

AFFDL-TR-74-155

12

FG

AD A 023 621

ANALYSIS OF SHOCK-ABSORBING CONCEPTS FOR BIRD-PROOF WINDSHIELDS OF ADVANCED AIR FORCE VEHICLES

*STRUCTURAL DEVELOPMENT BRANCH
STRUCTURES DIVISION*

FEBRUARY 1976

TECHNICAL REPORT AFFDL-TR-74-155
FINAL REPORT FOR PERIOD APRIL 1972 - NOVEMBER 1974

Approved for public release; distribution unlimited

AIR FORCE FLIGHT DYNAMICS LABORATORY
AIR FORCE WRIGHT AERONAUTICAL LABORATORIES
Air Force Systems Command
Wright-Patterson Air Force Base, Ohio 45433

DDC
RECEIVED
APR 28 1976
B

NOTICE

When Government drawings, specifications, or other data are used for any purpose other than in connection with a definitely related Government procurement operation, the United States Government thereby incurs no responsibility nor any obligation whatsoever; and the fact that the government may have formulated, furnished, or in any way supplied the said drawings, specifications, or other data, is not to be regarded by implication or otherwise as in any manner licensing the holder or any other person or corporation, or conveying any rights or permission to manufacture, use, or sell any patented invention that may in any way be related thereto.

This report has been reviewed by the Information Office (OI) and is releasable to the National Technical Information Service (NTIS). At NTIS, it will be available to the general public, including foreign nations.

This technical report has been reviewed and is approved for publication.

Werner R. Jansen

WERNER R. JANSEN
Project Engineer

FOR THE COMMANDER:

Larry G. Kelly

LARRY G. KELLY, Chief
Structural Development Branch
Structures Division

Approved for	
NTIS	With Section <input checked="" type="checkbox"/>
D-G	With Section <input type="checkbox"/>
UNCLASSIFIED	<input type="checkbox"/>
JUSTIFIED	
BY	
DISTRIBUTION/AVAILABILITY CODES	
Dist.	Avail. or Special
A	

Copies of this report should not be returned unless return is required by security considerations, contractual obligations, or notice on a specific document.

UNCLASSIFIED

SECURITY CLASSIFICATION OF THIS PAGE (When Data Entered)

REPORT DOCUMENTATION PAGE		READ INSTRUCTIONS BEFORE COMPLETING FORM
1. REPORT NUMBER 14 AFFDL-TR-74-155 ✓	2. GOVT ACCESSION NO.	3. RECIPIENT'S CATALOG NUMBER
4. TITLE (and Subtitle) 6 ANALYSIS OF SHOCK-ABSORBING CONCEPTS FOR BIRD-PROOF WINDSHIELDS OF ADVANCED AIR FORCE VEHICLES. ✓		5. TYPE OF REPORT & PERIOD COVERED 2 Final Report April 72 - November 74 ✓
7. AUTHOR(s) 10 Werner R. Jansen ✓		8. CONTRACT OR GRANT NUMBER(s) 16 AF-13681 17 1368021
9. PERFORMING ORGANIZATION NAME AND ADDRESS Structural Development Branch (FBS) ✓ Air Force Flight Dynamics Laboratory Wright-Patterson Air Force Base, Ohio 45433		10. PROGRAM ELEMENT, PROJECT, TASK AREA & WORK UNIT NUMBERS Project No. - 1368 Task No. - 136802 Work Unit No. - 13680229
11. CONTROLLING OFFICE NAME AND ADDRESS Air Force Flight Dynamics Laboratory AFFDL/FBS Wright-Patterson Air Force Base, Ohio 45433		12. REPORT DATE 11 February 1976
14. MONITORING AGENCY NAME & ADDRESS (if different from Controlling Office)		13. NUMBER OF PAGES 275 (12) 284 ✓
		15. SECURITY CLASS: (of this report) UNCLASSIFIED
		15a. DECLASSIFICATION/DOWNGRADING SCHEDULE
16. DISTRIBUTION STATEMENT (of this Report) Approved for public release; distribution unlimited.		
17. DISTRIBUTION STATEMENT (of the abstract entered in Block 20, if different from Report)		
18. SUPPLEMENTARY NOTES		
19. KEY WORDS (Continue on reverse side if necessary and identify by block number) Aircraft Shock Absorption Dynamic Analysis Windshield Impact Finite Difference Method Bird Strike Collision		
20. ABSTRACT (Continue on reverse side if necessary and identify by block number) → Shock-absorbing windshields and mounting frames are required in advanced AF aircraft to permit mission continuance after a hit by a bird in low level, high speed flight. Analytical structural models of → (over)		

DD FORM 1 JAN 73 1473 / EDITION OF 1 NOV 65 IS OBSOLETE

UNCLASSIFIED
SECURITY CLASSIFICATION OF THIS PAGE (When Data Entered)

012070

UNCLASSIFIED

SECURITY CLASSIFICATION OF THIS PAGE(When Data Entered)

(Cont'd of P1473A)

→ bird strike-proof, high visibility window systems are optimized using existing glazing materials, designs for realistic environmental conditions, and the influencing factors of proposed shock absorbing mechanisms. Theoretical results generated are compared with published experimental data. Parametric studies of structural response due to impact loading and damping of dynamic stresses due to energy absorption were performed to provide preliminary design data for windscreen protection against bird strike.



UNCLASSIFIED

SECURITY CLASSIFICATION OF THIS PAGE(When Data Entered)

FOREWORD

This is a report of an in-house effort conducted under Project 1368, "Advanced Structures for Military Aerospace Vehicles"/ Task 136802, "Structural Integration for Advanced Military Aerospace Vehicles"/Work Unit 13680229, "Bird-Proof Windshields for Military Aircraft" in the Structures Development and Integration Group, Structural Development Branch, Structures Division AF Flight Dynamics Laboratory. The principal investigator for this work was Mr. Werner R. Jansen, Aerospace Engineer.

The author gratefully acknowledges the interests and advices of Drs. R. Sandhu and G. Sendekyj, Structures Division. The assistance of Maj. R. Zollner, Tech Mgr of Structures Development and Integration Group is greatly appreciated.

This report covers work from April 1972 to November 1974, and was released by the author in December 1975.

AFFDL-TR-74-155

TABLE OF CONTENTS

SECTION	PAGE
I INTRODUCTION	1
1. Bird Strike Environment	3
2. General Windshield Criteria	4
3. Bird Proof Design Considerations	7
4. USAF Requirements	9
II APPROACH TO PROBLEM	11
1. Principle of Shock Absorption	16
2. Shock Absorbing Frame	26
3. Pane Visco-Elastic Interlayers	30
III FINITE DIFFERENCE ANALYSIS METHODS	32
1. Introductory Comments	32
2. Finite Difference Formulation of Dynamic Beam Equations	35
3. Curved Beam Equations	41
4. Finite Difference Formulation for Flat Plate	50
5. Finite Difference Idealization of Windshield (F-111)	81
a. The F-111 Windshield	81
b. The General Equations	82
c. The Geometry	84
d. Stiffnesses	86
e. Boundary Conditions	90
f. Mass Properties	91
g. Computer Program	91
IV APPLICATIONS	92
1. Analysis of Specific Square Panel Test (WT-18)	92
a. Finite Difference Solution	95
b. Preliminary Optimization of Mounting Frame	103
2. Theory/Test Correlation of Windshield (F-111)	117
V RESULTS, CONCLUSIONS AND RECOMMENDATIONS	140
APPENDIX I ASSESSMENT OF WINDSHIELD STRUCTURAL MATERIALS	143
1. Window Pane Materials	147
a. Laminate Glass	147
b. Flexible Interlayers	149
c. Acrylic Composite Windshield	151
d. High Strength Toughened Glass	152
e. Polycarbonate Plastic Sheet	155
2. Frame Design Data	159
3. Relevant Leading Edge Data	165

TABLE OF CONTENTS (CONT'D)

SECTION	PAGE
APPENDIX II SURVEY OF EXPERIMENTAL DATA	167
1. Bird Strike Experiments	167
a. Bird Guns, Test Frames, Instrumentation	167
b. Motion Picture Observations	169
c. Empirical Strength Design Formulae	170
d. Empirical Impact Force Equations	176
e. Bird Impact of Leading Edges, Fan Blades	177
2. Windshield Experiments Other than Bird Strike	178
3. Other Impact Analyses	179
a. Transient Beam Analysis	179
b. Elastic-Plastic Analysis of Plane Structures	181
c. Explosively Loaded Aluminum Shells	184
d. Hailstone Analysis	185
e. Other Computer Programs	185
APPENDIX III DESCRIPTIONS OF FINITE DIFFERENCE COMPUTER ROUTINES	186
1. Flat Plate Program	186
a. Introduction	186
b. Basic Program Listing	191
c. Different Versions "ONE" and "TWO"	193
2. Plate Program for Case WT-18	195
3. Conical Shell Segment Program	197
a. Introduction	197
b. Discussion of Program Listing	198
4. F-111 Windshield and Plotting Program	200
a. Introduction	200
b. Time Dependent Variables	200
c. Fixed Variables	204
d. Input Data	208
e. Calculation Procedure	210
APPENDIX IV COMPUTER PROGRAM LISTINGS	211
REFERENCES	266

ILLUSTRATIONS

FIGURE		PAGE
1	Shock Absorbing Window Frame.	14
2	Manner in Which a Bird Proof Windshield Panel Resists a Bird Strike	17
3	Mass-Spring-Damper System	18
4	Eigenvalues of Quadratic Eigenvalue Problem	21
5	Frequencies of Quadratic Eigenvalue Problem	22
6	Normalized Amplitudes of Quadratic Eigenvalue Problem .	23
7	Photo-Mechanically Measured Deflections of Shot WT-18 .	25
8	Principle of Viscous Damping System	27
9	Beam Finite Difference Model for Impulsive Loading. . .	40
10	Analog Network for Beam Impulse Loading	42
11	Variables of the Curved Beam Equations.	45
12	Variables for One Quadrant of Circular Ring Problem . .	47
13	Determination of Virtual Bending Moment	49
14	Symmetrical Impact Loading of Square Plate.	55
15	Central Bending Moment for Hard and Shock-Absorbing Window Mount.	57
16	Deflections W_0 and W_3 for Shock-Absorbing Design. . . .	59
17	Max. Center Deflections of Plate.	65
18	Time Histories of Center Deflection	66
19	Time Histories of Mid Edge Deflection	68
20	Maximum Center Stresses of Plate.	69
21	Maximum Mid Corner Stresses of Plate.	70
22	Center and Mid Edge Stresses.	71

ILLUSTRATIONS (CONT'D)

FIGURE		PAGE
23	Kinetic Energy in Impacted Windshield.	73
24	Effect of Viscous Interlayer Material on Panel Stresses	75
25	Determination of Windshield Contour.	85
26	Side View of F-111 Windshield/Crew Module.	87
27	F-111 Windshield/Mounting System	88
28	Original Test Data of Shot WT-18	94
29	26"x26" Test Panel Mounting Fixture.	100
30	History of Deflections for Shot WT-18.	102
31	Eight-Track Histories of Three Analog Runs	105
32	Deflections X_F (Trace 2) and $X_W - X_F$ (Trace 5) of Analog Runs.	108
33	MIMIC X-Y Plots of Corresponding Window Pane Deflections, X_{WF} , and Frame Deflections, X_F	113
34	Strain Gage Locations for Case FM-1.	122
35	Transcripts of Oscillograph Traces for Shot FM-1	124
36	Theoretical Strain Gage Readings of FM-1	126
37	"Ten-Twenty" Glass Stress Profile.	154
38	Typical Window Pane/Mounting Frame Concepts.	160
39	Calculated Static Flight Load Deflections for Different Mounting Concepts.	161
40	Pressure Cycle Used for Composite Laminate Testing	180
41	Beam Response Due to Impulsive Load.	182
42	Sequence in Cyclic Loop for Calculating Finite Differences.	188

ILLUSTRATIONS (CONT'D)

FIGURE		PAGE
43	Distribution of Constants in Finite Difference Scheme. .	190
44	View of 17x17 Finite Difference Grid	201
45	Typical Locations of Variables in Grid	202
46	Geometrical Arrangement of Radial Dimensions	206

TABLES

TABLE		PAGE
I	Description of Windshield Bird Strike Incidences	2
II	Windshield Design Criteria, Considerations and Requirements	5
III	Material Properties of F-111 Windshield/Canopy	56
IV	Edge Deflections of Hard Spring Supported Plate	76
V	Extreme Stresses and Deflections	77
VI	Parametric Investigation of Mounting Conditions for Plate	78
VII	Material Properties Considered in the Analysis of Panel Shot WT-18	96
VIII	Equal Mass and Pyramidal Load Distributions for Different Practical Grid Sizes	98
IX	Comparative Results at Different Grid Sizes	99
X	Identification of Eight-Track Analog Computer Records	107
XI	Eight-Track Parameters for Series (B) Analog Computer Runs	110
XII	Maximum Deflections, X_{WF} , from MIMIC X-Y Plots for Series (B) Parameters	111
XIII	Series (B) Analog and MIMIC Runs for Square Impulse, $(F_0/M_W) \cdot t_I = \text{const}$	116
XIV	F-111 Windshield/Crew Module Bird Strike Tests at AEDC	118
XV	Impact Time Histories for Shots FM-1, FM-2 and FM-7	120
XVI	Impact Load Computer Input for Shot FM-1	121
XVII	Input Data Chart for Case FM-1 of Bird Impacted F-111 Windshield	133
XVIII	Test Results of Stretched Acrylic Composite Windows	168

SYMBOLS*

E_{kin}	Kinetic Energy (pound-in)
EI_x, EI_y	Bending Stiffness (pound-in ²)
M_x, M_y	Bending Moment (pound-in)
Q_{tot}	Impact Load (pound)
r	Radius of Conical Shell (in)
t	Thickness of Pane (in)
u, w	Deflection (in)
\dot{u}, \dot{w}	Velocity (in sec ⁻¹)
\ddot{u}, \ddot{w}	Acceleration (in sec ⁻²)
V_x, V_y	Shear Load (pound)
x, y	In-plane Coordinates
Δt	Time Increment (sec)
$\Delta x, \Delta y$	Finite Differences (in)
ϵ	Elastic Strain at Outer Fiber (in/in)
ρ	Mass Density of Material (pound-sec ² /in ⁴)
σ	Stress Level at Outer Fiber (ksi, psi)

(*Basic symbolism; other symbols used by choice as indicated in the text.)

AFFDL-TK-74-155

SECTION I

INTRODUCTION

Efficient bird-proof design is a requirement for military aircraft to reduce losses due to bird strike and to reduce acquisition cost by reducing aircraft buys required to maintain the fleet size.

A stringent Air Force requirement is to operate aircraft in take-off, landing, and low level, high speed penetration modes where maximum crew protection is afforded for mission accomplishment. Windshields and canopies of aircraft are continuously vulnerable. In 1971, a F-111 airplane was lost as a result of a bird strike (Reference 1,2, and Table 1).

Aircraft bird strike hazard programs may fit into two categories, (1) concerned with the overall bird strike problem (collision avoidance), and (2) with the design of the aircraft itself to withstand the damaging effects of bird strikes. Bird impact resistance of aircraft transparencies under dynamic conditions is the theme of this report.

Development of conceptionally new bird proof windshield systems is costly. Design modifications of existing windshield systems that otherwise perform perfectly may be elaborate too. Therefore, one should consider other means of bird strike alleviation. The objective of Reference 3 was to determine the general feasibility of using the deflected air stream or pressure field caused by vanes, fuselage shaping, or shock waves to prevent bird strikes on aircraft windshields. This study concluded that bird strike prevention by means of deflected air flow using vanes, fuselage shaping, or shock waves, was not a feasible concept.

TABLE I
DESCRIPTION OF WINDSHIELD BIRD STRIKE INCIDENTS

YEAR	TYPE & MODEL AIRCRAFT	AIRCRAFT SPEED	PHASE OF FLIGHT	FLIGHT ALTITUDE	TYPE BIRD	BRIEF
1970	RF-4C	360KT	Low Level	500' AGL	Unknown	At an overseas location, this crew was flying a low level photo mission when they hit a large bird which penetrated the right side of the front canopy bow. The canopy failed, with large cracks running the length of the remaining canopy. A large 2' x 3' hole existed directly over the front seat. Several pieces of the canopy flew into the rear cockpit and struck the navigator. Fortunately, both crew members had their dual visors in place. Crew was covered with debris but were able to return to base and land successfully.
1971	F-111	492KT	Low Level	500' AGL	Turkey Vulture	Aircraft was on a day low level training mission when it struck a large turkey vulture. The bird penetrated the right windshield and entered the cockpit showering both crew members with glass and other debris. The pilot was unable to regain control of the aircraft due to severe windblast which negated communications and blurred vision. Both crew members successfully ejected in the capsule without major injury. However, both sustained minor cuts and bruises.

(From Reference 2)

In this report, techniques for reducing bird damage to USAF aircraft and air crew compartments are examined. Design concepts that would result in cockpit enclosures which can withstand bird impact are analyzed. Considerations include force-time loading factors, material response, attachment design, and structural transition zones.

1. BIRD STRIKE ENVIRONMENT

An international conference on bird strike on aircraft held in Sept. 1969 revealed that bird incidents involving aircraft in the vicinity of airports had significantly decreased (References 4 and 5). The only measures offering any real assurance of reducing the enroute hazard are those of bird-proofing the aircraft. This approach consists of increasing the strength and the energy-absorbing capabilities of the vulnerable parts of the aircraft that are likely to be subjected to bird impacts. Reference 2 indicates that the other approach to the problem, that of trying to avoid the birds, also appears to be a possible solution. Although a great deal of effort has been devoted to this concept, success is not in sight.

In response to AF Systems Command Document "Coordinating Committee on Bird Strike" of 1972 and Technical Need TN4-10 "Integrated Design Concepts to Provide Aircraft Windscreen Bird Strike Protection", a design concept for a bird-proof, high-visibility windshield by means of controlled shock isolation has been proposed ("Proposal of Bird Proof Windshield", AFFDL/FBS, March 1972). The AFSC document suggested a two phase effort attempting to treat the windscreen bird strike problem as an integrated design approach using and optimizing various specific techniques, such as deflectors, wind-

shield shaping, specific operations, materials, structural strength, etc., in order to achieve the total objective of adequate windscreen bird proof designs.

This concept was pursued to determine feasibility. A detailed DDC literature search (Reference 6) showed no analysis methods and data with respect to shock-absorbing windows.

2. GENERAL WINDSHIELD CRITERIA

Design criteria for a tandem side opening canopy, within the scope of structural finite element analysis conducted prior to 1972, lacked the requirement of proofing against bird strike. The magnitude of the design operating stresses in a canopy structure must be reliably known to insure both minimum weight and structural integrity. Minimum weight is required since the canopy ejection thruster size increases as the canopy weight increases. And, when pilot ejection through the canopy glass is required, the glass must be as thin as possible (Reference 7). The windshield must also satisfy strength requirements in new load carrying concepts as part of the external shell of the fuselage, subjected to the pressure differential due to aerodynamic and pressurization loads totaling several tons (Reference 8).

Visibility thru the windshield at all times during inclement weather is an obvious requirement for aircraft (Table II). In addition to the strength and optical requirements, electrical and thermal properties must be considered. A satisfactory electrical conducting film must have a high level of light transmission and good electrical properties for heating and demisting

TABLE II
WINDSHIELD DESIGN CRITERIA, CONSIDERATIONS AND REQUIREMENTS

Life Cycle General Design Criteria

Structural Static and Fatigue Strength

Environmental Fracture Toughness

Impact Resistance Against Bird, Hail, Bullet

Cyclic Pressure and Temperature Service Capability

Weathering Resistance

Optics and Field of Vision Qualification

Design Considerations*

Weight

Abrasion Resistance

Bird Impact Resistance

Cabin Pressure Retention

Ice Protection

Fail-Safe Characteristics

Fog Protection

Size

Contour

Design Requirements*

Temperature Requirements

Heat/Power Requirements

Thermal Design

Electrical Design

(* From Reference 9)

(Reference 10). Its adherence and lamination strengths are certainly adjunctive requirements.

Even bullet impact has to be considered as a plausible risk, either from outside the aircraft or fired from within (Reference 8). Hail stone impact, with masses up to bird size masses, also needs to be considered (Reference 11). Reference 12 notes that there is no test evidence to compare the damage to windscreens caused by hail and bird strike directly, and that the bird impact requirement is the most severe from an overall strength point of view. However, hail can cause extensive damage to the outer plies of a laminated windscreen.

An indicator used for qualifying windscreen panels against panel failure is the mean unit time between failures (MTBF). In the early sixties this mean unit time for the Boeing 707 was 6,700 hours (Reference 13). Reference 14 gives failure rates for the 747. The cumulative results of all the design changes as of November 1972 were that the mean time before repair (MTBR) had been raised from a low of about 1,400 hrs. in early 1971 for the original design to a level of over 6,000 hrs. for the current "balanced" laminated design. Over 25 percent of the removals were for causes not attributable to windshield performance per se. This data does not separately identify the stiff main ply interlayer or the improved seal, and the MTBF of the latest configuration is undoubtedly much higher.

Design criteria for curved and flat transport and helicopter windshields for environmental conditions may best be illustrated by the technical data of the Sierracin Windshield Flight Environment Simulator (WFES). This

mirror-image wind tunnel set-up (Reference 15) permits simultaneous representative accelerated life testing, within a time span of less than 20 minutes, of two windshields under entirely different test conditions. These conditions include continuous pressure and temperature cycling for selected flight profiles, outside temperature range from -100°F using liquid nitrogen to 150°F , pressures up to 15 psi, air velocity (flow pattern) over windshield up to 200 kt (far surpassing the maximum convective heat transfer coefficient of sea level air that most transport windshields can encounter in flight; external heat transfer rates equivalent to 800 kt at 35,000 ft), high speed rain simulation, humidity testing, ultraviolet testing, continuous windshield and frame deflection measurements, and visual and photographic observation. The WFES makes it possible to evaluate the reliability of current and newly upgraded designs in a short time span, possibly prior to actual production of the design. Representative flight cycles can be programmed at rates of 150 cycles per day.

3. BIRD PROOF DESIGN CONSIDERATIONS

The loads generated due to bird impact at usual flight speeds are impressive. A 4 pound bird at an impact velocity of 500 ft/sec causes 1500 psi compressive stress over an assumed area of 20 in² which is equivalent to 30,000 pounds (Reference 16).

Conventional design practice has to consider, and usually results in a trade-off between several influencing factors (Reference 17). In bird-proof designs for high speed flight, however, impact strength along with shock absorbing capacity is predominant and several of the conventional factors may be neglected.

Therefore, a reasonable basic specification is that the transparency should withstand a bird of a specified weight at a specified speed (Reference 18). A more detailed requirement in the civil aviation field is to resist a 4 pound bird at maximum true airspeed in operational service up to an altitude of 8,000 feet considering the most adverse temperature conditions. The Federal Aviation Agency (FAA) has, for several years, required a specific level of bird impact resistance for crew station transparencies on Transport Category aircraft. FAA regulation FAR 25 requires a windshield, with all its plies broken, not to be penetrated nor to shatter into the pilot's face (Reference 19).

The frequency of bird strikes on 707 and 720 jet liners has been less than one per 50,000 flight hours. None of these produced penetrations affecting flight safety. Bird penetration had not occurred once in over 500,000 flight hrs in 1961 (Reference 20). Reference 20 does not report how often cockpit windows were impacted by birds; however, it does reflect, that bird strike is no problem for the 707 and 720 windshields, and that there is indeed a bird-proof category of airplanes flying today. Reference 17 states that windshields can be made bird resistant by adding vinyl interlayers to the windshield assembly and heating the assembly to reduce its brittleness. Also, windshield panes and their supporting structures directly in front of the pilots should be designed to withstand bird impact requirements generally specified in MIL-A-008860A (USAF).

Results of investigations lend themselves directly to Specification MIL-A-008865A (USAF) for windshield/canopies and support structure and

to AFSC DH2-1 Design Handbook revisions. A follow-on effort ("Windshield Bird Strike Structure Criteria - Phase II", AFFDL-FB, Sept 1973) has been proposed to review the criteria developed under Phase I (Reference 21) to recommend new bird strike data collection, windshield structural proof tests, compliance tests, and flight limitation restrictions.

4. USAF REQUIREMENTS

The USAF probability of bird strikes is much lower than that for commercial aircraft (1965-1972 ICAO data), being .055/1000 flight hrs. Extrapolation of data shows 356 bird strikes annually on the average with up to 1/3 of these to be expected on crew enclosures.

A four pound bird as a criteria for impact resistant rating has been found to be statistically sound. It is reported that less than 5% of the strikes on all airplanes involve birds heavier than four pounds (Reference 20). Most USAF bases are located inland while many large commercial airports are near large bodies of water and major cities. This may account for the great number of sea gulls and pigeons struck by commercial airliners. The average USAF flight may also be of longer duration than the average airline flight of approximately 75 min. and above the main bird flight altitudes.

For an update of criteria, Reference 21 was prepared considering the possibility that future USAF aircraft may require windshields capable of resisting the impact of a bird while flying at velocities up to Mach 1.2 at sea level.

The minimum requirement for the F-111 Improved Windshield Program is a 4 pound bird impact at 500 kt true air speed (KTAS). The F-111 Transparencies Development Plan of Project 1926 requires proof testing for four (4) aircraft life times of 6000 flight hours utilizing cyclic thermal, pressure, and mechanical loading envelopes.

The mission envelope for the B-1 compares with the one of the F-111 for low level penetration and dictates the need for a similar proven bird resistant windshield concept, except that shielding against a 4 pound bird at 650 mph (565 KTAS) is required. The design of the windshield on the B-1 is based on transparency state-of-the-art as it existed in 1970, when bird impact technology was not nearly as well developed as it is now, and consequently was not incorporated in the B-1 Airframe System.

SECTION II
APPROACH TO PROBLEM

The methodology has to meet the following objectives: (1) prove the feasibility of bird-proof design with existing high strength glazing materials of laminated construction in combination with novel window frame concepts capable of absorbing part of the shock energy; (2) prove the validity of the mathematical model developed for determination of fail-safe configurations by comparing estimated results and actual test data of related efforts to optimize for essential parameters; and (3) determine beneficial applications of conceived design concepts and existing material configurations to suit adverse bird strike conditions and other environmental influences.

As the manufacturer of a bird proof windshield/canopy is usually required to dimension it for structural limit conditions, additional variables, such as location of impact, should be considered. The safety margin should be based on dynamic maximum stresses in the mounted window pane due to the design allowable impact relative to the dynamic stresses resulting from an ultimate impulse loading causing catastrophic failure of the window/mounting frame system. The problem is to understand the functional relationship between stresses and impulse for several particular design details.

A first approximation of the required pane thickness can be calculated from the Grashof equation for rectangular plates (Reference 10) with deflection which is small as compared to the dimensions of sides. This equation relates the dimensional parameters, pressure differential, and allowable stress for a plate with unrestrained edges.

The structural load experienced by an impacted windshield may be estimated by assuming conditions of 1.2 Mach at 500 ft altitude (1336 ft/sec) and a bird dimension of 8 inches. Impact time is .0005 sec., acceleration is 1,336,000 ft/sec², and one half of the flight speed is taken as the final speed of the bird. The force of impact is 166,000 pounds and the mass is 0.124 pound-sec²/ft. The normal force acting on the windshield, inclined at 24°, is 67,500 pounds. Assuming this load equally distributed over a window area of 600 in², the instant transverse pressure, p, is 113 psi.

"Quasi-static" solution for a plate of dimensions, s, and thickness, t, with all edges fixed and uniform load over the entire surface (Reference 22) gives the following maximum stress, σ_{max} , at mid-edge and maximum elastic deflection, w_{max} , at the center of the plate:

$$\sigma_{max} = .31 \frac{p \cdot s^2}{t^2} \quad (1)$$

$$w_{max} = .014 \frac{p \cdot s^4}{E \cdot t^3} \quad (2)$$

For one case calculated, deflection was $w_{max} = .77$ in, and the material must be stronger than $\sigma_{max} = 9.35$ ksi. The deflections and stresses would be different if mass inertia effects were taken into account.

Another approach to the windshield bird strike is the classical vibration problem. The plate is hit for an instance of time, then unloaded, and vibrates at an undamped frequency. The amplitude of vibration changes due to the severity of impact impulse. An estimation for the frequency, f, is in Reference 23.

The first mode of free vibration of a mounted square plate of specific density, ρ , is:

$$\omega_s^2 \sqrt{\frac{S}{D}} = 35.99 \quad (3)$$

where,

$$D = \frac{E \cdot t^3}{12(1-\nu^2)} \quad (4)$$

$$f = \frac{\omega}{2\pi} \quad (5)$$

A sample calculation within the parametrical range of interest (see Section III-4) shows that the time for one cycle of vibration varies between .008 and .015 sec. This indicates that a high speed impulse, typically lasting 0.0005 sec, is much shorter than the vibrational time.

The shock absorbing window pane/mounting frame (Figure 1) represents another aspect of bird strike which accounts for the total energy received due to impact. At the end of impact, this energy is almost entirely kinetic energy of the system, and practically no energy has been converted into potential or absorbed energy. The sum of these three energies (kinetic, potential and absorbed) is constant, that is

$$E_{imp} = E_{kin} + E_{pot} + E_{abs} = \text{const.} \quad (6)$$

The kinetic energy of the one-degree-of-freedom transverse movement of translational mass elements dominates and can be taken to represent the kinetic energy, E_{kin} , in Equation 6. The potential energy, E_{pot} , consists of the elastic bending energy in the pane and frame in the longitudinal and lateral directions, and the energy in the translational and rotational springs along

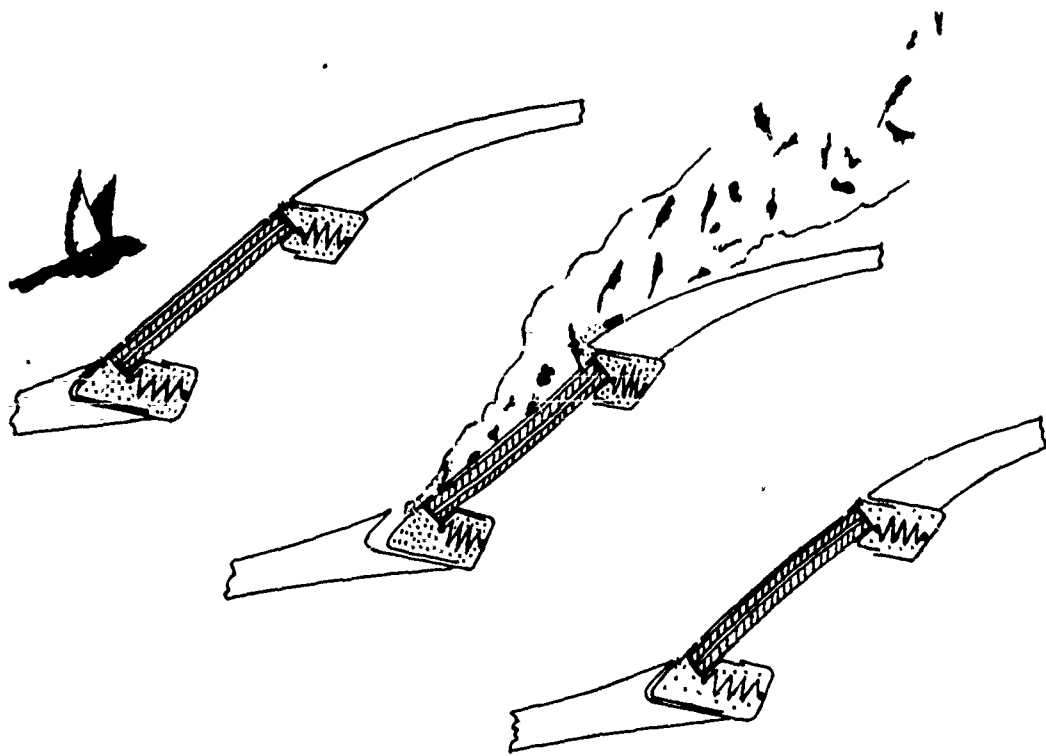


Figure 1. Shock Absorbing Window Frame

the boundary of the pane in the window mount. The absorbed energy, E_{abs} , is composed of the viscous material behavior of the pane and the viscous effectiveness of the shock absorbing frame.

Reference 24 indicates that the need to streamline the aircraft to minimize aerodynamic drag is in direct conflict with the requirement for good pilot vision. The existing windshield for the F-111 B aircraft has a 21.5° baseline. A 30° windshield was proposed providing improved visibility. The modification would have increased the susceptibility to destructive bird strike energy by a factor of $(\sin 30^\circ / \sin 21.5^\circ)^2 = 1.858$.

Designed shock-absorption for the purpose of stress variation is technically feasible (Reference 25). Time and distance can be varied to stop a moving mass. The resultant stress can be varied by tailoring the shock absorbers to fit a particular requirement. Active shock isolation has been defined practically (Reference 26). This seems to be more economical for continuous requirements. Substantial R&D effort should go into flight hardware integration of a particular proven concept.

The original bird proof designs consisted primarily of laminated tempered glass with polyvinyl-butylal (PVB) interlayers (Reference 16). Bird impact testing of laminated windshields made with PVB plastic has shown that impact resistance is primarily a function of the interlayer thickness, the percent plasticizer content in the plastic interlayer, the flexibility of the supporting structure, and the temperature of the plastic interlayer.

Two techniques exist for achieving bird proof designs at higher flight velocities. One technique relates to the optimally designed mounting frame of Figure 1 with capacity to accommodate a sufficient part of the shock

energy thereby reducing dynamic peak bending stresses in the pane shortly after impact. The second uses the laminated glazing concept (Figure 2) with cushioning, transparent rubber-like interlayer materials which are stronger than PVB under identical conditions and available at maximum allowable thickness for optical qualification. Separate and combined effects of these concepts were investigated.

1. PRINCIPLE OF SHOCK ABSORPTION

The principle of structural shock-absorption due to impact loading may be explained as follows. The sudden application of impact force causes the window mounting to vibrate in a transient manner and in many natural modes simultaneously (Reference 27). For a qualitative understanding, a simplified analysis is given herein where the masses are considered to be concentrated and the flexible members to be massless (Figure 3). The equations of motions of such a system are:

$$\begin{aligned} m_w \ddot{x}_w + k_w (x_w - x_f) &= F(t) \\ m_f \ddot{x}_f + c_f \dot{x}_f + k_f x_f - k_w (x_w - x_f) &= 0 \end{aligned} \quad (7)$$

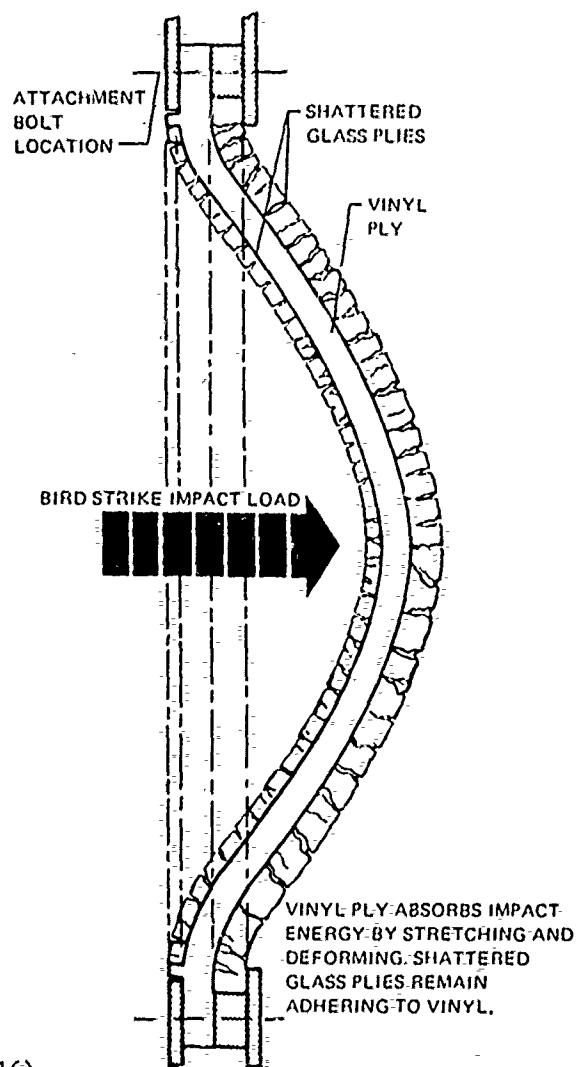
(t=0: $x_w=0, \dot{x}_w=0, x_f=0, \dot{x}_f=0$)

where the effective mass of the window

$$m_w = k_w / \omega_w^2 \quad (8)$$

is defined by the bending stiffness and the first mode of vibration. These equations may be solved by one of several methods. An accurate solution is only useful for a special case. For our purpose, a discussion of the nature of the solution is appropriate.

Bird impact is adequately represented by an impulse, Q, which may have



(REFERENCE 16)

NOTE: DATA SUPPLIED BY LOCKHEED.

Figure 2. Manner in which a Bird Proof Windshield Panel Resists a Bird Strike

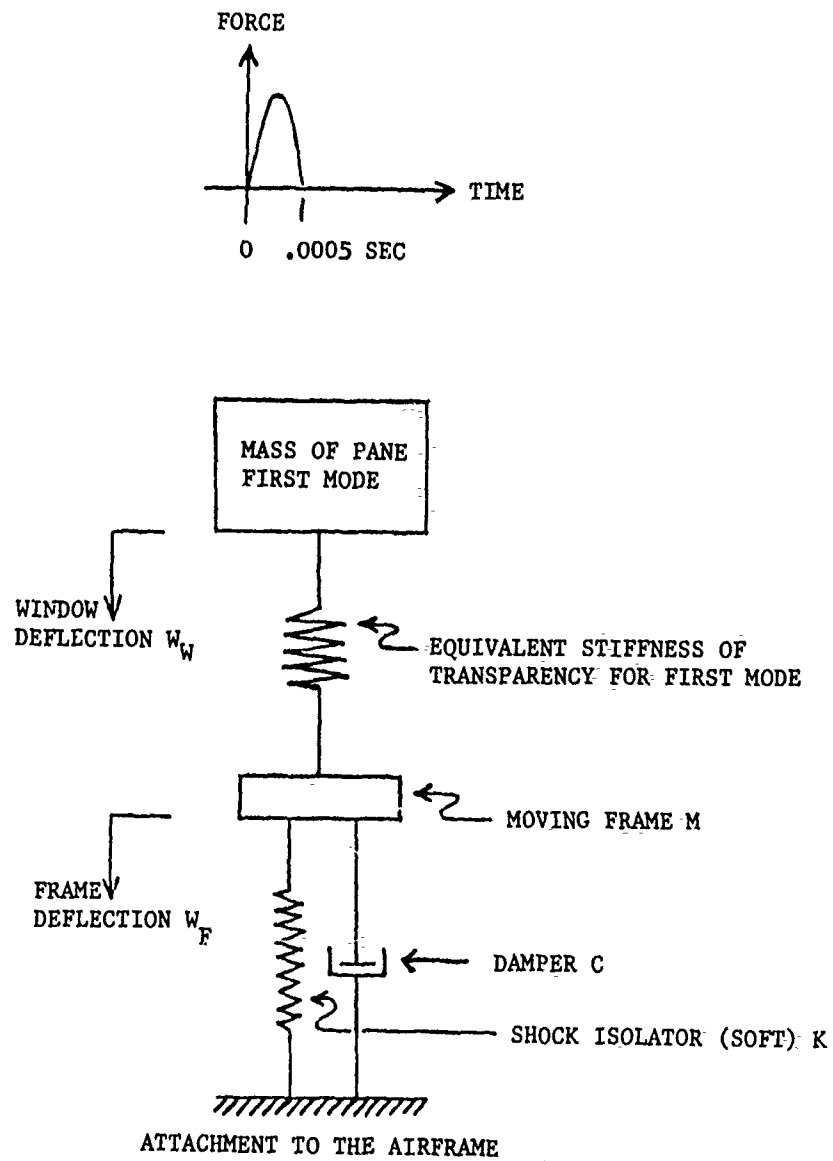


Figure 3. Mass-Spring-Damper System.

the force varying as a half sine wave, i.e.,

$$Q = \int_0^{\frac{\pi}{\omega}} F(t) dt$$

$$F(t) = F_0 \sin \omega t \quad (0 \leq t \leq \frac{\pi}{\omega}) \quad (9)$$

$$F(t) = 0 \quad (t \geq \frac{\pi}{\omega})$$

The duration of this load is on the order of .0005 sec at Mach 1.2. If this is very short compared to the natural periods of motion of this system, the impulse will cause a displacement, x_w , and the frame mass is restrained by the shock isolation spring. A soft spring allows motion of the frame mass and this in turn acts to reduce the stresses in the plate.

In the limiting case of an extremely soft isolation spring, the plate with its frame acts as if its edges were free. This is the optimum condition to resist breaking due to bird impact because the plate is allowed to move. However, a maximum displacement is technically allowable. In the practical case, the flexibility of support consists of a mixture of torsional and transverse flexibilities.

Two types of transient stresses must be considered during impact. These are bending stresses due to the relative displacement ($x_w - x_f$), and dynamic bending stresses due to the inertia of the pane and the difference in acceleration of the pane center and the window support, ($\ddot{x}_w - \ddot{x}_f$). These direct stresses are to be superposed on initial stresses due to aerodynamic pressure and thermal expansion. The initial stresses reflect the effects of aerodynamic contour, pressure differential, and thermal shock. It is anti-

icipated that the pane, sized for impact resistance, will also take the stresses due to the flight environment.

The resonance conditions of the undamped system of Figure 3 are given by:

$$\lambda_{1,2} = \frac{1 + \frac{k_f m_w}{k_w m_f} + \frac{m_w}{m_f}}{2} \pm \left(\frac{\left(1 + \frac{k_f m_w}{k_w m_f} + \frac{m_w}{m_f} \right)^2 - \frac{k_f m_w}{k_w m_f}}{4} \right)^{\frac{1}{2}} \quad (10)$$

$$\omega_{1,2} = \left(\frac{k_w}{m_w} \lambda_{1,2} \right)^{\frac{1}{2}}$$

$$a_{w1} = \frac{1}{1 - \lambda_1} a_{f1} ; \quad a_{w2} = \left(1 + \frac{k_f}{k_w} - \frac{m_f}{m_w} \lambda_2 \right) a_{f2}$$

This type of dynamic system vibrates in one of the modes (ω_1 or ω_2) with deflections $w_{w1,2} = a_{w1,2} \cdot \sin(\omega_{1,2} t + \phi)$ and $w_{f1,2} = a_{f1,2} \cdot \sin(\omega_{1,2} t + \phi)$ in phase, yielding $\phi=0$ (Reference 28). With m_w , m_f , k_w and k_f positive and real, a three-parameter analysis with m_w/m_f ranging between 10^{-2} and 10^2 , $k_w/k_f=1$ thru 10^3 , and $k_w/m_w=10$ thru 10^5 was conducted. The eigenvalues (λ_1 and λ_2), circular frequencies $\omega_{1,2}$ (sec^{-1}), and normalized amplitudes in the form, $-a_w/a_f|_1$ and $+a_f/a_w|_2$ are shown in Figures 4, 5 and 6. Assuming the softest frame support shown in Figure 6, $k_w/k_f=1000$, the amplitudes of the frame, a_{f1} and a_{f2} , are the largest with increasing mass ratios m_w/m_f , which is equivalent to decreasing frame masses, m_f .

A direct solution of the mass-spring-damper system (Figure 3) was obtained using the analog computer for different mounting conditions of PPG Industries flat 26" x 26" panel test, WT-18, performed under AFFDL Contract F33615-73-C-3099. This study indicated that substantial reductions of impact stresses in

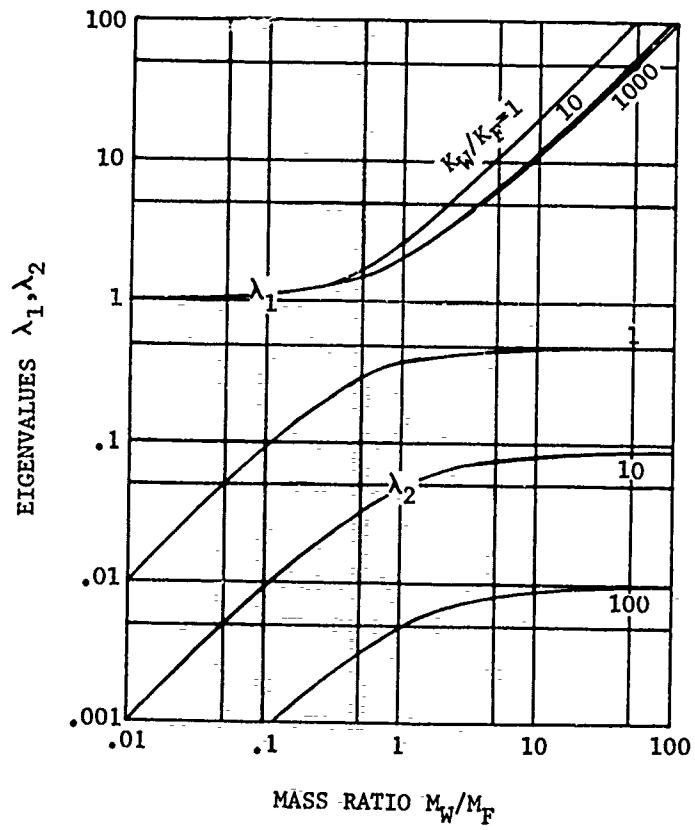


Figure 4. Eigenvalues of Quadratic Eigenvalue Problem

	ω_1		ω_2			
M_W/M_F	.01		1		100	
K_W/K_F						
1.	(A)	(G)	(B)	(H)	(C)	(I)
1000.	(D)	(J)	(E)	(K)	(F)	(L)

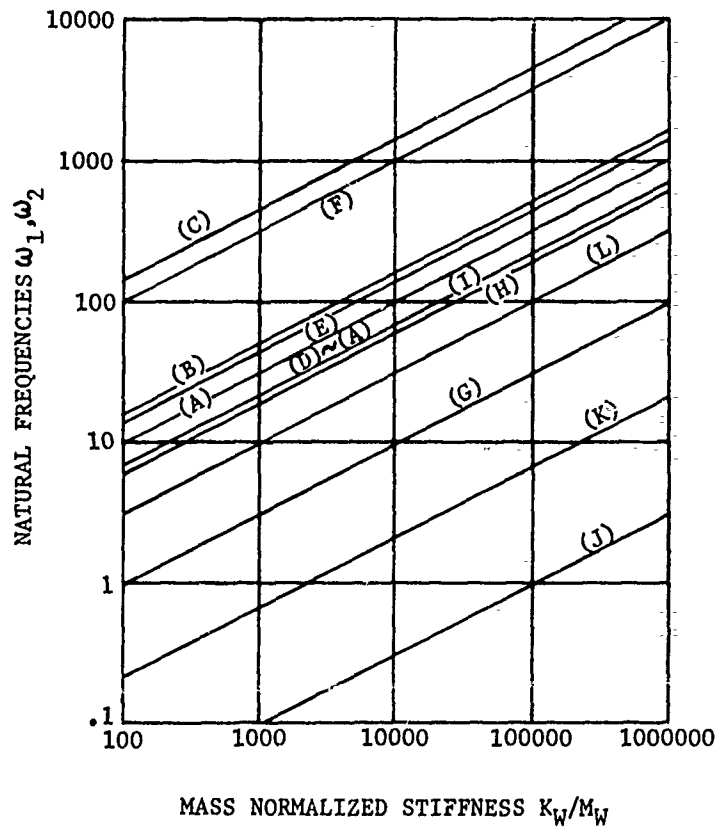


Figure 5. Frequencies of Quadratic Eigenvalue Problem

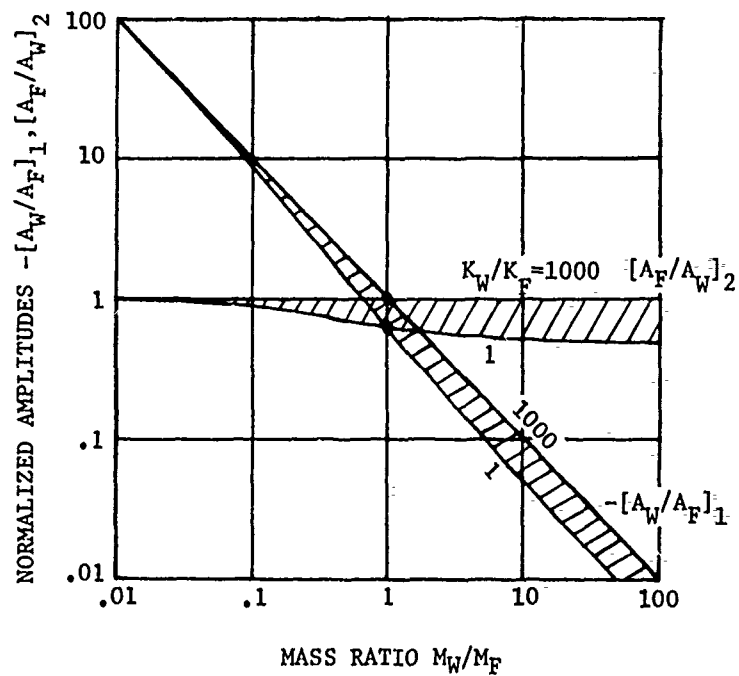


Figure 6. Normalized Amplitudes of
Quadratic Eigenvalue Problem

the pane could be achieved. Optimization was performed by trial and error.

The original test deflection data (Figure 7, lower diagram, a photo-mechanical record of the quasi-rigidly mounted pane) were curve-fitted for the following three parameters:

- (1) impulse per unit mass of window, $F_0 t_I / M_W$ (in/sec)
- (2) natural frequency, $\sqrt{K_W / M_W}$ (rad/sec),
- (3) damping factor, C_W / M_W (rad/sec).

$F_0 t_I / M_W$ was simulated as a square wave for convenience in the calculations.

Since a constant frequency model was used to simulate the actual data curve, which is non-linear shortly after impact, two calibrations were applied. Calibration "A" (Equations 13) was to get both curves in agreement past the second amplitude, which resulted in an initiation of the simulated time history. Calibration "B" (Equations 14) averaged the first four amplitudes such that the origins of both time histories and the fifth amplitudes were congruent.

Calibration (A):

$$\begin{aligned} F_0 t_I / M_W &= 1,060 \text{ in/sec} & (t_I \sim 10^{-3} \text{ sec}) \\ \sqrt{K_W / M_W} &= 410 \text{ rad/sec} & (13) \\ C_W / M_W &= 68 \text{ rad/sec} \end{aligned}$$

Calibration (B):

$$\begin{aligned} F_0 t_I / M_W &= 1,200 \text{ in/sec} & (t_I \sim 10^{-3} \text{ sec}) \\ \sqrt{K_W / M_W} &= 467 \text{ rad/sec} & (14) \\ C_W / M_W &= 76 \text{ rad/sec} \end{aligned}$$

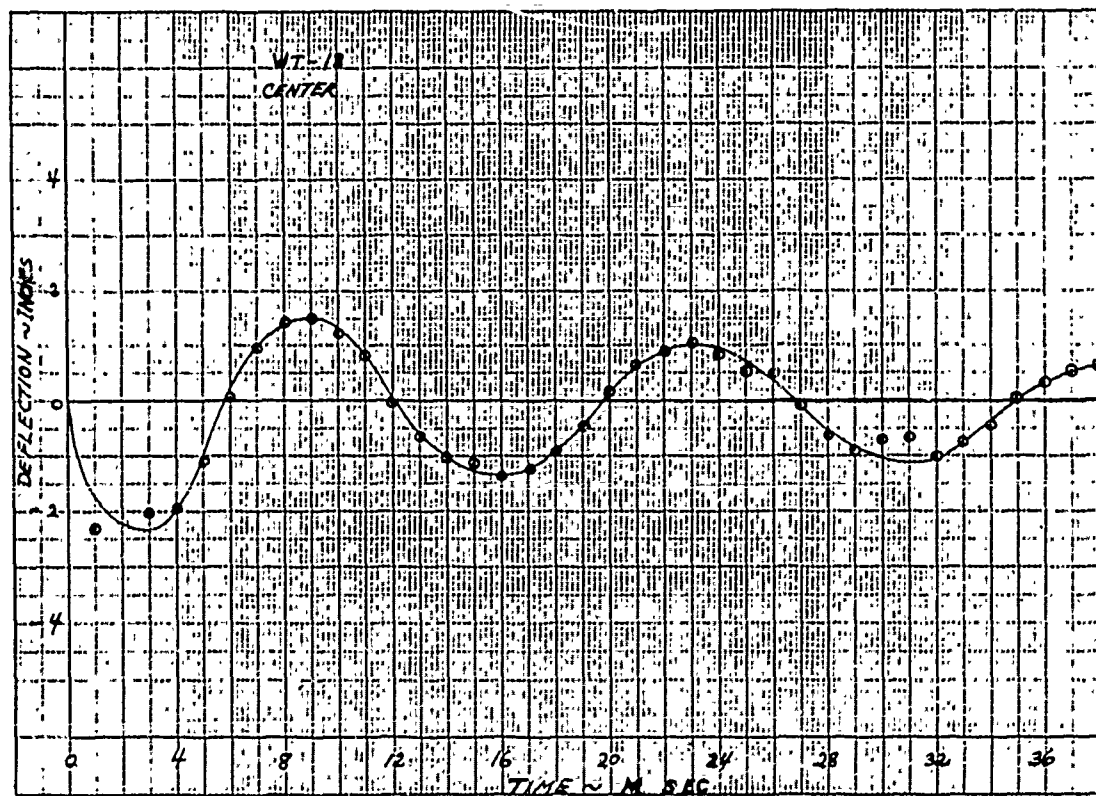
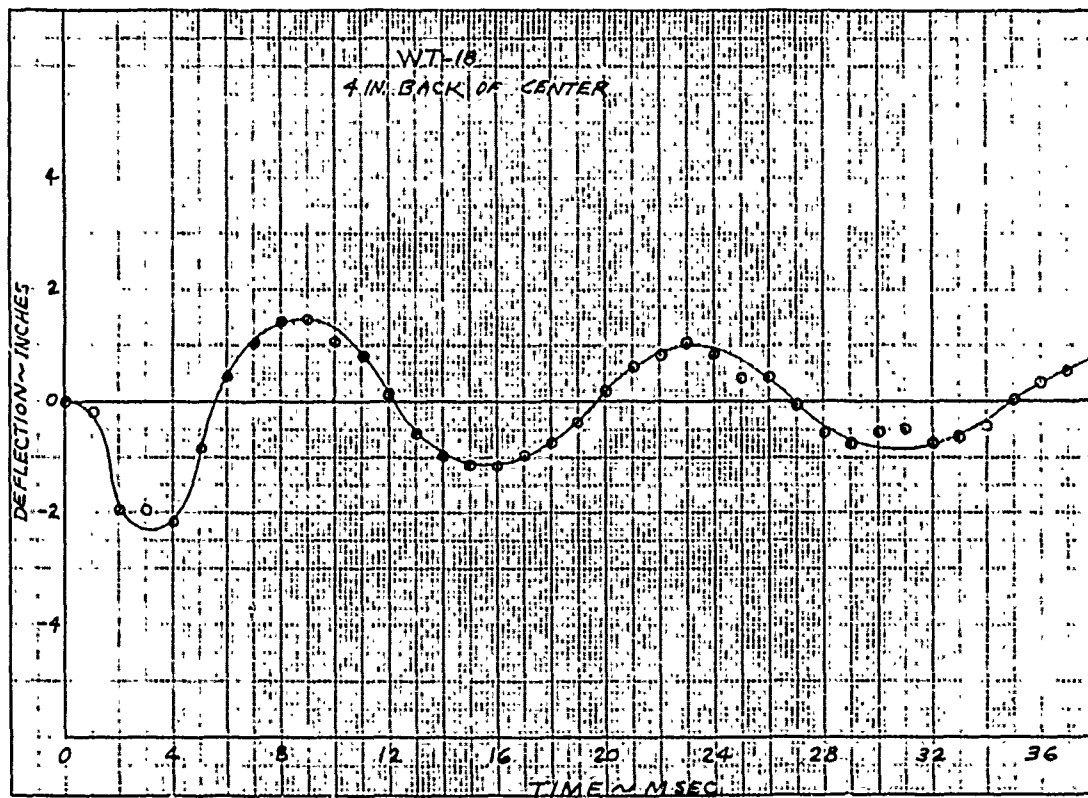


Figure 7. Photo-Mechanically Measured Deflections of Shot WT-18

Then, the original analog circuit for the rigidly mounted window pane was modified to represent a dampened, flexible mount for the pane. This modification added three additional parameters:

- (4) mounting frame - window mass ratio, M_W/M_F ,
- (5) stiffness ratio, K_F/K_W , and
- (6) dampening ratio, C_F/C_W .

Results for panel test WT-18 are discussed in Section IV-1b.

2. SHOCK ABSORBING FRAME

One configuration of mounting frame for damping the impact load is composed of a two-part hollow sliding frame containing viscous fluid that is released thru orifices under impact. Steel springs in the frame provide deceleration of the impacted window and spring-back to the original position. The frame contains distributed orifices which open to the outside. They dissipate energy by controlled release of fluid (Figure 8) under impact pressures. Other damping devices, such as an expendable low density cellular crushing material developed for the Apollo crew couch impact strut assembly (Reference 6), may be feasible.

When a viscous fluid system is used, the fluid has to remain functional in the operational temperature regime. The system must provide sealing characteristics as required for cabin pressurization and against atmospheric moisture. A fluid could reduce maintenance of the system. Replacement of the fluid after expenditure is possible with auxiliary pumping equipment, even under flight conditions. There should be no adverse interference of the fluid with the mechanical springs.

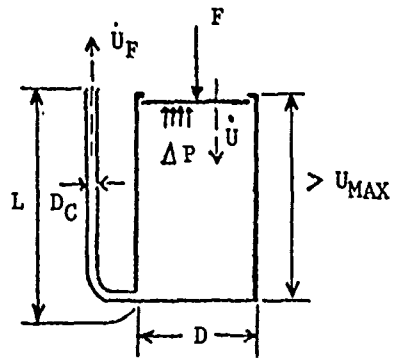


Figure 8. Principle of Viscous Damping System

Impact activated expenditure of the fluid to the outside should eliminate any danger of spillage into the cabin interior. The fluid must be non-corrosive, may act as a lubricant for the sliding mechanism, must not be a fire hazard or toxic, and must not block visibility after release. Spring-back of the frame to its original position after impact is necessary for reconstitution of aerodynamic cleanliness and supersonic flight performance of the vehicle. The spring mechanism has to absorb and discharge that part of the impact energy required to overcome the aerodynamic drag on the windscreen and frictional sliding forces during the spring-back phase. The frame must accommodate detrimental changes due to aerodynamic heating or cold spells at take-off, as well as static and dynamic flight loads, and different impact loads including eccentric impact.

Although a detailed design of the viscous flow damping system is not presently anticipated, its principle of performance could be explained (Figure 8) and a preliminary numerical evaluation (Reference 29) conducted. The pressure drop, Δp , due to viscous friction in small diameter capillary tubes reacts the load due to impact, F (Equation 15). A number of pipes, N , spread circumferentially around the frame should be capable of providing necessary release of the viscous fluid at a displacement, u_{\max} , during the relatively short response time of impact.

$$\Delta p = 4F/\pi D^2 \quad (15)$$

$$\dot{u}_F = (1/N) \cdot (D/d)^2 \cdot \dot{u} \quad (16)$$

$$\Delta p = \lambda \cdot (L/d) \cdot (8_F/2) \cdot \dot{u}_F^2 \quad (17)$$

$$\lambda = 64/Re \quad (\text{for } Re \leq 2320) \quad (18)$$

$$Re = \dot{u}_F \cdot d / \nu_F \quad (19)$$

$$F = (8\pi L/N)(D/d)^4 \cdot \rho_F \cdot \nu_F \cdot \dot{u} \quad (20)$$

$$F = k_{\dot{u}} \cdot \dot{u} \quad (21)$$

In the preliminary design cycle, the law of continuity for incompressible fluids (Equation 16) is used. The application of Bernoulli's equation for stationary flow conditions (Equation 17) includes the factor $\lambda L/d$ to take into account the kinematic fluid friction at the walls of the capillary tubes. Equation 18 defines the factor λ which is laminar for $Re \leq 2320$. Combination of Equations 15 thru 19 yields Equations 20 and 21, defining the viscous damping coefficient ($k_{\dot{u}}$) which should assume the value 10 pound-sec/in for an impact load (F) of 50,000 pounds and a frame velocity (\dot{u}) of 5000 in/sec. $k_{\dot{u}} = 10$ is technically feasible (Reference 30). Assuming a diameter ratio, $D/d=150$, with the equivalent piston diameter, D, and that of the capillary, d, a length of the capillary, $L=2$ in, a fluid of water-like density with $\rho_F=.00009$ pound-sec²/in⁴, and a kinematic viscosity (like that of mineral oil at R.T.) $\nu_F=1$ centi-stokes $\approx .0015$ in²/sec, the number of capillary tubes necessary is $N=344$.

Another technically feasible concept of impact absorption (the hollow rubber unit type) was treated theoretically and confirmed by experiment (Reference 31). The force-deflection characteristics of various shapes and geometrical dimensions were determined.

3. PANE VISCO-ELASTIC INTERLAYERS

Good interlayers must have shock-absorbing capability, optical transparency, and adhesive strength (Reference 16). Poly-vinyl-butyril (PVB) is one of the early interlayer materials, and has become the standard of comparison. Design details for interlayers have been suggested in Reference 32. One design has metal reinforced interlayer edges with the extended sheet metal bolted to the windscreen frame with parting agents at all bonded edges and individual laminations at the areas of high local load concentrations. The necessity of these design details challenges low cost low weight effective design. A 1/4-inch soft vinyl cushion between main plies and abrasion shield did not improve the panel resistance to bird weight (Reference 33).

The following approximate formulation for elastic flexural stiffness, EI, for the laminated window pane was chosen for use in the analysis:

$$EI = b \left(\sum_{\substack{\text{upper} \\ \text{layers}}} E_i t_i e_i^2 + \sum_{\substack{\text{lower} \\ \text{layers}}} E_i t_i e_i^2 \right) \quad (22)$$

$$\sum_{\substack{\text{upper} \\ \text{layers}}} E_i t_i e_i^2 = \sum_{\substack{\text{lower} \\ \text{layers}}} E_i t_i e_i^2 \quad (23)$$

where E_i = effective Young's modulus of layer i
 t_i = thickness of layer i
 e_i = distance of layer i from neutral plane

The position of the neutral plane is determined by iteration. The elastic properties, E_i , can be estimated. They are dependent on the type of material, manufacturing process, rate of loading (strain rate), and temperature (Reference 34, page 56).

Little is presently known about the shock-absorbing behavior of highly plastic interlayers and their effectiveness in the laminated arrangement. More research has to be undertaken to understand the behavior of the PVB interlayers. The type of test data needed to simulate are those of Reference 35.

To simulate the viscous damping, the elastic bending moment - slope relationship (the first term of Equation 24 in finite difference notation along a distance Δx at a location n) is modified to include rates of change of deflection slope (second term of Equation 24) accounting for the viscous damping component of bending moment distribution in the pane.

$$M_n = \left[(\Theta_{n+\frac{1}{2}} - \Theta_{n-\frac{1}{2}}) EI_n + (\dot{\Theta}_{n+\frac{1}{2}} - \dot{\Theta}_{n-\frac{1}{2}}) k_{vsx} \right] / \Delta x_n \quad (24)$$

Material data on viscous damping due to plate bending dependent on actual bending curvature rate, $\dot{\theta}$, were not found in the literature. The damping coefficient, k_{vs} , in Equation 24 represents a viscous moment of inertia. It is composed of strain rate force coefficients, $k_{\dot{\epsilon}_n}$, in the individual layers acting at distances, d_n , from a mid-layer axis such that the moments of upper and lower layers balance; that is,

$$k_{vs} = b \left(\sum_{n=1}^{n=\text{upper layers}} k_{\dot{\epsilon}_n} t_n d_n^2 + \sum_{n=1}^{n=\text{lower layers}} k_{\dot{\epsilon}_n} t_n d_n^2 \right) \quad (25)$$

The effective influence of this definition of damping coefficient upon plate dynamics has been observed in the follow-on analysis, considering k_{vs} as a bulk parameter constant throughout the finite difference model of plate.

SECTION III
FINITE DIFFERENCE ANALYSIS METHODS

1. INTRODUCTORY COMMENTS

At times, generation of closed form solution to the governing differential equations is not feasible. In case of structural problems, the reason for this may either be the complexity of the boundary condition of realistic structures, or the necessary description of nonlinear material behavior. Under such circumstances, however, an approximate solution may be obtained using numerical techniques. One of these techniques is the finite difference method. This is a procedure that transforms a continuous system, described by differential equations, into a discrete one consisting of algebraic equations. The independent variables are divided into a number of segments of suitable length and the differential operators are replaced by suitable finite difference operators, expressed in terms of the displacements at pivotal points. The choice of the number of pivotal points and the order of the operators affects the accuracy of the solution.

The following three ways are available to improve the accuracy:

(1) Increasing the number of divisions improves the quality of results; however, with larger number of divisions inaccuracies due to round-off errors tend to be significant. In addition, computational time increases rapidly with the number of divisions.

(2) Accuracy of the results can also be improved by using higher order difference operators. This may result in unwieldy equations making the numerical operations tedious.

(3) Another way to obtain better accuracy is to use Richardson's extrapolation technique (Reference 36) which consists of determination of the displacements, etc. for three different values of the number of divisions and extrapolation of the results. This technique presupposes that the successive values of calculated displacements, etc. approach monotonically to the correct solution from one side.

In dynamic problems, the solution procedure is started by assuming all time dependent variables to be zero. Then, loads are applied and accelerations are calculated. These are numerically integrated to give local displacements. The stresses in the structure due to the displacements are used to compute new loads. The procedure is then repeated continuously. Transient and stationary dynamic as well as static problems may be solved this way. In the static case, the load has to be slowly applied to keep accelerations causing vibrations at a minimum.

The very efficient marching solution procedure used herein does not require matrix operations. Calculations are straight forward and results are achieved in split seconds computer time. Accuracy of results increases with smaller increments of time and finite difference divisions.

Another advantage for using the finite difference methods, as described in the sub-sections below, has been found. One ready-to-use finite element analysis routine, NASTRAN, for determining the transient dynamic response was found to use 10 to 100 times more computer time per run than the finite difference analysis. It may be pointed out that results obtained with finite elements are more precise than with finite difference technique. However,

high accuracy is not required at the preliminary design state. Dozens of exploratory computer runs are required for initial understanding of the unknown dynamic behavior of the new structure. In addition, little is known at this time about the proper choice of sophisticated finite elements from the many available to achieve the accuracy that suits the realistic structure.

Based on the objectives, preliminary dynamic impact load design methods for bird proof, shock absorbing, high visibility windshield/mounting frame systems of advanced AF vehicles were developed. These methods are both general and systems oriented, employing realistic material and structural data of the window/mounting frame systems as the variable input. Bending of the two-dimensional structure was analyzed using elementary cross beam arrangements with a variety of window mounting conditions. Different cases and end attachments were considered in the beam element equations.

The static straight beam model has been expanded into a dynamic (Reference 37, Chap.8, Dynamic Analysis), two-dimensional model with structural curvature added in one dimension (References 37 and 38). Computer routines were developed and analyses conducted for:

- (a) the flat plate (square or rectangular),
- (b) the ideal conical shell segment,
- (c) the windshield portion of a F-111 type crew station, employing straight and curved finite difference equations as derived from the exact representative differential equations for beams, and selectively dimensioned.

Relevant information for the use of these routines is provided in Appendix III. The routines are listed in Appendix IV. CDC 6600 Fortran Extended

Version 3.0 was used as the computer language. Memory size required is 50K to 100K octal. The programs, as available on cards, use a card reader and a list device. Evaluated results of these routines are reported in Section IV.

2. FINITE DIFFERENCE FORMULATION OF DYNAMIC BEAM EQUATIONS

To illustrate the use of the finite difference method for solving dynamic problems, consider the flexural response of a straight beam under the action of time varying loads. The differential equation describing the flexural motion of the beam is

$$EI \frac{d^4 w}{dx^4} = q(t) + m \frac{d^2 w}{dt^2} \quad (26)$$

where E , I , and m are the Young's modulus, section moment of inertia, and mass respectively. In general, E , I , and m can vary with position along the beam. Moreover, $q(t)$ is the externally applied load.

The formulation of the problem is completed by specifying initial conditions and boundary conditions at the support of the beam. Letting subscript b refer to the support at $x = b$, the boundary conditions can be written as

$$(V)_b = -K_{wb} \cdot (W)_b \quad (27)$$

$$(M)_b = -K_{\theta b} \cdot (\theta)_b \quad (28)$$

where $\Theta = \frac{dw}{dx}$, (29)

$$M = EI \frac{d\Theta}{dx}, \text{ and} \quad (30)$$

$$V = -\frac{dM}{dx} \quad (31)$$

are the slope, bending moment and shear force, respectively. Equation 27 is the boundary condition of an elastic transverse support, while Equation 28 is the boundary condition for a rotational support. In particular, $K_{wb} = 0$, $K_{wb} = \infty$, $K_{eb} = 0$, and $K_{eb} = \infty$ correspond to free, rigid, pinned, and clamped supports, respectively. Finally, assuming that the beam is undeflected at time $t = 0$ and, that $q(0) = 0$, the initial conditions are

$$w = M = \Theta = V = \frac{d^2w}{dt^2} = 0 \quad \text{at } t = 0 \quad (32)$$

Even though Equation 26, with boundary conditions given by Equations 27 and 28, and initial conditions specified by Equations 32, can be solved by classical methods, the finite difference approach will be used, which will prove necessary when attempting to solve the curved windshield problem. In the finite difference approach, the partial differential equation (Equation 26) is replaced by an approximate difference equation which is then solved numerically. The accuracy of the solution depends on the accuracy of the finite difference approximation of the differential equation.

In applying the finite difference method, it is convenient to replace Equation 26 by a sequence of first order differential equations which are then replaced by finite difference equations. Upon introducing the auxiliary variables V , M , Θ , a and v , Equation 26 can be replaced by the following six first order equations:

$$-\frac{dV}{dx} = q(t) + m a \quad (33.1)$$

$$V = -\frac{dM}{dx} \quad (33.2)$$

$$M = EI \frac{d\Theta}{dx} \quad (33.3)$$

$$\Theta = \frac{dw}{dx} \quad (33.4)$$

$$a = \frac{dv}{dt} \quad (33.5)$$

$$v = \frac{dw}{dt} \quad (33.6)$$

Upon dividing the beam into n increments and the time variable into equal increments of duration, Δt , Equations 33 replaced by finite differences are:

$$V_{n+\frac{1}{2},t} - V_{n-\frac{1}{2},t} = -\left(q_{n,t} + m_n \cdot a_{n,t}\right) (\Delta x)_n \quad (34.1)$$

$$M_{n+1,t} - M_{n,t} = -V_{n+\frac{1}{2},t} (\Delta x)_{n+\frac{1}{2}} \quad (34.2)$$

$$\Theta_{n+\frac{1}{2},t} - \Theta_{n-\frac{1}{2},t} = \left(\frac{M}{EI}\right)_{n,t} (\Delta x)_n \quad (34.3)$$

$$w_{n+1,t} - w_{n,t} = \Theta_{n+\frac{1}{2},t} (\Delta x)_{n+\frac{1}{2}} \quad (34.4)$$

$$v_{n,t} = v_{n,t-\Delta t} + a_{n,t} \Delta t \quad (34.5)$$

$$w_{n,t} = w_{n,t-\Delta t} + v_{n,t} \Delta t \quad (34.6)$$

where subscripts $n-\frac{1}{2}$, n , $n+\frac{1}{2}$, $n+1$ refer to distinct locations of these variables in increasing order of steps, $\Delta x/2$, along the beam (see Figure 9). Equations 34.5 and 34.6 represent the Euler backward integration procedure for solving Equations 33.5 and 33.6.

It should be noted that the finite difference operators used in Equations 33.1 thru 33.4 are of the second order type with symmetrical placement of the pivotal locations at $n-1/2$, n , $n+1/2$, and n , $n+1/2$, $n+1$, respectively. Equations of this type, yielding an error proportional to $(\Delta x)^2$, could be replaced for higher accuracy by the fourth or sixth order first - difference operators $[D(y_0)]$ of Table 9.27 of Reference 28.

Boundary conditions, Equations 27 and 28, are not sufficient in the finite difference solution scheme. They must be supplemented by additional conditions. Mac Neal (Reference 37) indicates that assumed edge distributions one-half finite difference interval, $\Delta x/2$, beyond the ends of the beam should be used. The two required edge distributions, based on the assumption of linear change of variables beyond the beam boundaries, are

$$V_{b+\frac{1}{2},t} = 2V_{b,t} - V_{b-\frac{1}{2},t} \quad (35.1)$$

$$\Theta_{b+\frac{1}{2},t} = 2\Theta_{b,t} - \Theta_{b-\frac{1}{2},t} \quad (35.2)$$

Combination of Equations 28, 34.3 and 35.2 yields the slope at edge b:

$$\Theta_b = \frac{\Theta_{b+\frac{1}{2}}}{1 - \frac{K_{\theta b} (\Delta X)_b}{2EI}} \quad (36)$$

The assumed linear variation in Equations 35 could be replaced by higher order polynomials using additional values of the variables at $b + 1.5$, $b + 2.5$, etc. for the left-hand and $b - 1.5$, $b - 2.5$, etc. for the right-hand boundary of the beam (Figure 9).

An example solution for a beam of cell size, n , demonstrates the computation procedure. For simplicity, Δx , EI , and m are assumed constant at any pivotal location. The following numbers and types of finite difference equations exist for the solution: $n+1$ each of Equations 34.1 and 34.3, n each of Equations 34.2 and 34.4, and two (2) each of Equations 27, 28, 35.1 and 35.2, for the left and right boundary of the beam. These algebraic equations may be assembled in matrix notation in the format:

$$\left| \ddot{w}(t) \right|_{n+1} = - \frac{1}{m} \left| q(t) \right|_{n+1} + \frac{EI}{m(\Delta x)^4} \left[A \right]_{n+1} \left| w(t) \right|_{n+1} \quad (37)$$

with $[A]$ being a symmetric $n + 1$ by $n + 1$ coefficient matrix.

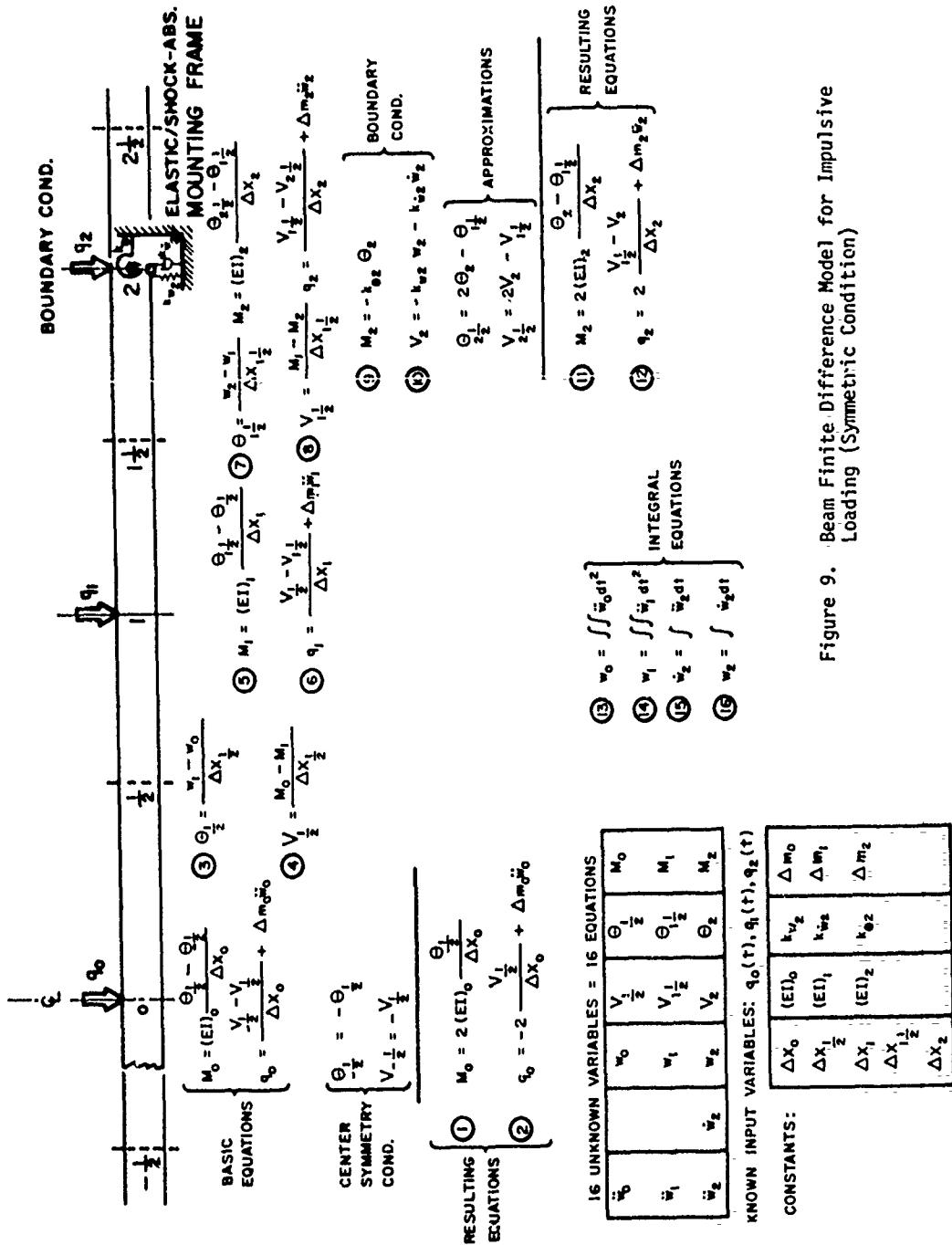


Figure 9. Beam Finite Difference Model for Impulsive Loading (Symmetric Condition)

At the end of time step $N = 1$: $q(1)|_{n+1} \neq 0$, $w(1)|_{n+1} = 0$ and the calculated accelerations $\ddot{w}(1)|_{n+1} \neq 0$. Repeated application of $n + 1$ equations each (Equations 34.5 and 34.6), with $a = \ddot{w}$, yield new values $w(N + 1)|_{n+1}$ to be inserted again into the computational scheme of Equation 37.

The following computational approach via the analog computer represents a continuous solution in time of the dynamic structural problem. The finite difference equations for the straight beam shown in Figure 9 may be analoged by an electrical wiring diagram (Figure 10) representing an actual computer network which will give the desired solutions. Limited computer hardware available in the Analog and Hybrid Computer Facility at WPAFB is a restriction on this method. This is indicated by the number of analog components necessary for the fairly simple beam finite difference model for impulse loading under symmetrical conditions (Figure 10).

3. CURVED BEAM EQUATIONS

The curved beam differential/difference equations are needed for modeling the curved geometry of the windshield in one or two directions. In case of the F-111 windshield of single curvature, the curved beam equations are applied only in one direction. The finite difference analysis procedure is similar to the one for the straight beam. However, the static equations were not generalized to include the dynamic term, $(d^2w/dt^2) \cdot m(x)$, as in Equation 26. The reason for this is that the

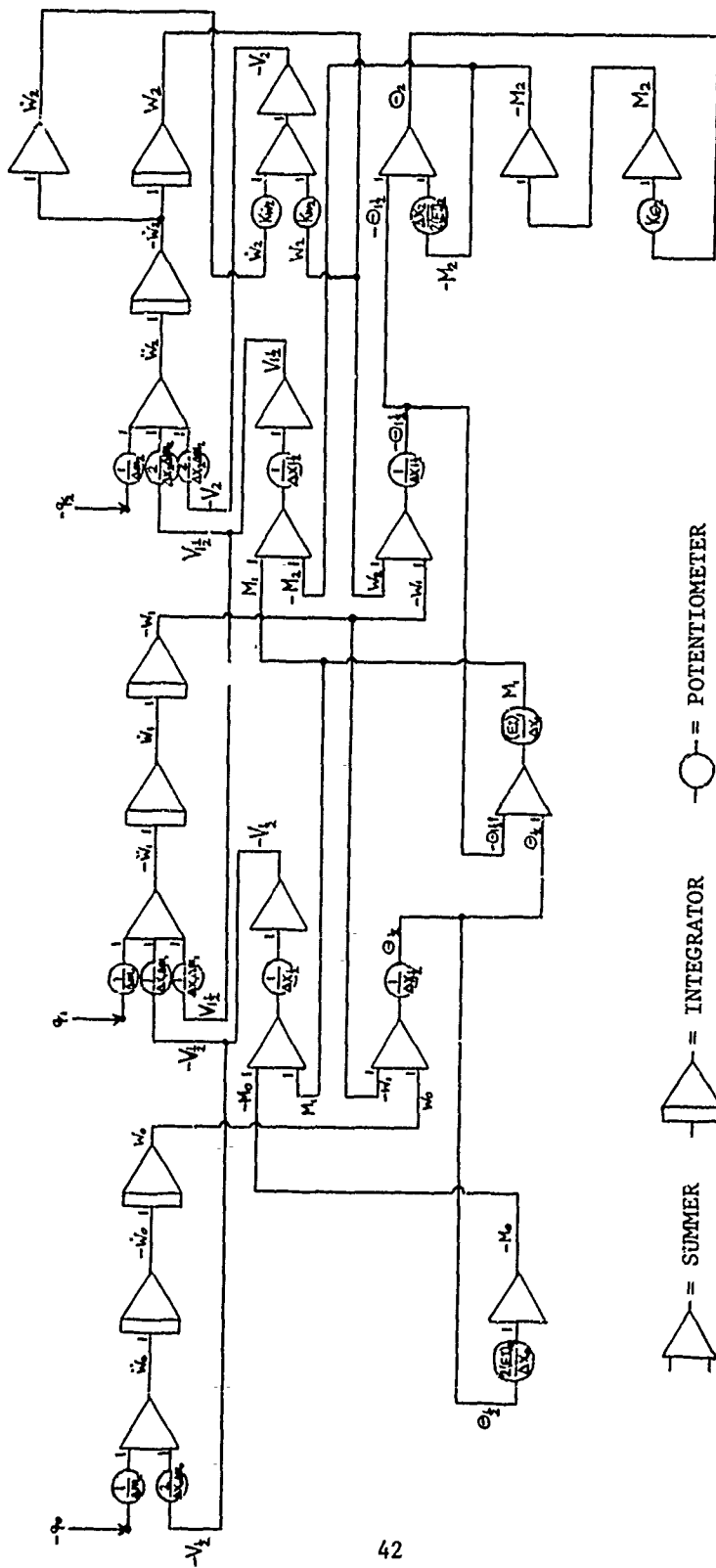


Figure 10. Analog Network for Beam Impulsive Loading

finite difference mass inertia of the flat plate and single curved plate (Sections III-3 and III-4, respectively) is applied only once at the intersections of the cross beam arrangement.

The static equation for the curved beam comparable to the one for the straight beam may be written either as

$$q_n - F_t = \frac{EI}{r^3} \left(\frac{d^4 u_n}{d\phi^4} + \frac{d^2 u_n}{d\phi^2} \right) \quad (38)$$

$$F_{t1} - q_t - \frac{dq_n}{d\phi} = \frac{EI}{r^3} \left(\frac{d^6 u_t}{d\phi^6} + \frac{d^4 u_t}{d\phi^4} \right)$$

or
$$\frac{dF_n}{d\phi} = F_t - q_n \quad (39.1)$$

$$\frac{dF_t}{d\phi} = -F_n - q_t \quad (39.2)$$

$$\frac{dM}{d\phi} = -F_n r \quad (39.3)$$

$$\frac{d\theta}{d\phi} = \frac{Mr}{EI} \quad (39.4)$$

$$\frac{du_n}{d\phi} = u_t + \theta r \quad (39.5)$$

$$\frac{du_t}{d\phi} = -u_n \quad (39.6)$$

$$(F_n)_{n+1} - (F_n)_n = \left[(F_t)_{n+\frac{1}{2}} - (q_n)_{n+\frac{1}{2}} \right] \left(2 \sin \frac{\Delta\phi}{2} \right)_{n+\frac{1}{2}} \quad (40.1)$$

$$(F_t)_{n+\frac{1}{2}} - (F_t)_{n-\frac{1}{2}} = \left[(-F_n)_n - (q_t)_n \right] \left(2 \sin \frac{\Delta\phi}{2} \right)_n \quad (40.2)$$

$$(M)_{n+\frac{1}{2}} - (M)_{n-\frac{1}{2}} = (-F_n)_n \left(2r \sin \frac{\Delta\phi}{2} \right)_n \quad (40.3)$$

$$(\theta)_{n+1} - (\theta)_n = \left(\frac{Mr}{EI}\right)_{n+\frac{1}{2}} (\Delta\phi)_{n+\frac{1}{2}} \quad (40.4)$$

$$(u_n)_{n+\frac{1}{2}} - (u_n)_{n-\frac{1}{2}} = [(u_t)_n + (\theta r)_n] \left(2 \sin \frac{\Delta\phi}{2}\right)_n \quad (40.5)$$

$$(u_t)_{n+1} - (u_t)_n = (-u_n)_{n+\frac{1}{2}} \left(2 \sin \frac{\Delta\phi}{2}\right)_{n+\frac{1}{2}} \quad (40.6)$$

The variables in the curved beam equations (Figure 11) are:

(1) dependent variables,

normal force, F_n (pound)

tangential force, F_t (pound)

bending moment, M (pound-inch)

(2) external loads,

normal load, q_n (pound/rad)

tangential load, q_t (pound/rad)

(applied along centerline of ring of radius, r (in),
per angular increment, $\Delta\phi$ (rad))

(3) local dependent variables,

normal displacement, u_n (in)

tangential displacement, u_t (in)

slope of deflection, θ (rad)

These, the basic equations, and the corresponding network analogy for rings of constant or variable radii of curvature, loaded in-plane, are given in Reference 38. Although expressions for forces and deformations in circular rings are widely publicized (Reference 39), the validity of the curved beam analysis to be set up was initially verified. The finite difference Equations 39 were checked by comparing them with the

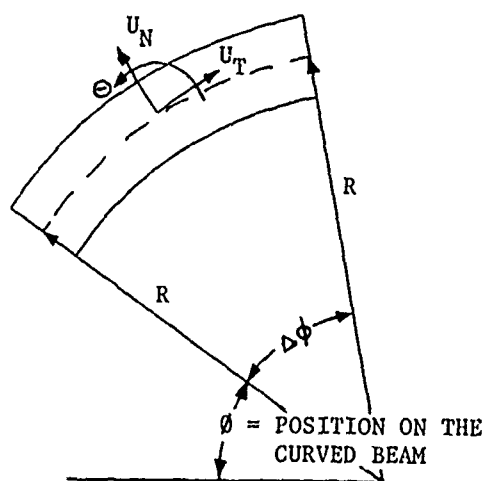
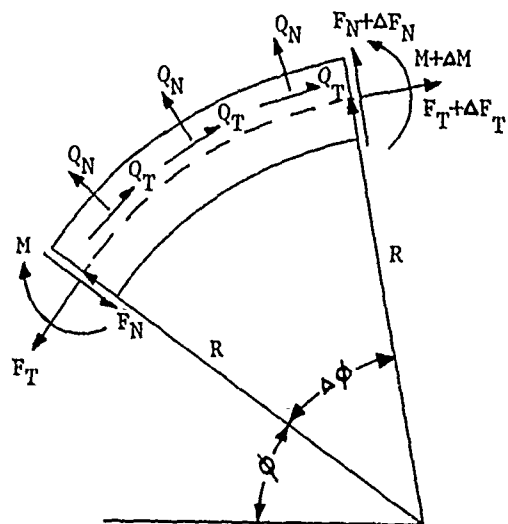


Figure 11. Variables of the Curved Beam Equations

explicit Equations 41 for the special case of a circular ring subjected to a pair of concentrated radial loads in equilibrium (Reference 37, Chap. 4 "Analogies for One-Dimensional Elements"), for $q_n = q_t = 0$:

$$F_n = P \sin \phi \quad (41.1)$$

$$F_t = P \cos \phi \quad (41.2)$$

$$M = Pr \left(\cos \phi - \frac{2}{\pi} \right) \quad (41.3)$$

$$v_n = \frac{Pr^3}{EI} \left(\frac{\phi}{2} \sin \phi + \frac{1}{2} \cos \phi - \frac{2}{\pi} \right) \quad (41.4)$$

$$u_t = \frac{Pr^3}{EI} \left(\left(\frac{1}{2} \cos \phi + \frac{2}{\pi} \right) \phi - \sin \phi \right) \quad (41.5)$$

$$\Theta = \frac{Pr^2}{EI} \left(\sin \phi - \frac{2\phi}{\pi} \right) \quad (41.6)$$

Table 4.2 of Reference 37 compares the numerical results of the exact solution based on Equations 41 and those of the approximate finite difference equations for four (4) cells per quadrant of ring. The agreement between the two solutions is shown in Figure 12.

The normal deflection, u_n , at any point ϕ , of the curved beam bent in the plane of initial curvature (Equation 41.4) was analytically derived for proof of accuracy. The changes of the horizontal and vertical diameters, at $\phi=0$ and 90° respectively, were checked against the solution derived by the method of unit loads (Reference 40, p. 94, Eq. (6)),

$$y_b = \int \frac{Mm}{EI} r d\phi \quad (42)$$

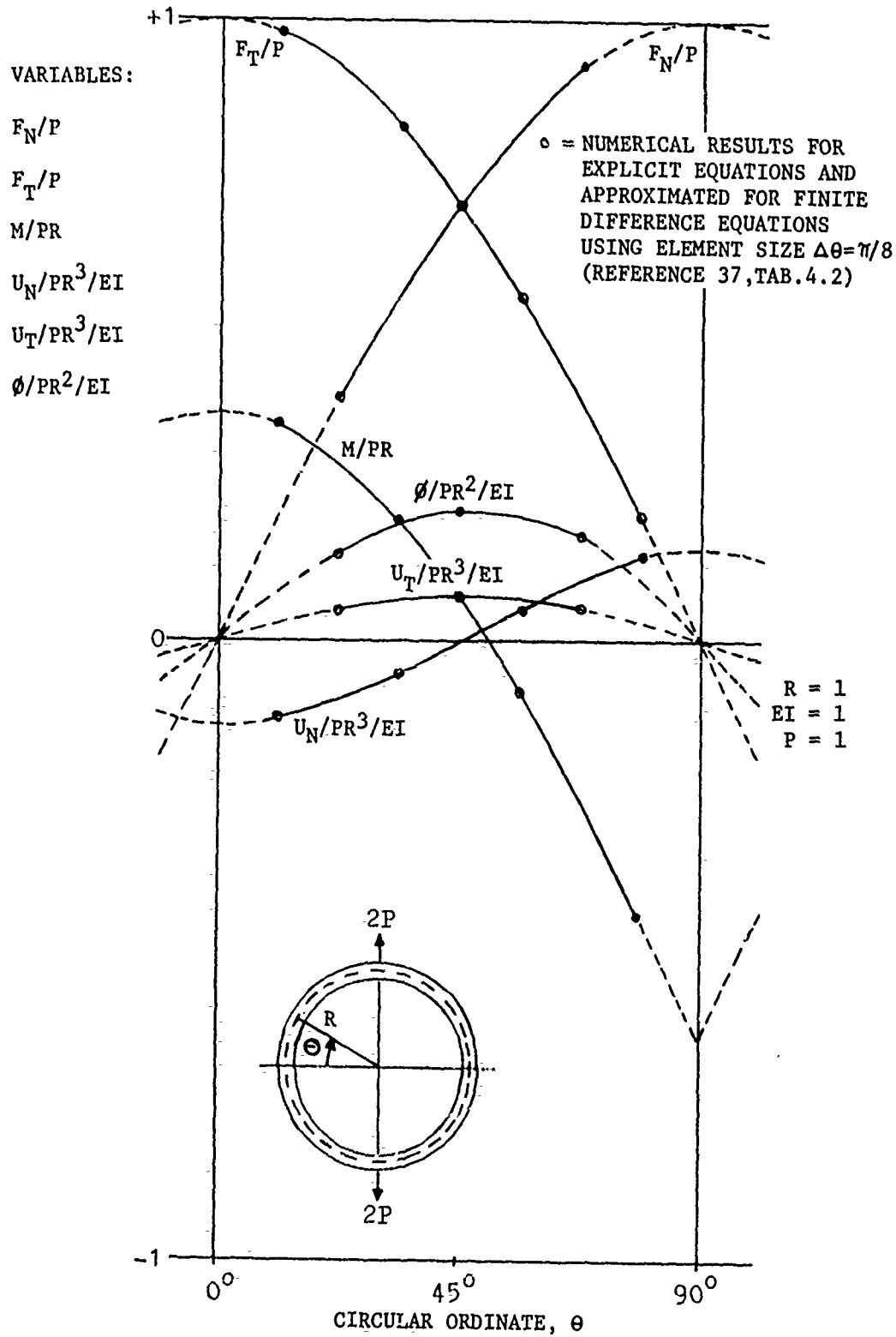


Figure 12. Variables for One Quadrant of Circular Ring Problem

with the bending moment, M , in the ring section (Equation 41.3) due to the actual loading, $2Q$, and the equation of a virtual bending moment, m , due to a virtual load, $2P$, acting normal at the section where $u_n = y_D/2$ is to be found. Instead of calculating u_n as a function of the angular ordinate, ϕ , use of the transformation, $\phi' = \phi + \pi/2$, is convenient with M having no abrupt changes in the assumed interval of integration, $0 \leq \phi' \leq \pi$. The variable of integration, ψ' , is introduced in both the intervals $0 \leq \psi' \leq \phi'$ and $\phi' \leq \psi' \leq \pi$.

$$M = Qr \left(\sin \psi' - \frac{2}{\pi} \right) \quad (43)$$

This is not the case with the virtual bending moment, m (Figure 13).

At $\psi' = \phi'$, m is zero and changes its sign.

The results of products of moments, Mm , and their integrations, for $0 \leq \psi' \leq \phi'$ are

$$Mm = 2PQr^2 \left(-\frac{1}{2} \cos \phi' \sin^2 \psi' + \frac{1}{2} \sin \phi' \sin \psi' \cos \psi' + \frac{1}{\pi} \cos \phi' \sin \psi' - \frac{1}{\pi} \sin \phi' \cos \psi' \right) \quad (44)$$

$$\int_0^{\phi'} Mm d\psi' = 2PQr^2 \left(-\frac{1}{\pi} + \frac{1}{\pi} \cos \phi' + \frac{1}{4} \sin \phi' - \frac{1}{4} \phi' \cos \phi' \right)$$

For $\phi' \leq \psi' \leq \pi$:

$$Mm = 2PQr^2 \left(\frac{1}{\pi} \sin \phi' \cos \psi' - \frac{1}{\pi} \cos \phi' \sin \psi' - \frac{1}{2} \sin \phi' \sin \psi' \cos \psi' + \frac{1}{2} \cos \phi' \sin^2 \psi' \right) \quad (45)$$

$$\int_{\phi'}^{\pi} Mm d\psi' = 2PQr^2 \left(-\frac{1}{\pi} - \frac{1}{\pi} \cos \phi' + \frac{1}{4} \sin \phi' - \frac{1}{4} \phi' \cos \phi' + \frac{\pi}{4} \cos \phi' \right)$$

The normal deflection, u_n (Equation 41.4), is given by

$$u_n = \frac{r}{2EI} \left(\int_0^{\phi'} Mm d\psi' + \int_{\phi'}^{\pi} Mm d\psi' \right)$$

$$= \frac{Pr^3}{EI} \left(\frac{1}{2} \sin \phi' + \left(\frac{\pi}{4} - \frac{\phi'}{2} \right) \cos \phi' - \frac{2}{\pi} \right)$$

$$= \frac{Pr^3}{EI} \left(\frac{\phi}{2} \sin \phi + \frac{1}{2} \cos \phi - \frac{2}{\pi} \right) \quad (46)$$

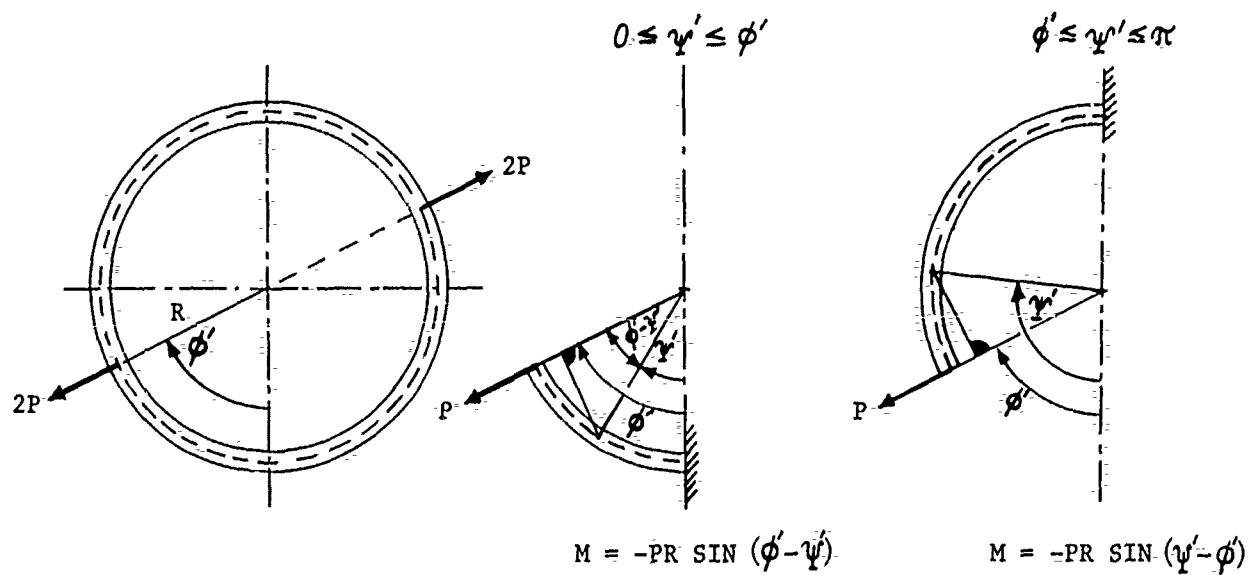


Figure 13. Determination of Virtual Bending Moment (M)

which is in agreement with

$$\begin{aligned} u_n(\phi=0) &= -.137 \frac{Pr^3}{EI} \\ u_n(\phi=\frac{\pi}{2}) &= .149 \frac{Pr^3}{EI} \end{aligned} \quad (47)$$

taken from Reference 40, chapter 8, table VIII -formulas for changes in horizontal and vertical diameters of circular rings and arches.

In addition to the six finite difference Equations 39, six boundary conditions and assumed edge distributions are required for solution of the curved beam problem. Four of the boundary conditions and edge distributions are identical with those required for the straight beam. Equations 27, 28, 35 do apply, where V has to be replaced by the normal internal shear, F_n , and M, ϕ are variables along the curved beam.

Two more equations are needed. The tangential load, F_t , at the upper and lower boundary was selected such that the internal load, F_t , at the center of external load application, f_n , is zero, that is

$$(F_t)_{\text{centerload}} = 0 \quad (48)$$

Furthermore, fixed tangential supports were assumed at the two boundaries, that is

$$(u_t)_b = 0 \quad (49)$$

4. FINITE DIFFERENCE FORMULATION FOR FLAT PLATE

In finite difference formulation, the flat plate is replaced by a grid of straight beams in rectangular x- and y- directions. The cross beams are interconnected by forcing the local deflections, $w_{x,y,t}$ (instantaneous results of numerical double-integration of Equations 34.5 and 34.6)

to be the common deflections of the two intersecting beams. In this idealization, torsional rigidities of the beams are neglected.

Replacing the pivotal indices of Equations 34, such as $n-1/2$, n , $n+1/2$, $n+1$ by combinations of $x-1/2$, x , $x+1/2$, $x+1$ and $y-1/2$, y , $y+1/2$, $y+1$, the left side of Equation 34.1 may be replaced by the finite differences of the shear forces, V , in the two directions. Assuming that $\Delta x = \Delta y = \Delta s =$ constant, the finite difference equations for the shear forces are

$$\begin{aligned} (V_x)_{x+\frac{1}{2},y,t} - (V_x)_{x-\frac{1}{2},y,t} + (V_y)_{x,y+\frac{1}{2},t} - (V_y)_{x,y-\frac{1}{2},t} = \\ -Q_{x,y,t} + (\Delta M)_{x,y} \cdot \ddot{w}_{x,y,t} \end{aligned} \quad (50.1)$$

where Q and ΔM are loads and masses, respectively.

Each of Equations 34.2, 34.3, and 34.4 may be assumed to represent a beam in x - and y - direction. Thus,

$$(M_x)_{x+1,y,t} - (M_x)_{x,y,t} = - (V_x)_{x+\frac{1}{2},y,t} \cdot \Delta s \quad (50.2)$$

$$(M_y)_{x,y+1,t} - (M_y)_{x,y,t} = - (V_y)_{x,y+\frac{1}{2},t} \cdot \Delta s \quad (50.3)$$

$$(\Theta_x)_{x+\frac{1}{2},y,t} - (\Theta_x)_{x-\frac{1}{2},y,t} = \left(\frac{M_x}{EI_x}\right)_{x,y,t} \cdot \Delta s \quad (50.4)$$

$$(\Theta_y)_{x,y+\frac{1}{2},t} - (\Theta_y)_{x,y-\frac{1}{2},t} = \left(\frac{M_y}{EI_y}\right)_{x,y,t} \cdot \Delta s \quad (50.5)$$

$$w_{x+1,y,t} - w_{x,y,t} = (\Theta_x)_{x+\frac{1}{2},y,t} \cdot \Delta s \quad (50.6)$$

$$w_{x,y+1,t} - w_{x,y,t} = (\Theta_y)_{x,y+\frac{1}{2},t} \cdot \Delta s \quad (50.7)$$

when Δs is a grid parameter. As in the straight beam problem, pairs of boundary conditions and distributions, for left and right edges, in x- and y-directions are needed.

Equations 50 could be written for variable finite difference grid spacings, $(\Delta x)_{x,y}$ and $(\Delta y)_{x,y}$. In this case, any rectangular plate could be treated with stepped changes from grid line to grid line of plate properties or geometrical irregularities (as reinforcements or cut-outs).

The bending stiffnesses may be determined, as for the homogeneous plate of thickness, t :

$$(EI_x)_{x,y} = E_x \cdot \frac{t^3 (\Delta y)_{x,y}}{12} \quad (51.1)$$

$$(EI_y)_{x,y} = E_y \cdot \frac{t^3 (\Delta x)_{x,y}}{12} \quad (51.2)$$

Using Equations 50.2 and 50.3, stresses at the surfaces of the pane are given by

$$\sigma = \frac{6 \cdot M}{\Delta s \cdot t^2} \quad (52)$$

where M is the calculated bending moment. This equation is valid for $\sigma \leq F_{yield}$. For higher stresses, a fictitious stress, F_b , referred to as the bending modulus of rupture is defined by

$$F_b = \frac{M \cdot c}{I} \quad (53)$$

where M is the ultimate bending moment (determined from tests of similar beams), I is the moment of inertia of the cross section, and c is the distance from the beam neutral axis to the extreme fiber.

Throughout the analysis, external shock loads are introduced at the nodal points of the finite difference grid. The dynamic loading condition applied analytically is a schematic distribution of the impact load, Q_{tot} , representing a pressure mound that varies with time. Methods for determining Q_{tot} are given in References 41 and 42. Motion pictures of experimental tests make it possible to estimate the windshield area covered by the traveling, decelerating mass of the bird (Appendix II-1).

The mass (Equation 54) is distributed similarly to the stiffnesses (Equations 51) between the beams:

$$(\Delta M)_{x,y} = \rho \cdot (\Delta x)_{x,y} \cdot (\Delta y)_{x,y} \cdot t \quad (54)$$

The marching procedure, starting out at one edge of the plate and considering one grid line after the other, is as follows:

Calculate all

- (1) e_x and e_y , inside of plate and at the edges (Equations 50.6 and 50.7),
- (2) σ_x and σ_y , at boundaries (Equations 28, 35.2, 50.4 and 50.5),
- (3) M_x and M_y , at supported edges (Equation 28),
- (4) V_x and V_y , at supported edges (Equation 27),
- (5) M_x and M_y , inside of plate and at the boundaries (Equations 50.4 and 50.5)
- (6) V_x and V_y , inside and at boundaries (Equations 50.2 and 50.3),
- (7) \ddot{w} , inside and at boundaries (Equation 50.1),
- (8) \dot{w} , w (Equations 34.5 and 34.6, respectively),
- (9) Repeat (1) thru (8) for next time step, at time interval, Δt , etc.

This marching procedure is sketched in Appendix III-1 (Figure 42, Sequence in Cyclic Loop for Calculating Finite Differences). It may be noted, that the program variables are discussed in Appendix III-1.

The following parametrical example illustrates the use of the flat plate analysis method. Requirements for mounting a flat rectangular windscreen were determined on the basis of a parametric screening of mounting conditions. A 2' x 2' window pane (Figure 14) of variable thickness (1" average) having the stiffness of polycarbonate at 200°F and up to 5 times that stiffness was assumed to be impacted by a pyramidally distributed load impulse (1/2 millisecond), $Q_{tot} \leq 100,000$ pounds. The flat plate routine of Appendix IV-2 was used.

With the arbitrary grid size of $6 \times 6 = 36$ (13 x 13 including mid mode points) for a square panel of sides of 2 ft, the grid parameter is $\Delta s = 4$ inch. At a pane thickness of $t = 1$ inch, the bending moment of inertia, $I = t^3 \cdot \Delta s / 12$, is 0.5 in^4 .

Two principal design parameters, Q_{tot} , and plate thickness, t , can be varied so that stresses due to M_x and M_y (in this case +3467 pound-in), remain below the assumed shatter strength of the polycarbonate ($F_{tu} = 5.2 \text{ ksi}$ at 200°F (Table III)). In addition, the deflection is restricted to plus or minus 1 to 2 inches at any location. The effects of flexible supports along the frame boundaries were investigated by assuming parametric ranges of technically achievable values for the frame stiffness and the other boundary parameters. Extreme values occurred at the center, mid edge and corner locations for the square, symmetrical case.

Figure 15 shows the effects of both a hard and a soft shock-absorbing window mount on the bending moment at the center of the plate

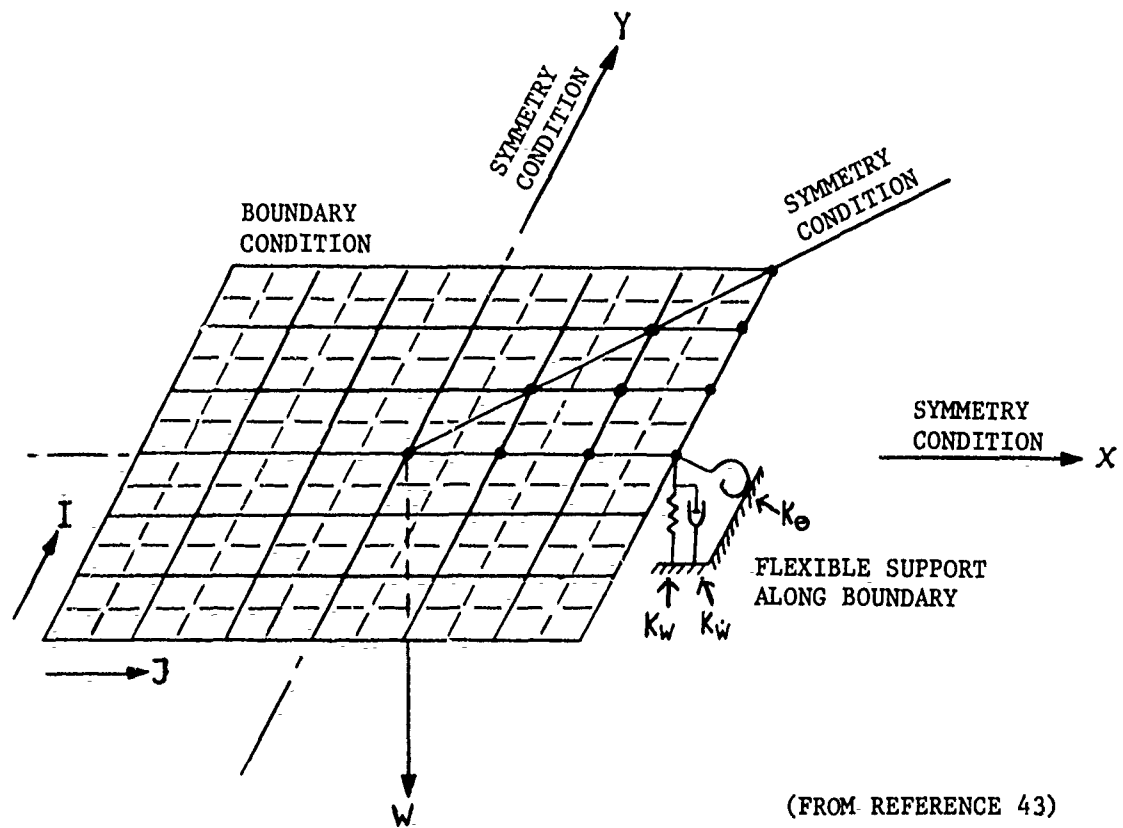


Figure 14. Symmetrical Impact Loading of Square Plate

TABLE III
MATERIAL PROPERTIES OF F-111 WINDSHIELD/CANOPY

	polycarbonate		Al 2024	Ti 6-4	Ti 6-6-2
	RT	200 °F	RT	RT	RT
$E \cdot 10^6$ (psi)	.315	.24	10.5	16	16.5
E_c			10.7	16.4	
F_{ty} (ksi)			55	140	160
F_{tu}	9.4	5.7 ⁺	63	150	170
e_{ult} %	126	155	12	6	8

(⁺ 5.2 ksi (Reference 44))

	MOUNTING CONDITION	
	HARD	SOFT
TOTAL LOAD	59,000 POUNDS	
TIME OF IMPACT	.0005 SEC	
VISCOUS DAMPING	10 POUND-SEC/IN	
SPRING CONSTANT	10,000	25 POUND/IN
ABSORBED ENERGY	28	1890 POUND-IN

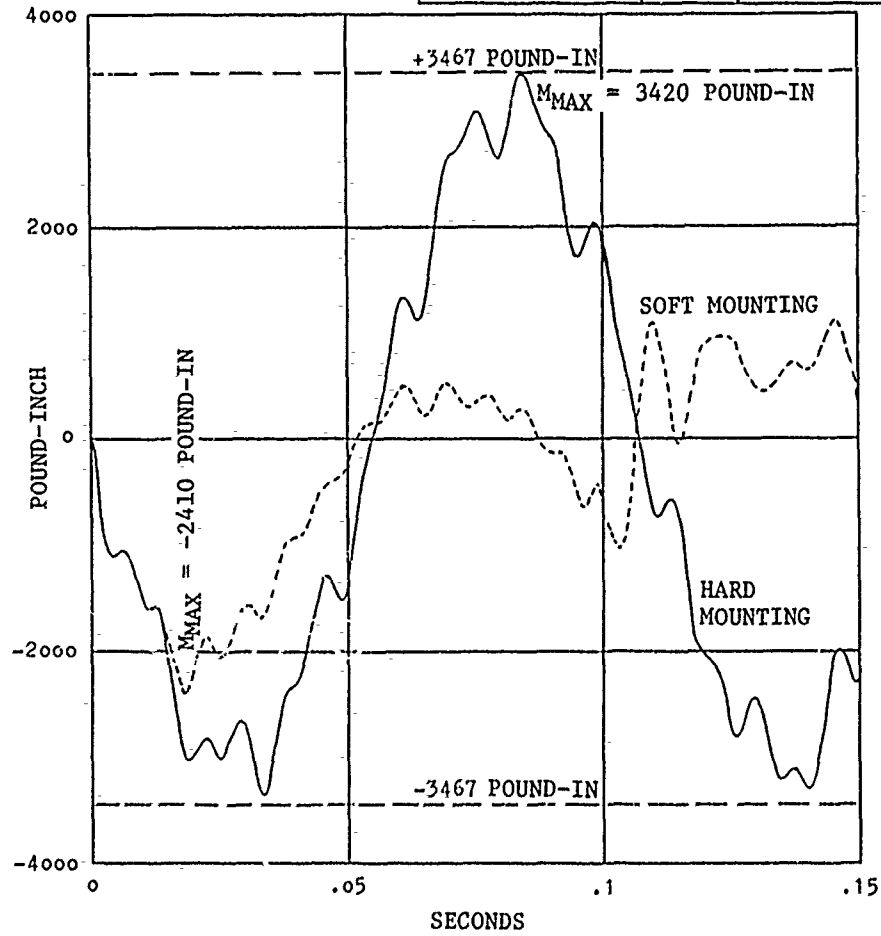


Figure 15. Central Bending Moment for Hard and Shock-Absorbing Window Mount

(Figure 14). The dashed lines are the upper and lower bounds on shatter strength indicating that $Q_{tot} = 50,000$ pounds is close to the failure load. Figure 16 shows the mid pane deflection, w_0 , and mid frame deflection, w_3 , for the shock-absorbing case (soft mounting) of Figure 15.

Using a Young's modulus, $E=0.2 \cdot 10^6$ psi, representative of the pane stiffness for polycarbonate at elevated temperature, the pane bending stiffness, $EI(1-\nu^2) \sim EI_x = EI_y$, in the longitudinal and transverse direction, is of the order of 10^5 pound-in². The bending stiffness of the frame, EI_f , is 10^6 pound-in². Finite difference distribution of bending stiffness is shown in Appendix III-1 (Figure 43).

Total mass and mass distribution for a pane volume of 24" x 24" x 1" = 576 in³ and specific mass density of polycarbonate (6.2 lb/ft²) is $(4)(6.2)/((32.2)(12)) = .064$ slugs. Twenty-five mass allocations, ΔM , are required at 25 nodal points of the interior, and 24 allocations of $\Delta M/2$ at the boundary in case of the 6 x 6 mesh resulting in $\Delta M = .064/37$ slugs. An effective frame mass totaling $\Delta M_f > \Delta M/2$ has to be added to $\Delta M/2$ at the edge of the frame.

Simulation of dynamic mounting must be as realistic as possible. In this plate model, mounting design is represented by the four properties, K_w , K_w^* , K_e and K_e^* varying with impact behavior of the window/frame system (Figure 43 of Appendix III-1). Spring constants, K_w , distributed at the nodal points along the frame, may act continuously, or as $K_w(1)$, while the frame is deflected downward, and as $K_w(2)$ during the upward mode of deflection. The latter scheme simulates the design mentioned above. $K_w(1)$ models effective viscous damping during the first quarter cycle (Figures 1 and 7).

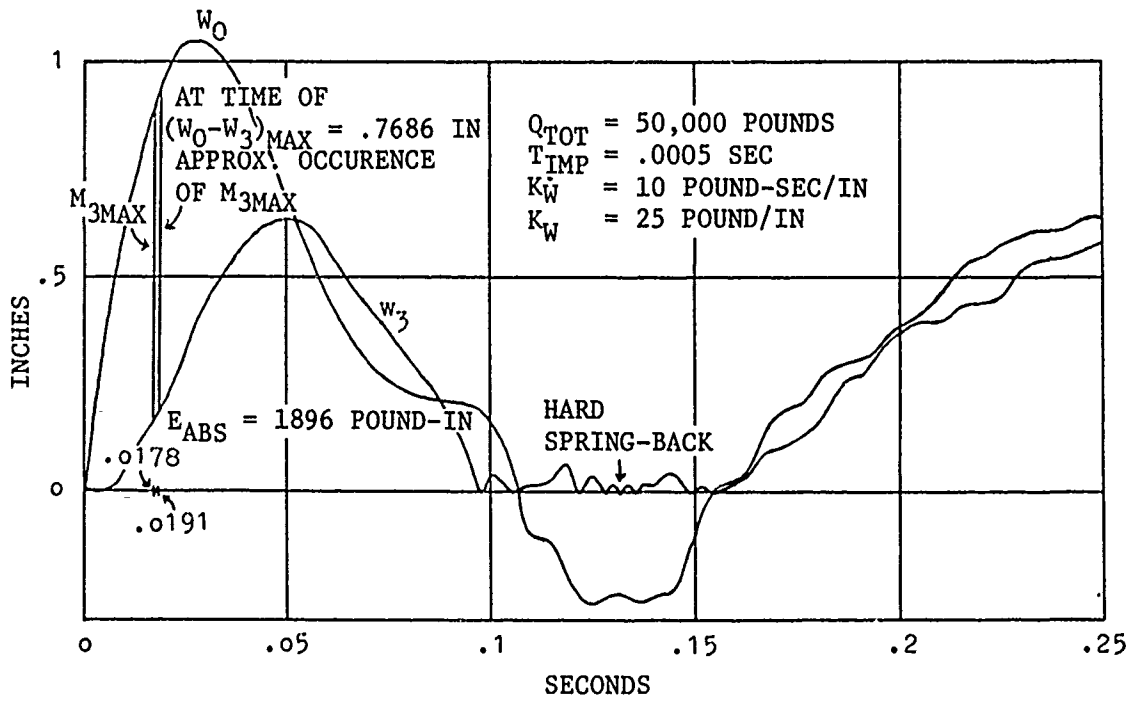


Figure 16. Deflections W_0 and W_3 for Shock-Absorbing Design

After release of the damping fluid, less effective damping, $K_w(2)$, takes over. The clamp-in conditions, K_θ and K_θ^* , are assumed different during downward and upward deflection. Typical values for the mounting system are $K_w(1) = 25$ pound/in (soft spring), $K_w(2) = 1,000,000$ pound/in (hard spring back), $K_w(1) = 10$ pound-sec/in (highly efficient viscous damping), $K_w(2) = .5$ pound-sec/in (less efficient damping), and $K_{\theta x} = K_{\theta y} = 100,000$ pound-in/rad (stiff clamp-in). An actual mounting system may have a variable distribution of these four mounting properties to achieve an improved shock absorption.

Initially, the pyramidal impulse load distribution (Figure 43.3, Appendix III-1) yields unit loads of $Q_1 = Q_{tot}/35$, and $Q_2 = 2 \cdot Q_1$, $Q_3 = 3 \cdot Q_1$. Q_{tot} can be in the 10^5 pound range equivalent to 10^3 psi average pressures if equally distributed. This load occurs during 5 time steps, N , of duration $\Delta t = .0001$ sec each. After impact, a nominal unit load of 0.1 pound or any other constant pressure load is assumed to act at the previously impacted nodal points. Time steps at a rate of less than 10 per milli second were utilized after the duration of impact to decrease the overall computational effort.

Using the above input data, the dependent variables have values in the following ranges:

slopes of deflection, θ_x and θ_y	$\pm 10^{-2}$ (rd) or $\pm 10^0$ (deg)
bending moments, M_x and M_y	$\pm 10^3$ (pound-in)
shear loads, V_x and V_y	$\pm 10^2$ (pound)
normal accelerations, \ddot{w}	$\pm 10^5$ (in/sec ²)
velocities of displacement, \dot{w}	$\pm 10^2 - 10^3$ (in/sec)
deflections, w	± 1 (in)

Energies in the finite difference scheme for the 6 x 6 grid size plate are calculated as follows. For convenience, the node and mid node points are numbered consecutively. Thus the node points have odd subscripts. At the beginning of time history at which impact starts, the three energies considered (Equation 6) are:

$$E_{kin}(t=0) = E_{pot}(t=0) = E_{abs}(t=0) = 0 \quad (55)$$

E_{kin} is newly determined at every time step, N:

$$E_{kin} = \frac{1}{2} \cdot \sum_{i=1,3,5 \dots 13} \cdot \sum_{j=1,3,5 \dots 13} \Delta M_{ij} \cdot \dot{w}_{ij}^2(t) \quad (56)$$

E_{pot} and E_{abs} are supplemented at every time step, N:

$$E_{pot}(t + \Delta t) = E_{pot}(t) + \Delta E_{pot}(t + \Delta t) \quad (57.1)$$

$$E_{abs}(t + \Delta t) = E_{abs}(t) + \Delta E_{abs}(t + \Delta t) \quad (57.2)$$

E_{pot} consists of the following components:

$$\Delta E_{pot} = \Delta E_{potEI} + \Delta E_{potke} + \Delta E_{potkw} \quad (58)$$

ΔE_{potEI} is the change of elastic potential energies in the x- and y- directions due to pane as well as window frame bending. ΔE_{potke} and ΔE_{potkw} are elastic energies stored in the rotational and transverse spring attachment systems around the perimeter of the window.

They are given by:

$$\begin{aligned} \Delta E_{potEI}(t) = & \sum_{i=3,5,7 \dots 11} \cdot \sum_{j=1,3,5 \dots 13} (\Theta_{x i+1,j}(t) - \Theta_{x i-1,j}(t)) [(\Theta_{x i+1,j}(t) - \Theta_{x i-1,j}(t)) \\ & - (\Theta_{x i+1,j}(t-\Delta t) - \Theta_{x i-1,j}(t-\Delta t))] \frac{EI_x}{\Delta x} \\ & + \sum_{i=1,3,5 \dots 13} \cdot \sum_{j=3,5,7 \dots 11} (\Theta_{y i,j+1}(t) - \Theta_{y i,j-1}(t)) [(\Theta_{y i,j+1}(t) - \Theta_{y i,j-1}(t)) \\ & - (\Theta_{y i,j+1}(t-\Delta t) - \Theta_{y i,j-1}(t-\Delta t))] \frac{EI_y}{\Delta y} \end{aligned} \quad (59)$$

$$\begin{aligned} \Delta E_{\text{pot } k_{\theta}(t)} = & \sum_{i=1 \text{ and } 13} \cdot \sum_{j=1,3,5 \dots 13} k_{\theta x j} \theta_{x i j}(t) (\theta_{x i j}(t) - \theta_{x i j}(t - \Delta t)) \\ & + \sum_{i=1,3,5 \dots 13} \cdot \sum_{j=1 \text{ and } 13} k_{\theta y i} \theta_{y i j}(t) (\theta_{y i j}(t) - \theta_{y i j}(t - \Delta t)) \end{aligned} \quad (60)$$

$$\begin{aligned} \Delta E_{\text{pot } k_w(t)} = & \sum_{i=1 \text{ and } 13} \cdot \sum_{j=1,3,5 \dots 13} k_{w j} W_{i j}(t) (W_{i j}(t) - W_{i j}(t + \Delta t)) \\ & + \sum_{i=1,3,5 \dots 13} \cdot \sum_{j=1 \text{ and } 13} k_{w i} W_{i j}(t) (W_{i j}(t) - W_{i j}(t + \Delta t)) \end{aligned} \quad (61)$$

Bending stiffnesses of the pane or the frame, EI_x and EI_y , were assumed constant with time, t . Spring constants, k_w , k_{θ_x} and k_{θ_y} , may vary with time. ΔE_{abs} consists of the following components:

$$\Delta E_{\text{abs}} = \Delta E_{\text{abskv}} + \Delta E_{\text{absk}\dot{\theta}} + \Delta E_{\text{absk}\dot{w}} \quad (62)$$

ΔE_{abskv} is the visco-elastic energy in x-and y- direction absorbed in the damping interlayers of the pane as well as frame due to stretch-damping occurring. $\Delta E_{\text{absk}\dot{\theta}}$ and $\Delta E_{\text{absk}\dot{w}}$ are visco-elastic energies absorbed in the built-in damping system of the frame. The energies are given by

$$\begin{aligned} \Delta E_{\text{abskv}(t)} = & \sum_{i=3,5,7 \dots 11} \cdot \sum_{j=1,3,5 \dots 13} (\dot{\theta}_{x i+1,j}(t) - \dot{\theta}_{x i-1,j}(t)) [(\theta_{x i+1,j}(t) - \theta_{x i-1,j}(t)) \\ & - (\theta_{x i+1,j}(t - \Delta t) - \theta_{x i-1,j}(t - \Delta t))] \frac{k_{v s x}}{\Delta x} \\ & + \sum_{i=1,3,5 \dots 13} \cdot \sum_{j=3,5,7 \dots 11} (\dot{\theta}_{y i,j+1}(t) - \dot{\theta}_{y i,j-1}(t)) [(\theta_{y i,j+1}(t) - \theta_{y i,j-1}(t)) \\ & - (\theta_{y i,j+1}(t - \Delta t) - \theta_{y i,j-1}(t - \Delta t))] \frac{k_{v s y}}{\Delta y} \end{aligned} \quad (63)$$

where viscous damping constants of the pane or the frame, $k_{v s x}$ and $k_{v s y}$ were assumed constant with time.

$$\begin{aligned} \Delta E_{abs} k\dot{\theta}(t) = & \sum_{i=1 \text{ and } 13} \cdot \sum_{j=1,3,5 \dots 13} k_{\dot{\theta}xj} \dot{\theta}_{xij}(t) (\theta_{xij}(t) - \theta_{xij}(t-\Delta t)) \\ & + \sum_{i=1,3,5 \dots 13} \cdot \sum_{j=1 \text{ and } 13} k_{\dot{\theta}yi} \dot{\theta}_{yij}(t) (\theta_{yij}(t) - \theta_{yij}(t-\Delta t)) \end{aligned} \quad (64)$$

$$\begin{aligned} \Delta E_{abs} k\dot{w}(t) = & \sum_{i=1 \text{ and } 13} \cdot \sum_{j=1,3,5 \dots 13} k_{\dot{w}j} \dot{w}_{ij}(t) (w_{ij}(t) - w_{ij}(t+\Delta t)) \\ & + \sum_{i=1,3,5 \dots 13} \cdot \sum_{j=1 \text{ and } 13} k_{\dot{w}j} \dot{w}_{ij}(t) (w_{ij}(t) - w_{ij}(t+\Delta t)) \end{aligned} \quad (65)$$

Constants, $k_{\dot{\theta}x}$, $k_{\dot{\theta}y}$ and $k_{\dot{w}}$, can vary with time.

Stepwise summation yields potential energy (E_{pot}), kinetic energy (E_{kin}), and absorbed energy (E_{abs}) in the system. E_{pot} , E_{kin} and E_{abs} are zero before impact. At the end of impact, E_{pot} , the total energy received is at its maximum and $E_{kin} \sim 0$, since the motion of the window/frame system has barely started. Several different computer runs showed $E_{pot} + E_{kin} + E_{abs}$ to be almost constant, in agreement with a true structural system, and that E_{abs} really picks up during the first quarter cycle using effective viscous damping. After the first quarter cycle, $E_{pot} + E_{kin}$ is the total energy remaining in the window frame system.

During incorporation of the energy equations into the computer routine, E_{abs} was assumed to be absorbed by the frame at the 24 nodal points at a viscous damping of $K_w(1)=10$ pound-sec/in. Typical frame deflection was .054" and the time was .03 sec for the first quarter cycle. The estimated result was $E_{abs} \sim 24$ pound-in (one case of low energy absorption). By comparison, the "flat plate routine" resulted in 16.8 pound-in. E_{pot} and E_{kin} results are similar.

Mean intervals of oscillations (usually hundredths of seconds) or frequencies may be obtained by plotting time histories of variables. The state of forced vibration is experienced during the short time of impact and periodic free vibration thereafter. Zero crossings of time histories of bending moments at the center of the plate, at the frame, and elsewhere show similar occurrences (although at different times) as observed in the case of one computer run of a 1/4 sec real time event. First, the bending moment changes from negative to positive at .067 sec after impact, the next crossing from positive to negative is at .115 sec; the third crossing is at .1885 sec and the fourth one at .2468 sec. A full oscillatory cycle occurs within .12 sec. This is equivalent to ~ 8 cys/sec.

Dynamic behavior of the typical window pane with shock-absorbing support structure is presented in Figures 17 thru 24 and Tables IV thru VI. The following constants were used in the parametric study: s^2 size, $s=2$ ft (square); load $Q_{tot}=100,000$ pounds (pyramidal); time, $t_{imp}=.0005$ sec; mass, $m=.77$ slugs/ft²/in; frame stiffness, $EI_f=5 \cdot EI$ (pane) pound-in².

For the original grid size, $\Delta s=4''$, and a time step, $\Delta t=.0001$ sec, no solution instability occurred. After completion of the original study, the erroneous mass assumption became obvious (with $m=.77/12=.064$ being realistic, rather than .77 slugs/ft²/in). In addition, a lower $Q_{tot}=15,000$ pounds (pyramidal) was taken to be more typical of an inclined panel impact. Using the new m and Q_{tot} , a high percentage of the parametric series of runs became unstable under certain conditions of EI , k_w , k_θ , k_w , etc. Quantitative stability limits of these conditions

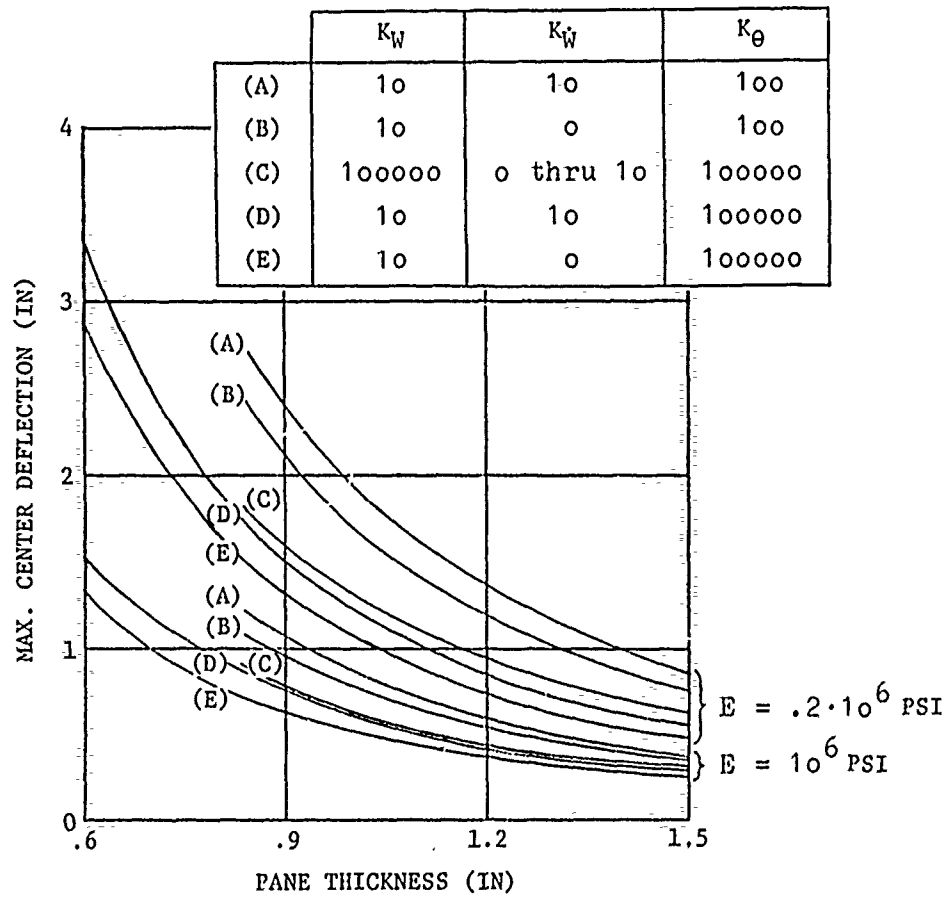


Figure 17. Max. Center Deflections of Plate

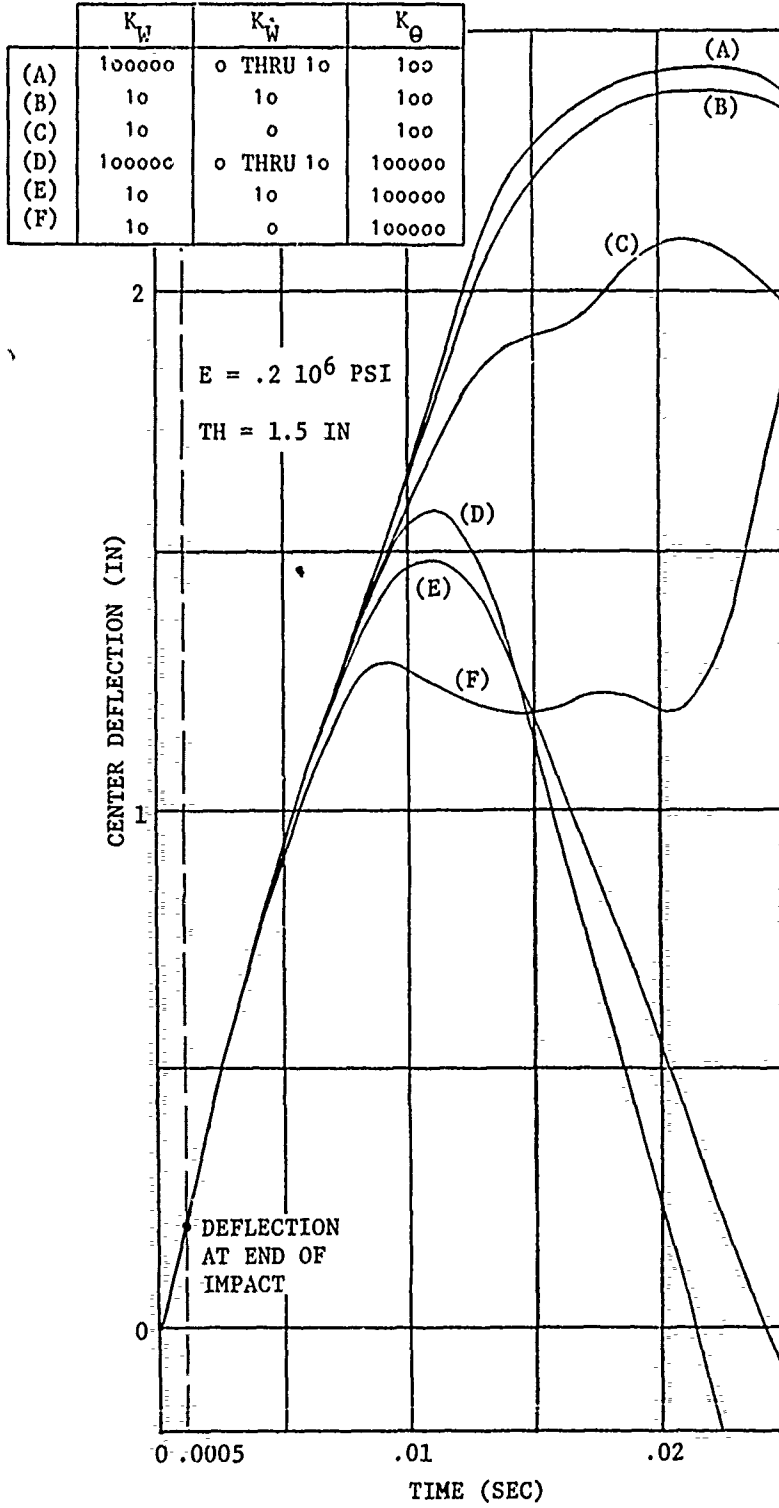


Figure 18. Time Histories of Center Deflection

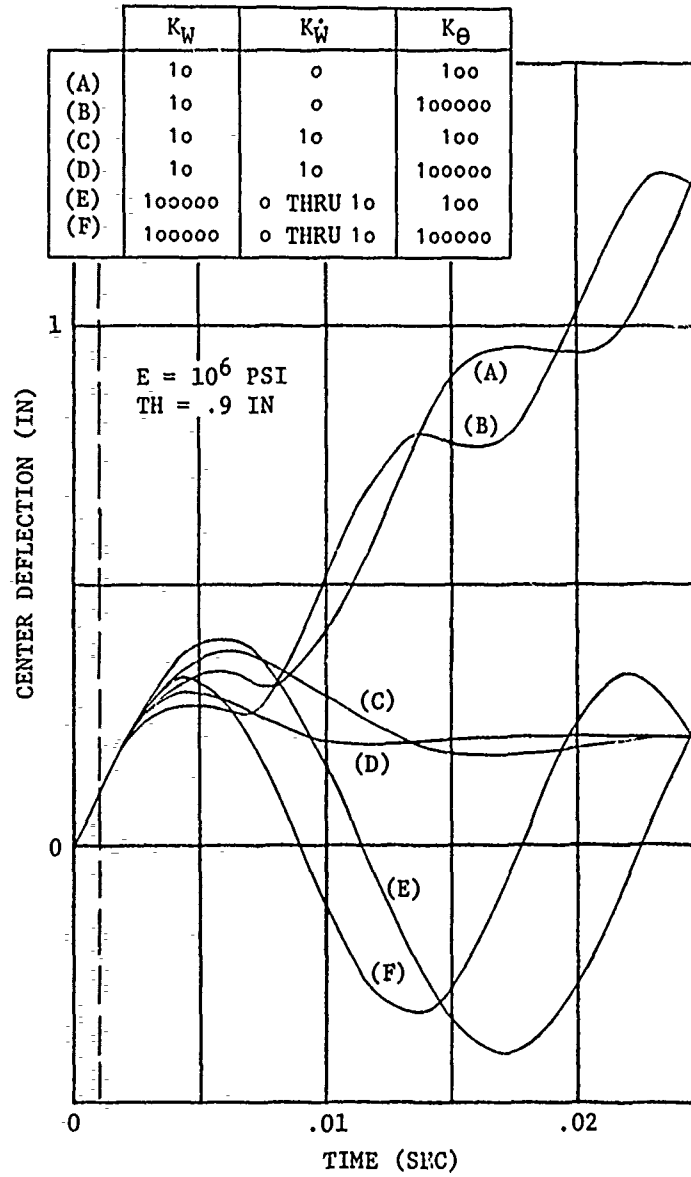


Figure 18 (Concl.)

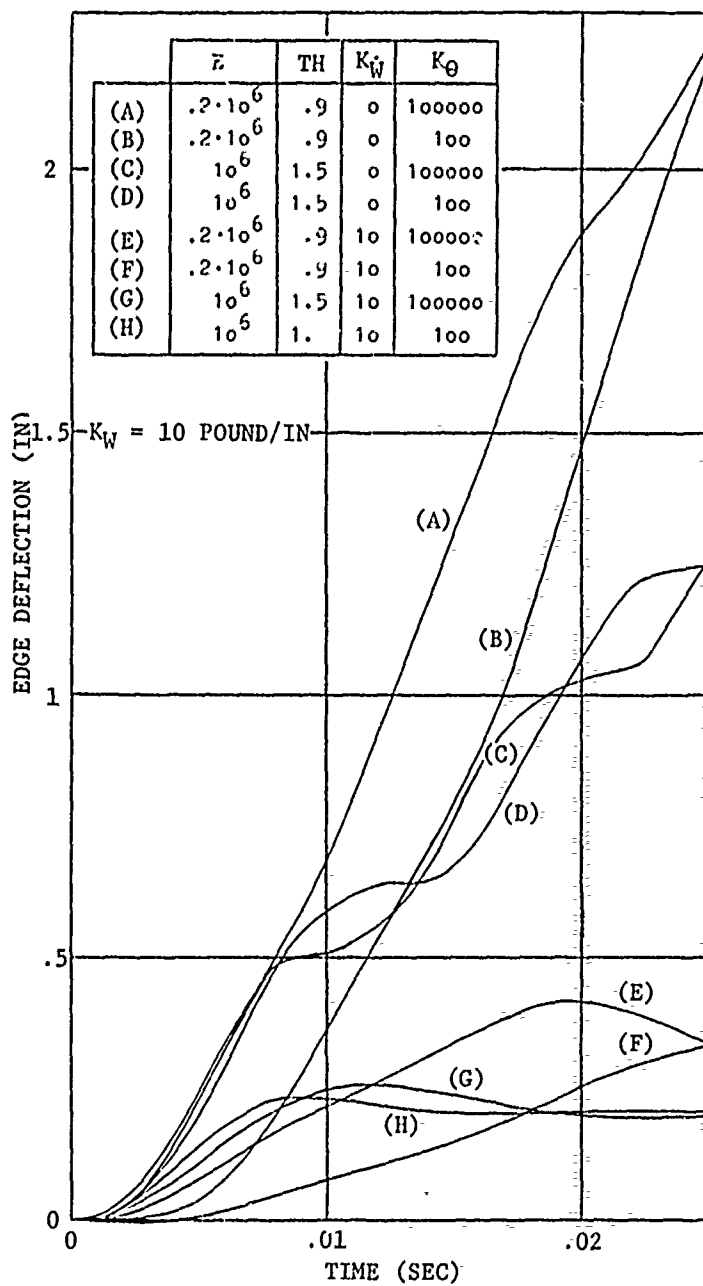


Figure 19. Time Histories of Mid Edge Deflection

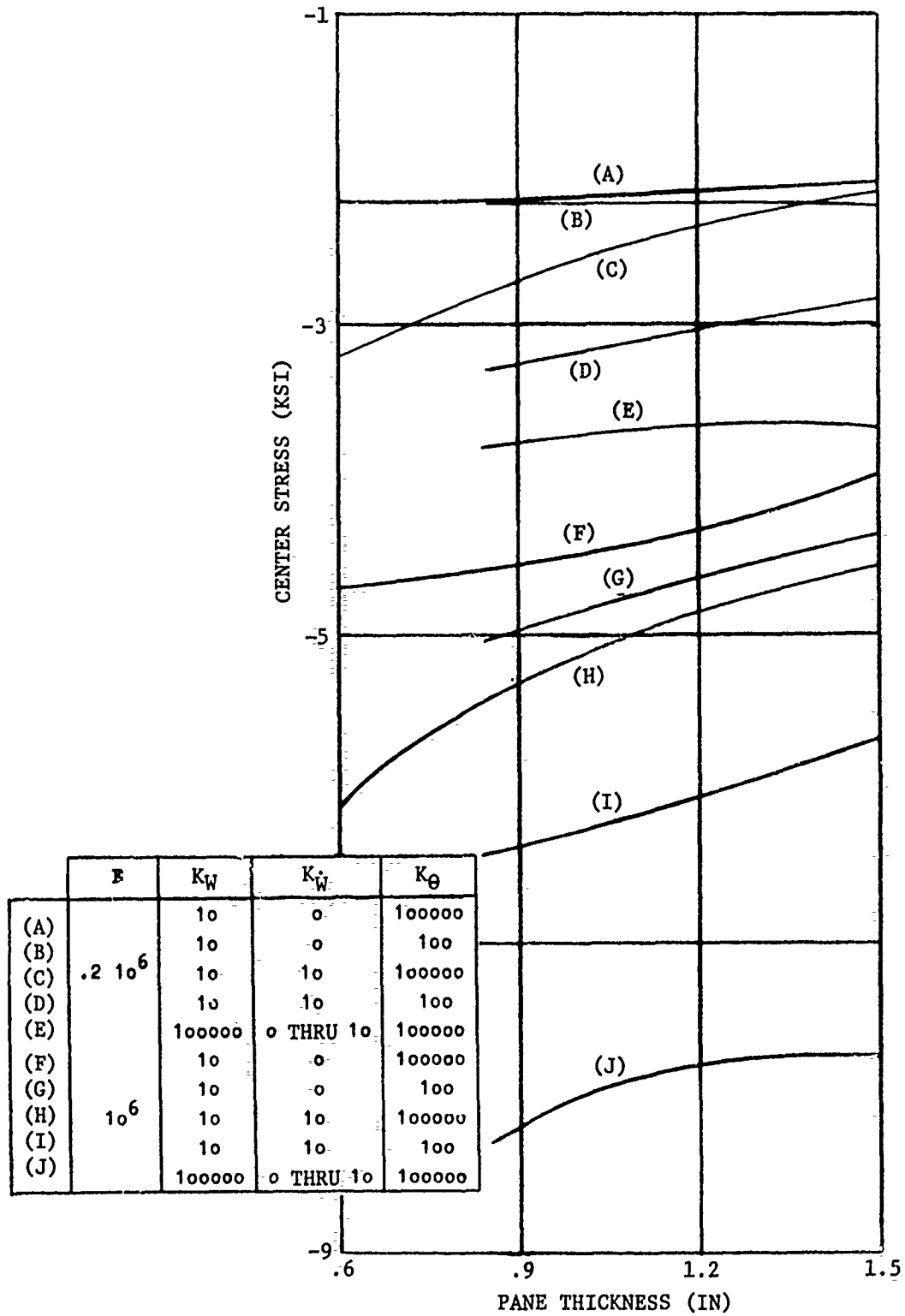


Figure 20. Maximum Center Stresses of Plate

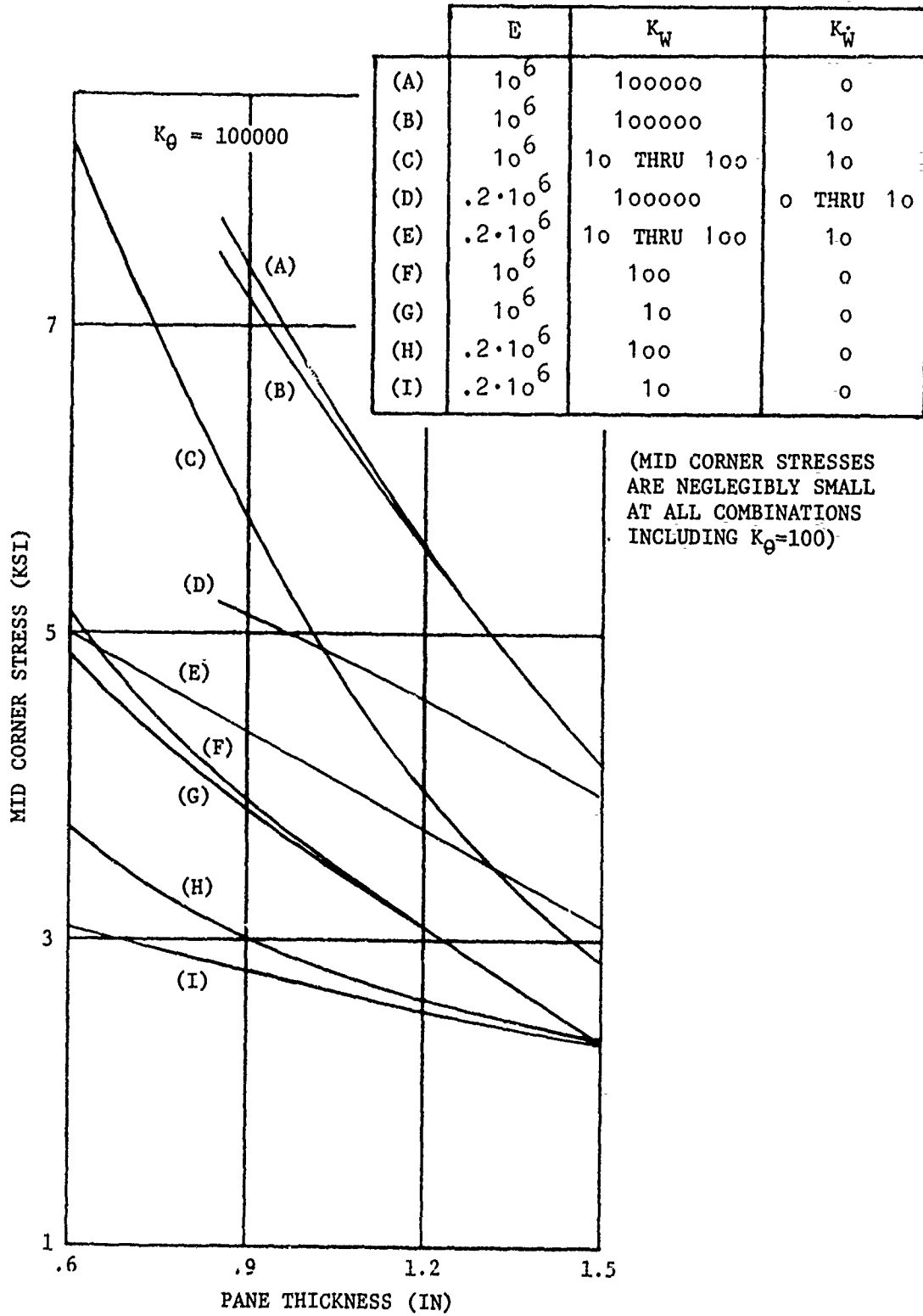


Figure 21. Maximum Mid Corner Stresses of Plate

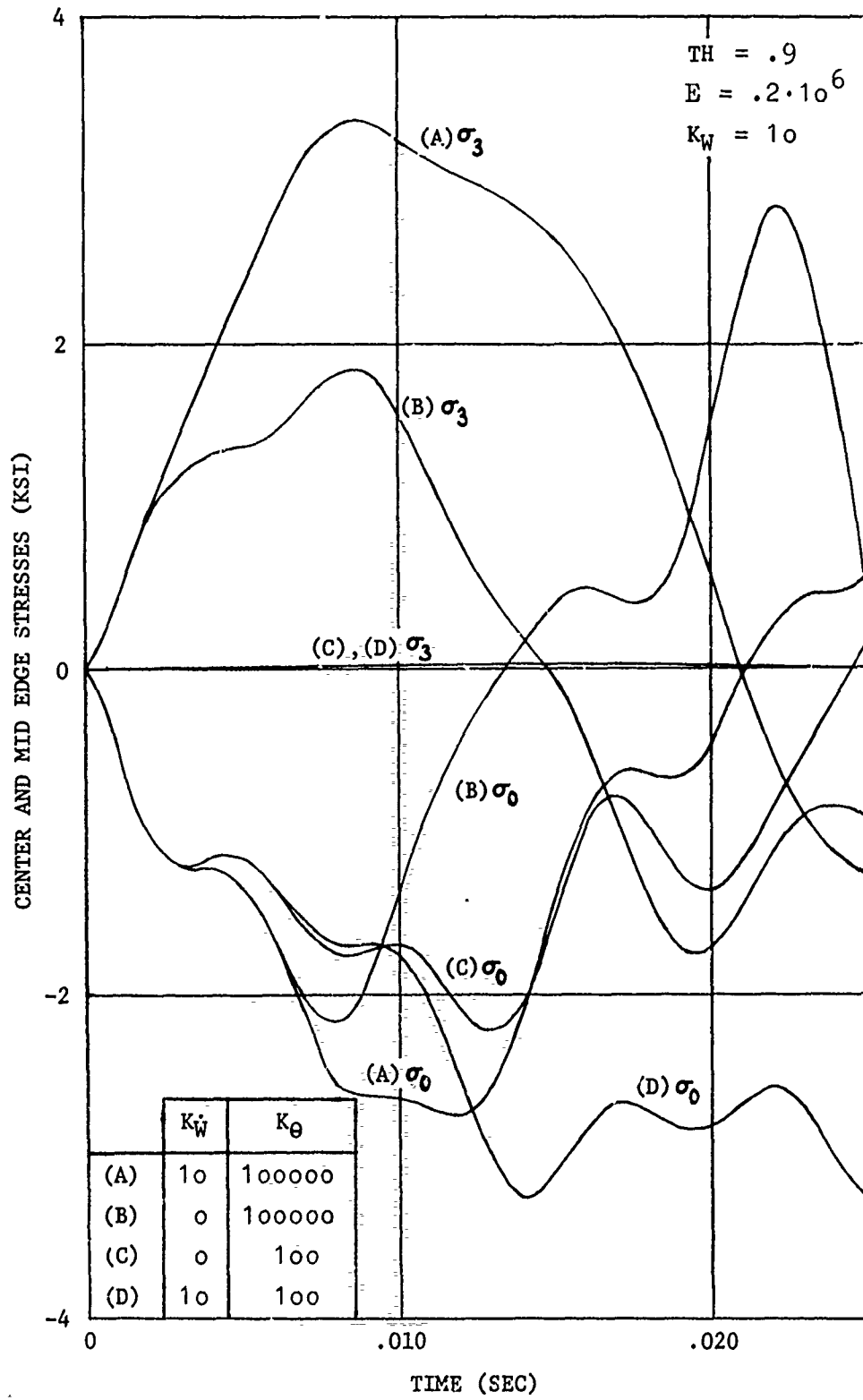


Figure 22. Center and Mid Edge Stresses

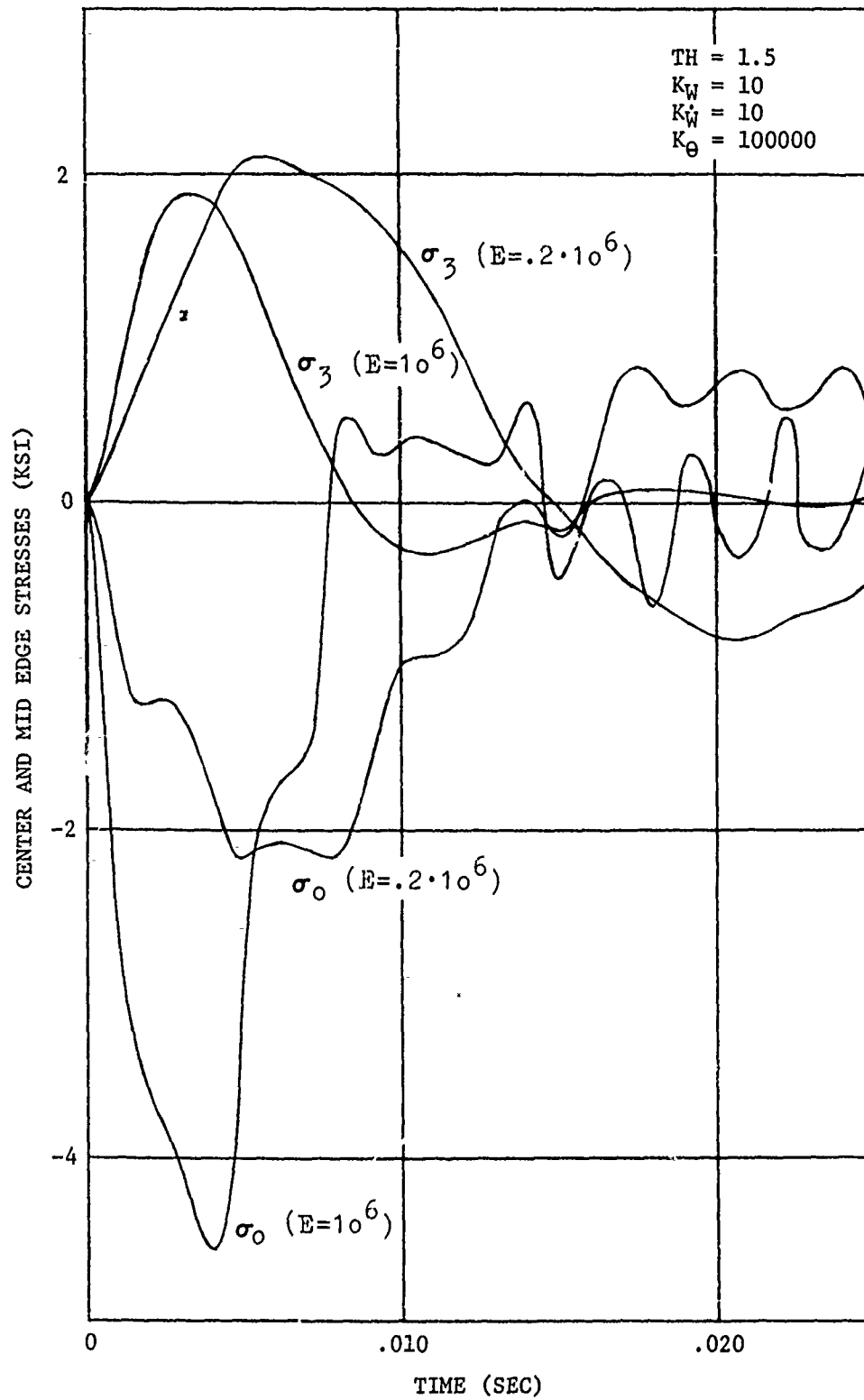


Figure 22. (Concl.)

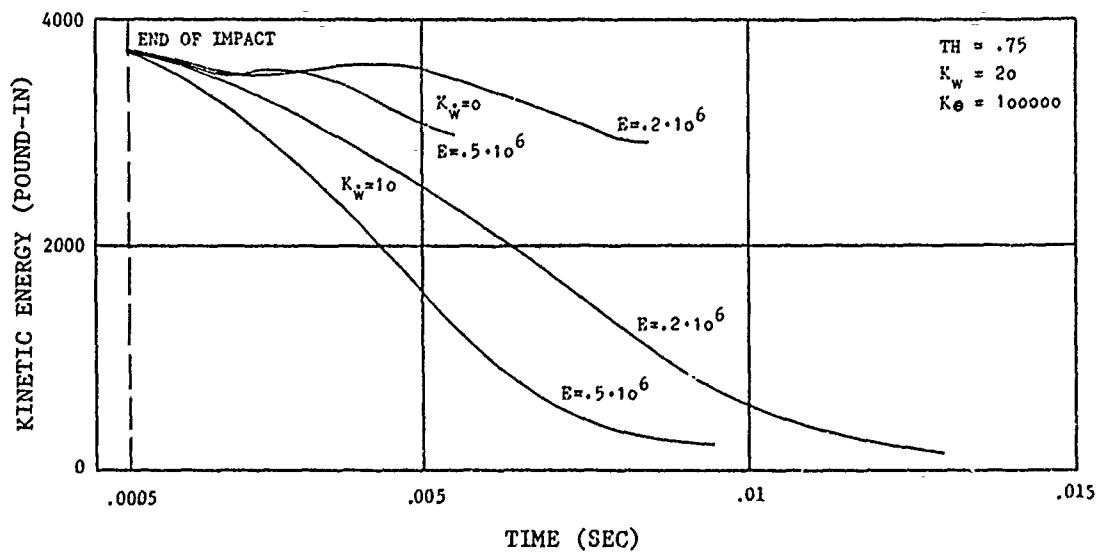
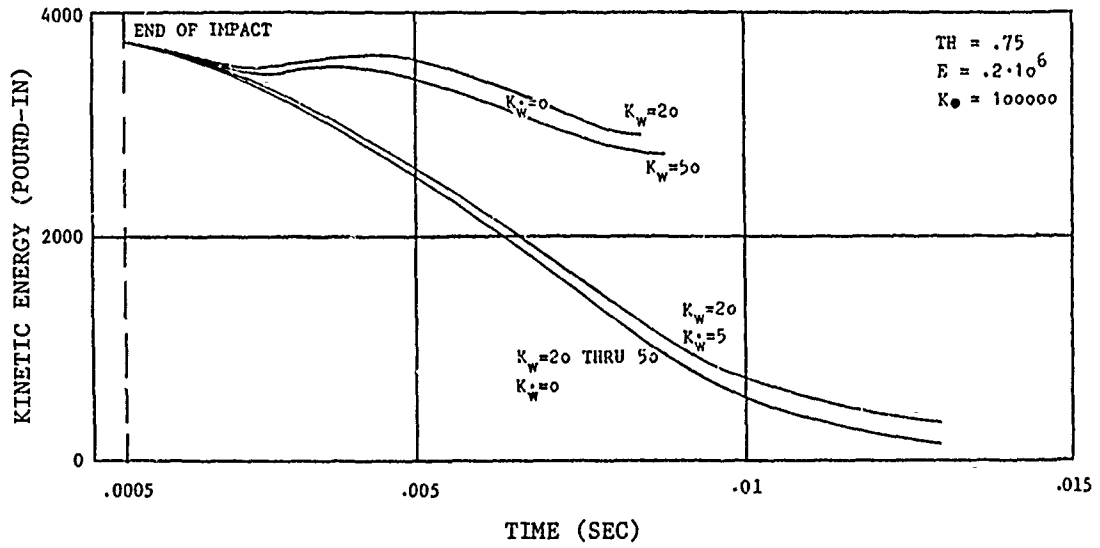


Figure 23. Kinetic Energy in Impacted Windshield

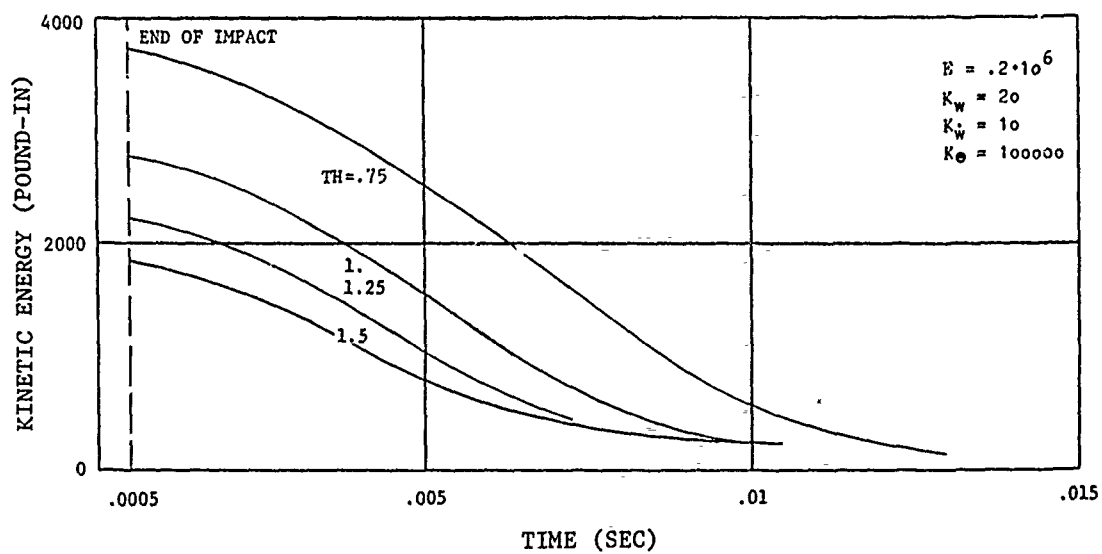


Figure 23. (Concl.)

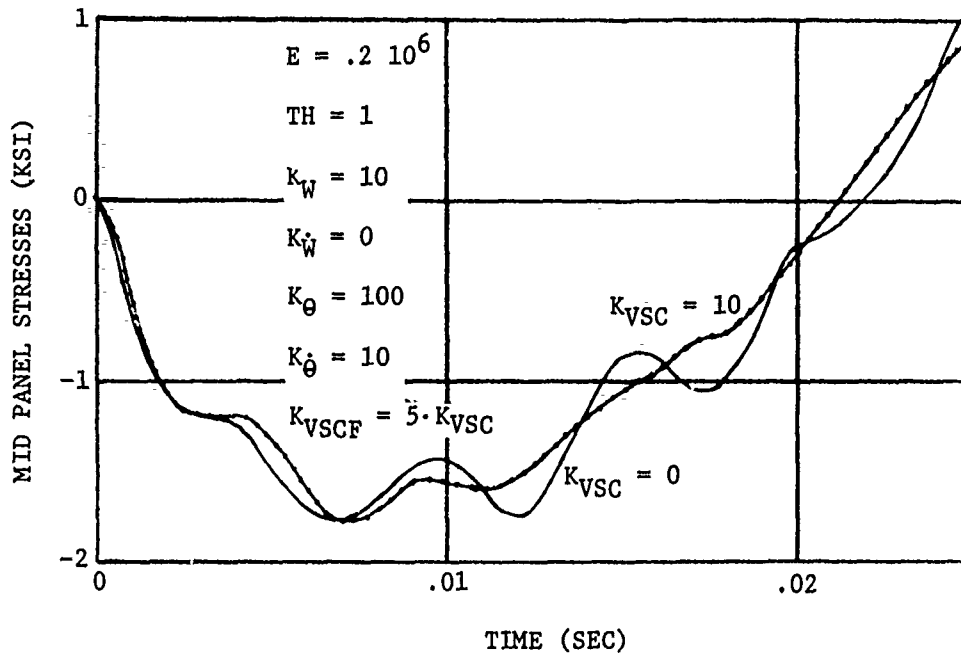


Figure 24. Effect of Viscous Interlayer
Material on Panel Stresses

TABLE IV
EDGE DEFLECTIONS OF HARD SPRING SUPPORTED PLATE

E	th	k_w	k_e	w_{3max}	w_{3min}
$.2 \cdot 10^6$.9	0	100000	.033	—
$.2 \cdot 10^6$.9	0	100	.0034	—
10^6	1.5	0	100000	.0122	-.0132
10^6	1.5	0	100	.0101	-.0099
$.2 \cdot 10^6$.9	10	100000	.0054	-.0032
$.2 \cdot 10^6$.9	10	100	.0033	—
10^6	1.5	10	100000	.0121	-.0123
10^6	1.5	10	100	.0094	-.0093

TABLE V
EXTREME STRESSES AND DEFLECTIONS

$k_w = 10$	σ (time) for $k_{vsc} = 10$	σ_3	w_0	w_3	comments: for $t \leq .025$, every 10th time interval						
	σ (time) for $k_{vsc} = 0$										
$k_e = 100$	-2.00 (.011) 1.37 (.025)	stresses neglegibly small at $k_e = 100$	1.68 (.019)	2.12 (.025)	σ_0 looks favor- able, however undamped w_3 too high						
	-1.73 (.008) 1.88 (.025)		1.70 (.019)	2.12 (.025)							
$k_e = 100000$	-2.00 (.007) 2.07 (.020)	1.63 (.008) -1.47 (.018)	deflections smaller than those at $k_e = 100$		X						
	-2.17 (.007) 2.84 (.020)	1.74 (.008) -1.71 (.018)									
$k_e = 100$	-1.67 (.007) .89 (.025)	X	1.69 (.025)	2.04 (.025)							
$k_e = 10$	-1.77 (.007) 1.19 (.025)		1.66 (.025)	2.05 (.025)							
$k_e = 100000$	-1.98 (.007) 1.99 (.020)	1.63 (.007) -1.36 (.017)	X								
	-2.15 (.007) 2.71 (.020)	1.72 (.007) -1.62 (.018)									
$k_e = 100$	-2.93 (.013) -2.81 (.022)	X									
$k_e = 10$	-3.17 (.013) -3.16 (.023)										
$k_w = 10$	-2.57 (.010) 1.33 (.024)					3.10 (.008) -1.52 (.025)	1.19 (.010) -.20 (.025)	.38 (.018)			
	$k_e = 100000$					-2.59 (.011) 1.60 (.025)	3.15 (.008) -1.53 (.025)	1.20 (.010) -.23 (.025)	.39 (.018)		
$k_w = 10$					-2.66 (.013) -2.51 (.021)	X					
$k_e = 100$	-2.58 (.017) -2.80 (.023)										
$k_w = 10$	-2.53 (.010) 1.30 (.025)				3.08 (.008) -1.50 (.025)			1.18 (.010) -.19 (.025)	.38 (.018)	σ_0 dampens out σ_3 too high w_0 tolerable w_3 is small	
$k_e = 100000$	-2.54 (.011) 1.55 (.025)				3.13 (.008) -1.52 (.025)			1.19 (.010) -.22 (.025)	.39 (.018)		
$k_e = 10$											

TABLE VI
PARAMETRIC INVESTIGATION OF MOUNTING CONDITIONS FOR PLATE

trans- lational spring support	rota- tional clamp	viscous frame damping	max. dyn. stress	frame plus window max. deflection	impact energy absorption	conclusion
soft	soft	effective	medium	acceptable	medium	less efficient
		ineffective	not investigated			
hard	not too hard	effective	low	small	high	good design practice*
		ineffective	medium	critically large	poor	inefficient
	soft	effective	medium	acceptable	medium	less efficient
		ineffective	not investigated			
hard	hard	effective	high	acceptable	poor	inefficient
		ineffective	very high	small	poor	current design

(* viscous interlayer damping effective only at high frequency / high amplitude responses of pane)

could have been easily investigated. Instead, $\Delta t = .00001$ sec was arbitrarily used, and all parametric runs investigated became stable again.

The maximum center deflections, $w_{\text{omax}}(\text{in})$, which occur first after impact were calculated and are selectively reported in Figure 17 for both a soft pane material ($E = .2 \cdot 10^6 \text{psi}$) and a very stiff one ($E = 10^6 \text{psi}$) for pane thicknesses between .6" and 1.5". The following mounting parameters, k_w , k_w' , and k_θ , were assumed equally distributed along the boundary:

$$k_w = 10 \text{ thru } 100,000 \text{ pound/in,}$$

$$k_w' = 0 \text{ thru } 10 \text{ pound-sec/in,}$$

$$k_\theta = 100 \text{ thru } 100,000 \text{ pound-in/rad.}$$

The viscous constants, k_ϕ , k_{VSC} and k_{VSCF} , initially were assumed zero to demonstrate the influencing effect of k_w' alone. Curves plotted in Figure 17 are the peak deflections taken from Figure 18.

Maximum deflections, $w_{3\text{max}}$, for the pane at the middle of the reinforced edge, equaling the amount of the local spring deflection, occur at time $>.025$ sec in case of the soft spring of $k_w = 10$ pound/in (Figure 19), except for cases (E), (G) and (H). $k_w = 100,000$ pound/in causes negligible maximum deflections, w_3 , at the middle of the edge.

Surface stresses occurring at the center and the mid edge of the plate are shown in Figures 20, 21, 22. For the typical ranges considered, time histories of kinetic energies, E_{kin} , are shown in Figure 23.

The viscosity effect of the interlayer represented by k_{VSC} , has been investigated for 32 different combinations of parameters represented by

$k_w=10$ and $100,000$ (pound/in),
 $k_w^*=0$ and 10 (pound-sec/in),
 $k_\theta=100$ and $100,000$ (pound-in/rd),
 $k_\theta^*=0$ and 10 (pound-in-sec/rd),
 $k_{vsc}^*=0$ and 10 (pound-in²-sec/rd).

It was observed that use of $k_{vsc}=10$ tends to flatten peak variations of stresses in the original curves of $k_{vsc}=0$. In addition, curves for $k_{vsc}=10$ lag behind those for $k_{vsc}=0$ (Figure 24). The set of parameter combinations was screened for extreme values of stresses, σ_0 and σ_3 , and deflections, w_0 and w_3 .

The effectiveness of shock absorption in dampening the oscillating stresses is shown in Figures 20 and 21. The peak stress of the first cycle for the damped system usually is slightly lower than the maximum stress for the undamped one.

The undamped stress reversals, rather than the one-time stress peak of the damped case, may be the reason for fatigue failure. For the undamped system, the possibility of local build-up of peak stresses exists, as the sum of kinetic and potential energy in the system theoretically remains constant. As time elapses after impact, energy dissipation by natural causes, not accounted for in this simplified analysis, could have occurred.

The largest tolerable deflections during the time history after impact (Figures 17, 18, 19) are another design restriction. A trade-off decision has to be made between soft springs (yielding higher deflections and lower pane stresses), and harder ones. A matrix of criteria

for design of the flat impact resistant windshield has been prepared using the limited number of results and is presented in Table VI. Low maximum dynamic stresses, acceptable frame and window maximum deflections and high impact energy absorption result, from using technically feasible soft translational springs, hard rotational clamps and effective viscous damping units.

The influence of the shape of impact pressure mound (such as constant vs. pyramidal distribution), the time-load profile (such as one-minus-cosine vs. square wave), the effect of geometrical eccentricity and severity/rapidity of impulse ($Q_{tot1} \cdot t_{imp1} = Q_{tot2} \cdot t_{imp2} = \text{const}$), may be investigated for "hard, medium and soft" boundary parameters. Equally distributed loads cause higher stresses at clamped edges than pyramidal loads. Eccentricity of impact may create higher stresses (shifted from the center of the pane towards one edge), along with overall lower deflections. Rapidity of impact, $t_{imp1} < t_{imp2}$ causes higher stress concentrations for very short periods of time. The advantage of a less severe $Q_{tot2} < Q_{tot1}$, however, should be determined.

5. FINITE DIFFERENCE IDEALIZATION OF WINDSHIELD (F-111)

a. The F-111 Windshield

The structural model for the F-111 Crew Module considers the wind-screens to the left and right held together by the head beam, with sills acting as lateral supports, a bow in the front attached to the bulk-head, and an unsupported arch in the rear, which simultaneously acts as

part of the frame of the hatch. The stiffness and mass properties of these parts and the edge reinforcements of the window panes were estimated from the details of the drawings. The head beam is 2 times stiffer than the arch. The bow is 8 times stiffer than the arch and the sills are over 20 times stiffer than the arch. The elastic support of the remaining module structure relative to the windscreens can only be guessed, and production runs show how important this input is.

b. The General Equations

As in the case of finite difference formulation for the flat plate, the F-111 windshield is replaced by a cross beam arrangement consisting of curved beams in x-direction and straight beams in y-direction. Further, it is an applied case of the basic monolithic conical shell segment with right and left window panes, and support members consisting of front bow, right and left sill, aft arch and center head beam.

The finite difference equations valid in both the general shell and windshield case, contain the following variables in the radial x-direction:

- (1) bending moment (pound-in), M_x ,
- (2) normal deflection (in), u_n ,
- (3) tangential internal force (pound), F_t ,
- (4) slope (rd), θ_x ,
- (5) normal force (pound), F_n ,
- (6) tangential deflection (in), u_t .

They are related by six (6) first-order curved beam difference equations.

Variables in the longitudinal y-direction, related by four (4) first-order straight beam difference equations, are:

- (1) moment (pound-in), M_y ,
- (2) normal deflection (in), u_n ,
- (3) slope (rd), θ_y ,
- (4) normal force (pound), V .

Tangential force, F_t , is equivalent to circumferential tension, and normal force, F_n , to radial shear. F_n could be used as an indicator of the shear stress distribution in the window pane. V is the shear force in the longitudinal direction.

The following are the general finite difference equations:

$$(F_n)_{x+\frac{1}{2},y,t} - (F_n)_{x-\frac{1}{2},y,t} - (F_t)_{x,y,t} \left(2 \sin \frac{\Delta\phi}{2}\right)_{x,y} + (V)_{x,y+\frac{1}{2},t} - (V)_{x,y-\frac{1}{2},t} = - (Q_n)_{x,y,t} - (\Delta M)_{x,y} (\ddot{u}_n)_{x,y,t} \quad (66.1)$$

$$(F_t)_{x+1,y,t} - (F_t)_{x,y,t} = - (F_n)_{x+\frac{1}{2},y,t} \left(2 \sin \frac{\Delta\phi}{2}\right)_{x+\frac{1}{2},y,t} - (Q_t)_{x+\frac{1}{2},y,t} \quad (66.2)$$

$$(M_x)_{x+1,y,t} - (M_x)_{x,y,t} = - (F_n)_{x+\frac{1}{2},y,t} \left(2 r \sin \frac{\Delta\phi}{2}\right)_{x+\frac{1}{2},y,t} \quad (66.3)$$

$$(M_y)_{x,y+\frac{1}{2},t} - (M_y)_{x,y,t} = - (V)_{x,y+\frac{1}{2},t} (\Delta y)_{x,y+\frac{1}{2}} \quad (66.4)$$

$$(\theta_x)_{x+\frac{1}{2},y,t} - (\theta_x)_{x-\frac{1}{2},y,t} = \left(\frac{M_x}{EI_x}\right)_{x,y,t} (r \cdot \Delta\phi)_{x,y} \quad (66.5)$$

$$(\theta_y)_{x,y+\frac{1}{2},t} - (\theta_y)_{x,y-\frac{1}{2},t} = \left(\frac{M_y}{EI_y}\right)_{x,y,t} (\Delta y)_{x,y} \quad (66.6)$$

$$(u_n)_{x+1,y,t} - (u_n)_{x,y,t} = \left[(u_t)_{x+\frac{1}{2},y,t} + (\theta_x)_{x+\frac{1}{2},y,t} (r)_{x+\frac{1}{2},y} \right] \left(2 \sin \frac{\Delta\phi}{2}\right)_{x+\frac{1}{2},y} \quad (66.7)$$

$$(u_n)_{x,y+\frac{1}{2},t} - (u_n)_{x,y,t} = (\theta_y)_{x,y+\frac{1}{2},t} (\Delta y)_{x,y} \quad (66.8)$$

$$(u_t)_{x+\frac{1}{2},y,t} - (u_t)_{x-\frac{1}{2},y,t} = - (u_n)_{x,y,t} \left(2 \sin \frac{\Delta\phi}{2}\right)_{x,y} \quad (66.9)$$

The following equivalencies exist between the flat plate Equations 50 and Equations 66:

66.1 \leftrightarrow 50.1
 66.3 \leftrightarrow 50.2
 66.4 \leftrightarrow 50.3
 66.5 \leftrightarrow 50.4
 66.6 \leftrightarrow 50.5
 66.7 \leftrightarrow 50.6
 66.8 \leftrightarrow 50.7

Equations 66.2 and 66.9 account for the effects of curvature, tangential load, F_t , and tangential displacement, u_t , respectively.

Equation 66.1 is the balance-of-force equation for calculating the normal accelerations, \ddot{u}_n . \ddot{u}_n is integrated (Equation 34.5) to find normal velocities, \dot{u}_n , and integrated again for displacements, u_n (Equation 34.6).

As in case of the flat plate, boundary conditions and edge distributions are satisfied by Equations 27, 28, 35.1 and 35.2.

The details of the algorithm (marching procedure) for calculating the time dependent variables of Equations 66, are similar to the ones for the flat plate (page 53).

c. The Geometry

The principal geometrical dimensions of the F-111 windshield were either found in original drawings or estimated as closely as possible. The actual radii for bow and arch, R_{min} and R_{max} , are given in Figure 25 (Notations in capital letters, such as RMIN and RMAX, are used for these and all the other variables in the FORTRAN program of Appendix IV). The central angles of the cone segment (Figure 25), minimum at bow and maximum at arch, ϕ_{min} and ϕ_{max} , are:

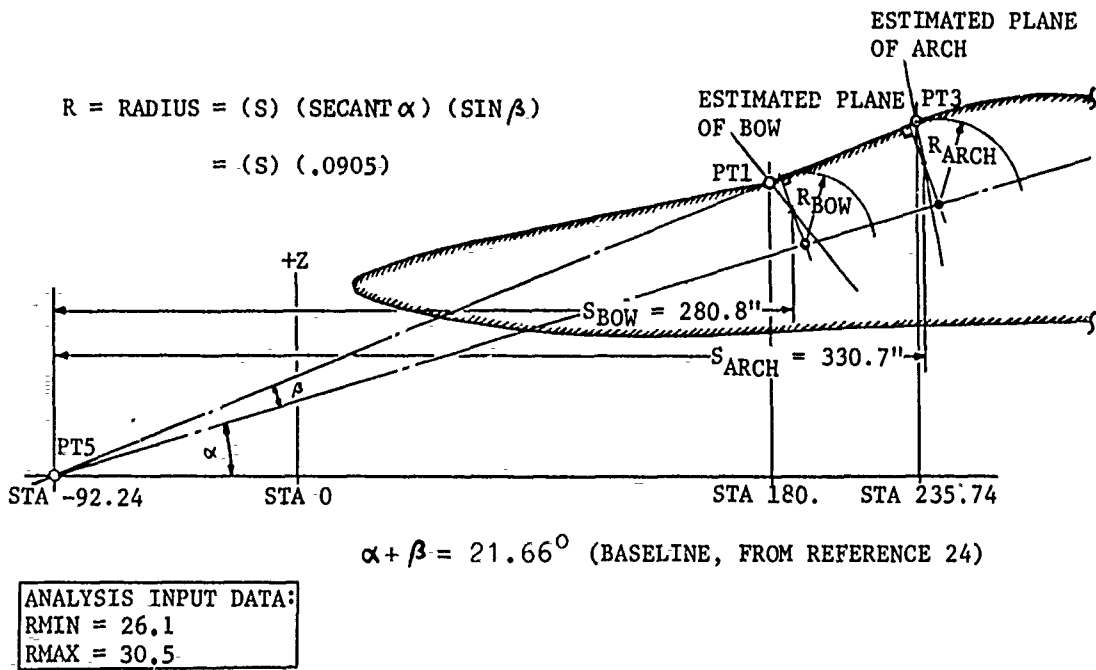


Figure 25. Determination of Windshield Contour

$$\phi_{\min} = 180^\circ - 2 \arcsin ((26.1-10.9)/26.1) = 108.9^\circ \quad (67.1)$$

$$\phi_{\max} = 180^\circ - 2 \arcsin ((30.5-21.8)/30.5) = 146.8^\circ \quad (67.2)$$

The geometry of the window is further described by the thickness, t (in), of the window pane. L_{hea} is the length of the head beam (in), and L_{sill} is the length of the sill (in) (Figure 26).

Estimated effective widths for generation of the finite difference grid for the edge members are:

$$W_{\text{hea}}=3, W_{\text{sill}}=3.5, W_{\text{bow}}=3, W_{\text{arc}}=2 \text{ inch.}$$

d. Stiffnesses

Pane stiffness is reflected in Young's modulus, E_{pane} (pound/in²), and bending stiffness per inch of width in the longitudinal direction for head beam, sill, bow and arch, EI_{hea} , EI_{sill} , EI_{bow} and EI_{arc} (pound-in) and transverse per inch of length, EI_{thd} , EI_{tsl} , EI_{tbw} and EI_{tac} (pound-in) (Figure 27).

Estimated effective longitudinal and transverse bending stiffnesses (Reference 45) for the frame, including the titanium sheet reinforcement strips (.03" x 2.2" at upper and .045" x 2.2" at lower side) with a pane thickness of .4" are $EI_{\text{hea}}=6,040,000$; $EI_{\text{sill}}=66,000,000$; $EI_{\text{bow}}=20,000,000$; $EI_{\text{arc}}=2,760,000$ (pound-in²) along the frame. The bending stiffness effect of edge reinforcements with the titanium stripping accounts for 160,000 pound-in² along the frame and is included in the above values. Table III presents the material properties for polycarbonate (Reference 46). Values of EI_{sill} and EI_{bow} are estimates rather than precise data, because of the unknown supporting stiffnesses provided by the structural opening of the module.

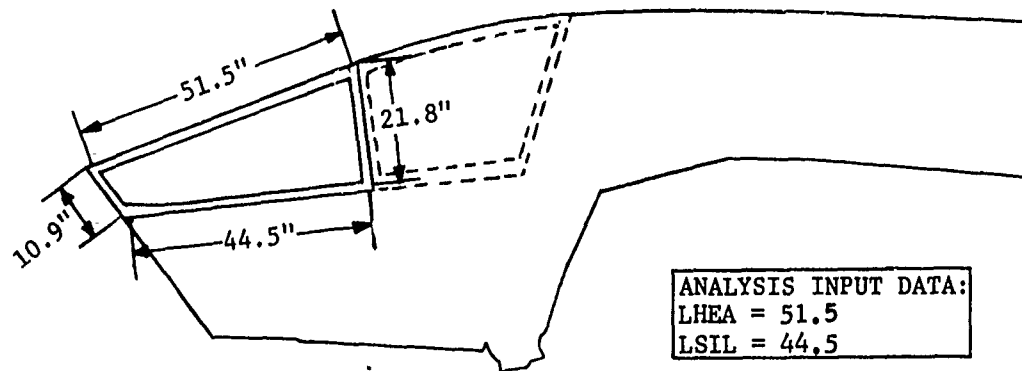


Figure 26. Side View of F-111 Windshield/Crew Module

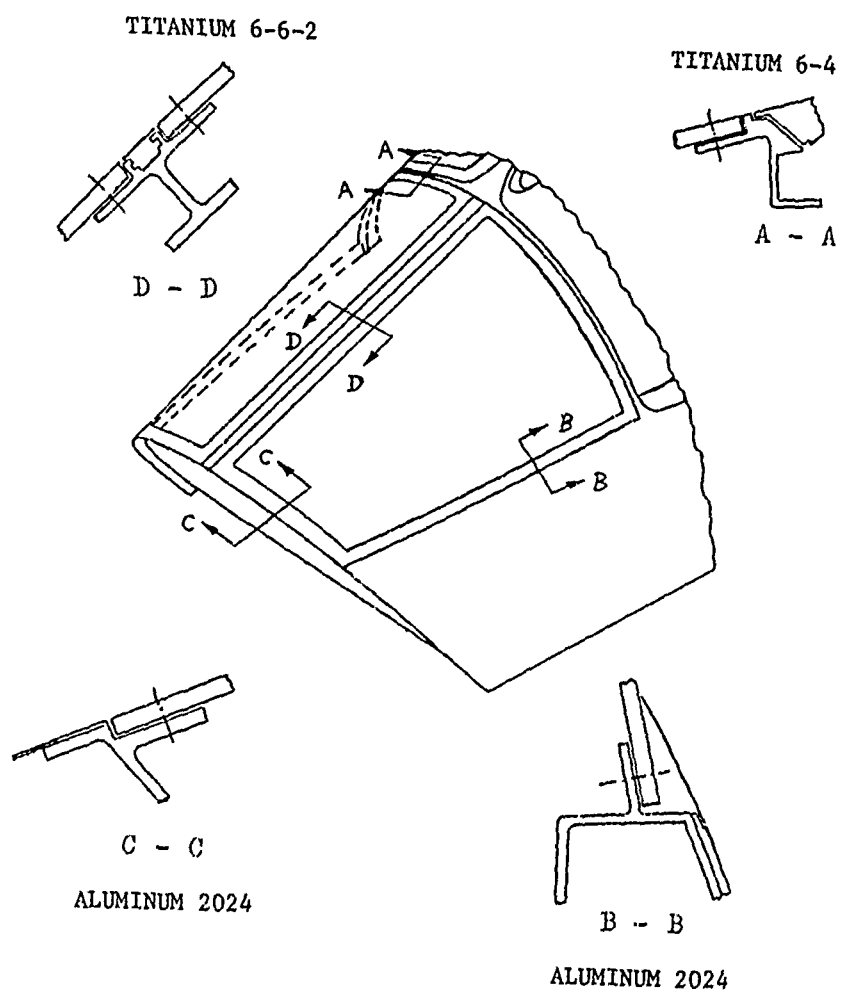


Figure 27. F-111 Windshield/Mounting System

The EI_t values in the transverse direction are much smaller than the EI values in longitudinal direction and represent partly the transverse bending stiffnesses of the flanges to which the reinforced glazing edges are mechanically fastened. Stiffness values of critical cross sections ($I/in=(\text{flange thickness})^3/12$) are thought too low to be representative of mounting stiffnesses. Considering one half the thickness of the standard glazing of 0.4 in^2 , $I/in=\text{flange thickness} \cdot (0.2'')^2$ was assumed. The resulting values are: $EI_{thd} = 73,500$; $EI_{ts1} = 84,000$; $EI_{tbw} = 84,000$; $EI_{tac} = 64,000$ (pound-in).

Bending stiffness in both the circular and longitudinal direction of the conical windshield are:

$$EI_x = E_{\text{pane}} (t^3/12) (\Delta y) \quad (68)$$

$$EI_y = E_{\text{pane}} (t^3/12) (\Delta s) + \Delta EI_y \quad (69)$$

$$\Delta EI_y = (\text{Curv}) \cdot E_{\text{pane}} \cdot t (1 - \cos(\Delta\phi/2))^2 \cdot r^2 \cdot (\Delta s) \quad (70)$$

where $\Delta s (=r \cdot \Delta\phi)$ is the finite difference along the arch, and ΔEI_y is an effect of curvature contributing to the gross longitudinal stiffness. Considering the finite difference element as an arch, the neutral axis is located parallel to the base of the arch at a distance less than the height of the arch. Ignoring the first term in Equation 69, the fraction, Curv , was graphically determined to be 3% or less. In the analysis, a variation of Curv between 0 and 0.2 has been used. Additionally, Curv is assumed to vary as a function of arch deflection to represent the realistic situation.

e. Boundary Conditions

The attachment conditions of the window pane to the frame and of the frame to the support opening of the module structure is simulated by elastic spring type boundary conditions for the sill, the bow, and the arch (excluding the head beam). The sill and the bow are considered to be rotationally as well as transversely very stiff compared to the arch. A 100:1 stiffness ratio was assumed with reasonably flexible values of 1000(pound/in) and 1000(pound/rd) for the arch resulting in the following values:

$K_{\text{unsil}} = 100,000$	$K_{\text{osil}} = 100,000$
$K_{\text{unbw}} = 100,000$	$K_{\text{obow}} = 100,000$
$K_{\text{unac}} = 1,000$	$K_{\text{oarc}} = 1,000$

In this preliminary study, these parameters were varied, and the effects on amplitude and frequency responses of stresses and deflections were analyzed.

While Curv accounts for the effect of the curvature on bending stiffness in the window pane, a correction factor (Cor) is used for the actual increased bending stiffnesses at the windshield corners.

The viscous type translational damping at all four edges is negligible in the conventional windshield frame of the F-111 fleet; therefore 0.1 (pound-sec/in) is considered a reasonable value. Variation of the effect of this property, as well as in rotation, has been explored.

$K_{\text{unsil}} = 0.1$	$K_{\text{osil}} = 0.1$
$K_{\text{unbw}} = 0.1$	$K_{\text{obow}} = 0.1$
$K_{\text{unac}} = 0.1$	$K_{\text{oarc}} = 0.1$

f. Mass Properties

All mass properties are based on the following specific densities, ρ (pound-sec/in⁴), for titanium (0.000414), aluminum (0.000258) and polycarbonate (0.000112).

Estimated mass properties of frame per running inch (pound-sec²/in²), based on the dimensions on original drawings (Reference 45) and specific densities, for the head beam, sill, bow and arch, (with the mass of the reinforced window edges, ~ 0.0013 , added in each case) are: $M_{\text{hea}} = 0.00054$, $M_{\text{sill}} = 0.00071$, $M_{\text{bow}} = 0.00043$ and $M_{\text{arc}} = 0.00038$. The types of mass elements, ΔM , at the corners are:

$$\Delta M = \Delta x \cdot M_{\text{bow}} + \Delta y \cdot M_{\text{sill}} \quad (71)$$

Along the frame,

$$\Delta M = \Delta x \cdot M_{\text{bow}} \quad (72)$$

Mass properties of windshield (window pane) calculated from windshield dimensions are:

$$(\Delta M)_{x,y} = \rho \cdot (\Delta S)_{x,y} (\Delta \gamma)_{x,y} t \quad (73)$$

with $\rho = 0.000112$ and $t = 0.9$.

g. Computer Program

The computer program developed for special features of the windshield in the F-111 module (Appendix III-4) incorporates the following possibilities: (a) a choice of loading history, (b) any location of impact, and (c) any boundary conditions, except for the fixed tangential support. Typical cases for the F-111 windshield may be found in Section IV-2.

SECTION IV
APPLICATIONS

This section contains the numerical results obtained for square panel test WT-18 and the F-111 windshield test FM-1 using the finite difference analysis method. These results are compared with available experimental data.

1. ANALYSIS OF SPECIFIC SQUARE PANEL TEST (WT-18)

One phase of a contractual effort by PPG Industries (Reference 47) was devoted to preliminary impact testing of 18 flat 26" x 26" panels of 14 types of pane construction. The panels were bolted into a test frame at an angle of 23°. Except for two failures caused by the frame during sorting-out runs, results were predictable.

The following is a summary of the 18 test cases (Reference 47). Two of the specimens, WT-1 and WT-2, were monolithic polycarbonate and both failed by shearing of the panes along the top edges of the frame. The others were laminated: three of three, one of four, two of five, six of seven, one of eight, and three specimens of nine layers each. The materials used, in order of application and with range of thickness indicated were: polycarbonate (0.093" - 0.766"), PPG proprietary interlayers (0.09" and 0.12"), stretched acrylic (0.06" - 0.125"), Herculite II (0.11"), and as-cast-acrylic (0.06" - 0.125"). Total pane thickness was 0.75" thru 1.041". Pane edges were simply stepped down to thicknesses from 0.359" thru 0.451". In seven panels, the pane edges were composed of monolithic polycarbonate and eleven panels of two layers of polycarbonate with one

PPG interlayer. Total panel weights varied from 20.25 thru 30.5 pounds (specific weights of 4.68 thru 7.48 pound/ft²). Weights of birds were 3.91 to 4.18 pounds. The actual speed varied between 96.5% and 114.7% of the intended speed. Range of final velocities was 755.1 thru 908.2 ft/sec (447 thru 538 kt). The kinetic energies at impact were from 35,398 pound-ft in shot WT-2 to 53,496 pound-ft in shot WT-5.

Eleven failures occurred and were typically described as: panel completely or center of panel blown out; bird penetrated from top edge shear; bird bounced but had 45° yaw and top edge of frame suffered permanent set; several cracks in polycarbonate; and panel bulged. On nine of these panels the permanent set was from 1/16" to 1/2". Of the seven tests with no penetration occurring, shots WT-9 at 44,077 pound-ft total kinetic energy of impact and WT-18 at 45,353 pound-ft were acceptable with good residual visibility. The critiques of the remaining five tests are: structural deficiency; improper damping frame; 9/16" permanent set and 0 degree residual visibility; crack in polycarbonate middle ply and 7/16" permanent set; spall of stretched acrylic.

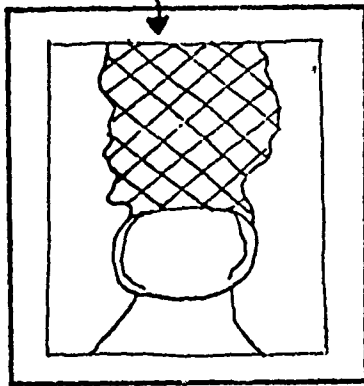
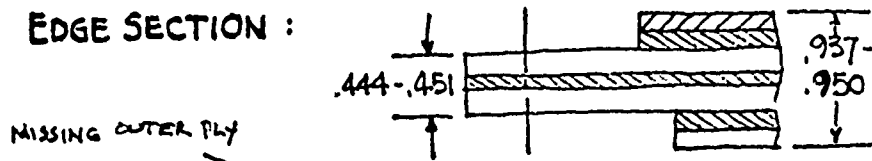
Figure 28 gives one of the original data forms prepared for each individual test. The corresponding set of deflection histories, calculated from motion picture frames, at the center of the panel and 4 inches back of the center are shown in Figure 7. Test shot WT-18, presented in Figure 28, was one of the most successful tests and has been simulated for this reason.

SAMPLE CODE : 9030-7A

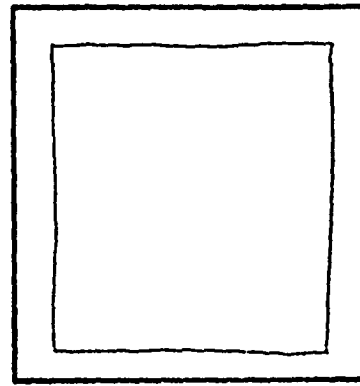
CONSTRUCTION : .125" ACRYLIC - .120" 1/L - .188" PC - .090" 1/L - .188" PC -
.120" 1/L - .125" PC

THICKNESS : .956" AREAL DENSITY : 5.96 LB./FT² PANEL WT. : 23.75 LB.

EDGE SECTION :



(FRONT)



(REAR)

RESULTS ON 3-30-73 @ 64°F AND 23° INSTALLATION ANGLE

SHOT NO. : WT-18 SPEED : INTENDED : 850 FPS
PRELIM. : 857.5" BIRD WT. : 4.00 LB.

REMARKS : $j \approx 0$ FINAL : 854.7"
(506 kt) (45,353 FT-LB)

BIRD BOUNCED. NO POLYCARBONATE CRACKING ON BACK PLY. NO SHEARING OR CRACKING ON TOP EDGE. BEST PERFORMANCE OF ALL PANELS SHOT ??? APPROX. 30% OF OUTBOARD PLY BLOWN OFF. GOOD ADHESION ELSEWHERE. RESIDUAL VISIBILITY EXCELLENT.

(FROM REFERENCE 47)

Figure 28. Original Test Data of Shot WT-18

a. FINITE DIFFERENCE SOLUTION

Using the material properties given in Table VII, the stacking sequence of the laminate is 0.125" acrylic, 0.12" interlayer, 0.188" polycarbonate, 0.09" interlayer, 0.188" polycarbonate, 0.12" interlayer, 0.125" polycarbonate, totaling ~ 0.956 ". The effective bending stiffness of the panel of shot WT-18 may be estimated using Equations 22 and 23, EI_{lam} per inch width $\sim 24,000$ pound-in² at a corresponding modulus of the laminated panel, $E_{MOD} = 0.33 \times 10^6$ psi, was used in the analysis.

Applying the equations for plate vibration (Equations 3, 4, 5), the theoretical vibration frequency, ω_{th} , is compared with the actual frequency, ω_{ac} , as determined from Figure 7. The plate naturally vibrates after the impact disturbance has diminished. An estimate is $\omega_{ac} \approx 2\pi / (0.015 \text{ sec}) = 420 \text{ sec}^{-1}$. With $D \sim EI_{lam} = 24,000$ pound-in², $\rho = 0.00011$ pound-sec²/in⁴, and $s = 26$ in, $\omega_{th} = 790 \text{ sec}^{-1}$ (88% higher than the actual vibration). The vibrational behavior of the heavy frame, not taken into account, may explain the actual slow down from 0.008 to 0.015 sec per cycle.

Proper choice of grid size, Δs , and time step, Δt , according to the condition, $(\Delta t / \Delta s) \cdot (E / \rho)^{1/2} > 1$, to achieve accuracy of prediction by finite differences, was based upon Reference 48. Using a time step, $\Delta t = 0.0001$ sec and an applicable $\sqrt{E / \rho} = 50,000$ in/sec, Δs has to be 5" or smaller. The square or rectangular flat plate program (Appendix IV-1) originally using a grid size, $NG = 13$, and in consequence the mass quotient, $NM = 37$, to calculate equal mass distribution, $DMM = MPANE / NM$, as well as the load quotient, $NQ = 70$, to determine unit load, $QTOT / NQ$,

TABLE VII
 MATERIAL PROPERTIES CONSIDERED IN THE
 ANALYSIS OF PANEL SHOT WT-18

64 °F	transparent polycarbonate plastic sheet MIL-P-83310	stretched acrylic sheet MIL-P-5425	polyvinyl butyral base flexible interlayer
tensile strength (ksi)	10.3	10.	3.
tensile modulus $\times 10^6$ (psi)	0.34	0.43	0.24
Poissons ratio	(0.3)	0.35	0.46
specific mass density (lb sec ² /in ⁴)	0.000112	0.000111	0.000102

for pyramidal impact loading, was modified for selective grid sizes up to $NG = 33$. Table VIII contains the values of NG , NQ and NM for the computer input. Grid size chosen for analysis of shot WT-18 is $NG = 21$. Table IX shows results for an unrelated case of the occurrences of maximum/minimum pane center stresses and deflections for different grid sizes. Values can be seen to converge at finer grid sizes. For grids, $NG \geq 25$, the program was found to be unstable. The cause of this instability was not investigated.

The test frame for the 26" square panel shots was made of 1/2" cold rolled steel with 32" x 32" outer and 24" x 24" inner dimensions (Figure 29 a). Attachment bolt holes were located 1/2" aft of the inside edge. 1/4" diameter bolts of 60 ksi strength at 1 1/4" center spacing were used. Four (4) clamps were used to hold this frame with the mounted pane on a very rigid support. Positioning of the clamps was varied initially from test to test until the best possible clamping positions were established, causing no plastic deformation of the frame under impact to avoid subsequent refurbishment of the frame after every shot. Clamp locations were fixed from shot WT-6 on (Figure 29 b). Locations of clamps were taken from the impressions of the clamps on the used hardware.

At a grid size of $NG = 21$, the clamping idealization is shown in Figure 29 b where the bolt-center lines (25" x 25") representing the lines of support are equivalent to one-directional support of the frame only. This arbitrary decision for simplicity of support condition neglects the rotational behavior of the frame.

TABLE VIII

EQUAL MASS AND PYRAMIDAL LOAD DISTRIBUTIONS FOR DIFFERENT PRACTICAL GRID SIZES

Grid Size NG	Quotient NM $DMM = \frac{MPANE}{NM}$	Quotient NQ Unit Load = $\frac{QTOT}{NQ}$
5	5	2
9	17	20
13	37	70
17	65	168
21	101	330
25	145	572
29	197	910
33	257	1160

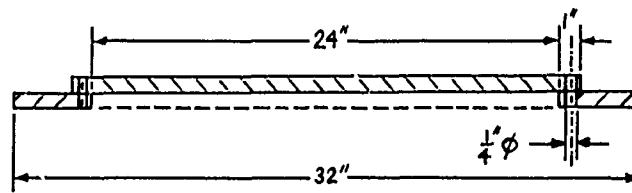
TABLE IX
COMPARATIVE RESULTS AT DIFFERENT GRID SIZES

grid size	max/min center stress ⁺ (ksi)	time of occurrence (sec)	max/min center deflection ⁺ (in)	time of occurrence (sec)
5	-60.7	0.005	33.3	0.005
	61.0	0.015	-33.2	0.015
9	-38.6	0.005	16.0	0.004
	40.2	0.012	-16.3	0.012
13	-31.4	0.005	13.4	0.004
	34.6	0.011	-13.5	0.011
17	-31.7	0.005	12.3	0.004
	31.4	0.010	-12.1	0.010
21	-31.6	0.003	11.6	0.004
	31.5	0.011	-11.7	0.010

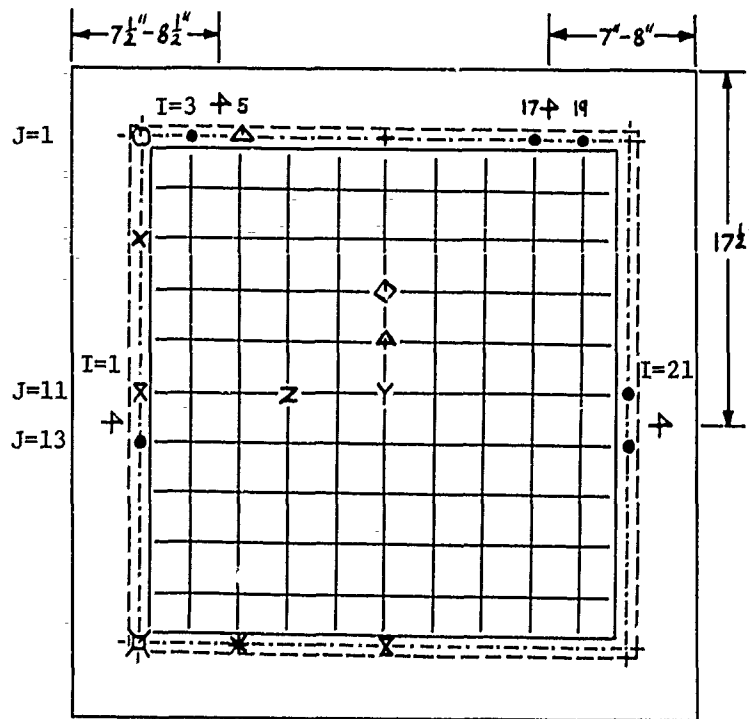
(discontinued because of instability of parameters of computer program (blow-up))

(⁺print-out recorded every 10th step)

panel size 25" squared
time step 0.0001 sec



(A) DIMENSIONS OF TEST PANEL MOUNTING FRAME



(B) CLAMPING IDEALIZATION, CHOICE OF GRID SIZE, NG=21, 12 SYMBOLS REPRESENT LOCATIONS FOR DEFLECTION HISTORIES IN FIGURE 28.

(↖ ACTUAL CLAMP LOCATIONS FOR WT-6 AND ON)

Figure 29. 26" x 26" Test Panel Mounting Fixture

The calculated bending stiffness of the frame, using the formula $EIF = E_{\text{steel}} \times \text{width} \times \text{thickness}^3/12$, is approximately 1.3×10^6 pound-in². Total mass of the pane without frame based on the weight given in Figure 28 is 0.0615 pound-sec²/in.

Total mass density of the frame is $\rho_{\text{steel}} \times \text{volume} = 0.72 \times 10^{-3} \times 224 \sim 0.16$ pound-sec²/in. The overall spring stiffness of the frame in the downward mode of deflection is assumed to be $k_w = 100,000$ pound/in and a very small number in the upward mode. Spring stiffness k_w in the upward mode due to clamping at the eight (8) idealized locations (Figure 29 b), is 100,000 pound/in. For a bird velocity of 854.7 ft/sec for WT-18, vertical impact and parallel sliding velocities at an inclination of 23° are 334 ft/sec and 786 ft/sec, respectively.

Using the normal velocity and the mass of a 4 pound bird in the force equation of Reference 42, the calculated force is 16,120 pounds. The impact time is 0.00133 sec or about 13 time steps of $\Delta t = 0.0001$ sec each. The effective bird dimension is ~ 5 ". Due to central impact, the sliding time is 0.00125 sec or longer. This yields the acting time of the impact pressure mound almost as long as it takes to slide across the pane towards the upper edge of the frame. A two step pyramidal load distribution was used in the analysis to account for the traveling pressure mound. It has a pyramidal central distribution lasting for time steps, NNNN=1 thru 7, and this distribution shifts midway between the center of plate and the upper frame (shift $J=J+6$) for NNNN=8 thru 12.

The following are the input data used to calculate the deflections at 12 different locations simulating shot WT-18 (Figure 30):

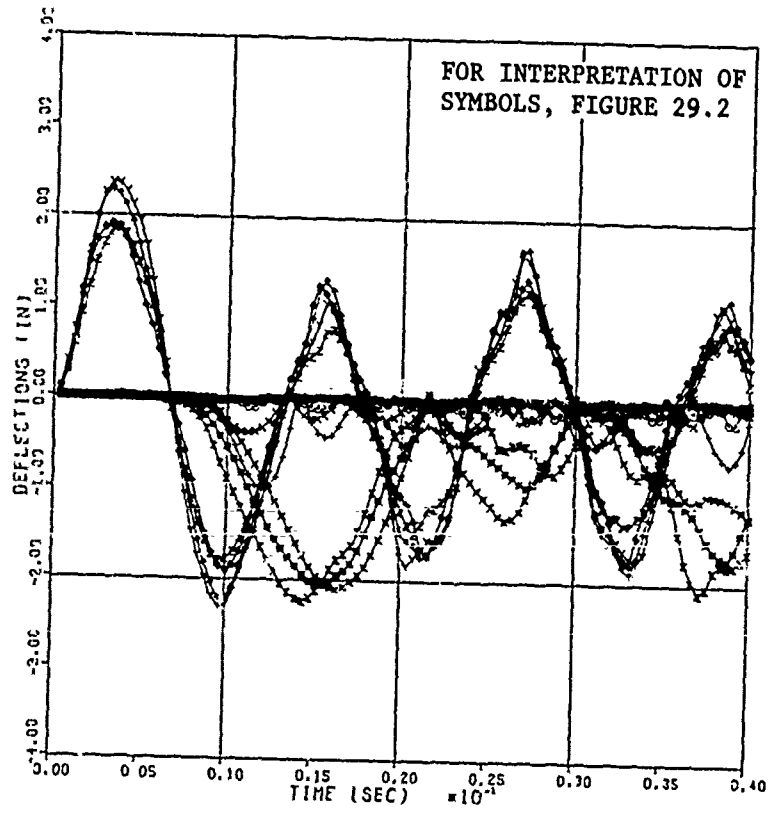


Figure 30. History of Deflections for Shot WT-18

Grid parameters - NG=21, NM=101, NQ=330

Panel dimensions - X=Y=25

Panel thickness - THICK=.956

E-module of laminated panel - EMØD=.329 E+6

Bending stiffness of frame - EIXF=EIYF=.129 E+6

Mass of pane element - DMM=0.0615/NM

Mass of frame element - DMF=0.1613/(2·NG-2)

Total impact load - QTOT=25,000

Time step - DT=0.0001

Spring stiffnesses chosen representing downward fixed support and upward free support at the eight clamping locations were: KW=100,000 (fixed) or 0.1⁻¹⁰ (free). Deflection data were calculated for 400 time steps totaling 0.04 sec. The data are plotted in Figure 30. The "Y" and "φ" marked curves in Figure 30 correspond closely with the test curves in Figure 7.

b. PRELIMINARY OPTIMIZATION OF MOUNTING FRAME

A scalar analysis of windshield/mounting frames had been conducted by means of the analog computer (or MIMIC) simulation language (References 49 and 50) as discussed in Section II-1. Series (A) and (B) runs for

$$M_W/M_F = \begin{Bmatrix} .1 \\ 1 \\ 10 \end{Bmatrix}, K_F/K_W = \begin{Bmatrix} .1 \\ 1 \\ 10 \end{Bmatrix} \text{ and } C_F/C_W = \begin{Bmatrix} .1 \\ 1 \\ 10 \end{Bmatrix},$$

(totaling twenty-seven (27) runs each) were conducted to: (1) find the range of parameters, M_W/M_F , K_F/K_W and C_F/C_W , representing quasi-rigidly mounted conditions; (2) find a difference between calibration assumptions (A) and (B), and (3) optimize mounting for lowest pane deflections relative to mount deflection, which is equivalent to lower dynamic stresses in the

pane. Follow-on runs were made for further optimization, an assessment of $F_0 t_I / M_W = \text{const}$, and vibration of the coupled system.

Using the values $M_W/M_F = \begin{Bmatrix} 1 \\ 10 \end{Bmatrix}$ and $K_F/K_W = 10$ at $C_F/C_W = \begin{Bmatrix} 0.1 \\ 1 \\ 10 \end{Bmatrix}$ resulted in extreme frame deflections, X_F , of only 10% of the pane deflections relative to ground reference, X_W . Therefore, deflections $X_W - X_F$, are approximately the same as in the unmounted case of infinite stiffness and mass of the frame (i.e. ratios $K_F/K_W = \infty$ and $M_W/M_F = 0$).

Figure 31.1 shows the eight-track histories of three cases of calibration (A), while Figure 31.2 shows the histories to calibration (B). Only slight individual differences in the two series of traces are observed. Table X identifies these analog records at the common tracing time factor of $2\text{mm} \approx 1\text{ ms}$. As an example, deflection variables, X_F (track 2), $X_W - X_F$ (track 5), and X_W (track 7) are at an identical scale and double that of X_W (track 1).

Figure 32 represents deflections, $20X_F$ at 2 V/L and $10(X_W - X_F)$ at 1 V/L, on tracks (2) and (5), respectively, for the mounted case with calibration (B). Run "1" in Figure 32.2 at $K_F/K_W = 1$, $M_W/M_F = 10$, and $C_F/C_W = 10$ gives the lowest window deflections (stresses) at these parameters. Runs "2", "3", "5" and "6" reveal that the frame limit deflection criterion arbitrarily set at approximately 2 inches has been exceeded in early time periods with the traces invalidated via built-in analog circuitry.

These analog runs were followed by further adjustments of the three parameters (Table XI). Use of the digital "MIMIC" code (References 49, 50) was supplemental (Table XII), and applied to cross-check results. For the entire series of runs of Table XI, the values $10(X_W - X_F)$ at 1 V/L for the flexible frame remained practically constant. $10(X_W - X_F)$

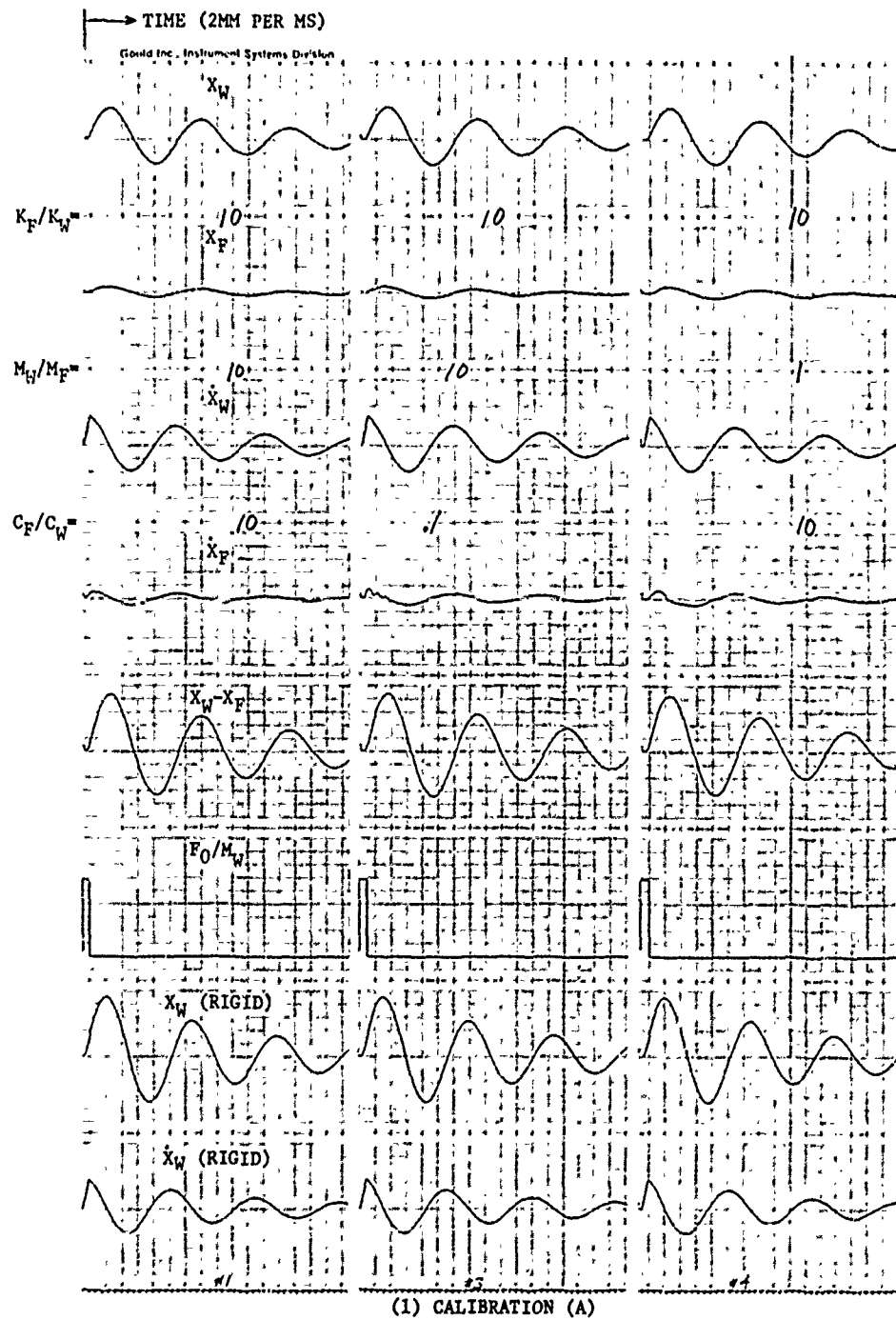
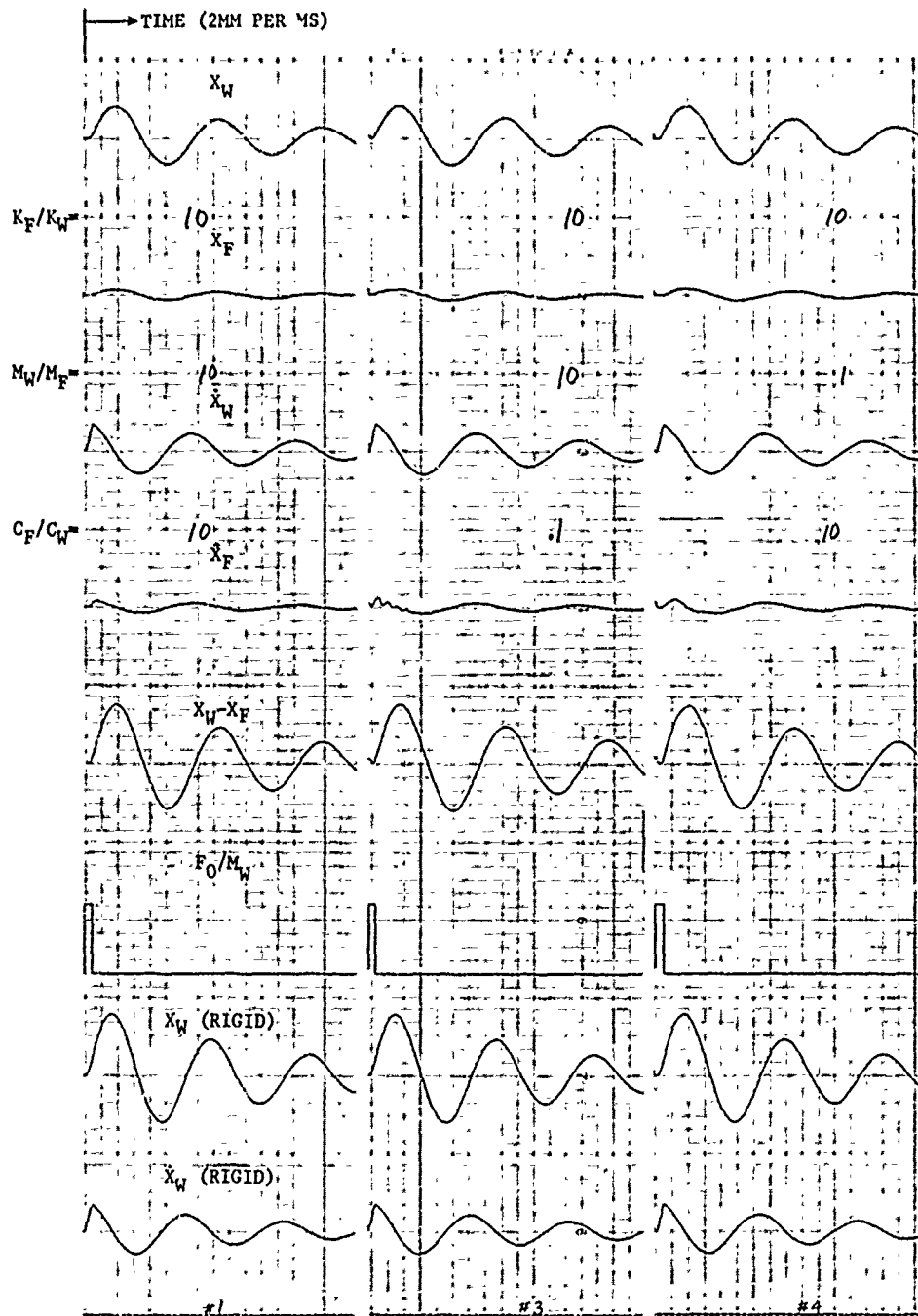


Figure 31. Eight-Track Histories of Three Analog Runs



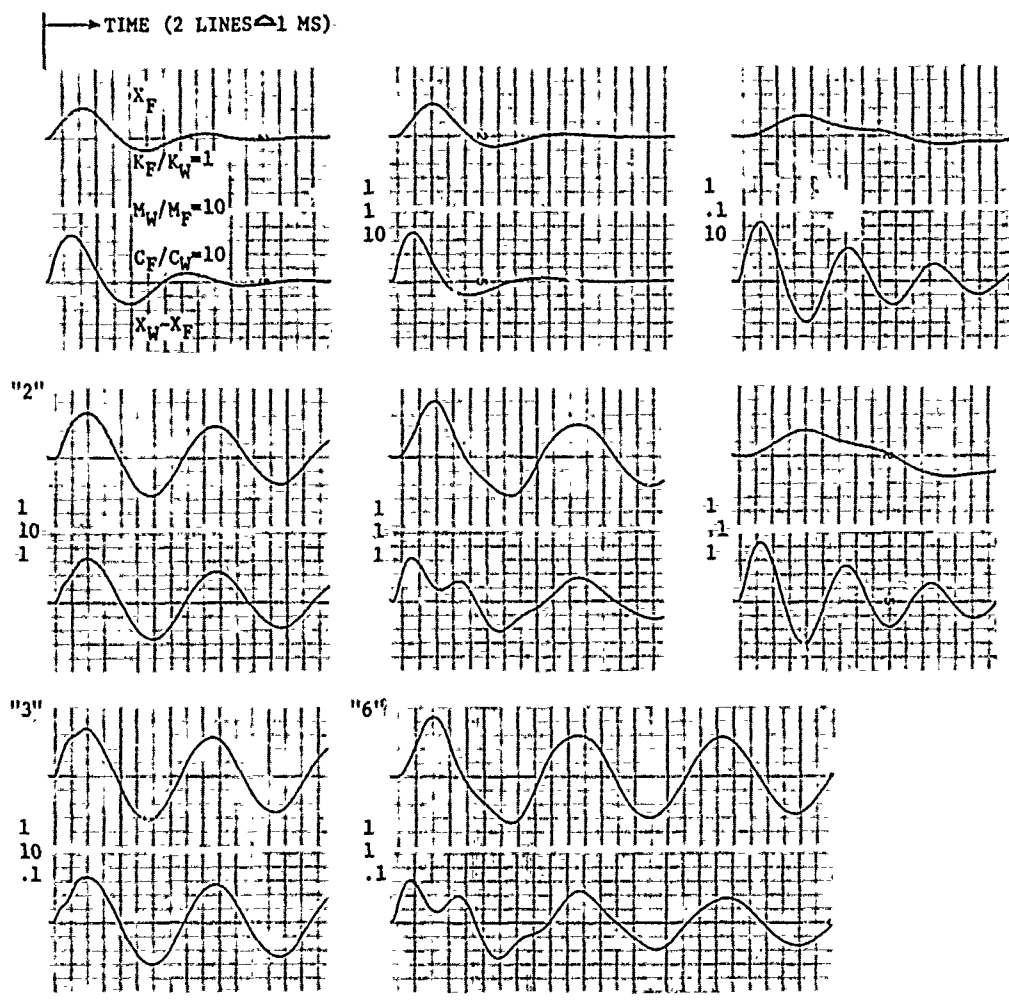
(2) CALIBRATION (B)

Figure 31. (Concl.)

TABLE X
IDENTIFICATION OF EIGHT-TRACK ANALOG COMPUTER RECORDS

track number	scale factored variable	recording parameter, V/L= analog volt output per line	
mounted frame	1	$10 X_W$	2
	2	$20 X_F$	2
	3	$.05 \dot{X}_W$	5
	4	$.05 \dot{X}_F$	2
	5	$10(X_W - X_F)$	1
rigid frame	6	$5 \cdot 10^{-5} F_0/M_W$	2
	7	$10 X_W$	1
	8	$.05 \dot{X}_W$	5

(See: Figure 31)



(1) PARAMETERS:

$$K_F/K_W=1$$

$$M_W/M_F = \begin{Bmatrix} 10 \\ 1 \\ .1 \end{Bmatrix}$$

$$C_F/C_W = \begin{Bmatrix} 10 \\ 1 \\ .1 \end{Bmatrix}$$

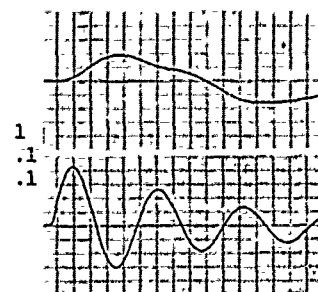


Figure 32. Deflections X_F (Trace 2) and $X_W - X_F$ (Trace 5) of Analog Runs

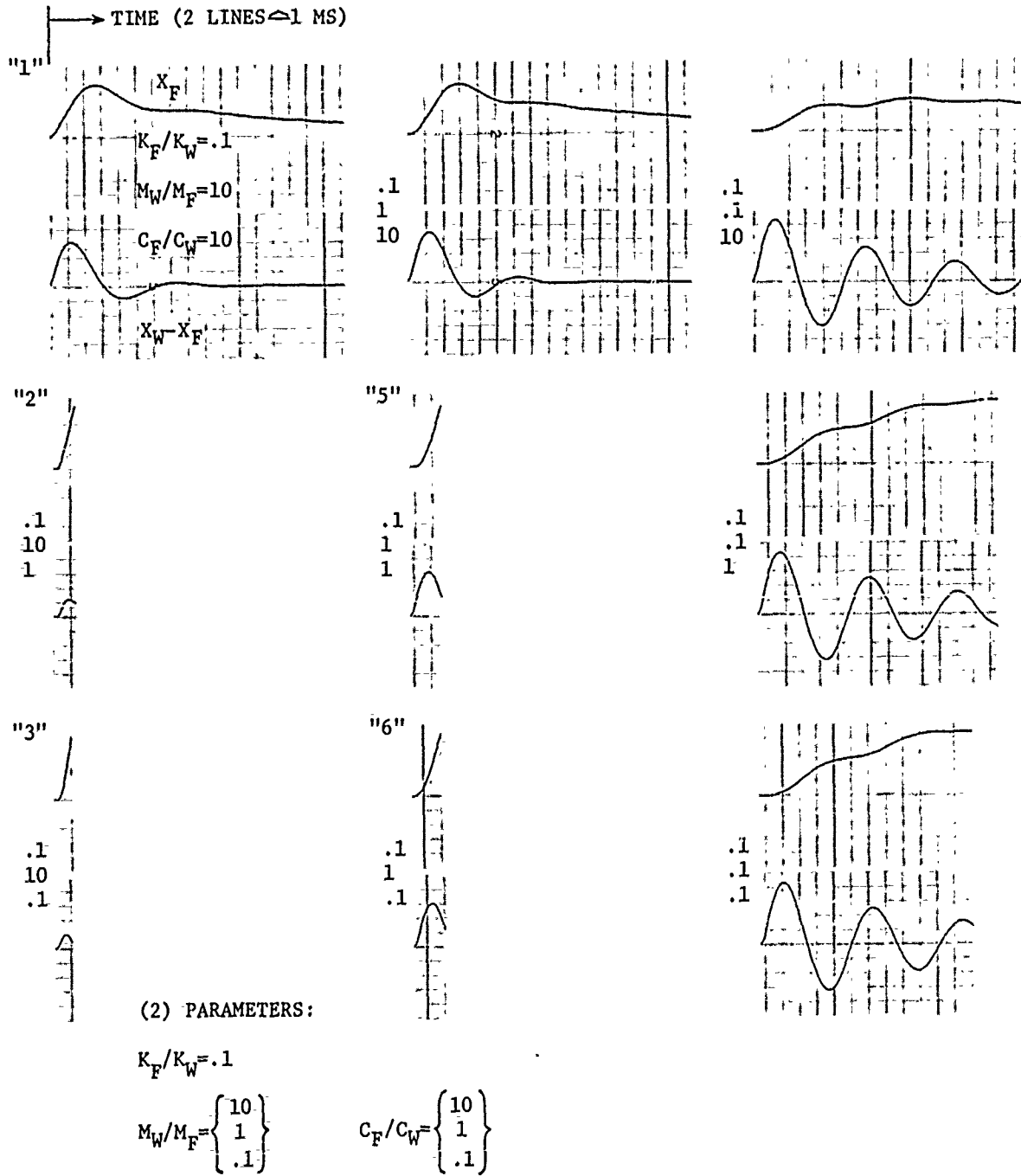


Figure 32. (Concl.)

TABLE XI

EIGHT-TRACK PARAMETERS FOR SERIES (B) ANALOG COMPUTER RUNS

Run	K_F/K_W	M_W/M_F	C_F/C_W	10 ($X_W - X_F$) at 1. V/L	
1	0.1	100	7	[lines] 13.4	
2	0.1	100	8		
3	0.1	100	9		
4	0.05	100	9		
5	0.01	100	9		
6	0.1	50	9		
7	0.05	50	9		
8	0.01	50	9		
9	0.1	10	9		
10	0.05	10	9		
11	0.01	10	9		14.8

Series (B): $(K_W/M_W)^{1/2} = 467 \text{ sec}^{-1}$
 $C_W/M_W = 76 \text{ sec}^{-1}$
 $F_O/M_W = 1.2 \times 10^6 \text{ in/sec}^2$ at $t_I = 10^{-3} \text{ sec}$

TABLE XII

MAXIMUM DEFLECTIONS, X_{WF} , FROM MIMIC X-Y PLOTS FOR SERIES (B) PARAMETERS

*** MIMIC SOURCE PROGRAM ***

```

*          CONSTANTS ARE M=MW/MF, K2=KF/KW, C2=CF/CW
          CON(M,K2,C2)
*          CONSTANTS ARE K1=(KW/MW)**2, C1=CW/MW, ZR=ZERO=0
          CON(K1,C1,ZR)
          PAR(FW,TI)
-----
          DT          .0005
*          F(T)=FW*MW T<TI; =ZR T=TI; =ZR T>TI
*          FBT=F(T)
          FBT        FSW(T-TI,FW,ZR,ZR)
          K3         K1*M
          K4         K3*(1.+K2)
          C3         C1*M
          C4         C3*(1.+C2)
*          THE MOUNTED FRAME
          D2XW      FBT-K1*(XW-XF)-C1*(D1XW-D1XF)
          D2XF      K3*XW-K4*XF+C3*D1XW-C4*D1XF
          D1XF      INT(D2XF,0.)
          D1XW      INT(D2XW,0.)
          XW        INT(D1XW,0.)
          XF        INT(D1XF,0.)
          XWF       XW-XF
          FIN(T,.04)
          OUT
          OUT(T, XWF, XF, FBT, FW, TI)
          PLOT(T, XWF, XF, FBT, FW, TI)
          END
    
```

Series (B): $FW = F_0/M_W = 1,200,000 \text{ in/sec}^2$

$K1 = K_W/M_W = 2.18089 \times 10^5 \text{ sec}^{-2}$

$C1 = C_W/M_W = 76 \text{ sec}^{-1}$

$TI = t_I = .001 \text{ sec}$

$ZR = 0.$

$M = M_W/M_F$

$K2 = K_F/K_W$

$C2 = C_F/C_W$

Run	K_F/K_W	M_W/M_F	C_F/C_W	$X_{WF} = X_W - X_F$ [in.]
1	.1	10	10	1.5
2			9	1.5
3			8.5	1.45
4			8	1.4
5			7	1.38
6			5	1.2
7			1	.6
8			.1	.7

for the rigid frame is about 1.53 times higher than the flexible values 10 $(X_W - X_F)$. X - Y plots of runs "1", "5", and "7" (Table XII, Figure 33) reveal the penalties of high frame deflections, X_F , for low window pane deflections, $X_{WF} = X_W - X_F$; for the latter two runs, MIMIC run "1" of Figure 33 is identical with analog run "1" of Figure 32.2.

The results of this preliminary optimization study of the frame properties, K_F/K_W , M_W/M_F and C_F/C_W , are useful in conducting a detailed finite difference optimization of the window mounting system that best suits impact case WT-18.

A study of varying F_0 and t_I (keeping $F_0 t_I / M_W = \text{const}$) was conducted by analog and duplicated by MIMIC runs (Table XIII). Results reveal a decrease in maximum excited amplitude response, $(X_W - X_F)_{\text{max}}$, by lowering F_0 / M_W and elongating t_I . This simulates heavier birds at lower impact velocities. Table XIII shows that the effort of mounting the window for shock absorption in case of the heavier birds becomes inefficient.

It is important to note that $1/2 \cdot K_W / M_W \cdot (X_W - X_F)_{\text{max}}^2$ is the maximum potential strain energy per unit window mass accumulated during the first downward mode of deflection after impact.

Vibration of the coupled system, with the traces X_F and $X_W - X_F$ nearly in phase, may be seen in Figure 32.1. At 2 lines per ms, runs "2" and "3" ($K_F/K_W=1$, $M_W/M_F=10$) indicate 38 1/2 lines per cycle or about 52 Hz. Run "6" ($K_F/K_W=M_W/M_F=1$) yields 46 Hz \sim 289 rad/sec. Using the system constant, $(K_W/M_W)^{1/2} = (218089)^{1/2} = 467 \text{ sec}^{-1}$, the upper λ_2 -line in Figure 4 (eigenvalues), and the (h) - line (of ω_2) in Figure 5, frequencies of the quadratic eigenvalue problem, satisfy the conditions of run "6" of Figure 32.1.

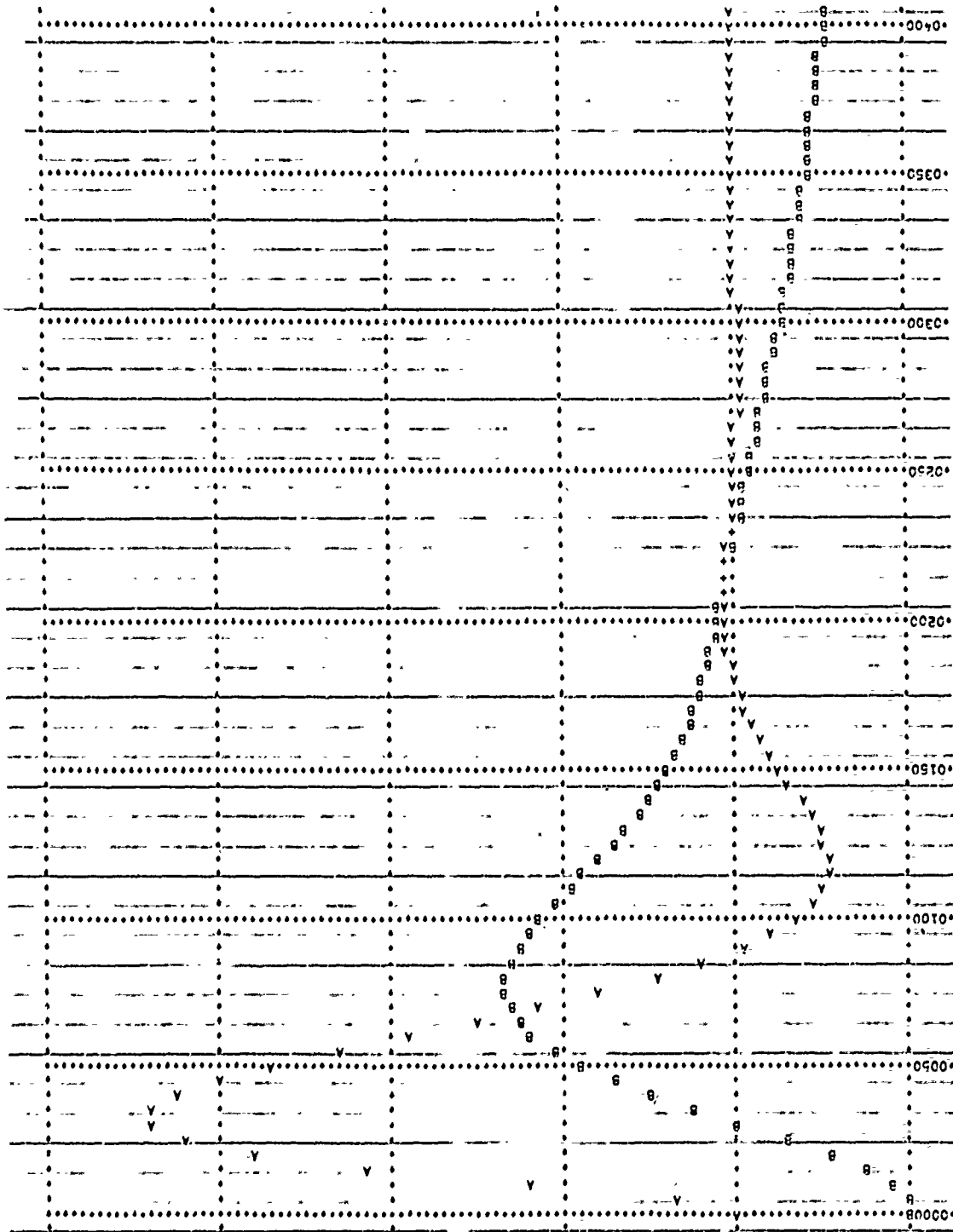


Figure 33. (Cont'd)

A*XF 0000
 B*XF 0000
 C2 7*0000E 00
 M 1*0000E 01
 K2 1*0000E-01

0000 1*0000
 0000 2*0000
 0000 3*0000
 0000 4*0000
 0000 5*0000

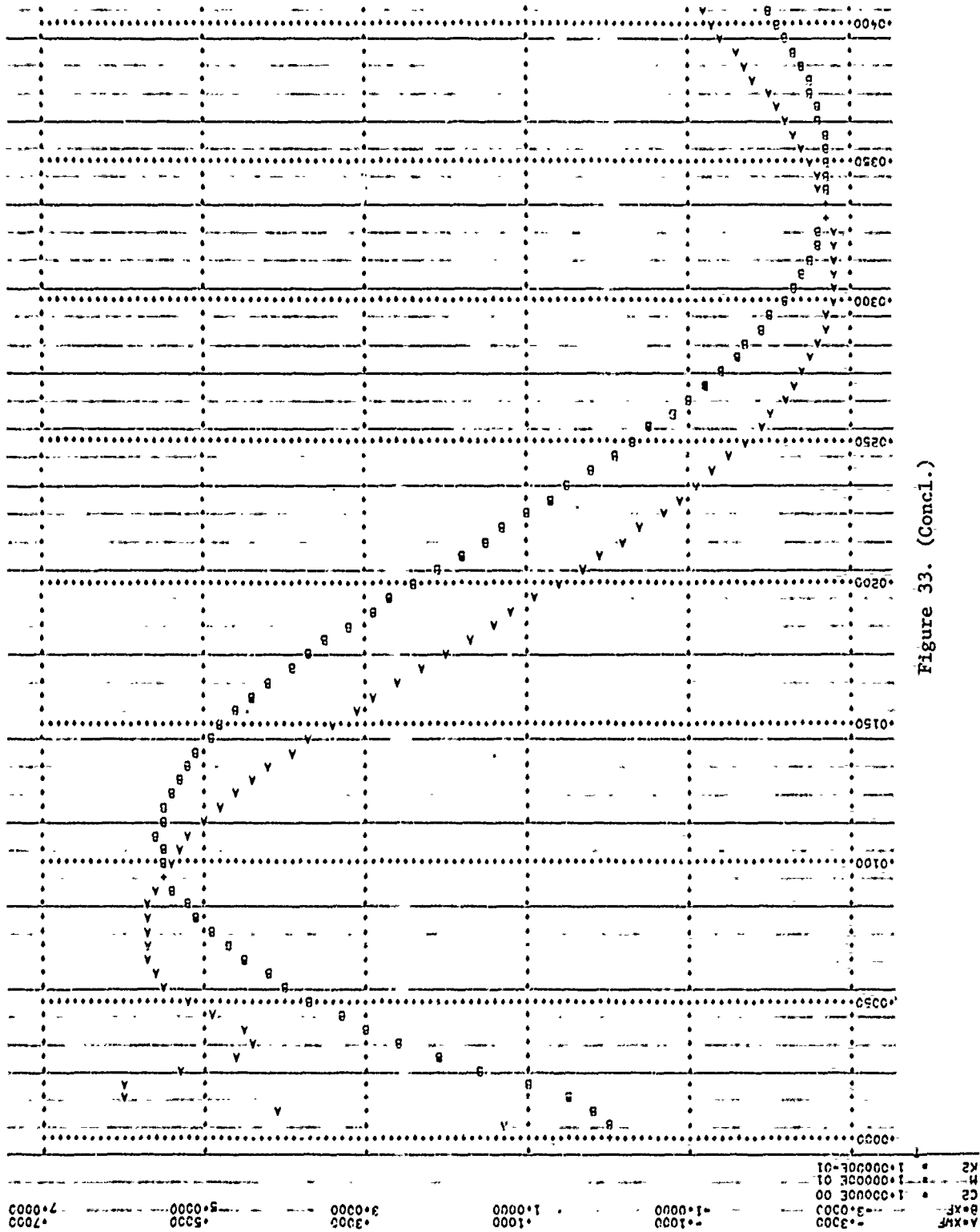


Figure 33. (Concl.)

TABLE XIII
 SERIES (B) ANALOG AND MIMIC RUNS FOR SQUARE IMPULSE,
 $(F_0/M_W) \cdot T_I = \text{CONSTANT}$

Constants:

$(K_W/M_W)^{1/2} = 467 \text{ sec}^{-1}$	$F_0 T_I = 1.2 \cdot 10^3 \text{ in/sec}$	$C_W/M_W = 76 \text{ sec}^{-1}$
$K_F/K_W = 0.1$	$M_W/M_F = 10$	$C_F/C_W = 9$

Analog Results (duplicated by MIMIC):

Run	T_I [ms]	mounted case $10(X_W - X_F)_{\text{max}}$ at 1 V/L [lines]	rigid case $10X_{W\text{max}}$ at 1 V/L [lines]
1	0.1	15	23
2	1	14.8	22.8
3	5	12	18
4	10	7	9.8

(10 lines = 1 inch deflection)

2. THEORY/TEST CORRELATION OF WINDSHIELD (F-111)

The finite difference analysis method (see Appendix IV-4 for computer program) was used to simulate the experimental strain gage readings of the windscreen/canopy of a bird strike exposed F-111 module, with gages mounted at designated locations in the vicinity of the T-intersection of arch and head beam (Reference 30). The glazing material of both F-111 windshields was monolithic polycarbonate (0.9" thick), impacted by a 4 pound bird. The records of the following shots: (1) on the center of one of the windshields, FM-1, (2) one at the corner of the windshield, FM-2, and (3) one at the center of the head beam, FM-7, were available for analysis (Table XIV). Shot FM-1 is compared herein with the theoretical results.

Theoretical impact loads for shots FM-1, FM-2, and FM-7 were estimated using the empirical power laws of References 33 and 34. They are presented in Table XIV. The calculations for shot FM-1 are: impact velocity, $V_{FM-1} = 932$ ft/sec, and angle of inclination, $\sim 22^\circ$, give normal velocity, $V_n = 349.5$ ft/sec, and parallel velocity, $V_t = 865$ ft/sec. The bracket of probable impact loading [(using the less severe MacAuley equation) $F = 0.05835 \times W^{2/3}$ (pound) $\times V^2$ (ft/sec), and the sinusoidal average of the original Mitchell equation, $2\hat{F}_1/\pi = 0.1156 \times W^{2/3}$ (pound) $\times V^2$ (ft/sec)] is 17,970 thru 47,900 pounds. Duration of impact is given by bird dimension/ $V_n = 0.00122$ sec (MacAuley) and $3/8$ bird dimension/ $V_n = 0.00045$ sec (Mitchell).

The common impulse, force \times time, is 21.85 pound-sec. Time of travel is distance/ $V_t = .00218$ sec. The bird disintegrated after having

TABLE XIV
F-111 WINDSHIELD/CREW MODULE BIRD STRIKE TESTS AT AEDC

shot No.	location of impact (in)	observed failure	measured velocity (ft/sec)	measured velocity (kt)	distance to travel (in)	time to travel (sec)	sinusoidal average loads (lb) (MacAuley)(Mitchell)	acting times (sec) (MacAuley)(Mitchell)	calculated impulse (lb-sec)
center of windshield FM-1	13 1/8 in. distance \perp from centerline head beam; 22 5/8 in. from centerline aft arc \parallel head beam	crack in corner	932	551	22 5/8	0.00218	17,970* 47,900*	0.00122 0.00045	21.9
corner of windshield FM-2	8 1/8 in. \perp from centerline head beam; 7 7/8 in. distance \parallel head beam from centerline aft arc	disintegration of arch (1 inch)	897	530.5	7 7/8	0.00079	15,750 42,550	0.0127 0.000477	20.0
center of head beam FM-7	center of 51.5 in. head beam	no failure after patch up of FM-2 damage.	901.8	534	25 3/4	0.00256	16,850 44,900	0.0124 0.000465	20.9

(*Load chosen for FM-1: 31,800lb)

covered .0012/.00218=55% (MacAuley) and .00045/.00219=20.6% (Mitchell) of the distance traveled over the windshield.

High speed photography of test FM-1 indicated that the impact load corresponds closer to the MacAuley load (17,970). The load initially was set at an arbitrary 127,200 pounds times a factor FRC (see notation FRC in Appendix IV-4). FRC = .15 was chosen, yielding 19,200 pound of load at initial impact, to match the experimental with the theoretical curves (Figures 35 and 36).

The idealized centers of impact in the nodal grid and the subsequent spread of the traveling debris over the windshield area were determined approximately using pertinent data from Table XIV. They are given in Table XV. Table XVI gives the input time histories of the normal and tangential load components, Q_n , and Q_t , respectively for the "F-111 windshield" subroutine, i.e.,

$$(Q_t)_{x-\frac{1}{2},y,t} = \frac{1}{2} Q_{x,y,t} (\sin \phi)_{x-\frac{1}{2},y} \quad (74.1)$$

$$(Q_n)_{x,y,t} = Q_{x,y,t} (\cos \phi)_{x,y} \quad (74.2)$$

$$(Q_t)_{x+\frac{1}{2},y,t} = \frac{1}{2} Q_{x,y,t} (\sin \phi)_{x+\frac{1}{2},y} \quad (74.3)$$

Figure 34 taken from Reference 35 shows the strain gage location for shot FM-1 and the corresponding idealized nodal point coordinates at which time histories of bending moments were determined. These bending moments were transformed into strains for the purpose of comparison.

The FM-1 case of the F-111 windshield is analyzed at fixed grid size (17 x 17) and with the window pane and frame parameters fixed at all trans-

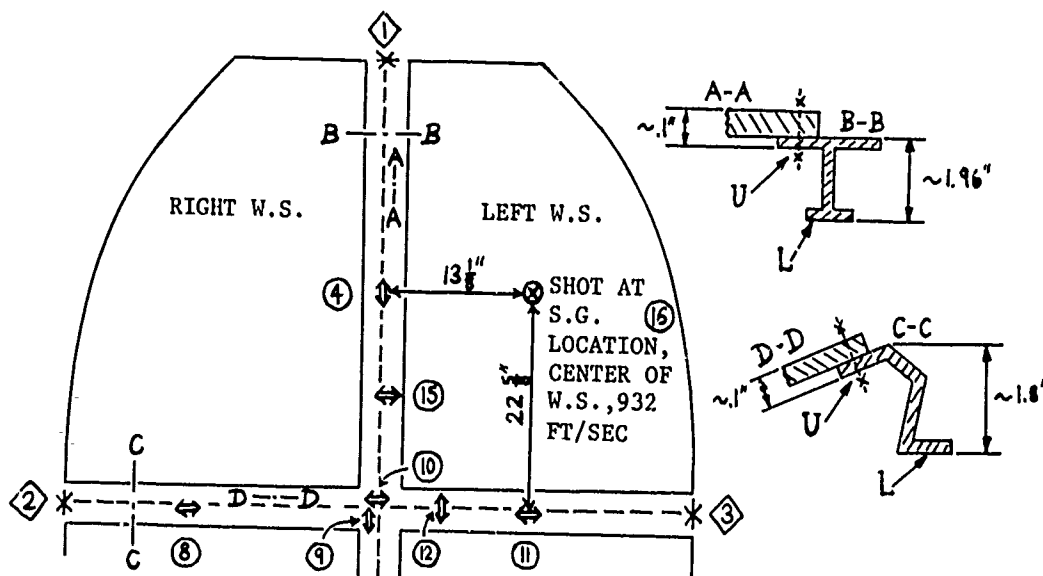
TABLE XV
 IMPACT TIME HISTORIES FOR SHOTS FM-1, FM-2 AND FM-7

% of FM-1 load Q(I,J)	nodal point		time step N	% of FM-2 load Q(I,J)	nodal point [†]		time step N	% of FM-7 load Q(I,J)	nodal point		time step N		
	I	J			I	J			I	J			
100	13	9	1 thru 5	100	11	15	1 thru 5	100	9	9	1 thru 5		
50	13	9 11	6 thru 9	50	11	15 17	6 thru 7	50	9	9 11	6 thru 10		
25	13	11 13	10 thru 13	(† approx. location of initial impact: I = 11, 10" distance from centerline of head beam, J = 15, 6.44" distance from centerline of arch head beam)								11 13	11 thru 15
12.5	13	13 15	14 thru 17									13 15	13 thru 20
6.25	13	15 17	18 thru 20									15 17	21 thru 24

(step $\Delta t = .0001$ sec)

TABLE XVI
 IMPACT LOAD COMPUTER INPUT FOR SHOT FM-1

	acting time steps									
	1	4	5	8	9	12	13	16	17	20
	calculated times (At = .0001 sec)									
	.0001	.0004	.0005	.0008	.0009	.0012	.0013	.0016	.0017	.0020
QT(4,9)	15900		7950		.1			.1		.1
QN(5,9)	31800		15900		.1			.1		.1
QT(6,9)	15900		7950		.1			.1		.1
QT(4,11)	.1		7950		3975			.1		.1
QN(5,11)	.1		15900		7950			.1		.1
QT(6,11)	.1		7950		3975			.1		.1
QT(4,13)	.1		.1		3975			1988		.1
QN(5,13)	.1		.1		7950			3975		.1
QT(6,13)	.1		.1		3975			1988		.1
QT(4,15)	.1		.1		.1			1988		.1
QN(5,15)	.1		.1		.1			3975		.1
QT(6,15)	.1		.1		.1			1988		.1
QT(4,17)	.1		.1		.1			.1		.1
QN(5,17)	.1		.1		.1			.1		.1
QT(6,17)	.1		.1		.1			.1		.1
Force components in pounds										994
										1988
										994



STRAIN GAGE NO.	THEORETICAL GRID LOCATION		DISTANCE FROM REFERENCE POINT (IN)		SECTION AND SURFACE LOCATION		ESTIMATED N.A. POSITION (IN)
	I	J	1	2			
④	9	9	①	28	B-B	L	0.98
⑮	9	13	①	25.5	A-A	U	0.5
⑧	13	17	②	17.5	C-C	L	0.9
⑨	9	17	①	52.5	C-C	L	0.98
⑩	9	17	②	36.5	C-C	L	0.9
⑫	7	17	③	31.5	D-D	U	0.5
⑪	5	17	③	17.5	C-C	L	0.9

(FROM REFERENCE 35)

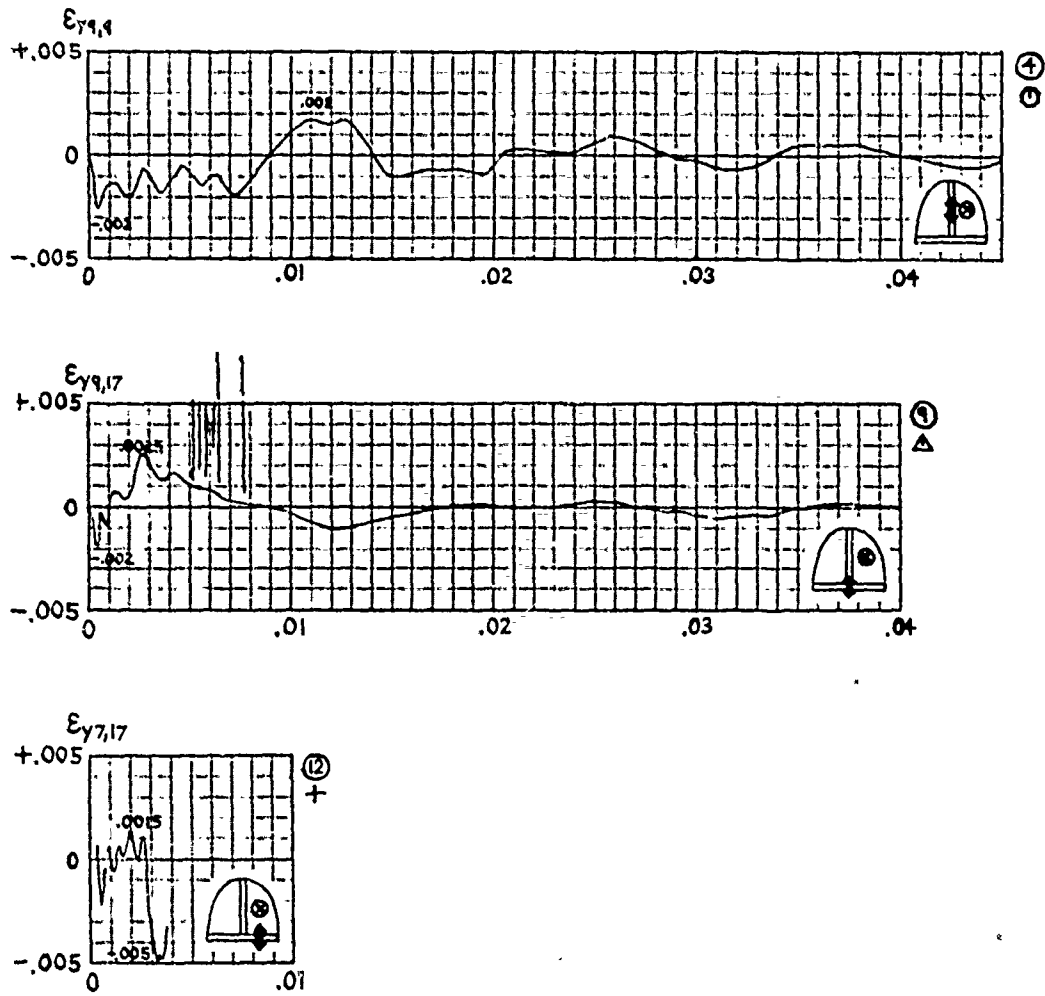
Figure 34. Strain Gage Locations for Case FM-1

ient time steps of computation. The input data for the computer program had to be assumed at various levels of confidence, by trial and error. The mass parameters of the bow and the sill (MBØW and MSIL), the constant representing viscosity of the pane (VISC), and most of the stiffness and damping properties of the boundaries at bow, sills and arch locations had to be experimented with. Other local adjustments necessary to match the theoretical results with the corresponding oscillograph traces from Reference 35, transcribed in Figure 35, were directly programmed in the computer code (Appendix IV-4: E1Y(9,7)=E1Y(9,7)*2. thru E1X(5,17)=E1X(5,17)/2.).

Figure 35 a shows three strains in the y-direction (direction of flight): $\epsilon_y 9,9$, $\epsilon_y 9,17$ and $\epsilon_y 7,17$. The last trace, $\epsilon_y 7,17$, should be considered partially invalid since the strain gage failed during the test. These three traces correspond to the series of curves shown in the upper portions of Figures 36. In Figure 35 b, four strain gage readings perpendicular to the longitudinal axis of the airplane are recorded. These strains, $\epsilon_x 9,13$, $\epsilon_x 13,17$, $\epsilon_x 9,17$ and $\epsilon_x 5,17$, correspond to the four curves shown in the lower portion of Figure 36.

As can be seen from these figures, discrepancies between the experimental (Figure 35) and theoretical results (Figure 36) were experienced. The inaccuracy of the model may be one reason for this.

In case of corner shot FM-2 at very low yield of the stiffer corner, acting load and time come close to the critical Mitchell condition. In case of the strain gage data of the center beam test, FM-7, damage from pre-



(A)

(FROM REFERENCE 35)

Figure 35. Transcripts of Oscillograph Traces for Shot FM-1

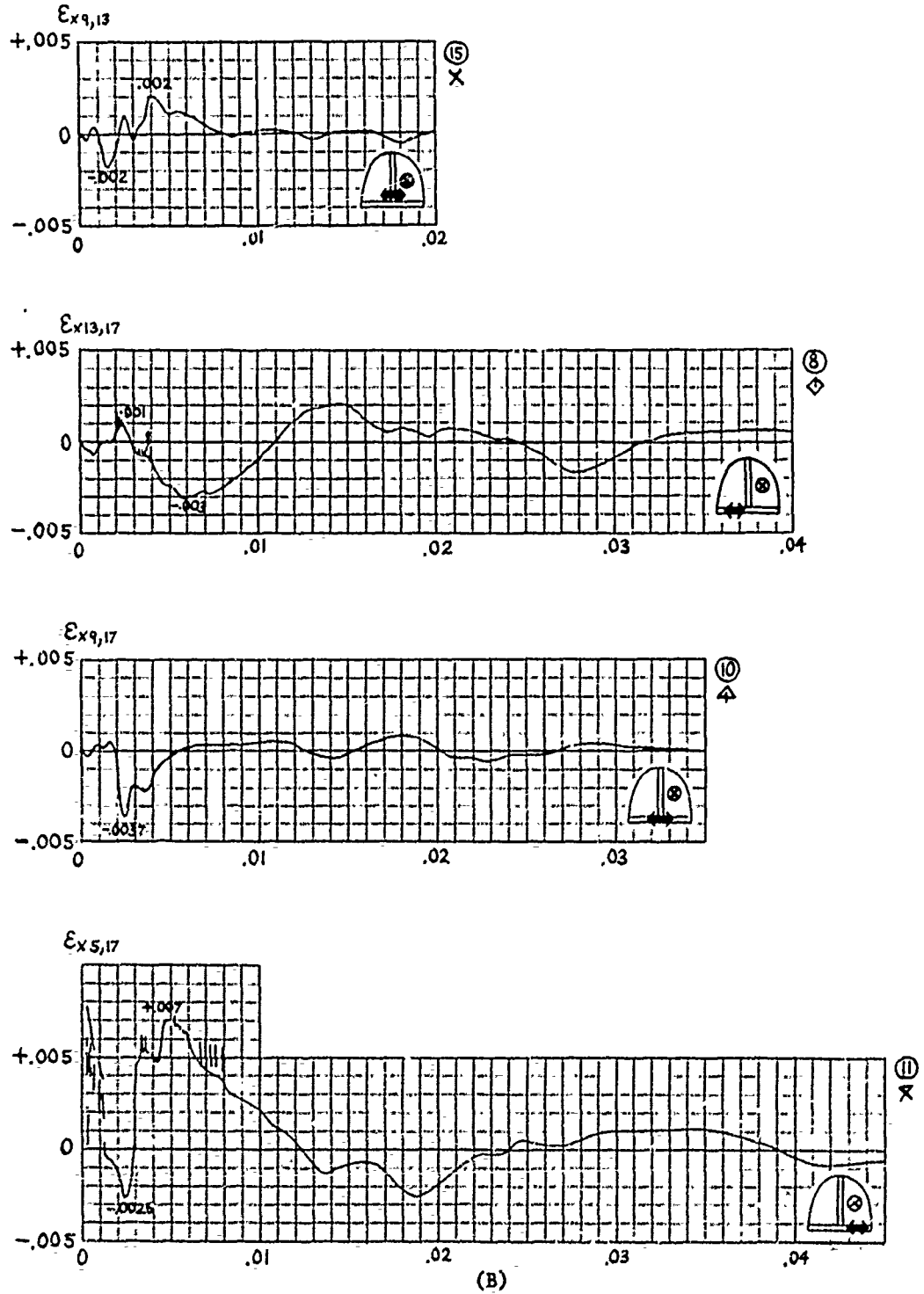


Figure 35. (Concl.)

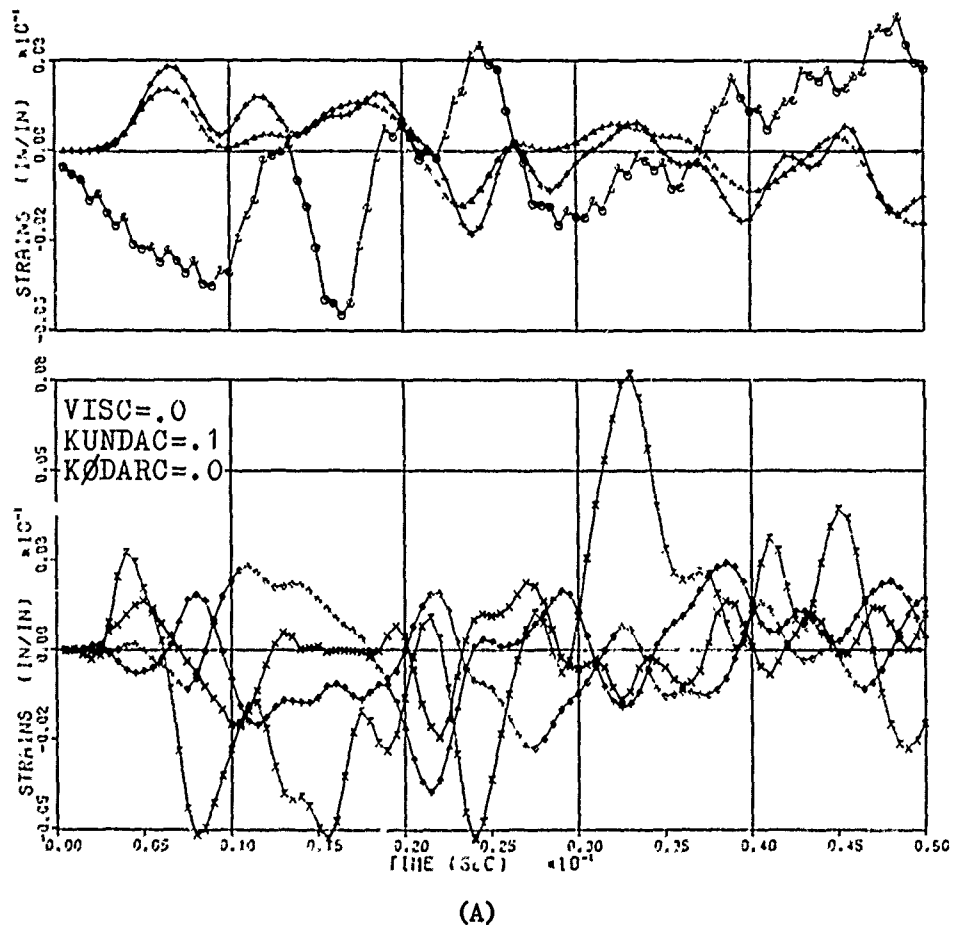
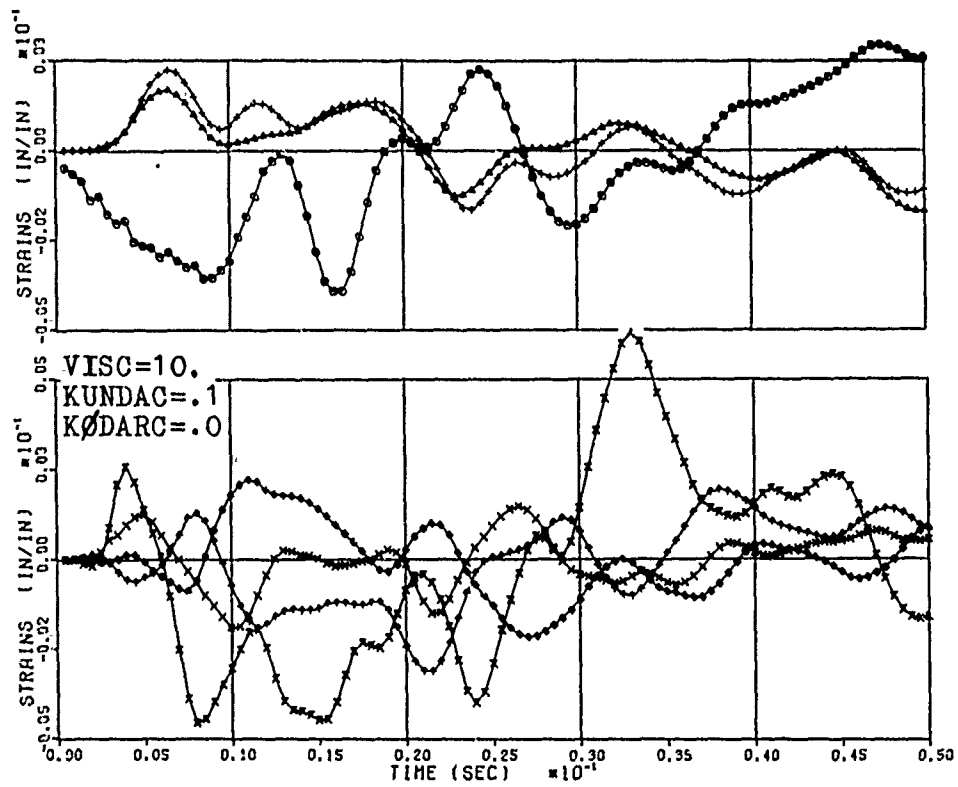
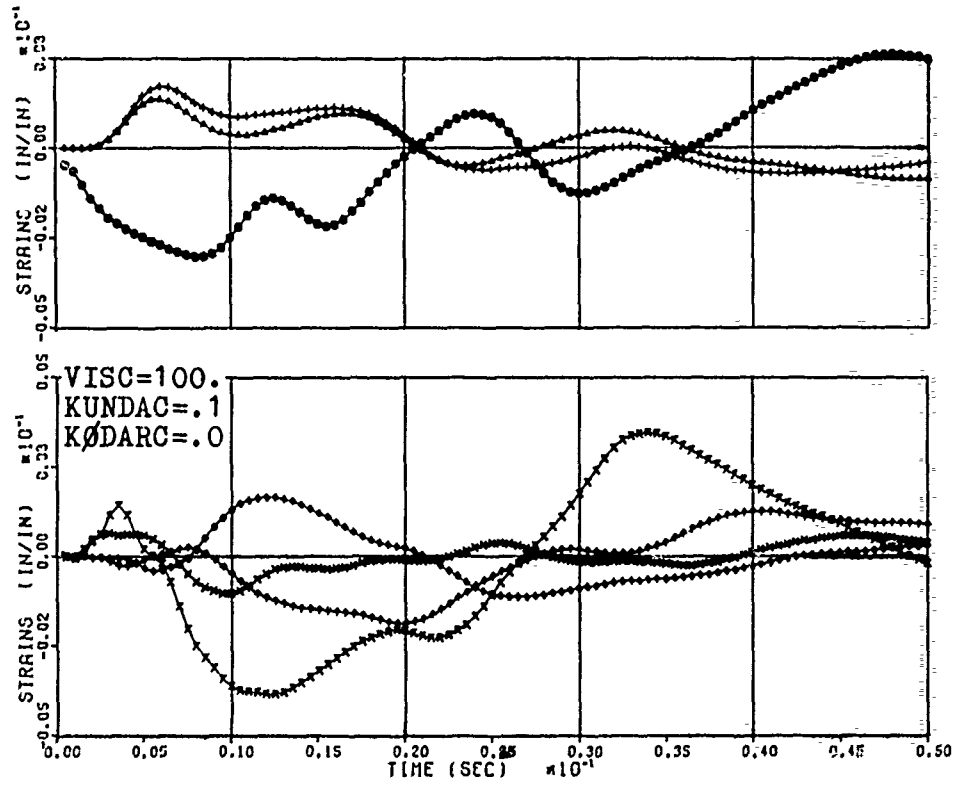


Figure 36. Theoretical Strain Gage Readings of FM-1



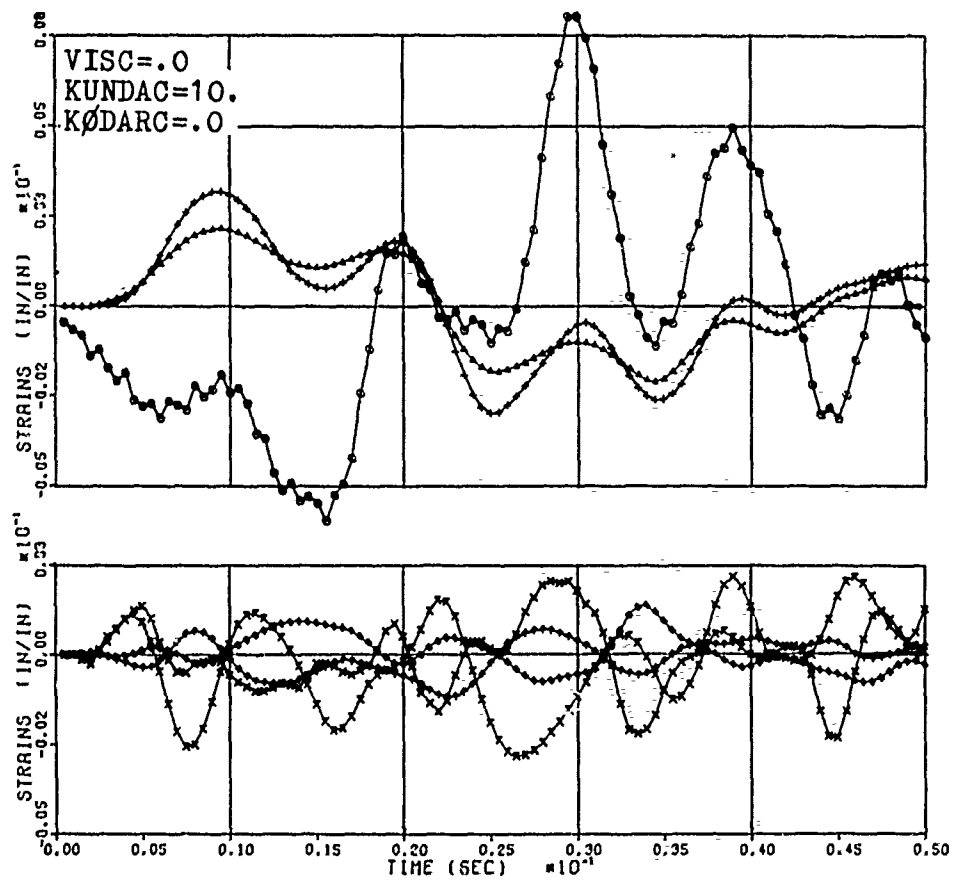
(B)

Figure 36. (Cont.)



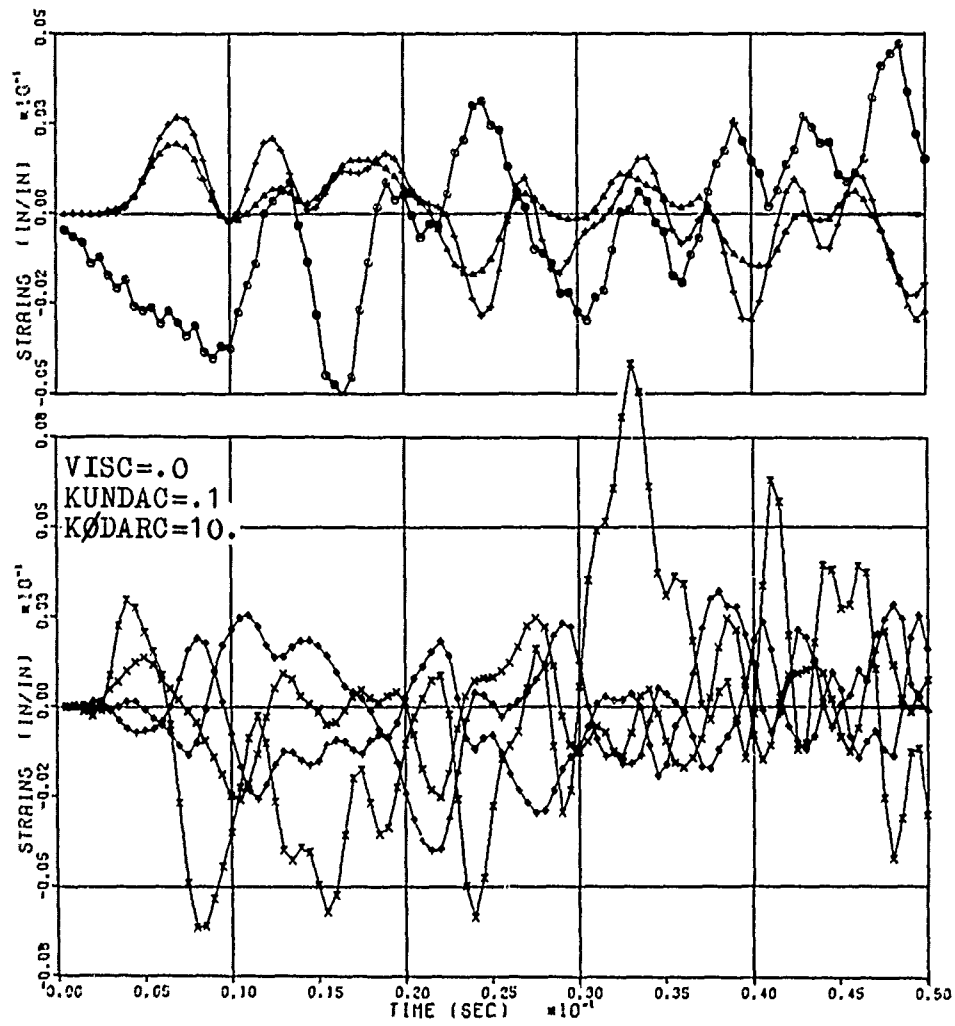
(C)

Figure 36. (Cont.)



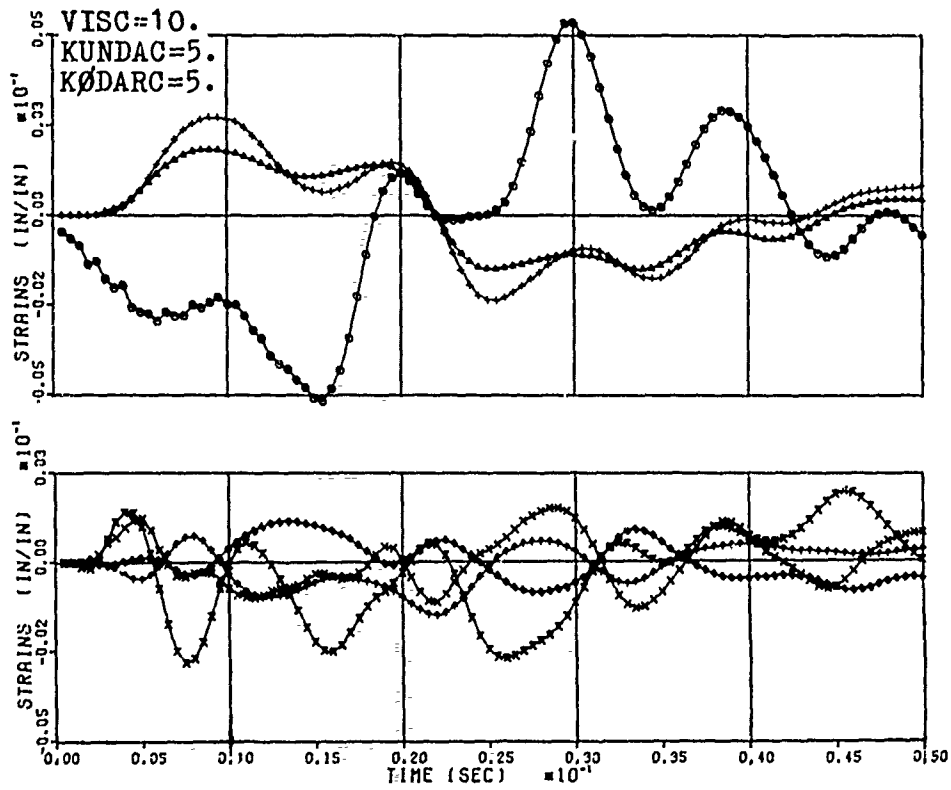
(D)

Figure 36. (Cont.)



(E)

Figure 36. (Cont.)



(F)

Figure 36. (Concl.)

vious tests and necessary strapping may have obscured performance of the module.

The computer input data for case FM-1 are shown in Table XVII. These data are in computer notation and the reader is referred to Appendix IV-4 for their identification.

A total of twenty-two stiffness and dampening parameters are considered in the computational scheme of FM-1. A parametrical study with just three value changes (low, medium, high) of each of these parameters would require about 3.135×10^{10} individual runs. It was determined, however, that local vibration characteristics can be influenced easily by local as well as overall parametrical changes. The parameters of the individual frame components, for example, the transverse and rotational dampening properties of the arch, KUNDAC and KØDARC, would have local influence upon the arch area. The parameters, EPANE and VISC, on the contrary, represent pane material characteristics and have overall influencing effects.

The strain gage data of case FM-1 was the only one readily available for use in the comparison of test data with theory. For this reason, only a small series of specific parameters was chosen to investigate their influence upon the strains at locations at which the strain gage data were recorded. Representative dampening parameters were selected to investigate the shock absorption provided. Parameters for the arch, representing a part of the frame, were chosen because it has much smaller stiffness than the head beam and therefore displaces more easily than the other frame components, and dampening is effective only due to displacement.

TABLE XVII
 INPUT DATA CHART FOR CASE FM-1 OF BIRD
 IMPACTED F-111 WINDSHIELD

DT	NNN	NP	CURV	ISHEAR	CØR
.0001	5000	5	.15	5	2

THICK	LHEA	WHEA	LSIL	WSIL
.9	51.5	3	44.5	3.5

RMIN	THMN	WBØW	RMAX	THMX	WARC
26.1	108.8	3	30.5	146.8	2

SPDEN	MHEA	MSIL	MBØW	MARC
.000122	.00054	.0085	.0052	.00038

EPANE	VISC
315000	variable

EIARC	EITAC	KUNAC	KØARC	KUNDAC	KØDARC
2960000	70000	200	10000	variable	variable

EIHEA	EITHD
640000	78000

EISIL	EITSL	KUNSL	KØSIL	KUNDSL	KØDSIL
1000000	100000	1000	10000	.1	.0

EIBØW	EITBW	KUNBW	KØBØW	KUNDBW	KØDBØW
10000000	100000	10000	100000	.1	.0

The parameters, in the nomenclature of the computer program (Appendix IV-4), are EPANE, VISC, KUNDAC and KØDARC. They are assumed equally distributed. EPANE = 315,000 pound/inch² is the calculated modulus of the pane, and the second chosen value, 200,000 pound/inch², represents a hypothetical low-modulus pane material. All assumed values of the remaining three parameters are simply "low-medium-high"; VISC = $.1 \times 10^{-10}$, 5, 10; KUNDAC = .1, 5, 10; KØDARC = $.1 \times 10^{-10}$, 5, 10.

A four do-loop set-up, a computer program modification, was used to generate all combinations of EPANE, VISC, KUNDAC and KØDARC. The different graphical plots of the strains in Figure 36 contain only five of these combinations. The pane stiffness for all six plots is 315,000 pound/inch². The remaining three parameters in order are: ($.1 \cdot 10^{-10}$, .1, $.1 \cdot 10^{-10}$), ($.1 \cdot 10^{-10}$, .1, 10), ($.1 \cdot 10^{-10}$, 10, $.1 \cdot 10^{-10}$), (10, .1, $.1 \cdot 10^{-10}$), (10, 5, 5), and (100, .1, $.1 \cdot 10^{-10}$), equivalent to parametrical runs "1", "3", "7", "19", "23" and a "hypothetical" one. The time span of T=.05 sec was covered by time intervals of DT = .0001 sec with the final time step NEND=500. The strains at every fifth step were plotted (NP=5). Similarly, tables of strains as well as deflections of all 54 runs were printed. The total of nine strains contain the seven at the recorded edge locations, and ϵ_x 5,9 and ϵ_y 5,9 at the initial impact location. The latter two strains were selected assuming that they represent the maximum stretch occurring in the pane. The print-outs of deflection histories consist of three groups of three columns each: UN(5,9), UN(5,13) and UN(5,17) tracing the route of impact on the impacted side, UN(9,9), UN(9,13) and UN(9,17)

along the head beam, and UN(13,9), UN(13,13), UN(13,17) at symmetrical locations of the opposite windshield. A matrix print-out of all variables (QN, QT, ØX, ØY, MX, MY, V, FN, FT, UN, UND, UNDD, UT) was generated for run "1" at every 50th time step (NP=50) to check the numerical ranges of all time-dependent variables. The original 17x17 matrices were printed in a reduced (clear) format containing no mid-way zero values.

These are general comments about the original strain data as compared with the six series of simulated strains. The transcripts of oscillograph traces seem to have much natural dampening when matched by the parametrical means provided in the model of FM-1. The strains in x- and y- direction oscillate quite smoothly with low peaks, and smooth vibration at the edges and corners is required not to crack and destroy the attachments. The simulation with VISC=100, KUNDAC=.1 and KØDARC=.1 x 10⁻¹⁰ (~0) looks favorable. A high value of VISC (Figure 36 f) has an effect on both the traces, longitudinal and lateral. However, it is felt that high overall dampening represented even by VISC=10 does not exist in the pane material.

Another initial observation is that the y-group and x-group of strains go independently thru similar changes (or one group is not affected at all) due to the individual change of one parameter. The reason that the four lateral strain gages oscillate at higher modes of vibration than the three longitudinal ones, an observation from all the charts of Figure 36, is a greater stiffness in flight direction than in lateral direction. Two of the longitudinal strain gages bend up, while one bends down, and three lateral gages bend up, while one bends down. This is due to the gage location.

A comparison of run "1" with "19" (Figure 36 a and d) shows that $VISC=10$ has little effect on changing strains without dampening provided by $KUNDAC$ and $K\phi DARC$. The three y-strains in "19" approach the original recordings of "1" (Figure 35). High translational rather than high torsional dampening (see case "7" vs. case "3") is more favorable for matching the strain gage recordings in the x-direction. The torsional dampening in "3" endangers the x-direction with high peak cyclic oscillation. The peaks are removed in run "7" with $KUNDAC=10$, but the frequency is still too high to match the experiment. Comparison of run "7" with run "23" shows that the x-strains in both the cases are almost identical, indicating that similar effects can be achieved via different means. Using run "23" as a new start for curve fitting, $VISC=20$ instead of 10, $KUNDAC=10$ instead of 5, and $K\phi DARC=2$ instead of 5 can be used for comparison.

The following comments result from an evaluation of the complete matrix print-out for run "1". All the matrices reflect non-symmetry due to the unsymmetrical loading condition. The matrices, printed every 50th time step for 500 steps, showed stability of solution during this time span. The results are of the same order of magnitude for all 54 different runs. The slopes, ϕX and ϕY , show maximum values of about ± 1.2 , initially, at the impact location. Later, at the 450th time step, the ± 1.1 limit for ϕX is exceeded at the opposite windshield area. This is due to the fact that run "1" contains practically no dampening of oscillations. On the second sheet of the print-out format, the matrices of moments, MX and MY , were calculated with values up to $\pm 1.2 \times 10^5$ pound-in. These were also computed

at the opposite side of impact from .03 sec on. The highest values typically occur at the sills for MX and at the front bow and arch for the MY moments. Vertical shear forces, FN and V, generate up to $\pm 2 \times 10^4$ pound, and tangential shear, FT, up to $\pm 5 \times 10^3$ pound. The third type of print-out sheet (UN, UND, UNDD, UT) initially shows the high values on the side of impact. Later, these are dispersed. High deflections, UN, in the pane, head beam and arch area are $\pm(1$ to 2) inches; velocities, UND, range less than $\pm 10,000$ inch/sec; accelerations, UNDD, less than $\pm 10^7$ inch/sec². Tangential displacements were calculated in the ± 1 inch range.

The strain and deflection histories of the 27 runs each of EPANE=315,000 pound/inch² (high) and 200,000 (low) have been compared. Both series were at 250 time steps with every 5th one (50) recorded. EPANE=200,000 pound/inch² caused overall lower frequencies of vibration. The first seven strains in the nine column strain tables pertaining to the metal edge frame members of the windshields indicate values with all strains up to $\pm .002$ in/in. The two-directional strains in the pane at the point of impact, the last two columns, are ten times those in the frame, in the range of $\pm .02$ in/in.

It is interesting to note the number of sign changes of strains, SX(5,9) and SY(5,9), in the tables as measures of frequency. SX(5,9) in the high stiffness case is both negative and positive at three different times. SY(5,9) is negative seven times and positive six times at higher frequency. During the first .025 seconds, strains SX(5,9) and SY(5,9) are a bit slower in the low stiffness case; negative three times and positive two times, negative six times and positive five times, respectively. The four x-strain gages oscillate at about the same frequency as SX(5,9); the three y-strain gages at about 1/3 of the frequency of SX(5,9).

The material response at impact grid location could be characterized as cyclic strain both of high frequency and magnitude. Peak values for case "1" are:

$$\begin{aligned} SX(5,9) &= -.0269, +.0118, -.0189, +.00804, -.00808, +.00686 \text{ and} \\ SY(5,9) &= -.0275, +.00448, -.00563, +.00553, -.00757, +.00081, -.014 \\ &\quad +.0128, -.0045, +.00593, -.00133, +.00692, -.00281 \text{ in/in.} \end{aligned}$$

The first peak values of strains, $SX(5,9)$ and $SY(5,9)$, are practically unchanged throughout all high stiffness cases. The peak strain reversals that follow the initial ones are very irregular from case to case. Higher cyclic stretch may be found in the x-direction rather than in the y-direction of windshield location (5,9).

Typical first strain reversals from minimum to maximum values for case "24" (high stiffness and combination 10, 5, 10) are: $\Delta SX(5,9) = .03579$ in/in and $\Delta SY(5,9) = .02895$ in/in. Second strain reversals (max/min) are $\Delta SX(5,9) = .02479$ in/in and $\Delta SY(5,9) = .00611$ in/in. The same strain reversals for the low stiffness case equivalent to "24" are; .0448 and .029 in/in for $SX(5,9)$; .03538 and .00744 in/in for $SY(5,9)$. This shows lower cyclic stretch for the stiffer pane. Here, stretch ratios of the two cases do not compare linearly with EPANE stiffness ratios.

Of further interest are the cases of cyclic stretch at impact location which do not repeat into the $\pm .01$ range. This is the case for $SY(5,9)$ in runs "12", "19", "20" and "21" (high stiffness). All $SX(5,9)$ exceed $\pm .01$ in/in at least twice after the first exceedance. A similar investigation could be conducted for the low stiffness cases.

The high and low modulus deflection histories (27 cases each) were investigated. Every deflection table contains three groups of three columns each, as mentioned previously. The first group of deflections on the impact side are characterized by higher values than the remaining deflections; up to two inches in the downward mode (positive values). The second group (head beam) possesses maxima up to 1.3 inch downward with 1 inch at the opposite side (third group).

The histories of the local deflections throughout the series are generally repetitive. These are the first deflection peaks and times of occurrence (for runs "1", "19", and "23") that have been found to differ to the largest extent in the first high deflection group:

$$UN(5,9) = 1.91(.002) / 1.85(.002) / 1.85(.002);$$

$$UN(5,13) = 1.9(.0045) / 1.8(.0045) / 1.8(.0045);$$

$$UN(5,17) = -.399(.0055) / -.368(.0055) / -.145(.005).$$

The second peak deflections are somewhat similar. The first peak deflections for the corresponding cases of lower pane stiffness are:

$$UN(5,9) = 2.45(.0025) / 2.36(.0025) / 2.36(.0025);$$

$$UN(5,13) = 2.36(.006) / 2.21(.0055) / 2.2(.0055);$$

$$UN(5,17) = -.396(.0065) / -.36(.0065) / -.124(.006).$$

Here, $EPANE = 200,000 \text{ pound/in}^2$ can be seen to cause higher deflections than $315,000 \text{ pound/in}^2$. Typical deflections at impact location are 1.91" and 2.45" for the high and low stiffness cases, respectively, yielding a ratio of 1:1.28 while the pane stiffness ratio is 1.58:1.

It may be concluded that the edge member strains in the impact environment of FM-1 undergo greater changes within the series of parametrical runs (see graphs of Figure 36) than the corresponding deflections.

SECTION V
RESULTS, CONCLUSIONS AND RECOMMENDATIONS

The feasibility of high-visibility bird-proof windshield design with existing glazing materials has been demonstrated. Novel window frame concepts with sufficient shock absorption capacity to accommodate part of the impact energy, thereby isolating the impacted window from damage, were examined.

The report presents the finite difference method of designing bird-proof windshields efficiently. It shows the parametrical design characteristics when using the developed computer routines and verifies the analysis method by simulating actual case data. The finite difference program modeling monolithic linear material under pure bending could be replaced by models of other material behavior including laminated arrangements. Modification of the computer routines, however, is not justified unless actual test data (combined deflection histories, strain gage readings, and details describing the material failure modes) are available. A more detailed bird impact model could be developed based on the results of realistic impact pressure distributions.

A computer program was developed using finite difference equations for the square window pane with attachment frame and shock absorbing mounting system under symmetric loading condition. Requirements on mounting conditions were determined by screening the appropriate parameters.

Flat plate analysis under realistic flight conditions of 1.2 Mach, an impact of a 4 pound bird, and technically achievable shock-absorption indicated that the dynamic peak stresses in the pane could be reduced

by 30% or more. This can be done by using a highly viscous damping system in connection with soft springs.

Damping represented by coefficients of 10 pound-sec/in at the boundary nodal points and spring constants of 25 pound/in acting at the same positions were found to be technically acceptable for the impact regime of up to 100,000 pound of 0.5 milli-sec duration. Spring-back deflections of the window frame went up to one inch (a technically acceptable compromise). Up to 90% of the energy was absorbed immediately after impact. Using the principle of conservation-of-energy and recording the time history of energies, it was found that the lowest dynamic stresses in the pane occurred for the mounting case for which highest amount of energy was absorbed.

The computer program, written to perform stress analysis of flat windscreen due to bird impact, was modified for conical shell analysis of fighter, bomber or attack aircraft windscreen canopies. A change from four to six first-order dynamic difference equations was necessary to account for the effect of curvature.

The input/output formats of the computer routines were modified to yield more fruitful information for design, and to avoid unstructured runs in the hit and miss experimentation for optimum systems performance. Energy absorbed and retained and extrema of stresses as functions of frequency response were accounted for by employing available mechanical properties (such as those for transparent polycarbonate plastic sheet).

Photomechanically recorded deflection data of the PPG laminated polycarbonate 26" x 26" test panel (shot WT-18) were successfully simulated.

The mass, stiffness and dampening parameters, M_f/M_w , K_f/K_w and C_f/C_w , for optimum mounting conditions were determined for this particular case using analog and MIC analysis techniques. This scalar approach, as described in the report, is an example of preliminary optimization of the best suitable window mount for an existing windshield.

Test data of the experimental strain gage readings of the bird strike on windscreen/canopy of an F-111 crew module (tests FM-1, FM-2 and FM-7) generated in a bird shot program at Arnold Engineering Development Center (AEDC), were provided by the Improved Windshield Protection ADP office. The conical finite difference computer program was used to analyze some of the data. Results have been matched successfully with strain gage readings for test FM-1. It was decided not to analyze data of test FM-2. In case of center beam hit FM-7, accumulated damage from previous tests and necessary strapping obscured the performance of the module.

The scope or recommended experimental work is to develop and physically demonstrate a shock absorbing window screen to ensure availability of the technology for future systems. The work should include three steps, namely to devise innovative concepts, to identify absorbed impact energies and to reduce maximum stresses of window pane as functions of the design parameters. Substantial effort should be devoted towards identification of those problem areas requiring additional research.

APPENDIX I

ASSESSMENT OF WINDSHIELD STRUCTURAL MATERIALS

The purpose of material assessment is to stimulate bird proof design by appropriate stacking of highly shock proof glazing materials and viscous, plastic interlayers at maximum allowable pane thicknesses for optical qualification. This consideration plus feasible end attachment to the mounting frame contributes to the accommodation of shock energy, thereby isolating the impacted window from damage.

An additional goal is to obtain transparency cross sections possessing the lowest life cycle cost that will meet the transparency/support structure system requirements. Sierracin's economical and innovative approach (Reference 51) of retro-fitting the upgraded Lockheed P-3 and Cessna T-37 windshields should be mentioned. The knowledge gained from these military programs is currently being applied to commercial aircraft windshields, such as the Boeing 747 and Lockheed L-1011 at substantial savings to the carriers.

The ability of different glazing materials and combinations of materials to withstand bird strike penetration and the failure modes that can be identified in case of damage varies widely (Reference 4). Actual windshields, of the F-4 for example, are known to have experienced initiation of breakage in the corners, which may suggest designing very stiff corners for specially vectored flexibility for stress relief. A suitable approach could be properly applied plastic paddings (Reference 27) and/or gussets.

The design variables for bird impact resistance are thickness of material, type of construction, edge attachment design, and supporting

structural frame (Reference 52) within the required geometry. A factor of safety to account for uncertainties should be applied to demonstrate enough strength of the windshield for thermal stresses since they occur due to thermal differential expansions or contractions. Lack of rigidity of the windscreen support structure generally results in lower bird impact resistance. Other poor design details which should be avoided are sharp corners, pre-existing material deficiencies, and poor quality of holes.

Too many laminas are disadvantageous for windshield strength (Reference 33). Windscreen panels laminated with PVB, with four .24" main plies of glass, instead of two .5" glass plies, tested at +50°C, indicate a reduction of failing speeds of approximately 20%. The shatter strength of laminated plate is highest at maximum specific strength of the laminas at optimum stiffness assuming the adhesives in the laminating process do not degrade the basic materials and weaken the laminated panel.

The bending stiffness of laminated plate with highly plastic interlayer(s) is reduced. Shear load distribution to account for shear deformation in addition to bending deflection should be considered in this type of laminate arrangement.

Proper design and fabrication of laminates must consider the compatibility of adherends having different thermal expansions. Optimally designed adhesive edge and corner bonds with the adhesive/glazing material interface behavior would distribute stresses evenly. This would eliminate fastener holes and corresponding stress concentration factors.

The major requirement for cockpit front windows to resist impact by bird and hailstones, makes some of the organic materials well suited to economical designs. Conforming to this requirement, the windows not only stop the missiles but retain a high degree of visibility after impact (Reference 53). A glass facing is often mandatory for the outside surface of these materials from the standpoint of durability (especially abrasion protection) and positioning of anti-icing films close to the outside for effectiveness.

The location of impact is another very important design factor (Reference 54). The failure strength of windscreens with four main ply laminations appears to be less critical for corner shots than those with only two main ply laminations. This supports arguments for tailored flexibility (and strength) where required (Reference 41, 42). No attempt should be made to design no-deformation characteristics into areas of probable bird strike. This would require immense strength (and weight) and it would not be practical except for small birds and low impact speeds. It is more practical to provide for yielding characteristics such that the impact is deliberately cushioned. The authors of References 41 and 42 mention other good design practices. Taper angles should be selected as sharp as practical. Surfaces should be kept perfectly smooth offering no projection against which the bird might pile up.

The bird impact problem is accentuated by the temperature effects due to kinetic heating of the interlayers (Reference 32), which on many present windscreen designs of sandwich-type assembly is taken into

consideration. Temperature of interlayers, particularly at their edges, where the panel is joined to windscreen frame have to be kept generally below 130°C, which is the upper thermal capability of organic materials. Proposed and on-going programs in the AF Materials Laboratory (AFML) include (Reference 1): efforts to develop a new adhesive and interlayer enabling the fabrication of polycarbonate composite windows; evaluation of abrasion resistant coatings for transparencies; and work on high temperature transparencies of polyarylsulfone for 400-500°F use.

An analysis must be conducted to determine the thermal windshield environment of subsequent design for measures to control temperature. The surface conditions of windshields at supersonic speed may be estimated using shock tables of air flowing around a cone. Assuming a cone opening angle of 22° (the approximate angle of inclination of a F-111 windshield), the steady flow condition for a low altitude case at $M_1=1.2$, ambient air pressure, $p_1=14.7$ psi, temperature, $T_1=520^\circ\text{Rankine}$, and density of air $\rho_1=0.07651$ pound/ft³ (density altitude=0), is as follows. A separated normal shock exists for these conditions with $p_2/p_1=1.513$, $T_2/T_1=1.128$, and $M_2=0.8422$. Indices 1 and 2 indicate conditions upstream of and after the shock, respectively. At a Prandtl number, $Pr=.7$, for air at 600°R, the recovery factor is $r=0.7^{1/3}=0.888$ (turbulent case). The conditions affecting the windshield at this low altitude case are: wall temperature, $T_2=198^\circ\text{F}$, pressure normal to surface, $p_2=22.2$ psi and (negligible) viscous drag friction of 0.026 psi. Similar calculations for a high altitude case of

$M_1=2.5$ at 50,000 ft, $p_1=1.69$ psi, $T_1=-67^\circ\text{F}$ and $\rho_1=.01161$ pound/ft³, indicate a conical shock wave of 34.3° opening angle, and the windshield conditions: $T_2=338^\circ\text{F}$ and $p_2=4.3$ psi.

Reference 32 contains a chart of skin temperature as a function of Mach number and altitude. At 0 degree incidence, .9 emissivity, and 2 ft distance from edge, the skin temperature in turbulent flow is fairly constant (100°C) for 40,000 to 120,000 ft altitude. In heat flow and thermo-stress analyses, discrepancies in the thermal properties must be considered. Typical values for glazing and frame materials are : coefficient of expansion for soda lime glass $\sim 9.$; PVB ($+25^\circ\text{C}$) 400.; and stainless steel ~ 20 in/in $^\circ\text{C} \times 10^{-6}$; and thermal conductivities of $\sim 15.$; ~ 2.5 ; ~ 90 Btu/ft²/h/ $^\circ\text{C}$ /in, respectively (Reference 32).

A full spectrum of fracture toughness data of glazing materials does not exist (Reference 16). The k-value of MIL-P-5425 and MIL-P-25690 acrylic sheet varies between 1 to 4 ksi $\sqrt{\text{inch}}$ as a function of temperature between -40°F and 150°F .

1. WINDOW PANE MATERIALS

a. LAMINATED GLASS

Basic glazing is characterized (Reference 32) as the one having the best optical properties, consistent strength, and stiffness over a wide temperature band, being unaffected by solvent attacks, and capable of maintaining strength when laminated. Glass is highly sensitive to fabrication and service induced scratches. High thermal conductivity

and low coefficient of expansion should be matched to that of the metal retaining frame.

The inherent brittleness of glass usually relegates it to a sandwich construction consisting of two or more layers of glass with a flexible plastic interlayer in between. Therefore, the thickness of the glass faces of the laminate have little effect on impact strength within reasonable limits, while the plastic interlayer at an optimum temperature has a dominant effect (Reference 16). Thin glass face sheets laminated to acrylic structural plies do not increase the penetration speed. They break at much lower speeds than the calculated failure speed of the composite (Reference 19). Laminated aircraft glazing is specified in MIL-G-25871A(1).

The average modulus of rupture of soda lime toughened glass is 27,000 psi, and of chemically toughened glass is 35,000 psi. 200°C is the suggested maximum temperature for operational use of glass. Cockpit enclosures for Mach 2.5 to 3 flight vehicles ($370^{\circ} \leq T \leq 560^{\circ} \text{F}$) of the non-laminated flat glass design showed the disadvantages of poor visibility, heavy weight (16 psf) and environmental control system (ECS) penalties.

Thermally toughened glass contains a built-in parabolic stress distribution through its thickness. The ratio of compression to central tension is 2 to 1 with the neutral layer at 21% of thickness below the surface (Reference 32). Moduli of rupture at rates of loading from 10,000 to 60,000 psi/min do not reflect strength behavior in rapid bird strike environment. The strength of flat glass, as represented by the modulus of rupture, is affected not only by the various strengthening treatments,

AFFDL-TR-74-155

but also by abrasion, which reduces the modulus drastically (Reference 16). In addition, the measured strength of a batch of specimens shows a wide scatter under identical test conditions.

Failure of combination glass windows is unpredictable. The 707 windshields are a combination of .2" semi-tempered glass outer ply, .38" hard PVB membrane interlayer with an electrical conductive coating, and .5" fully-tempered glass inner ply, sandwiched together and mounted in a rigid frame. Loading is a repetitive cycling of heat, cold, pressurization and pressure relief. High window heating is always required prior to descending from higher cruise altitudes. Thermal gradients thru the laminas are induced by temperatures of an average -40°F in outer atmosphere, 110°F in the PVB and 70°F inside. Holding pressure differential is 8.6 psi.

Bullet resistant glass is one of the recently developed cockpit survivability features of a close air support aircraft (Reference 55). The bullet-proof, bird-proof front windshield successfully defeated a 7.62mm armor-piercing projectile without generating any backface spallation.

b. FLEXIBLE INTERLAYERS

Interlayers of windshields must have good optical properties and adhesion to the basic glazing, chemical stability, solvent resistance, and high ductility over a wide temperature range (Reference 32). Bird impact tests of laminated windshields made with PVB plastic have shown impact resistance to be primarily a function of the interlayer thickness,

temperature, and the percent plasticizer content in the interlayer. PVB interlayers are most effective for penetration protection at 21% plasticizer, and heated to a temperature of about 90° to 100°F.

At lower or higher temperatures, the impact strength decreases rapidly (References 16 and 34). Differences in the behavior of glass or acrylic windows with thin (1 to 2 mm) PVB or cast-in-place (CIP) interlayers were found to be insignificant in the temperature range from 0° to 30°C (Reference 19). Windows with PVB interlayers of 5 mm thickness had to be at 18°C for comparative results.

Thick PVB interlayers play the part of an elastic member at 30° to 40°C. Temperature seems to have no influence on glass strength, only on PVB strength. The results of a theoretical study (Reference 56) indicate that for certain types of aircraft the time required for the entire vinyl layer of the windscreen to reach its optimum temperature may be greater than that required for the aircraft to clear the bird inhabited zone.

Under favorable conditions, ultimate strength of PVB interlayer material is about 2.7 ksi at a stiffness of 10^5 psi, and modulus of rupture is 3000 psi at 70°C. Changes of impact velocity up to 100 mph were experienced by modification of the flexibility of the supporting structure (Reference 34). In cases of bird-proof windshield designs (Reference 16), the thickness of the PVB interlayer was reduced 20% at the aft edges and corners to counter reduced flexibility there.

PVB is visually objectionable in thermal flight. It develops internal bubbles if exposed to temperatures above 160°F for very long periods, or 230°F for a few hours. The refractive index of plastic (as in PVB) is nearly the same as of glass (1.5 to 1.52). Haze in PVB at 2" thickness is less than 2%.

c. ACRYLIC COMPOSITE WINDSHIELD

In most glass windshields, the interlayer is structural, serving as the primary means for resisting bird impact, and also as the fail-safe member to prevent explosive decompression if the glass breaks (Reference 46). Where aircraft profiles require curved panels, plastic materials become an obvious choice (Reference 16). The first flat composite windshield was delivered to Douglas Aircraft Company as a part of a study of comparative bird-impact strength performed in 1961. In the case of the stretched acrylic plastic, its superior structural performance relegates the interlayer to merely a flexible bonding layer.

The effect of temperature in the range -40°C to +50°C on the failure speeds of acrylic windscreens is generally small. The stretched acrylic materials are more critical than glass at the lower temperatures, whereas the reverse is true for higher temperatures. Monolithic acrylic panel results show failure speeds approximately 15% lower than multi-laminated panels of the same total stretched acrylic thickness (Reference 54). When as-cast and stretched acrylic are bonded together to a flat window, they behave as if the window were completely made of as-cast acrylic (Reference 19).

Boeing's first choice for the 747 airplane was a pair of curved electrically-heated composite panels with less aerodynamic drag and cockpit noise (Reference 46). The main structure of the windshield is composed of

two layers of stretched acrylic .9" thick providing a fail-safe dual load path. Flat .05" thick front and back surface plies of chemically strengthened glass are flexed to the windshield for abrasion resistance, adding bending stiffness to the assembly. Surprisingly small peeling forces were found in these surface plies. The laminae are held together with 3 PVB interlayers. The windshield developed for the L-1011 of the same materials may be considered a novel design to carry heavy hoop-tension and shear loads as a part of the fuselage surface. At a curvature of 59", it is substantially larger (3 x 4 ft) and thinner than the 747 windshield.

One of the most advanced designs of stretched acrylic (Reference 51) is the windshield of the F-5E. It is a wrap-around configuration with a shallow viewing angle that requires an exceptional amount of care in processing. The processing machine stretches biaxially squares of acrylic from six feet to ten feet while it slowly cools in an environmentally controlled room. This is followed by a large scale optical grinding and polishing process.

d. HIGH STRENGTH TOUGHENED GLASS

Windshield design without birdproofing interlayers is possible if the plies carry' g the inflight loads can be provided with adequate impact strength. This is the case for stretched acrylic at lower speeds. Chemically toughened glass could be used (Reference 32) if it can be developed to a modulus of rupture of 50,000 psi. The latest types of toughened glass have gone a long way towards reducing the inherent weight advantage of plastics (Reference 57). Triplex 10-20 high strength glass is approximately

30% more resistant to bird impact than thermally toughened glass (Reference 54). The relationship between failing speed and total glass thickness was found to be linear and independent of the main ply composition.

The technique of defeating a bird, using inclined heavy gage glass panels, could be called bird-bouncing. The bird is deflected off the windscreen and the debris retains a high proportion of the initial energy (Reference 18). This is the design philosophy for glass windscreens as defined in Reference 58. The prime function of the glass is to resist bird-impact and pressure loads. When two or more sheets of heat-tempered plate glass are bonded together by flexible interlayers of PVB, the PVB provides a reserve load for pressurization. The layers of glass resist loads through bending, with the frame around the panel acting as a simple support. It is designed so that airframe loads are not transmitted through the transparency. The high modulus of rupture required for the impact resistance is achieved by artificially introducing a stress distribution in the glass (Figure 37). In the unloaded state the center is in tension while the surfaces are in compression. A large bending load has to be applied before the surface changes from compression to tension. The annealed strength of the glass has to be added to the compressive stress to calculate the moduli of rupture in bending.

Triplex has gained acceptance for manufacturing curved cockpit glazing for Boeing 747 windscreens. It is rated for impact resistant to a 4 pound bird at 427 kt (Reference 58). The windshields are composed of two panes of thermally toughened "10-20" glass, each 12 mm thick. In the A300B Airbus production (Reference 57) flat "10-20" windscreens will be used. They will be composed of two main plies, each 10 mm (.394") thick, and a facing ply of

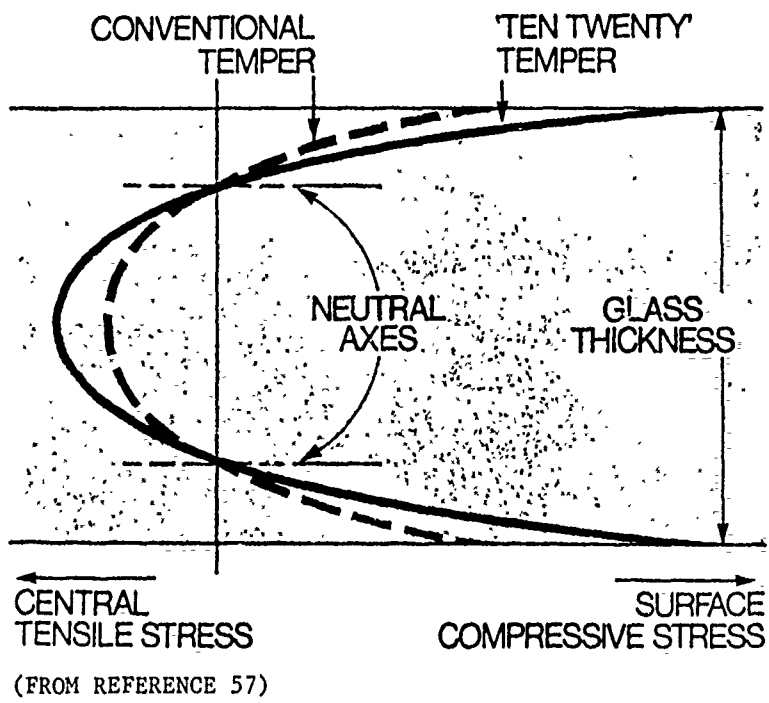


Figure 37. 'Ten-Twenty' Glass Stress Profile

flat .05" Chemcor glass. Corner bird strike under low temperature soak conditions is to be considered critical for the A300B windshield.

e. POLYCARBONATE PLASTIC SHEET

The most outstanding property of polycarbonate is its ductility. The stress-strain curve shows elastic-perfect plastic behavior with small instability at initial yielding. Its low abrasion resistance, however, requires surface plating with other materials. As a consequence, the impact strength of fusion-clad polycarbonate is much lower than that of unclad polycarbonate (Reference 46). This is caused by the brittle nature of the as-cast acrylic cladding and propagation of cracks through the fusion bonded surface into the polycarbonate. Sierracin developed a manufacturing process to overcome this problem. Instead of cladding, a thin glue line (.01") of flexible, high temperature resistant silicon resin bonds the polycarbonate with thin and flexible .01" - .025" inter-layer acrylic sheet.

The "230 series" of ductile protective coatings provide increased weathering resistance of polycarbonate as compared to hard Sierracote 220 coating (Reference 59). Specimens were impact tested with a specially shaped 40 pound weight of 1" diameter from a height of 7.5'. Impact strength was not adversely affected by the thin coating in the range of -65°F thru room temperature.

Another peculiarity of polycarbonate has been found. Notched Izod impact strength vs. material thickness data (Reference 60) indicates existence of a sharp ductile to brittle transition in polycarbonate at a

sheet thickness of about .18". The measured specific strength was 16.8 ft-pound/in for a specimen thickness of .125", and only 3.9 ft-pound/in for .1875". For this reason, it is desirable that polycarbonate in one eighth inch sheets be used as the primary structure.

Polycarbonate sheet is the most heat resistant transparent plastic currently available for production programs. Internal bubbling defines the upper limit for operating temperature and occurs after moderate (short) exposure at 315°F (350°) (Reference 46). Polycarbonate unfortunately, exhibits low light transmission and high haze content. Quality surface polishing of extruded sheet has to be extensively pursued during the windshield manufacturing process and is difficult to achieve. As a result, a change in the prime specification to a minimum of acceptance of 65% light transmission has been recommended by Rockwell International (Reference 44).

The most suitable grade polymer found for aircraft glazing is flat sheet "3000 S.L.", ultra-violet stabilized, water white grade polycarbonate from Farbenfabriken Bayer A.G. (Reference 61). Mechanical properties are identical to those of the other grades, $F_{ty}=64.8 \text{ MN/m}^2$ (1 psi = 6895 N/m²) at 20°C, and 60% reduction at maximum operating temperature of 140°C. Stressed and unstressed polycarbonates were found resistant to many aircraft fluids, but were immediately attacked by Skydrol 500 and bromochloromethane. MIL-P-83310 is the military specification for transparent polycarbonate plastic sheet.

In one test series, the response to bird impact of 27 different flat panels of polycarbonate (and acrylic) windshield materials was evaluated for

impact energy absorbing potential at non-penetration vs. pane thickness and angle of impact (Reference 62). In another impact experiment with a 4 pound bird at a Canadian test site (Reference 63), a 36" x 36" curved panel of polycarbonate in a representative windshield frame survived corner, center and edge shots at a top speed of 650 mph (\sim 500 kt). Composition of the panel was: 0.125" as-cast acrylic outer layer and \sim 1" plastic interlayer discontinued at the edges; 0.875" polycarbonate main structural ply, \sim 1" plastic interlayer; 0.15" polycarbonate splinter shield. Four (4) other concepts and one (1) of polycarbonate, were tested. In all penetration occurred.

In a more recent test, a two ply/interlayer polycarbonate pane (3' x 4' and 1" total thickness) was tested at 140°F with a 4 pound bird at 450 kt. The specimen showed an impression due to permanent plastic deformation approximately 2 1/2" maximum in depth and somewhat larger than the projected area of bird (Reference 64).

Rockwell International, Los Angeles Division, conducted an evaluation of glazing materials for the B-1 (Reference 44), and selected monolithic polycarbonate as the prime candidate, obviously due to its exceptionally high impact resistance over a wide range of temperature, and its strength at high temperature ($F_{tu} = 5.2$ ksi at 220°F). The main right and left windshields of the B-1 have the geometry of a single curved truncated cone with approximately a 50" average radius, covering an area of 2500 in² each, with a ratio of width/height of 2, and angle of inclination approximately 23° to 25°. Swedlow Inc. has been selected as subcontractor (Reference 65) to develop these bird-proof windshields for speeds over 650 mph. The operational

temperature requirement is in the -40 to 125°F temperature range and requires a thermal gradient study to be conducted. The structural build-up of the laminate in sequence of arrangement is: (1) .09" abrasion resistive acrylic ply at the outside, (2) vacuum deposited gold film underneath for de-icing and radar sensitivity, (3) .16" cast-in-place silicon, (4) .87" polycarbonate (the load carrying ply), (5) .05" cast-in-place silicon layer, and (6) .15" polycarbonate inside layer. This lamination totals 1.398" thickness, providing 70% transparency at 3% haze. The side and upper windows are claimed (Reference 66) to be bird-proof and temperature resistant. Side windows of the B-1 will be a laminated structure of polycarbonate and stretched acrylic plastic, while the upper windows - above the crew - will be monolithic polycarbonate. Special abrasion resistant coatings will be applied to the polycarbonate exteriors.

A more recent report on the B-1 windshield (Reference 15) states that it is by far the largest aircraft project ever undertaken and the most technical demanding. The composite transparency consists of two polycarbonate plies, two cast-in-place silicone interlayers, and a glass outer ply. It contains a Sierracote anti-ice heating element and coatings to provide radar reflection and static drain. The use of normal interlayer materials is precluded by the operating requirements of the B-1, particularly the high temperatures generated by near-supersonic speeds at low altitudes, which led to new processing techniques. Exceptional optical requirements are imposed on the windshield by its shallow viewing angle. It is further stated, that the light weight fighter YF-16 canopy is the largest and deepest drawn polycarbonate component ever formed.

2. FRAME DESIGN DATA

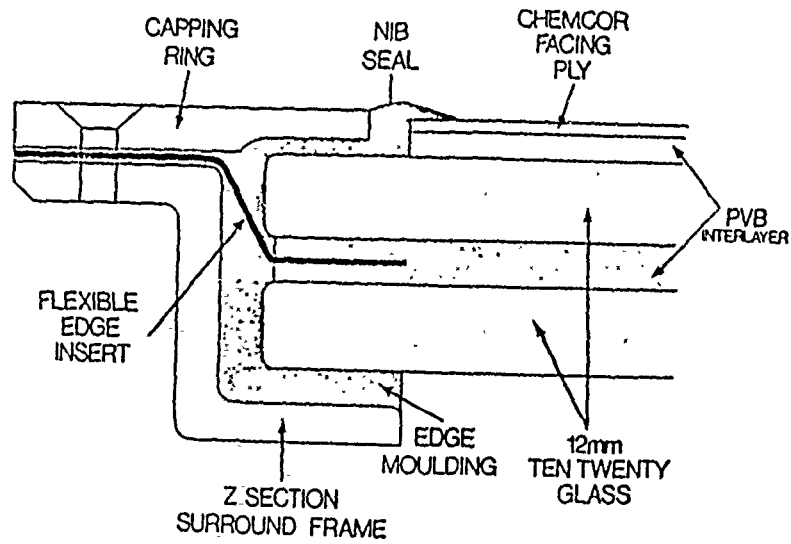
Edge attachment designs (Figures 38 and 39) have become more complex as the demands of enclosure requirements have increased (Reference 16). The development of the method of fixation and the rigidity of supports for a particular aircraft make it impractical to specify a certain design for a given set of parameters.

A manufacturer's handbook on glass aircraft windshields (Reference 67) states that some glass parts with no edge attachment are mounted in the airplane with a rubber channel similar to that used in automobiles some years ago. Others consist of metal inserts with molded vinyl and glass fabric-phenolic reinforcement, metal "Z" frames and metal retaining rings. The complexity of the edge attachment is a function of the structural and operating design parameters of the individual aircraft. One common mounting design concept for glass is "slip plane parting medium" to reduce delamination, edge chipping caused by temperature and pressure induced stresses. It distributes the stress over a larger area and minimizes the possibility of failure due to point stress loading.

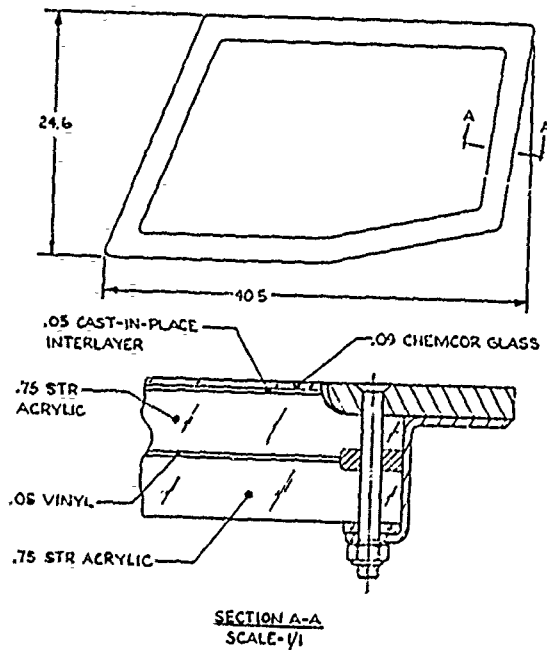
Conflicting recommendations were found concerning the effect of frame stiffness upon the bird impact resistance of windshields. A Civil Aviation Agency (CAA) report (Reference 16) states that windshields mounted in more flexible supporting structures resisted penetration at velocities about 100 mph higher than did identical panes mounted in the more rigid cockpit structure.

In Reference 18, the problem is seen as follows: the mounting attachment and frame must transmit the impact load in such a way that undue local

AFFOL-TR-74-155

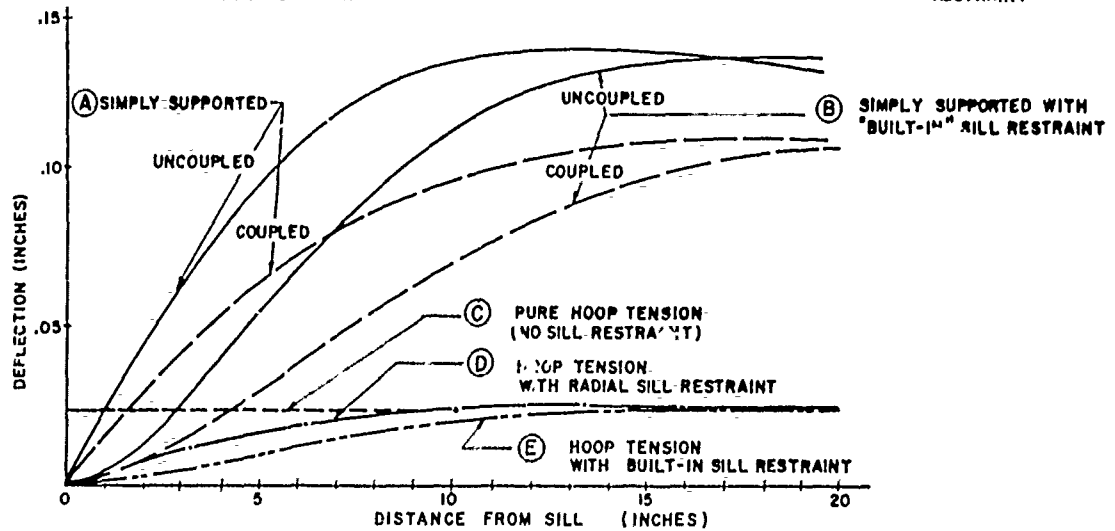
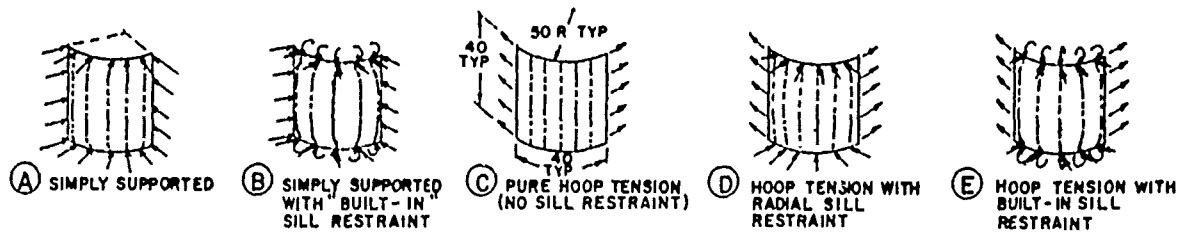


(1) EDGE SECTION OF BOEING 747 WINDSHIELD [REFERENCE 57]



(2) SIERRACIN WINDSHIELD DESIGNED FOR 4 POUND BIRD AT 472 MPH [REFERENCE 9]

Figure 38. Typical Window Pane/Mounting Frame Concepts



(REFERENCE 14)

Figure 39. Calculated Static Flight Load Deflections for Different Mounting Concepts

stress concentrations do not result in failure of the screen. Similarly, the frame should be able to accept these loads without local deformation causing stress concentration in the screen. A recent experimental investigation (Reference 53) indicated that windscreens should be mounted in a frame as rigid as possible to obtain the highest impact resistance. This is very important for thermally toughened glass windscreens which were shown to be particularly sensitive to reduction in frame stiffness. In Reference 58, however, use of the frame to absorb energy thru distortion during the bird strike is cited.

The points of contact between the glazing material and the enclosure frame have to be designed as load bearing to transmit all principal in-flight loads, and at the same time non-load bearing to accommodate the thermal expansion of the glazing material. Reference 16 concludes that the glazing material should be securely fixed within the supports, but should be free to expand or contract due to changes in temperature and with aging. The coefficient of thermal expansion of the frame should be matched as nearly as possible to that of the glazing (Reference 32). If this is not possible, the frame design should be such that compression stresses are created in the transparency.

The edge attachment for glass is different from that for a plastic glazing material. Reference 46 states the careful isolation of flat glass windshields from the fuselage loads (Figure 38.1) is required. Plastic windshields, especially the curved ones, can be bolted directly into the metal structure (Figure 38.2) so that cabin pressurization loads are carried by hoop tension, while bird impacts are absorbed by the windshield acting as an arch in compression. This permits the windshield and the surrounding

cabin structure to be loaded structurally in the most efficient manner. The 747 cockpit structure does not take full advantage of this "bolt-in" capability, but the Lockheed L-1011 does. Monolithic polycarbonate one-half inch thick with a bolt-through attachment has had success for particular aircraft applications (Reference 16). A clamped configuration gives generally better results than a bolted one (Reference 19). A well designed bolted attachment, however, can give practically the same results as a clamped design solution.

The method of fitting and attachment can present maintainability problems (Reference 68) because of residual strain due to initial fitting or subsequent change. For this reason, windshield panels are designed and developed already mounted in their frame for use in the Royal Air Force. The windshield assembly of the 747 airplane is similarly preinstalled in an aluminum frame (Reference 46). Installation into the aircraft is a simple metal-to-metal bolt-up with dry pressure seals, performed entirely from outside the airplane. Use of edge attachments (a means of fastening the side edges of the glazing to the enclosure and consisting of side beams, transverse frames and other reinforcements) may easily lead to greater stress concentrations than those the edge attachments were intended to eliminate (Reference 16). To minimize these stress concentrations, stresses in the materials should be uniformly distributed. In-flight experimental testing using strain measurements of instrumented panes and frames of cockpit windows is one way of achieving this (Reference 14).

Chapter 5 of Reference 69 provides information on fastening and joining techniques of reinforced plastics. It also furnishes data on the effects

of the use of different materials and joint parameters upon failure modes and fatigue strength. The consequence of bolting alone can be seen in higher stress concentration, vs. a greater risk of catastrophic operational failure in case of adhesive bonding. The following lap joint data for 0.063 in. thick 7075-T6 clad are selected to indicate two joining methods; however, they do not represent typical glazing/frame material joining characteristics. Lap joint strength for 3/16 in. diameter tapered interference fasteners at a spacing of 4 diameters, is 1700 pound/in. The stress concentration factor, k_t , is 3. Lap joint strength of an adhesive bond at a length/thickness ratio of 40 is 1900 pound/in; $k_t=1.5$ (Reference 70).

The following are a few results of efforts undertaken to provide improved windshield protection for the F-111. After a series of tests at AEDC/Tulahoma TN using a F-111 crew escape module with the original windshields replaced by several monolithic polycarbonate windshields and those of modified laminated polycarbonate Pittsburgh Plate Glass (PPG) proprietary plastic interlayers, the damage to the windshield frames was assessed.

The part of the ledge on the right hand arch (which had completely failed during one of the tests) supporting the windshield behind the impact location, was fractured in a combination of shear, bending and tension. The rest of the ledge failed primarily in shear except for 4-5 inches along the bottom of the arch. The arch had a slight rearward set. The center post had received moderate deformation due to a direct bird impact. As a result, a decision was made to reinforce the windshield support structure (Reference 47). A static stress analysis was conducted employing a NASTRAN computer model of the F-111 windshield/frame arrangement. The applied pressure

AFFDL-TR-74-155

load simulated the bird strike test condition FM-2 of Reference 35. In two computer runs, a structural configuration with a six inch corner radius added to the upper aft corner of the windshield arch and beam intersection was compared with the original design. The addition of the radius resulted in a reduction of 20% in the peak tension stresses in the mold line surface of the edge of the transparency.

Structural failures, as they occurred on the bird impacted F-111 windshield/canopy with modified laminated windshield and the reinforced aft arch manufactured by McDonnell Aircraft Company, was as follows. Two arch reinforcing members (1 right and 1 left) were tested first as designed and manufactured (Reference 71). Attachments indicated permanent set, such as flattening and torsional set, in the aft arch windshield mounting flange. Cast aluminum corner fittings on the aft arch were broken. Bolts sheared and kept the mounting flange from failing at that location. The badly damaged windshield and aft arch both held together and no material penetrated the cockpit in these tests. It was decided that the reinforcements were too strong. The amount of support provided by the arch reinforcing members was reduced by machining of the members and by use of a different fastener pattern. There was no bird penetration, but the arch and reinforcing member were too badly damaged to allow installation of further windshields for testing. Work was continued with further arch modifications. The results showed better bird resistance for the F-111 in terms of penetration at the pre-established goal of bird strike performance.

3. RELEVANT LEADING EDGE DATA

Non-penetration is recommended as the design requirement for leading-

edge structures for bird-strike resistance (Reference 72). Bird impact resistance is proportional to leading-edge skin thickness. An empirical design formula was developed based upon the penetration velocity of typical designs using L73 aluminum alloy and riveted construction. This velocity was measured as a function of bird weight (up to 4 pound), skin thickness, nose radius, rib thickness and pitch, and sweep angle. Conventional butt joints reduce the penetration velocity by 15%. Reduction of skin thickness between rib or joint attachment lines (up to 15%) by means of chemical etching or machining is ineffective in reducing penetration velocity.

Designs with other skin materials, such as L72 aluminum alloy, nickel and titanium alloys, a CFRP-L73 alloy laminate, and bonded construction, were also investigated. For high strength titanium and nickel alloy leading edge skins on adequately strengthened support structures, the penetration velocity is given by factor $0.8 \times \text{tensile strength of alloy} / \text{tensile strength of L73}$. A 1.1 mm thick reinforcement of the carbon composite inside the leading edge resulted in the laminated skin being much less resistant to bird impact than a light alloy skin of equivalent weight. Bonded nose construction using the cold curing epoxy Araldite (HSA process specification DHA455) increases the impact resistance.

APPENDIX II
SURVEY OF EXPERIMENTAL DATA

1. BIRD STRIKE EXPERIMENTS

A wealth of data from experiments with bird-impacted, mounted window panes exists. For example, Table XVIII summarizes data for stretched acrylic composite windows. These data, from different sources, may be interpolated for comparison purposes to account for single parametrical changes such as larger or thicker panes, different attachment conditions, higher impact velocities, and heavier birds.

The available experimental data is discussed in the following subsections.

a. BIRD GUNS, TEST FRAMES, INSTRUMENTATION

Performance capability of a Canadian compressed air bird gun with a 6 in. diameter barrel is 250 to 700 ft/sec, with the ability to extend the velocity to 1000 ft/sec using 4 to 8 pound birds (Reference 4). A considerable increase in the speed potential of the Royal Aeronautical Establishment Farnborough (R.A.E.) gun has been gained by sealing the muzzle of the barrel with a frangible 'Melinex' diaphragm and evacuating the air (Reference 12). Tests referred to in Reference 19 were performed with a bird gun at the Centre d'Essais Aéronautique de Toulouse (C.E.A.T.). R.A.E. systematically tested 25" x 19" panels with rounded corners (Reference 12), while the French Air Ministry used a typical frame of 520 mm by 820 mm (Reference 19).

Every actual windscreen installation for bird impact resistance should be validated by tests under the required operational conditions (Reference 54). Force-time relations, as they occur during in-flight bird strike, can

TABLE XVIII
TEST RESULTS OF STRETCHED ACRYLIC COMPOSITE WINDOWS

source	composition	dimension	edge attachment	angle of bird install. size	test speed	temperature condition	failure mode
Lockheed*	.062" polyester plastic outer pane, .325" poly-vinyl-butylal interlayer, .75" stretched acrylic pressure pane	19" x 35" nominal window size	interlayer with .061" 7178 SF Al metal insert at edges; 6 for #10 H.T. bolts spaced at 1 1/8" on centers and 1 1/4" dia. metal spacer each hole; bolted thru interlayer and stretched acrylic pane	?	345 kt (997 mph)	interlayer at optimum temperature	no penetration
Swedlow**	3 layers (1" total) of Swedlow stretched Acrilvue acrylic (Mil-P-25690A) and 2 layers (.5" total) of cast in place interlayer (SS-3530)	15" x 15"		30°	420 mph	-5° outer -28° center +11° inner to simulate specific descent after heating)	bird bounced off; slight spalling around the heads of the mounting bolts only
Swedlow** for Dassault Mystère 20 executive jet	.125" borosilicate glass, .1" cast in place interlayer, .5" stretched acrylic, .12" cast in place interlayer, .75" stretched acrylic	24" x 21"	pressure mounted	40°	436 mph	5.5° ambient	no failure
Lockheed*	.25" stretched acrylic outer pane, .19" cast-able interlayer, .75" stretched acrylic pressure pane, .35" air gap spacer, .08" acrylic inner pane heat resistant;	20" x 20"	2024-T4 aluminum insert in interlayer; #10 H.T. bolts spaced approx. 1.22" on centers thru metal insert, stretched acrylic, spacer and inner pane	?	490 mph 411 kt (474 mph)	interlayer at optimum temperature	failed no penetration
Sierracin***	.09" Chemcor glass, .05" cast in place interlayer, .75" stretched acrylic, .05" vinyl, .75" stretched acrylic	24.6" x 40.5" overall	see Fig. 14	?	472 mph over 500 mph	?	no damage minor damage would not have precluded continued flight

[*Reference 16, **Reference 73, ***Reference 9]

be simulated using air or powder guns instead of more expensive rocket sled tests. Each source of impact, however, requires calibration (Reference 74). Experience has shown that the projectile speed achieved is within 3% of that predicted from the calibration graphs (Reference 12). The means of visualizing what is taking place during an impact is a very important area of experimental investigation. Interferometric techniques using photomechanics and pulse and continuous wave lasers are used to determine impact resistant structural design features.

b. MOTION PICTURE OBSERVATIONS

A list of phenomena was prepared after a review of Douglas DC8/DC9/DC10 airplanes bird impact testing movies, photographs, and test results (Reference 75). The films reviewed showed the impact of 4 pound birds at 300-450 kt. The bird specimen ruptured immediately upon impact. The bird either bounced or bagged, if there was no penetration. Blood traces radiated from the point of impact. In oblique impact, the trace of splash radiated from the point of impact in all directions. The intensity of the trace was heavy along tangential velocity direction and reduced gradually in the opposite direction. The trace for the point of impact was smaller than the packaged cylinder diameter of bird.

A radial crack pattern was observed for glass laminates, while the pattern for stretched acrylic and chemically strengthened glass windshields radiated in all directions. The crack pattern in the tangential direction was centered at the point of impact and extended concentrically to a finite radius. Inside this radius there was permanent deformation. The crack pattern was similar on both inner and outer glass

face sheets. The cracks radiating approximately normal to the permanently deformed circular shapes were apparently not affected by the windshield edges.

From these observations the following hypotheses were developed (Reference 75). Bird impact at certain speeds is isothermal with no entropy change during impact. Total energy generated from the impact dissipates in splashing the bird and converts into internal strain energy of the windshield.

The material conforms according to its nature: linear elastic-perfect plastic, or work hardening. Momentum is transferred into the windshield instantaneously. The windshield subjected to an initial velocity after impact has no instantaneous displacement response. After that it is free from surface traction.

c. EMPIRICAL STRENGTH DESIGN FORMULAE

Two types of design equations have been derived from bird strike tests. One determines structural performance and the other estimates impact forces (Appendix II-1d).

The empirical equations for structural performance (References 10, 12 and 19) give the relationships between the thickness of monolithic glass or plastic panel, the bird weight, the aircraft speed, and panel mounting angle with the trajectory. Mott (Reference 12) in his equations further considers clamping width, main ply thickness, main ply composition, temperature and impact position. Poullain and Clamagirand (Reference 19) investigated shape, size, and contour characteristics of the windows, and found that a reduction in the window radius would appreciably increase the

critical impact speed of the curved panel.

Similar equations were developed for the thickness of the vinyl interlayer of a laminated panel as well as for newer materials. The variation of impact damage (assuming failure speed proportional to the reciprocal of the cosine of the sweep back angle (Reference 12)), deviated from Newton's law ($m \cdot v^2$) for test data recorded from thermally toughened glass panels of .8" total glass thickness according to $m \cdot v^3$ (Reference 18). The formulae for the rectangular shape of Reference 19, are different for different materials and use v^2 and (weight of bird)^{2/3} for any glass and acrylic material.

As the failure analysis of bird-impacted windshield was mostly experimental, empirical design formulas were established based on the test data. One of the early formulas for toughened glass is

$$t = .136 (1 - .348 \cos \alpha) e^{(V \cdot \cos \alpha / 873)} \quad (75)$$

where t , V , and α are the thickness in inches, penetration speed in mph for a 4 pound bird, and windscreen angle between direction of impact and normal to windshield, respectively. This formula is valid for clamp-mounted panes ranging in thickness from 1/4 to 1 1/4 inch, and $\alpha = 40^\circ$ to 60° (Reference 18). At an angle of 50° , 500 (600) mph would require a thickness of 4 (8) inches of toughened glass to avoid penetration of a 4 pound bird.

Tests on transparencies (Reference 18) have indicated that penetration velocity is proportional to one over the cube root of the bird mass, M . The proportionality constant for a vinyl sandwich panel specific thickness under identical conditions is

$$MV^3 = 5.1 \cdot 10^7 \quad (76)$$

and for stretched acrylic it is $6.75 \cdot 10^8$ with M varying from 1 to 8 pounds and V in mph. The design formula for 20% plasticized PVB for the total PVB thickness is

$$t = .05 \cdot e^{(V \cdot \cos \alpha / 180)} \quad (77)$$

$V \cos \alpha$ varies only 5% at a range of $\alpha = 41^\circ$ to 46° . Penetration resistance decreases substantially, as the temperature departs from the optimum. Scatter of data occurs due to mounting conditions (Reference 18). In one case, identical screens failed around the edge attachment at 376 mph in December, and at 460 mph at 63°F outside temperature in July. The main vinyl layer was at 40°C in both tests. The design formula obviously does not include the temperature of the edge attachment and the quality of mounting design.

A laminated stretched acrylic panel with PVB interlayers of .875" total thickness, inclined at 45° , defeated a 4 pound bird at 320 mph (Reference 18). This speed is some 20-40% higher than that for toughened glass at the theoretical glass speed of 265 mph. The high penetration speeds of the laminated stretched acrylic/polyvinyl composite panel reflect optimized mounting attachments.

It has been observed over the years (Reference 54) that the impact energy of the bird to produce similar damage is a constant value, and that the failing speed is proportional to the reciprocal of the cosine of the sweep-back angle. For thicker windscreens, the above formulas predict failure speeds below the speeds achieved in clamped edge panel tests. If compared on the basis of weight and not thickness, the stretched acrylic windscreens

would be twice as resistant as those of thermally toughened glass, and 1 1/2 times as resistant as Triplex's "10-20" high strength glass.

The following formulas are for thermally toughened glass, stretched acrylic, and "10-20" glass, respectively (Reference 54).

$$V(\text{mph}) = 400 \cdot t(\text{in}) / (\sqrt{W(\text{pound})} \cdot \cos \alpha) \quad (78)$$

$$V(\text{mph}) = 470 \cdot \sqrt[3]{t(\text{in})} / (\sqrt{W(\text{pound})} \cdot \cos \alpha) \quad (79)$$

$$V(\text{mph}) = 520 \cdot t(\text{in}) / (\sqrt{W(\text{pound})} \cdot \cos \alpha) \quad (80)$$

(W = bird weight, t = total thickness of specified material)

These equations do not reflect support lengths. Panels of 25" x 19" and 32" x 20" were tested. No information is presently available that reflects the effects of panel size and shape in such an empirical equation. Similar equations were derived independently (Reference 19) and are reported for comparison:

(i) Laminated Glass of several plies with thin layers of PVB in between (1 to 3 mm), tested at ambient temperature:

$$e^{3/2} C = v^2 p^{2/3} \sin \alpha \cdot \lambda \quad (81)$$

If all the plies do not have the same tempering:

$$e^{3/2} \left(\frac{e_1 C_1 + e_2 C_2 + \dots}{e} \right) = v^2 p^{2/3} \sin \alpha \cdot \lambda \quad (82)$$

where e = total thickness of glass in mm; e_1 = thickness of ply with coefficient C_1 ; e_2 = thickness of ply with coefficient C_2 (thickness of PVB not taken into account); C = strength coefficient for bird impact complying with specification

FAR 25 (no penetration of bird or shattering).

(ii) Stretched Acrylic windows:

$$e^2 C = v^2 p^{2/3} \sin \alpha \cdot \lambda \quad (83)$$

where e = total thickness without interlayer; $\lambda = 1$ for civil aircraft; .5 for side windshield of fighters; .35 for wrap around fighter windshield.

(iii) As-cast Acrylic flat windows of civil aircraft and front windshield of a fighter: The equation is the same as for stretched acrylic, but with $C = 28$, $\lambda = 1$. Curved side windows of fighter aircraft:

$$48 e^2 = v^2 p^{4/3} \sin \alpha \quad (84)$$

for 25" to 35" curvature.

The formulae fit 520 mm x 820 mm test frame size. At edge rebates not too deep, e is the pane thickness. Otherwise, the speed is very similar to that for the thickness in the rebate area.

A typical requirement for helicopter windshields is to defeat bird impact in the velocity range of 200 to 250 mph (Reference 76). Specimens manufactured and tested by Pittsburgh Plate Glass of .25" stretched acrylic and the light weight glass configuration failed at impact speeds as low as 100 mph, when impacted with a 4 pound bird at room temperature. In comparison, the penetration velocity for .25" monolithic polycarbonate is approximately 250 mph. It is the same for composite designs of glass and polycarbonate weighing 4.5 pound/ft². Table XVII provides test data from different sources for stretched acrylic composite aircraft windshields.

The resistance to bird impact of the modified 2' x 2' size windshield of the Canadian Air Force CL-41 Tutor aircraft has been investigated (Reference 77) utilizing the high speed rocket sled facility at Holloman AFB, NM.

Two (2) layers of vinyl (25 parts plasticizer), .18" and .12" thick were added to the original .45" laminated glass windshield (inner and outer layers semi-tempered, center tempered glass) and attached to the frame. Prior to modification, the main glass yielded a penetration velocity of only 127 mph for collision with a 4 pound bird. At the indicated air speed of 298 mph (IAS), a 3.5 pound chicken did not penetrate the right-hand panel, which was at a temperature of 70°F. Penetration did occur at this speed into the left hand panel, which was cooled to a temperature 30°F below that for maximum strength of the vinyl. Using the M.E. 106 formula for vinyl, the theoretical penetration speeds for .12", .18" and .3" thicknesses are 210, 290 and 415 mph, respectively. This reveals that the add-on design modification partly utilized the material strengths of the PVB.

The following example indicates how misleading windshield designs for high impact energy can be arrived at by extrapolating empirical formulae such as the one of Reference 84 for medium impact speeds. It is estimated that a windshield of laminated vinyl-glass required to defeat the impact of a four (4) pound bird at 1.2 Mach and 500 ft. altitude, has to be 2.75" thick. At this material thickness, luminous transmission is an estimated 50%, which is far below the acceptable value.

Flat 25" x 19" panels of thermally strengthened glass with rounded edges and clamped edge conditions have been tested in connection with the development of the Concorde windscreen (Reference 54). Impact of a four pound bird at a speed of 512 mph is the operational requirement. Experimentally observed penetration speeds were considerably higher than those predicted using the formula of R.A.E. Tech. Mem. 106 (1952) while not being as high as those

predicted by the newer formula of Note 373 of 1967. In the experiments, the edge attachment featured a relatively stiff light alloy cast mounting frame, two alternative widths of packing pieces and clamping rings (.84" and .6" encastration), rubber gaskets and no glass-to-metal contact. No appreciable differences in impact behavior between the two encastration widths were observed. The forward facing abrasion screen was reduced in size to form an edge rebate to permit clamping of the main load bearing plies only. Deflections were determined by measuring the distance between the glass face and the displaced plunger rod. Accuracy of the measurements was probably better than 10% measuring deflections of .08" to .28". Comparable deflections for polycarbonate windshields are several inches. Data for a different Concorde test panel (Reference 54) of the thermally strengthened glass "10-20" are as follows: three (3) main plies laminated together with PVB, 1.15" total thickness, size 820 mm x 520 mm (32 1/4" x 20 1/2"), rounded corners, tested at 7°C ambient temperature, 53° declined. This panel satisfied the operational requirements.

d. EMPIRICAL IMPACT FORCE EQUATIONS

Impact forces due to birds hitting a non-denting plane at relative normal velocities, V , are tabulated in Reference 42. The minimum possible impact force,

$$F = MV^2/2s \quad (85)$$

caused by the change of velocity to zero in the time available, was obtained by assuming constant deceleration rate. As a baseline, this force was deter-

mined for a 2 pound herring gull of 4" effective bird dimension, s . The bird dimension was scaled for larger and smaller birds as the cube root of bird weight. If a sinusoidal acceleration were assumed, the peak acceleration would be $\pi/2$ times mean acceleration. Forces would be greater if the bird carcass did not spread, as it would result in the acceleration taking place in a shorter distance than " s ". In the case of an oblique impact at an angle of incidence, α , the relative normal velocity is $V \cdot \cos \alpha$ instead of V .

A bird acts as a semi-rigid object forming a three-dimensional mound (Reference 41). This mound is assumed to be $1/4$ of the effective bird dimension in height. With no structural deformation, its acceleration occurs during the linear motion of the center of gravity of the bird through a distance of $3/8 s$. The formula for sinusoidal peak force for normal impact (Reference 41),

$$\hat{F} = .702 \cdot W^{2/3} \cdot V^2 \quad (86)$$

(W in pound, V in kt)

was experimentally verified in connection with work on engine intake bird deflectors from readings of pressure transducers fitted to inclined rigid grills supporting the deflector plate and measuring both the vertical and horizontal forces (Reference 72). The formula

$$P = .685 \cdot W^{2/3} \cdot V^2 \cdot \cos \alpha \quad (87)$$

was found to be valid in the range of $W = .1$ thru 2.25 kg, $V = 105$ thru 320 kt and $\alpha = 45$ thru 75° .

e. BIRD IMPACT ON LEADING EDGES, FAN BLADES

Equations 86 and 87 were also applied to other impacted structures, such

as wing leading edges (Reference 72). The response of composite material cantilever beams to soft body impact representing bird impact on jet engine fan blades was studied in Reference 78. Agreement between the experimental results and one degree of freedom - classical beam theory for free-clamped, free-hinged and free-free modes of attachment was found to be good. Extension of this work to a two-degree of freedom lumped parameter model has provided excellent predictions of measured torsional vibrations induced by impact. The second part of these studies deals with the transmission of planar forces, created by a pressure profile, from low modulus transparencies, such as homogeneous, laminated and fiber reinforced materials, into different types of adjoining fuselage structure.

2. WINDSHIELD EXPERIMENTS OTHER THAN BIRD STRIKE

An analysis method is mentioned (Reference 79) that predicts the temperatures of and heat transfer within window materials by both conduction and radiation. The heat balance equations in the computer routine account for emission, attenuation, and absorption of radiant energy within the glaze. The heat transfer test results provide experimental data on realistic window components. This effort could be considered a prerequisite for conducting thermal stress and failure analysis of window systems in thermal flight environments.

The thermal shock profile of a windshield is the temperature variation thru the transparency assembly at the specific flight profile that produces the maximum temperature differential. The thermal shock temperature-time history of the original glass windshield of the F-111, repeated for 75 cycles

of 1600 sec each, is typical for high performance aircraft windshields. This windshield was composed of .11" Herculite II, .08" interlayer, .11" Herculite II (Reference 80). The inner and outer initial test temperatures were $T_1 = -35^\circ\text{F}$ and $T_2 = -18^\circ\text{F}$, respectively. The temperature differential was high during half of the flight cycle, T_1 peaking at 350°F and T_2 at 275°F .

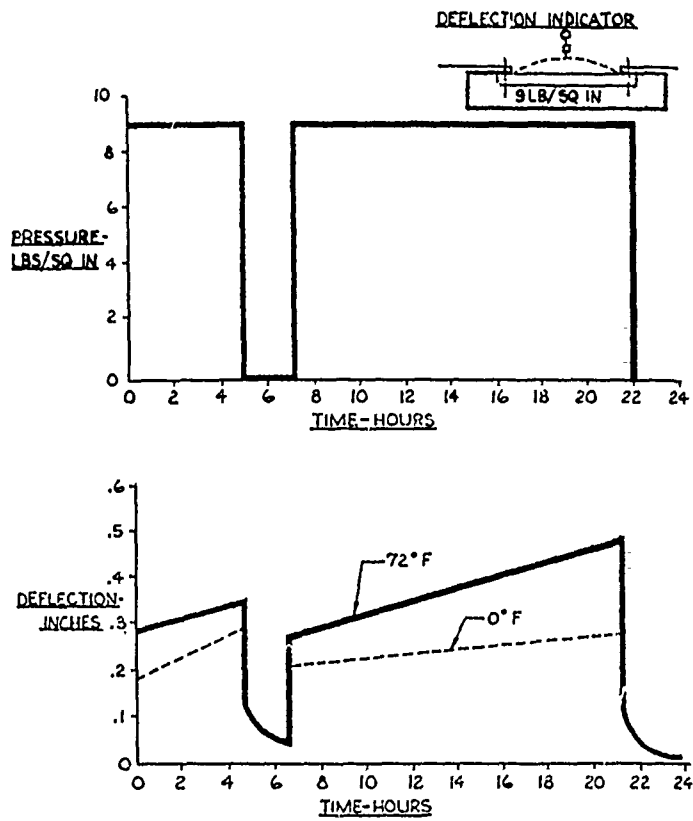
The development of one windshield required extensive structural testing of the materials as well as the interlaminar bonds (Reference 9). The tests were oriented toward pressurization loading in one, and separate impact performance tests in another program. The pressurization loading was simulated in a test rig using a composite windshield of 1.7" total thickness and subjecting it to over 1,000 hrs of cyclic loading at a range of temperatures from -65°F to 70°F . Figure 40 shows the pressure cycle used in the investigation. The windshield survived without damage and greatly increased the understanding of the structural capabilities of this type of windshield.

3. OTHER IMPACT ANALYSES

The following research investigations were found to be valuable back-up information.

a. TRANSIENT BEAM ANALYSIS

Transient analysis was conducted to investigate the impact behavior of a free-free beam under an impulsive force applied at the beam center in Reference 81. Non-dimensional deflections, wEI/PL^3 , were computed in terms of non-dimensional beam location (actual location/tip location) for different



[REFERENCE 9]

Figure 40. Pressure Cycle Used for Composite Laminate Testing

non-dimensional instances of time,

$$\mathcal{T} = t/t_I \text{ with:}$$

$$t_I = \pi/\omega_0 \quad (88)$$

$$\omega_0 \approx \sqrt{\frac{EI}{ML^4}} \quad (\text{first mode of free vibration})$$

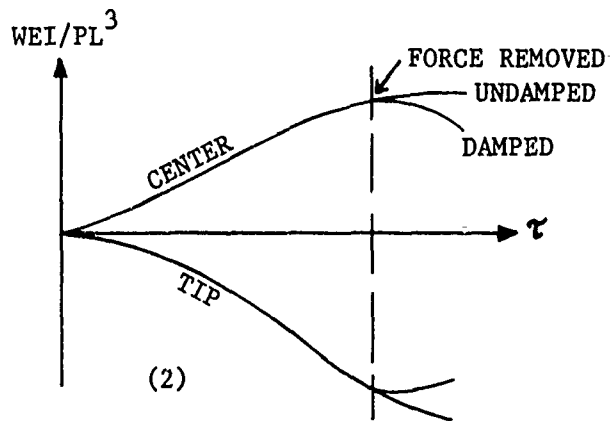
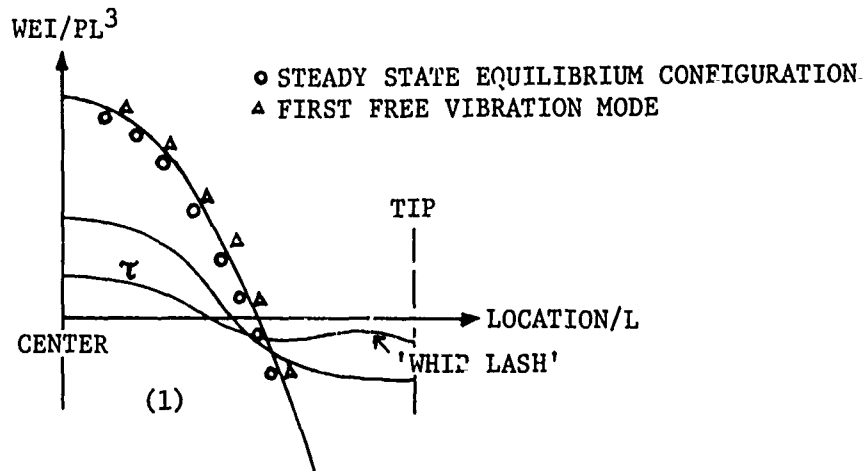
where M = mass of beam per unit length (pound-sec²/in²), and P/L = inertial load on the beam (pound/in). Figure 41.1 shows the initial deflectional response up to $\mathcal{T} = .25$. A "whip lash" motion of the end of the beam may be noted in the spanwise wave travel. The time histories of center deflection and tip deflection relative to the center of mass (the reference) are presented in Figure 41.2.

b. ELASTIC PLASTIC ANALYSIS OF PLANE STRUCTURES

The following is a description of a very elaborate elastic-plastic impact analysis (Reference 48):

(1) The elastic-plastic response of certain plane structures undergoing large deformations due to dynamic loading has been investigated. Various methods were used in loading the specimens. In some tests heavy lead rings were dropped on flat and pointed anvils. On other tests, stationary lead, copper and aluminum rings carrying weights around the periphery and those with no additional attached masses were subjected to contact explosives directed radially inward at a single point. Aluminum cantilevers, rectangular and triangular frames and semicircular arches were loaded by magnetomotive and explosive impulses.

(2) The aluminum rings with 5" to 6.5" outer diameter, 1/8" to 1/4"



[FROM REFERENCE 81]

Figure 41. Beam Response Due to Impulsive Load

radial thickness and up to 3/8" wide, were machined from tubing and annealed at 350°C for 15 min. The aluminum had the following mechanical properties: 14.9 ksi yield stress, 8 to 10 x 10⁶ psi elastic modulus and .2 to .82 x 10⁶ psi plastic modulus. Cantilevers and frames of aluminum were made from .032" to .036" thick aluminum sheet material, 10" long and 3" wide. The masses attached to the plane structures were 1/2 pound steel blocks.

(3) The sharp indenter initiated the plastic deformation process at a free falling speed of 14 ft/sec. Point explosive loading by No. 6 I.C.I. nylon detonators caused 1.5x10⁻² pound-sec impulses with detonative deformation times in the order of .01 sec. 0.37" diameter and 3/4" long mild steel bullets moving at 695 ft/sec were used in the high speed bullet impact tests. The distributed magnetomotive loading method imposed a prescribed uniform radial velocity on the ring. Magnetomotive as well as detonative loads delivered to the frames were calculated from the swing of 1.2 pound ballistic pendulum rigidly fixed to the frame. Initial structural velocities were determined to be 7800 to 9000 in/sec, requiring high speed photographing at 15,000 frames per second.

(4) The impact behavior of the ring subjected to impulsive point loads was simulated by large deflection-analysis assuming elastic-linear strain hardening or rigid-plastic material behavior and the formation of four plastic hinges: two stationary hinges at the point of impact and a point diametrically opposite, and two moving hinges. Rigid-plastic analyses were found to be valid only in cases for which the initial kinetic energy was an order of magnitude greater than the elastic strain energy of the structure at the onset of plastic deformation.

(5) Two analysis methods were used to investigate the loading of rings, and particularly arches, cantilevers and frames. One method assumed a simple approximate model of the ring, consisting of concentrated masses around the circumference connected to each other by weightless links possessing the strength properties of the material. The dynamic equation for each mass of the ring were solved. The second method utilizes Lagrange's energy equations. Both methods were in close agreement.

(6) Insignificant difference between the calculated and experimentally determined profile of the deformed structure were observed as long as the ratio of structural length to the link length remained more than ten: $\Delta s/s > 10$. Prediction improved with increasing number of nodal points. Time interval, Δt , cannot be chosen arbitrarily and depends upon the wave speed thru the structural link length, Δs . It was found that divergence occurs when

$$(\Delta t/\Delta s)(E/\rho)^{1/2} > 1 \quad (89)$$

Another analytical effort (Reference 82) demonstrated the injury reduction capability of energy absorbers. Existing statistical data on crash accelerations and man-weight distributions were used as inputs to a MIMIC computer program. Dynamic response indices and stroke lengths were computed for each acceleration-man-weight combination. This program can be used as a guideline in selecting candidate energy absorbers.

c. EXPLOSIVELY LOADED ALUMINUM SHELLS

The computer code PETRØS (Plastic-Elastic Transient Response of Cylindrical Shells with Large Deflections) used finite-difference method to calculate dynamically induced deformations of general, thin shells (Reference 83).

PETRØS handles symmetrical loading conditions only. No structural reinforcing supports were taken into consideration. Classical boundary conditions were employed. This program was reviewed to determine its ability to simulate the actual F-111 windshield bird strikes test results. The boundary conditions that can be handled and symmetry restrictions make the program inappropriate for simulating the F-111 windshield test results.

d. HAILSTONE ANALYSIS

The "DEPRØSS 3" program may be applicable to the bird strike impact problem once the failure criteria for transparencies material are clarified (Reference 75). This program analyzes the dynamic elastic-plastic axisymmetric responses of impulsively loaded plates and shells of revolution. Thomson and Hayduk adapted "DEPRØSS 3" with minor modifications in the initial velocity input section and the mass ratio of hailstone/plate, improving their previous work by including the effects of combined bending and membrane action. They succeeded in predicting the size of dents caused by hail impact.

e. OTHER COMPUTER PROGRAMS

The following programs can be used to simulate experimental bird strike test results. SABOR 5/DRASTIC V is applicable only for impact analysis of shells of revolution without stiffening members. MAGIC and NASTRAN have the required stiffened shell segment capability. In MAGIC, however, the transient force (or velocity) input response capability is lacking, while NASTRAN possesses it.

APPENDIX III

DESCRIPTION OF FINITE DIFFERENCE COMPUTER ROUTINES

User oriented descriptions of the four FORTRAN program versions developed: FLAT PLATE, PLATE WT-18, CONICAL SHELL SEGMENT, and F-111 W/S (FM-1) are presented in this appendix. These computer programs are based on the finite difference methods of Section III and were applied in the analyses of Section IV. Listings of the programs are provided in Appendix IV. For familiarizing the user with the programs, the appropriate card listings accounted for by numbering from the start of the individual program may be looked up as soon as they are referred to in the following guidelines.

All functions of executing the computations, such as assigning the time varying variables, zeroing variables for initial conditions, controlling variables, as of stiffness and support, and finally solving the structural finite difference equations, are contained in the four different, separate computer routines "MAIN". The only type of subroutine that has been established, provides graphical support to process output data by means of the CALCOMP plotter. This subroutine, "GRAPH", is listed only in connection with the F-111 W/S (FM-1) program. Similar subroutines may be devised and attached to the remaining programs.

1. FLAT PLATE PROGRAM

a. Introduction

Based on a mathematical model for impulse loading, a computer program for calculation of time histories using finite difference equations of the types of Equations 50 has been developed in the Analog and Hybrid

AFFDL-TR-74-155

Computation Branch, Computer Center, WPAFB, Ohio. This program (Reference 43) was written for a flat plate of 6 x 6 elements to consider flexural bending of the plate, rotational clamping stiffness of the attachment frame, and viscous damping and spring-back behavior of the mounting system. This required a 7 x 7 mesh that also needed half-way points. Variables were dimensioned in 13 x 13 arrays. "DØ" loops were used to define problem variables within the mesh and on the boundary. Numerical integration utilized the point slope formula (Euler's Method) which proved to be adequate for time steps smaller than .05 msec.

The sequence of operating in a marching procedure on the representative straight beam equations in cross-beam arrangement to calculate the instantaneous variables is shown in Figure 42. The "x" and "y" markings in the patterns represent the generation of numerical values of x- and y- variables, respectively. Initial conditions consider all variables (internal shear loads (VX, VY), bending moments (MX, MY), slopes of deflection (OX, OY), and displacements (W)) zero. Figure 43 reflects the optional distribution of constants in the finite difference scheme: distribution of bending stiffnesses (EIX, EIY, EIF), mounting properties (KW, KWD, KOX, KOY, KOXD, KOYD) along the edges, time dependent pyramidal impact loads (Q1>Q2>Q3) and mass properties (DMM, DMF).

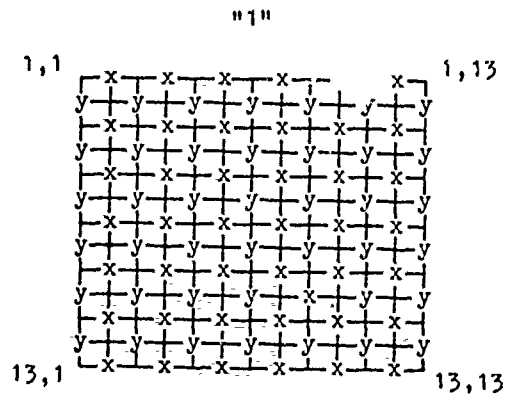
For reason of simplicity, the basic flat plate program is presented in its shortest form (Appendix IV-1). Bending stiffnesses are: $EIX=EIY=EIF=EI$. Mounting properties along the edges, KW,KWD and $KOX=KOY=KO$, are constant. Rotational dampening is avoided: $KOXD=KOYD=0$. The components of load can be specified at any grid point. Distributed loads must be treated as concentrated at the nodes. The pyramidal load distribution (Figure 43.3) is

AFFDL-TR-74-155

TYPICAL REPRESENTATIVE EQUATION

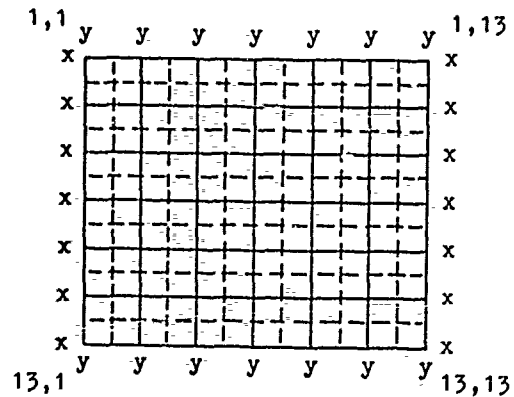
$\phi X(I,J) = (W(I+1,J) - W(I-1,J)) / DS$
 (AND FOR ϕY , INSIDE AND BOUNDARY)
 (LISTED AT LINES 67 AND 68 OF FLAT
 PLATE COMPUTER ROUTINE USED)

GENERATED PATTERN
 (FOR GRID SIZE $NX \cdot NY = 13 \cdot 13$)



$\phi X(1,J) = \phi X(2,J) / (1 + DS \cdot K \phi X / (2 \cdot EIC))$
 (AND FOR ϕY , BOUNDARY)
 (LINES 72 THRU 75)

"2"



$MX(II,J) = -K \phi X \cdot \phi X(II,J) \cdot SIGN$
 (AND FOR MY , BOUNDARY) (LINES 80 AND 82)

"2"

$VX(II,J) = (KW(I) \cdot W(II,J) + KWD(1K) \cdot WD(II,J)) \cdot SIGN$
 (AND FOR VY , BOUNDARY) (LINES 92 AND 102)

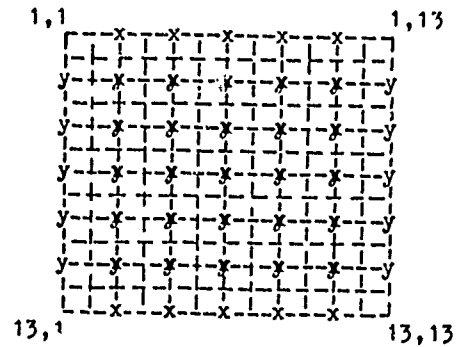
"2"

Figure 42. Sequence in Cyclic Loop for Calculating Finite Differences

AFDL-TR-74-155

$MX(II,J)=(\phi X(II+1,J)-\phi X(II-1,J)) \cdot EIC/DS$
(AND FOR MY, INSIDE AND BOUNDARY)
(LINES 109 AND 112)

"3"

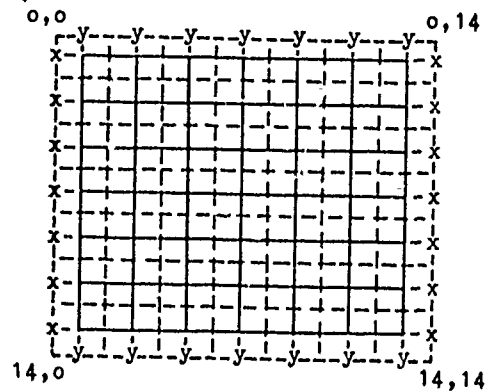


$VX(II,J)=(MX(II+1,J)-MX(II-1,J))/DS$
(AND FOR VY, INSIDE AND BOUNDARY)
(LINES 117 AND 118)

"1"

$VX0(I)=2 \cdot VX(1,I)-VX(2,I)$
(AND FOR VY0, ETC., OUTSIDE AND BOUNDARY)
(LINES 122 THRU 125)

"4"



$WDD(I,J)=(Q(I,J)-VXP+VXM-VYP+VYM)/DM$
(AND FOR WD AND W)
(LINES 141, 142 AND 144)

"5"

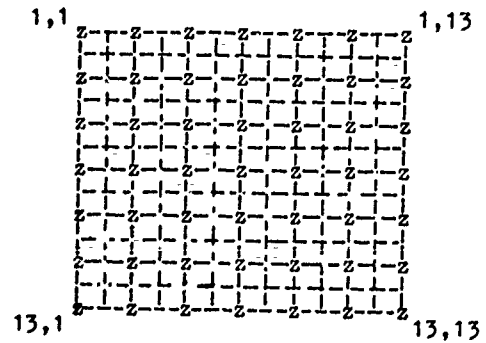
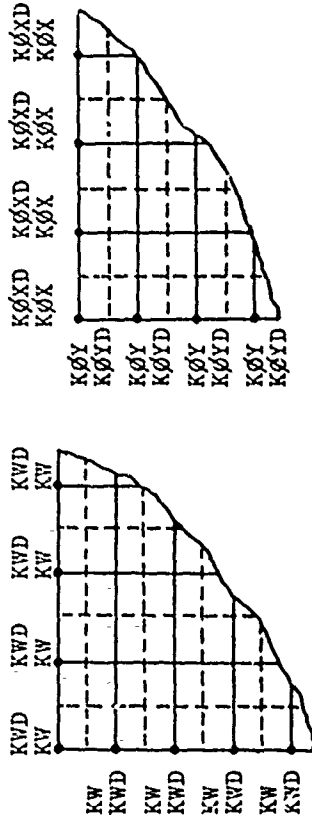
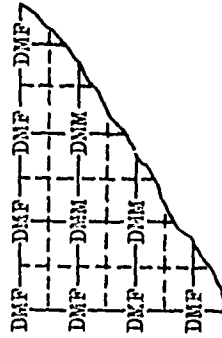


Figure 42. (Concl.)

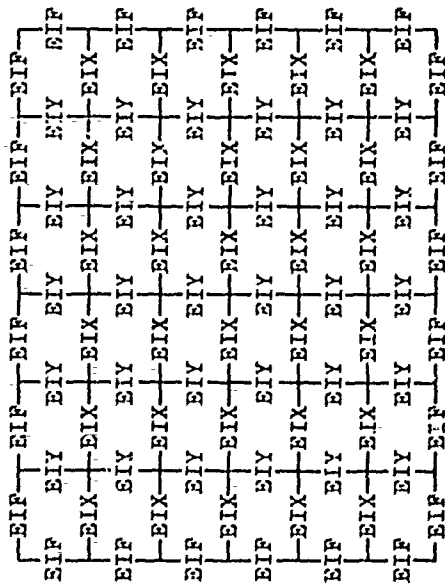
2. MOUNTING PROPERTIES KW, KWD AND KØX, KØXD, KØY, KØYD ALONG THE FRAME BOUNDARY:



4. MASS PROPERTIES DMM AND DMF:



1. DISTRIBUTION OF BENDING STIFFNESSES, EI AND EIF:



3. PYRAMIDAL LOAD DISTRIBUTION, Q1, Q2 AND Q3:

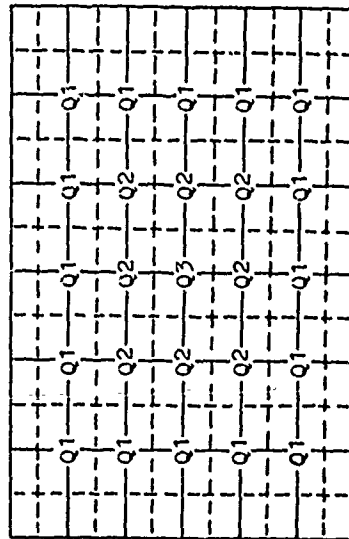


Figure 43. Distribution of Constants in Finite Difference Scheme

AFFDL-TR-74-155

presented as an example of external transient load application only. In the basic flat plate program, loads of .1 pound as "quasi-zero" loads remain constant at all interior nodal points and along the edges ($Q_1=Q_2=Q_3=Q$). All nodal masses are constant: $DMM=DMF=DM$.

b. Basic Program Listing

Program FLAT PLATE has been listed in two versions (Appendix IV-1) to demonstrate ways of simple modification of the same basic routine for versatile utilization. The unmodified listing is described first, excluding the three modifications each in the options "ONE" and "TWO" by computer card additions. For this purpose, the comment card statements are repeated with additional comments.

Following the title, FLAT PLATE PROGRAM FOR FIXED GRID SIZE (13 x 13), PARAMETRICAL RUN * * * * * ONE * * * * * (or PARAMETRICAL RUN * * * * * TWO * * * * *), the second comment is: ASSIGNING THE TIME VARYING VARIABLES. This is followed by dimensioning the variables W, WD, WDD, OX, OY, VX, VY, Q, MX and MY and the single array variables VX0, VX14, VY0 and VY14. To change the applicable problem size of the program to a grid size other than 13 x 13, the dimensions of these parameters as well as dimensional notations in the equations of the routine must be changed.

The comment INPUT DATA REQUIRED (NUMERICAL EXAMPLE IS ARBITRARY) is followed by six necessary plate constants. The geometry of the structure is determined by the grid parameter, DS, that reflects the side of the square panel in inches. The bending stiffness, EI (pound-inch²), of the pane and the frame boundary depends upon Youngs modulus (psi), grid size and pane thickness (inch). DM (pound-sec²/in) is the lumped, constant mass

at the grid point location. Boundary conditions are presented at the nodal edges: spring constant, KW (pound/in), rotational spring, KO (pound-in/rd), and viscous damping, KWD (pound-sec/in). In addition, there are three time variables controlling the program. As a numerical example: DT = .00001 (time step, sec) and NEND = 1000 (number of last time step) yield plate vibration of 1/100 sec real time. NP determines the print sequence, to suppress print-out at time steps not desired.

To SET INITIAL CONDITIONS, all distributed plate variables (13 x 13) are zeroed at time step, NNNN = 1, using a double DO-loop. These are:

OX(I,J), OY(I,J)	Slopes	(rd)
MX(I,J), MY(I,J)	Bending moments	(pound-in)
VX(I,J), VY(I,J)	Shear loads	(pound)
WDD(I,J)	Normal accelerations	(in/sec ²)
WD(I,J)	Velocities of displacement	(in/sec)
W(I,J)	Deflections	(in)

The external loads Q(I,J)=.1 are "quasi-zero" loads of .1 pound (or another small value) each and are assigned to stabilize the equations when the variables above eventually turn to very small values. Much higher loads, Q(I,J), replace this .1 pound loading in case of an impact load analysis (such as in run "TWO"). For another type of transient analysis, the DO-loop may be used to initially set WD(I,J) non-zero (run "ONE").

The MAIN DO-LOOP OF COMPUTATION PER TIME STEP NNNN is to DEFINE O-, M- AND V-VARIABLES IN 13 x 13 ARRAYS. This is the executing part of the routine with multi-nested DO-loops recalculating OX(I,J), OY(I,J), MX(I,J) etc.

In the sequence of determining the finite differences, the typical representative equations with line reference numbers (line numbers of run "ONE") are repeated from Figure 42: OX, OY INSIDE/BOUNDARY, (a) $OX(I,J) = (W(I+1,J) - W(I-1,J)) / DS$ (and for OY, inside and boundary) (listed at lines 66 and 67), (b) $OX(1,J) = OX(2,J) / 1. + DS \cdot KO / (2. \cdot EI)$ (and for OY, boundary) (lines 68 thru 71); MX, MY, VX, VY ON BOUNDARY, (c) $MX(II,J) = -KO \cdot OX(II,J) \cdot SIGN$ (and for MY, boundary) (lines 78 and 79), (d) $VX(II,J) = (KW(I) \cdot W(II,J) + KWD \cdot WD(II,J)) \cdot SIGN$ (and for VY, boundary) (lines 80 and 81); MX, MY INSIDE/BOUNDARY, (e) $MX(II,J) = (OX(II+1,J) - OX(II-1,J)) \cdot EI / DS$ (and for MY, inside and boundary) (lines 86 and 87); VX, VY INSIDE/BOUNDARY, (f) $VX(II,J) = (MX(II+1,J) - MX(II-1,J)) / DS$ (and for VY, inside and boundary) (lines 92 and 93); VX, VY OUTSIDE BOUNDARY, (g) $VXO(I) = 2. \cdot VX(1,I) - VX(2,I)$ (and for VYO, etc., outside and boundary) (lines 99 thru 102); CALCULATE WDD AND INTEGRATE, (h) $WDD(I,J) = (Q(I,J) - VXP + VXM - VYP + VYM) / DM$ (and for WD and W) (lines 114, 115 and 116). Finally, the IDENTIFICATION OF VARIABLES FOR PRINT-OUT and WRITING OUTPUT VARIABLES yields the required print-out at any time step NNNN. This is the END OF MAIN DO-LOOP.

c. Different Versions "ONE" and "TWO"

Example "ONE" is the first listing in Appendix IV-1. Comment cards inserted at three locations: BEGIN OF RUN "ONE" MODIFICATION and END OF RUN "ONE" MODIFICATION indicate the changes made to the basic program. Following SET INITIAL CONDITIONS (line 32), all time varying variables are zeroed, except for the quasi-zero load $Q(I,J) = .01$ (pound) and the initial velocity $WD(I,J) = 100$ (inch/sec). The main DO-loop of computation per time step, NNNN (lines 56 thru 157), is activated two times (lines 25 thru 159).

The first activation generates all time varying variables of five consecutive steps and print all these variables; the second one calculates 50 steps, printing every 10th step only. The reactivation of the DO-loop a second time is not necessarily required to get the results. This was done for ease of programming. It can be done with one use of the DO-loop.

For structural reasons as well as loading symmetry and symmetry of initial conditions, only parts of the generated patterns of numerical values are printed-out in such a way that no value in a pattern is repeated unnecessarily. This print-out is on the first and second page following the listing "ONE". It can be seen that zero values half way between the nodal points of grid generation are omitted. The WRITE and FORMAT statements under WRITING OUTPUT VARIABLES reflect the tabulation per page. Use of this basic 13 x 13 plate program for nonsymmetrical cases suggests that these statements are modified such that the entire pattern of numbers is printed.

The outer DO-loop, DO 3 NN=1, 3 (line 24), conducts two additional runs resulting in four more pages of print-out. The print-out on the third and fourth page has the same velocity, $WD(I,J)=100$, initially applied. The quasi-zero load, $Q(I,J)$, was set at .01 pound instead of .1 pound to show the difference. The generated numbers on first and third (and second and fourth) pages should be compared for similarity of results. The third and last run with reversed input signs, $WD(I,J)=-100$ and $Q(I,J)=-.01$, yields the output with the same numbers as the second run but with reversed signs.

Example "TWO" is the second listing in Appendix IV-1. Comment cards inserted at three locations show where the modifications to the basic program were made. The initial condition is a linearly increasing load at the center

of the plate, Q(7,7), rather than an initial non-zero velocity condition. The linear load increase is changed to a constant load level at .1 sec. Computation is terminated at .25 sec.

Two runs were conducted for comparison of results, using the loop, DO 1 NN=1, 2 (line 26). The first run required 1250 steps to yield .25 sec of time event; the second required 20 times as many. Displacements can be seen to increase almost linearly thru .1 sec and stay fairly constant from there thru .25 sec in both cases. The accelerations, WDD, reflect the highest deviations when comparing corresponding numbers of the two runs.

2. PLATE PROGRAM FOR CASE WT-18

This is an expansion of the basic flat plate program to simulate the deflection data of impact case WT-18. The comment cards of the listing (Appendix IV-2) are repeated with an explanation of the differences between this and the basic plate program. The self-explanatory title is FLAT PLATE PROGRAM FOR VARIABLE GRID SIZE (UP TO 21 x 21) SET UP FOR CASE WT-18.

All dimensioned variables are sized such that 21 is the maximum allowable grid size (ASSIGNING THE TIME-VARYING VARIABLES). The expanded variables as compared with those of the basic program are: displacement, W, is replaced by W, WMDT (deflection at previous time step); velocity, WD, and acceleration WDD remain the same; OX, OXMDT (slope at previous time step), OXD (rate of slope) for OX; OY, OYMDT, OYD for OY; VX, VY, Q, VX0, VY0 remain the same; VXPI and VYPI for VX14 and VY14, respectively; MX, MXEL (elastic component of bending moment), MXVC (viscous component of bending moment) for MX; MY, MYEL, MYVC for MY. The constant boundary conditions are replaced by

AFFDL-TR-74-155

these distributed ones: KW, KWD, KOX, KOY, KOXD and KOYD.

These are the pre-calculated parameters for grid sizes (VARIABLES FOR DIFFERENT GRID SIZES): L(1)=5, L(2)=9, L(3)=13, L(4)=17, L(5)=21, L(7)=29 and L(8)=33. One set of the variables, L, A and B may be chosen for grid size determination. A and B depend on grid size L.

Input data (INPUT DATA REQUIRED (CASE WT-18)) are expanded to side lengths X and Y instead of DS of the basic plate program. Any choice of N1=1 thru 8 selects the parameters L, A and B. The parameters EMOD, THCK, EIXF and EIYF stand for EI, and MPANE and MFRAME instead of DM. The basic KW, KWD and KO are replaced by KWDN (KW in downward mode), KWUP (upward), KWDC, KOXC, KOYC (all for local distribution). Added parameters KOXDC and KOYDC are rotational edge dampening; directional viscous in-pane and in-frame properties are KVSX, KVSX, KVSXF and KVSXF. QTOT is the total impact load that is pyramidally distributed. TQ is the impact time. DT, NEND and NP remain as in the basic program.

The reader is referred to lines 55 thru 73 for CALCULATION OF DEPENDENT VARIABLES. These are dependent grid (NG thru DY), stiffness (EIX and EIY), mass (DMM and DMF) and impact endurance constants (TQP, TQM) to set up the finite difference model. The DISTRIBUTION OF INITIAL CONDITIONS AND BOUNDARY CONSTANTS are lines 75 to 131, where the main DO-loop of computation begins. All (I,J) variables are zeroed for the first step NNNN=1 (lines 81 thru 98). Uniform distribution of boundary constants KW, KWD, KOX, KOY, KOXD, KOYD is accomplished (DOWNWARD AND UPWARD MODE OF KW). For SPECIAL CLAMPING FOR CASE WT-18, some KW values in the uniformly distributed pattern are selectively superposed by new values. The operations under DISTRIBUTE STABILIZING PERMANENT LOAD (lines 121, 122, 123), and SUPERPOSE PYRAMIDAL

IMPACT LOAD WT-18 (lines 127 thru 131) are self-explanatory.

All the following comments concern operations within the main DO-loop starting at line 135 (MAIN DO-LOOP OF COMPUTATION PER TIME STEP NNNN). IMPACT TIMING WT-18 (line 140) replaces the continuous quasi-zero load with the time dependent impact load distribution and reestablishes the continuous load after impact (line 36). The remaining comments are identical with those of the basic plate program: DEFINE O-, M- AND V-VALUES IN NG x NG ARRAYS; OX, OY INSIDE/BOUNDARY; ON BOUNDARY; MX, MY, VX, VY ON BOUNDARY; MX, MY INSIDE/BOUNDARY; VX, VY INSIDE/BOUNDARY; VX, VY OUTSIDE/BOUNDARY; CALCULATE WDD AND INTEGRATE; IDENTIFICATION OF VARIABLES FOR PRINT-OUT; WRITING OF OUTPUT DEFLECTIONS FOR WT-18 and END OF MAIN DO-LOOP.

The reader may compare the computational expansions of this program with the basic one. The sample of results printed out following the listing represents Figure 32 and is self-explanatory.

3. CONICAL SHELL SEGMENT PROGRAM

a. Introduction

The concept of finite difference techniques in the computer routine "flat plate" (Appendix IV-1) was applied in the development of the program for dynamic stress analysis of conical shell type windscreens and canopies. Such a program, which later could be used for typical systems hardware design, was not readily available at the time development. This monolithic conical shell routine of equal grid spacing and consistent properties (Appendix IV-3) was developed as a prerequisite for the F-111 windshield routine (Appendix IV-4).

The user should have no difficulties applying this basic code and gaining

further understanding of it by studying the F-111 applied code that is described in detail (Appendix III-4).

Serving as a proof for operational readiness of this dynamic shell program, symmetrical 17 x 17 stress and deflection matrices were observed as a result of a symmetrical impact loading history. The current listing is set up with initial velocity $WD(I,J)=50$ (in/sec) and provides symmetrical results. The example print-out at the end of the listing includes variables in reduced 17 x 17 matrix tabulation at time steps $NNNN=1$ and 4000, equivalent to .0001 and .4 seconds ($\Delta t=.0001$ sec) after the start of time history. The attached two by three, self-explanatory print-out tables were generated by the WRITE statements of lines 197 thru 230 (Appendix IV-3).

b. Discussion of Program Listing

Additional comments concerning the modifications necessary for a switch from the previously described flat plate geometry are provided. The reader is referred to Appendix III-1 for the basic comments still valid here. The title is self-explanatory: DYNAMIC CONICAL SHELL PROGRAM (17 x 17), ANY LOADING HISTORY, FIXED TANGENTIAL SUPPORT, X-VARIABLES: MX, UN, FT AND OX, FN, UT (6 FIRST ORDER DIFFERENCE EQUATIONS), Y-DIRECTION: MY, UN and OY, V (4 EQUATIONS COUPLED WITH X-VARIABLES).

ASSIGNING THE TIME-VARYING VARIABLES (line 9) incorporates the changes. The previously used plate variables W, WD, WDD are renamed by displacements, velocities and accelerations in normal directions: UN, UND, UNDD. The tangential displacement, UT, is newly introduced. Slopes OX and OY remain. Internal load, V, is replaced by FN, FT, V. External loads are QN and QT (normal and tangential) instead of Q. Masses DMM are calculated instead of using a constant distributed mass, DM. Additions are one-dimensional

AFFDL-TR-74-155

variables: FNO, FN1, VO, V1, R (radii), DX, DS, DTHX and THX (radial constants), and EIY. MX and MY remain the same.

INPUT DATA REQUIRED (NUMERICAL EXAMPLE IS ARBITRARY) are geometrical dimensions SIDE, RMAX, RMIN, THETA that replace DS of the flat plate program. A switch was made from parameter EI to THICK and E (thickness, Young's modulus), and specific density, SPDEN, instead of DM. Two-directional edge stiffnesses (KW) are KUN and KY; rates are: KUND and KYD. Rotational springs KOX and KOY stand for KO of the basic plate program (Appendix IV-1). DT, NEND and NP stay identical. The CALCULATION OF THE REMAINING INPUT is FINITE DIFFERENCES OF CONE SEGMENT, AVERAGE DENSITY OF ELEMENT, APPROXIMATE TANGENTIAL STIFFNESS INCLUDING EFFECT OF CURVATURE, and frame stiffness using the ASSUMPTION: FRAME = 5X SHELL STIFFNESS. These dependent constants are self-explanatory in lines 41 thru 72. For details, refer to the shell geometry explained in the context.

SET INITIAL CONDITION is required for variables UN, UND, UNDD, UT, OX, OY, MX, MY, FN, FT, V, QN, QT (lines 76 thru 94) prior to initiation of the MAIN DO-LOOP OF COMPUTATION PER TIME STEP NNNN to DEFINE O-, M-, and V- VALUES, and UN AND UT IN 17 x 17 ARRAYS. The computational steps in the DO-loops are: OX, OY INSIDE BY ALL UN AND UT INSIDE; OX, OY AT BOUNDARY BY INSIDE OX, OY, BOUNDARY CONDITIONS MX AND MY, AND APPROXIMATED OX, OY OUTSIDE THE BOUNDARIES; MX, MY AND FN, V AT BOUNDARY; MX, MY INSIDE AND AT EDGE BY OX, OY INSIDE; FN, V INSIDE AND AT EDGE BY MX AND MY; FN, V OUTSIDE THE BOUNDARY. An addition to the program is: FORWARD/BACKWARD CALCULATION OF FT, an alternate approach from the direct one to calculate FT. The equations are physically correct assuming a realistic distribution of FT. Use of Equation 40.1 instead, has resulted in "blow-

up" in the calculation procedure. CALCULATE UNDD AND INTEGRATE remains an unchanged procedure. As quoted for FT, the FORWARD/BACKWARD CALCULATION OF UT replaces Equation 40.2 for reasons of "blow-up". WRITING OF VARIABLES AND END OF MAIN DO-LOOP completes the algorithm.

4. F-111 WINDSHIELD AND PLOTTING PROGRAM

a. Introduction

This computer code is based on the basic shell program described and listed in Appendices III-3 and IV-3. The finite difference grid, dimensioned 17 by 17 in the present case (Figure 44), correspondingly requires as many 17 by 17 arrays of computer storage as variables employed at grid locations (Figure 45). About one quarter of these locations is actually utilized. This way, simplification of index notations in the operational equations is achieved. These equations could be rewritten in a compact form to eliminate this expenditure of storage. A more refined analysis could be conducted utilizing the mesh completely; however, the number of calculative steps would be several times larger.

At a grid size of 17 x 17, the running time of the current computer routine was less than 30 seconds per set of input data for the selected parameter print-out of a 2500 step history, totaling .25 seconds of real time. Computer time is reduced when print-out is kept at a minimum and not required at every time interval. In addition, non-sequential print-out could be triggered by desired threshold values of any timely variable.

b. Time Dependent Variables

The variables dimensioned I=1 thru 17 in radial (X) direction and J=1

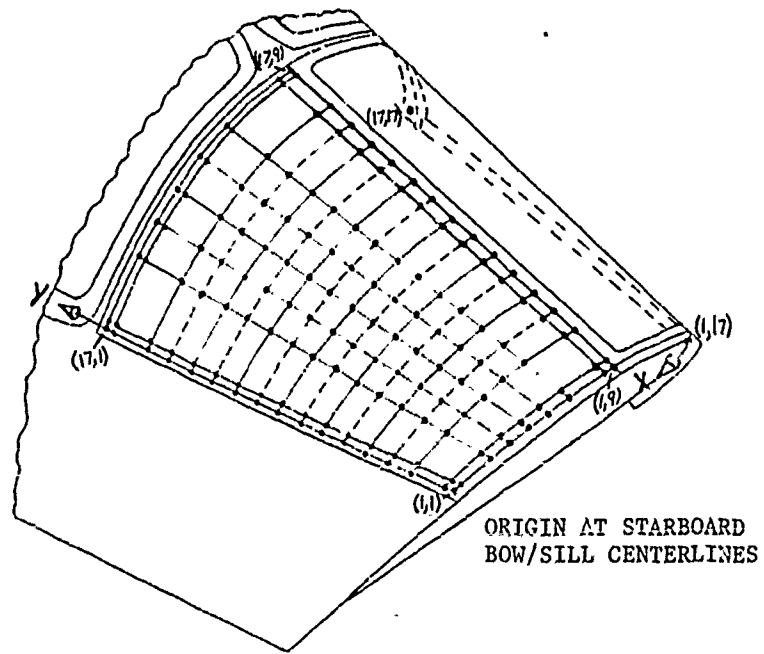


Figure 44. View of 17x17 Finite Difference Grid

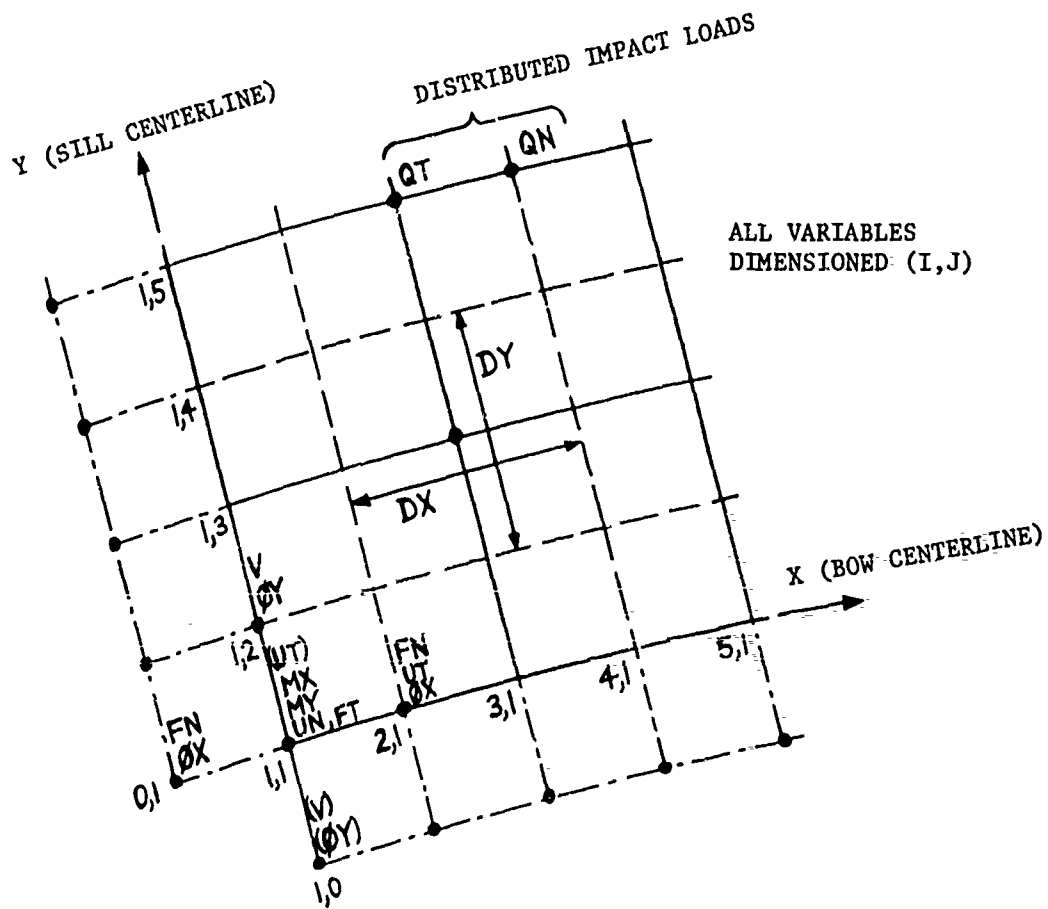


Figure 45. Typical Locations of Variables in Grid

thru 17 in longitudinal (Y) direction (Figure 45) are:

QN(I,J)	normal component of impulse force (pound)
QT(I,J)	tangential component (pound)
UN(I,J)	normal displacement (inch)
UNMDT(I,J)	normal displacement of previous time step (inch) (not used in current option, established for control of attachment_conditions)
UND(I,J)	normal velocity (in/sec)
UNDD(I,J)	normal acceleration (in/sec ²)
UT(I,J)	tangential displacement (inch)
ØX(I,J)	radial slope of deflection (rad)
ØXMDT(I,J)	radial slope of previous time step (rad)
ØXD(I,J)	rate of slope of radial deflection (rad/sec)
ØY(I,J)	longitudinal slope of deflection (rad)
ØYMDT(I,J)	slope of previous time step (rad)
ØYD(I,J)	rate of slope of deflection (rad/sec)
MX(I,J)	radial bending moment (pound-in)
MXEL(I,J)	elastic component of bending moment (pound-in)
MXVC(I,J)	viscous component (pound-in)
MY(I,J)	longitudinal bending moment (pound-in)
MYEL(I,J)	elastic component of bending moment (pound-in)
MYVC(I,J)	viscous component (pound-in)
FN(I,J)	internal normal load in radial direction (pound)
FT(I,J)	radial tangential load (pound)
V(I,J)	shear load in longitudinal direction (pound)

The histories of the normal and tangential load components, QN and QT, at time step NNNN are:

$$QT(I-1,J) = \text{SIN}(\text{THX}(I-1,J)) * Q(I,J) / 2.$$

$$QN(I,J) = \text{COS}(\text{THX}(I,J)) * Q(I,J)$$

$$QT(I+1,J) = \text{SIN}(\text{THX}(I+1,J)) * Q(I,J) / 2.$$

The present computer routine contains the Q(I,J) data of bird impact case FM-1 as a built-in, but flexible, input (see Section IV-4).

One dimensional arrays of order 17 for definition of normal loads outside the grid, FN0, FN18, V0, V18 are defined from the assumption of approximate boundary conditions of related variables to satisfy the number of equations required for solution of unknown variables.

c. Fixed Variables

Two-dimensional arrays of order 17x17 are:

DM(I,J)	mass distribution (pound-sec ² /in)
DX(I,J)	finite differences of radial secant (inch)
DS(I,J)	finite radial arch difference (inch)
DY(I,J)	longitudinal finite difference distance (inch)
THX(I,J)	radial angular spacing (rad)
DTH(I,J)	related angular expression (rad)
SNDTH(I,J)	angular expression
CSTHTH(I,J)	angular expression (inch)

EIX(I,J) radial inplane bending stiffness (pound-in²)
 EIY(I,J) longitudinal bending stiffness (pound-in²)
 KUN(I,J) translational spring mounting (pound/in)
 (only utilized at the edges)
 KØX(I,J) rotational sill stiffnesses (pound-in/rad)
 KØY(I,J) rotational bow or arch stiffnesses (pound-in/rad)
 KUND(I,J) viscous translational dampening (pound-sec/in)
 KØXD(I,J) viscous rotational sill dampening (pound-in-sec/rad)
 KØYD(I,J) rotational bow or arch dampening (pound-in-sec/rad)

One-dimensional arrays of order 17:

RD(J) radii, variable in longitudinal direction (inch)
 CIRC(J) arch lengths (inch)
 TH(J) central angles (rad)
 SD(I) variable longitudinal lengths (inch)

Determination of finite differences in the x-direction is as follows:
 RD(1) and RD(17) are minimum and maximum radii, RMIN and RMAX respectively,
 assuming a grid size of 17 (Figure 44). Radii of bow, RD(2), and arch,
 RD(16), are based on given bow and arch widths in proportion to the size
 of grid in the y-direction. The radii, RD(2) thru RD(16) vary linearly.
 All the other radial variables are as indicated in Figure 46.

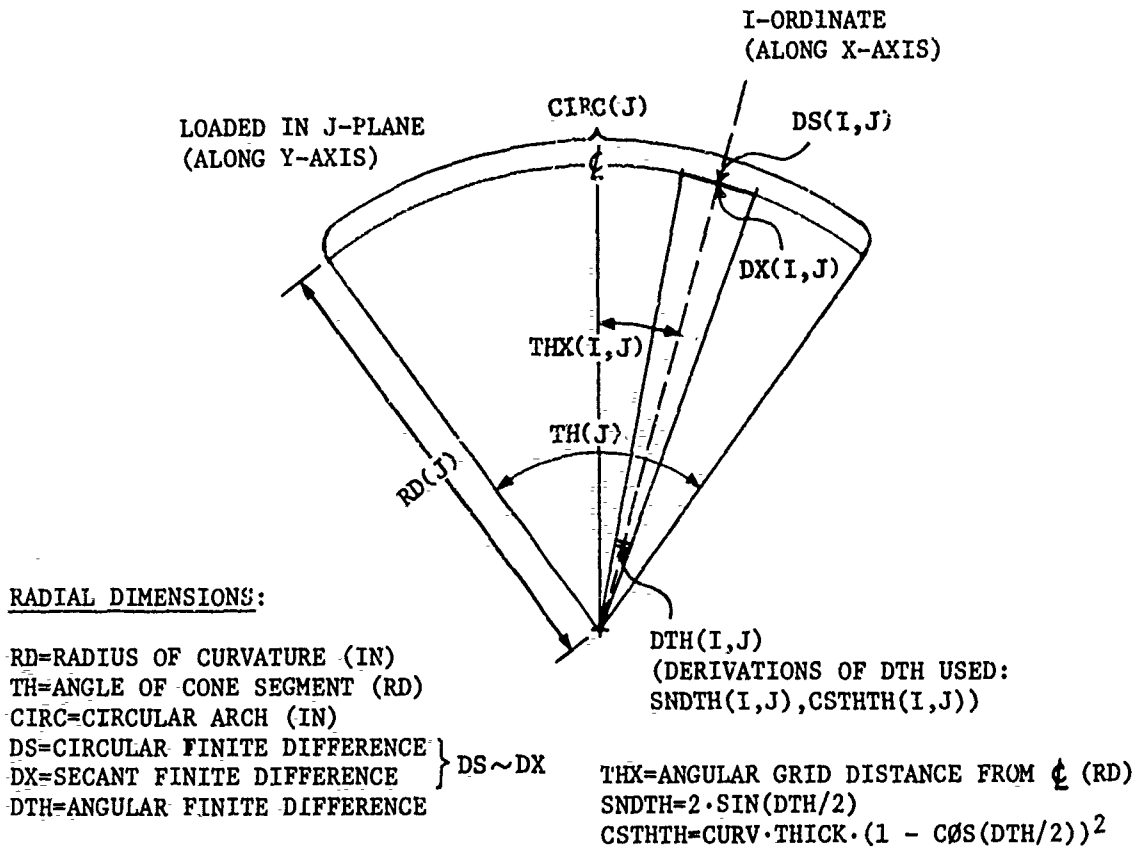


Figure 46. Geometrical Arrangement of Radial Dimensions

AFFDL-TR-74-155

The types of mass elements, $DM(I,J)$, developed at the corners (1,1), (17,1), (1,17) and (17,17) are:

$$DM(1,1)=DX(1,1) \cdot MBOW + DY(1,1) \cdot MSIL$$

For MBOW and some other constants in the following equations, see the input data

Along the frame:

$$DM(2,1)=DX(2,1) \cdot MBOW$$

Mass properties of the windshield (window pane) calculated from windshield dimensions:

$$DM(I,J)=SPDEN \cdot DS(I,J) \cdot DY(I,J) \cdot THICK$$

In-plane pane stiffnesses:

$$EIX(I,J)=EPANE \cdot THICK^3 / 12 \cdot DY(I,J)$$

$$EIY(I,J)=EPANE \cdot THICK^3 / 12 \cdot DS(I,J)$$

$$+CURV \cdot EPANE \cdot THICK(1 - \cos(DTH(I,J)/2)) \cdot RD(J)^2 \cdot DS(I,J)$$

The stiffnesses along, and transverse to, the frame (sill, head beam, arch, bow) are calculated using corresponding eight boundary stiffnesses, such as EIARC, EITAC.

When some of the attachment restraints or stiffnesses are not effective (equal to zero), very small values were actually used to stabilize the calculation procedure.

d. Input Data

An example input for operation of the computer routine is provided in Table XVII showing the time increment of each step, DT, the number of calculative steps after which the program stops, NEND, and the frequency of print-out, NP. CURV is a constant to account for additional bending stiffness due to curvature. The index, ISHEAR, set equal to the location of centerline of impact, arranges the string lengths of "forward and backward" solutions of tangential equations. COR considers the increased stiffnesses in the corners.

A description in sequence of the remaining variables in Table XVII:

THICK	thickness of window pane (inch)
LHEA	length of head beam (inch)
WHEA	width of head beam (inch)
LSIL	length of sill (inch)
WSIL	width of sill (inch)
RMIN	actual radius of bow (inch)
THMN	minimum central angle of cone segment (rad)
WBØW	width of bow (inch)
RMAX	actual radius of arch (inch)
THMX	maximum central angle of cone segment (rad)
WARC	width of arch (inch)
SPDEN	specific density of window pane (pound-sec ² /in ⁴)
MHEA	mass of head beam per running inch (pound-sec ² /in ²)
MSIL	mass of sill (pound-sec ² /in ²)
MBØW	mass of bow (pound-sec ² /in ²)

MARC	mass of arch (pound-sec ² /in ²)
EPANE	Young's modulus (pound/in ²)
VISC	pane viscous constant (pound-in ² /rad)
EIARC	bending stiffness of arch (pound-in ²)
EITAC	transverse stiffness of arch (pound-in ² /in)
KUNAC	spring mounting of arch (pound/in)
KØARC	rotational arch stiffness (pound-in/rad)
KUNDAC	viscous translational arch dampening (pound-sec/in)
KØDAC	viscous rotational arch dampening (pound-in-sec/rad)
EIHEA	bending stiffness of head beam (pound-in ²)
EITHD	transverse stiffness of head beam (pound-in)
EISIL	bending stiffness of sill (pound-in ²)
EITSL	transverse stiffness of sill (pound-in)
KUNSL	spring mounting of sill (pound/in)
KØSIL	rotational sill stiffness (pound-in/rad)
KUNDSL	viscous translational sill dampening (pound-sec/in)
KØDSL	viscous rotational sill dampening (pound-in-sec/rad)
EIBØW	bending stiffness of bow (pound-in ²)
EITBW	transverse stiffness of bow (pound-in)
KUNBW	spring mounting of bow (pound/in)
KØBØW	rotational bow stiffness (pound-in/rad)
KUNDBW	viscous translational bow dampening (pound-sec/in)
KØDBØW	viscous rotational bow dampening (pound-in-sec/rad)

e. Calculation Procedure

The calculations start by zeroing the variables for initial conditions ($I=1,17$ and $J=1,17$): UN, UND, UNDD, UT, OX, OY, MX, MY, FN, FT, V. Load inputs to initially stabilize equations are quasi-zero loads of .01 pounds everywhere on the grid for QN, and QT on the right side ($I=1,8$), $QT=0$ at the center line ($I=9$), and $QT= -.01$ on the left side ($I=10,17$). The calculation continues similar to the "flat plate" routine of Appendix IV-1. Plotted results for this example may be found at the end of the listing of this program (Appendix IV-4): the three page 17×17 matrix print-out per time step, NNNN, at .025 sec and .05 sec ($DT = .0001$, $NEND = 500$, $NP = 250$). The print-out of the selected strain and deflection histories (of case "1", see page 272) is self-explanatory. Here, $NP = 5$ yields 100 values per column. For further details, the user is referred to the comments in the program listing which are practically identical with the basic conical shell program that was adapted to this bird strike case, FM-1. One then simply follows the FORTRAN statements in both the listings (Appendix IV-3 and 4).

APPENDIX IV
COMPUTER PROGRAM LISTINGS

The attached FORTRAN IV source programs:

1. FLAT PLATE, one starting at page 222, the other at 231,
2. PLATE WT-18 (page 236),
3. CONICAL SHELL SEGMENT (page 245), and
4. F-111 W/S (FM-1) on page 256,

contain built-in input parameters and flexible input data. A modest amount of printed output has been generated at selected time steps.

The source decks of the computer programs described herein can be obtained by contacting AFFDL (FBS/JANSEN), W-PAFB, OH, 45433, (513)255-5548.

```

1      C
2      C FLAT PLATE PROGRAM FOR FIXED GRID SIZE (13X13)
3      C PARAMETRICAL RUN *****
4      C
5      C PROGRAM MAIN(OUTPUT,TAPE6=OUTPUT)
6      C
7      C ASSIGNING THE TIME-VARYING VARIABLES
8      C
9      DIMENSION N(13,13),MO(13,13),NDO(13,13),OX(13,13),OY(13,13),VX(13,
10     C13),VY(13,13),Q(13,13),VX0(13),VY0(13),VX14(13),VY14(13)
11     REAL MX(13,13),MY(13,13)
12     REAL KO,KH,KWD
13
14     C INPUT DATA REQUIRED (NUMERICAL EXAMPLE IS ARBITRARY)
15     C
16     OS=*.
17     EI=20000.
18     DM=.302
19     KW=10000.
20     KMO=1.
21     KO=10000.
22     CT=.0031
23
24     C BEGIN OF RUN ***** MODIFICATION
25     DO 3 NN=1,3
26     DO 2 N=1,2
27     NP=1
28     IF(N.EQ.2) NEND=100
29     IF(N.EQ.2) NP=20
30     C END OF RUN ***** MODIFICATION
31     C
32     C SET INITIAL CONDITIONS
33     C
34     WRITE(6,1)
35     FORMAT(1H1)
36     DO 10 J=1,13
37     DO 16 I=1,13
38     Q(I,J)=.01
39     IF(NN.EQ.2) Q(I,J)=.1
40     IF(NN.EQ.3) Q(I,J)=-.1
41     W(I,J)=0.
42     MO(I,J)=100.
43     IF(NN.EQ.3) MO(I,J)=100.
44     C END OF RUN ***** MODIFICATION
45     MDD(I,J)=0.
46     OX(I,J)=0.
47     OY(I,J)=0.
48     VX(I,J)=0.
49     VY(I,J)=0.
50     MX(I,J)=0.
51     MY(I,J)=0.
52
53     16
54     C
55     C MAIN DO-LOOP OF COMPUTATION PER TIME STEP NNNN
56     DO 1000 NNNN=1,NEND
57     T=0.7*NNNN

```

```

60 C DEFINE O,M AND V VALUES IN 13X13 ARRAYS
C
C DO 20 J=1,13,2
C CX,OY INSIDE/BOUNDARY
C
C DO 30 I=2,12,2
OX(I,J)=(M(I+1,J)-M(I-1,J))/DS
OY(J,I)=(M(J,I+1)-M(J,I-1))/DS
OX(1,J)=OX(2,J)/(1.+DS*KO/(2.*EI))
OX(13,J)=OX(12,J)/(1.+DS*KO/(2.*EI))
OY(J,1)=OY(J,2)/(1.+DS*KO/(2.*EI))
OY(J,13)=OY(J,12)/(1.+DS*KO/(2.*EI))
C
C MX,MY,VX,VY ON BOUNDARY
C
C DO 40 II=1,13,12
SIGN=1.
IF(II.EQ.1) SIGN=-1.
MX(II,J)=KO*OX(II,J)*SIGN
MY(J,II)=-KO*OY(J,II)*SIGN
VX(II,J)=(KM*M(II,J)+KMD*MO(II,J))*SIGN
VY(J,II)=(KM*M(J,II)+KMD*MO(J,II))*SIGN
C
C MX,MY INSIDE/BOUNDARY
C
C DO 50 II=3,11,2
MX(II,J)=(OX(II+1,J)-OX(II-1,J))*EI/DS
MY(J,II)=(OY(J,II+1)-OY(J,II-1))*EI/DS
C
C VX,VY INSIDE/BOUNDARY
C
C DO 60 II=2,12,2
VX(II,J)=(MX(II+1,J)-MX(II-1,J))/DS
VY(J,II)=(MY(J,II+1)-MY(J,II-1))/DS
C
C CONTINUE
C
C VX,VY OUTSIDE BOUNDARY
C
C DO 70 I=1,13,2
JX(I)=2.*JX(I,I)-JX(2,I)
VX(I,I)=2.*VX(I,3)-VX(12,I)
VY(I,I)=2.*VY(I,1)-VY(I,2)
J*14(I)=2.*JY(I,13)-V*(I,12)
C
C CALCULATE WDD AND INTEGRATE
C
C DO 80 J=1,13,2
DO 80 I=1,13,2
VXP=VX(I,J)
IF(I.NE.13) VXP=VX(I+1,J)
VYM=VY(I,J)
IF(I.NE.1) VYM=VY(I-1,J)
VYP=VY(I,I)
IF(J.NE.13) VYP=VY(I,J+1)
VYM=VY(I,I)

```

```

115 IF(J.NE.1) VYH=VY(I,J-1)
    MDD(I,J)=(Q(I,J)-VXP+VXM-VYP+VYM)/DM
    MO(I,J)=MO(I,J)+DT*MDD(I,J)
    M(I,J)=M(I,J)+DT*M(I,J)
    CONTINUE
120 IF(MOD(MNHN,MP).NE.0) GO TO 1000
C IDENTIFICATION OF VARIABLES FOR PRINT-OUT
C
    WRITE(6,100)
    FORMAT(* TIME SLOPE OX (OY) SHEAR VX (VY)* )
125 C MX (MY) MOMENT
C WRITING OUTPUT VARIABLES
C
    WRITE(6,101) T,OX(2,1),OX(2,3),OX(2,5),OX(2,7),MX(1,1),MX(1,3),
    CHX(1,5),MX(1,7),VX(2,1),VX(2,3),VX(2,5),VX(2,7)
    FORMAT(13E10.3)
130 WRITE(6,102) OX(4,1),OX(4,3),OX(4,5),OX(4,7),MX(3,3),MX(3,5),
    VX(3,7),VX(4,1),VX(4,3),VX(4,5),VX(4,7)
    L.VX(3,7),VX(4,1),VX(4,3),VX(4,5),VX(4,7)
135 FORMAT(10X,4E10.3,10X,3E10.3,4E10.3)
    WRITE(6,103) OX(6,1),OX(6,3),OX(6,5),OX(6,7),MX(5,5),MX(5,7),
    CVX(6,1),VX(6,3),VX(6,5),VX(6,7)
140 FORMAT(10X,4E10.3,20X,2E10.3,4E10.3)
    WRITE(6,104) MX(7,7)
    FORMAT(80X,E10.3)
    WRITE(6,200)
    FORMAT(* ACCELERATION MDD VELOC
    QTY MO DISPLACEMENT M*)
145 WRITE(6,201) MDD(1,1),MDD(1,3),MDD(1,5),MDD(1,7),MO(1,1),MO(1,3),
    MO(1,5),MO(1,7),M(1,1),M(1,3),M(1,5),M(1,7)
    FORMAT(10X,12E10.3)
201 WRITE(6,202) MDD(3,3),MDD(3,5),MDD(3,7),MO(3,3),MO(3,5),MO(3,7),
    CH(3,3),M(3,5),M(3,7)
202 FORMAT(20X,3E10.3,10X,3E10.3,10X,3E10.3)
150 WRITE(6,203) MDD(5,5),MDD(5,7),MO(5,5),MO(5,7),M(5,5),M(5,7)
    FORMAT(30X,2E10.3,20X,2E10.3,20X,2E10.3)
203 WRITE(6,204) MDD(7,7),MO(7,7),M(7,7)
    FORMAT(40X,E10.3,30X,E10.3,30X,E10.3/)
C
C END OF MAIN DO-LOOP
C
160 CONTINUE
C BEGIN OF RUN ***** MODIFICATION
2 CONTINUE
3 CONTINUE
C END OF RUN ***** MODIFICATION
STOP
END

```


TIME	SLOPE OX (OY)	SLOPE OY (OX)	MOMENT MX (MY)	MOMENT MY (MX)	VELOCITY X (Y)	VELOCITY Y (X)	SHEAR VX (VY)	SHEAR VY (VX)	DISPLACEMENT X (Y)
.200E-02	.182E-02	.277E-01	.380E-01	.357E-01	.908E+01	.138E+03	.190E+03	.104E+03	.435E+01
	.155E-03	.122E-01	.122E-01	.119E-01	-.856E+02	-.129E+03	-.129E+03	.127E+03	.150E+01
	.104E-04	.129E-02	-.156E-02	-.151E-02	-.688E+02	-.688E+02	.179E+02	.151E+02	.155E+01
	ACCELERATION X (Y)	ACCELERATION Y (X)	VELOCITY X (Y)	VELOCITY Y (X)	MOMENT MX (MY)	MOMENT MY (MX)	VELOCITY X (Y)	VELOCITY Y (X)	DISPLACEMENT X (Y)
	.655E+04	.608E+05	.413E+05	-.449E+05	.275E+02	.317E+02	.309E+02	.309E+02	.175E-03
	-.626E+05	-.531E+05	-.594E+04	.180E+05	-.109E+02	.457E+02	.475E+02	.475E+02	.118E-01
		.594E+04	.412E+05	.412E+05		.123E+03	.123E+03	.122E+03	.118E-01
									.165E+00
									.222E+00
									.209E+03
TIME	SLOPE OX (OY)	SLOPE OY (OX)	MOMENT MX (MY)	MOMENT MY (MX)	VELOCITY X (Y)	VELOCITY Y (X)	SHEAR VX (VY)	SHEAR VY (VX)	DISPLACEMENT X (Y)
.400E-02	.613E-03	.144E-01	.406E-01	.541E-01	.307E+01	.520E+02	.203E+03	.270E+03	.716E+00
	.654E-03	.208E-01	.528E-01	.597E-01	.610E+02	.610E+02	.610E+02	.270E+02	-.106E+00
	.609E-03	.141E-01	.210E-01	.209E-01	-.159E+03	-.159E+03	-.159E+03	-.194E+03	-.147E+01
	ACCELERATION X (Y)	ACCELERATION Y (X)	VELOCITY X (Y)	VELOCITY Y (X)	MOMENT MX (MY)	MOMENT MY (MX)	VELOCITY X (Y)	VELOCITY Y (X)	DISPLACEMENT X (Y)
	-.549E+04	-.316E+05	.244E+05	-.257E+05	.179E+01	.451E+01	.639E+01	.518E+01	.294E-03
	.289E+05	.383E+04	.383E+04	-.219E+05	-.203E+02	-.218E+02	-.218E+02	.177E+02	.502E-01
		.424E+05	-.385E+05	-.385E+05	.307E+02	.307E+02	.307E+02	.117E+03	.502E-01
			-.728E+04	-.728E+04				.213E+03	.582E-02
									.165E+00
									.382E+00
									.165E+00
									.567E+08
TIME	SLOPE OX (OY)	SLOPE OY (OX)	MOMENT MX (MY)	MOMENT MY (MX)	VELOCITY X (Y)	VELOCITY Y (X)	SHEAR VX (VY)	SHEAR VY (VX)	DISPLACEMENT X (Y)
.600E-02	.832E-03	.161E-01	.406E-01	.538E-01	.216E+01	.805E+02	.203E+03	.269E+03	.787E+00
	.234E-03	.247E-01	.651E-01	.902E-01	.831E+02	.831E+02	.831E+02	.182E+03	-.375E-01
	.536E-05	.132E-01	.383E-01	.544E-01	-.134E+03	-.134E+03	-.134E+03	-.179E+03	.272E+00
	ACCELERATION X (Y)	ACCELERATION Y (X)	VELOCITY X (Y)	VELOCITY Y (X)	MOMENT MX (MY)	MOMENT MY (MX)	VELOCITY X (Y)	VELOCITY Y (X)	DISPLACEMENT X (Y)
	-.119E+04	-.121E+05	.122E+05	-.783E+04	.190E-01	.140E+01	.312E+01	.941E+00	.129E-03
	.159E+05	.159E+05	.159E+05	-.617E+05	.229E+02	.229E+02	.243E+02	.111E+02	.129E-03
			-.173E+04	-.617E+05	.310E+02	.310E+02	.310E+02	-.377E+02	.686E-01
									.686E-01
									.429E+00
									.793E+00
TIME	SLOPE OX (OY)	SLOPE OY (OX)	MOMENT MX (MY)	MOMENT MY (MX)	VELOCITY X (Y)	VELOCITY Y (X)	SHEAR VX (VY)	SHEAR VY (VX)	DISPLACEMENT X (Y)
.800E-02	.107E-02	.291E-01	.532E-01	.603E-01	.536E+01	.146E+03	.266E+03	.302E+03	.179E+01
	.711E-03	.248E-01	.489E-01	.544E-01	-.218E+02	-.218E+02	-.218E+02	-.294E+02	-.231E+00
	.166E-03	.729E-02	.128E-01	.106E-01	-.180E+03	-.180E+03	-.180E+03	-.249E+03	.267E+00
	ACCELERATION X (Y)	ACCELERATION Y (X)	VELOCITY X (Y)	VELOCITY Y (X)	MOMENT MX (MY)	MOMENT MY (MX)	VELOCITY X (Y)	VELOCITY Y (X)	DISPLACEMENT X (Y)
	-.572E+03	-.516E+04	.601E+04	-.374E+04	.259E-01	.858E+00	.372E+01	.641E+01	.204E-03
	.254E+05	.254E+05	.254E+05	-.139E+05	.168E+02	.168E+02	.152E+02	.378E+02	.204E-03
			-.526E+05	-.250E+05	-.632E+02	-.632E+02	-.632E+02	-.944E+02	.123E+00
									.489E+00
									.493E+00
TIME	SLOPE OX (OY)	SLOPE OY (OX)	MOMENT MX (MY)	MOMENT MY (MX)	VELOCITY X (Y)	VELOCITY Y (X)	SHEAR VX (VY)	SHEAR VY (VX)	DISPLACEMENT X (Y)
.100E-01	.860E-03	.225E-01	.411E-01	.483E-01	.430E+01	.112E+03	.206E+03	.242E+03	-.466E+00
	.135E-02	.208E-01	.192E-01	.163E-01	-.118E+03	-.118E+03	-.118E+03	-.150E+03	-.150E+01
	.635E-03	.784E-02	.499E-02	.510E-02	-.709E+02	-.709E+02	-.709E+02	-.552E+02	-.698E+00
	ACCELERATION X (Y)	ACCELERATION Y (X)	VELOCITY X (Y)	VELOCITY Y (X)	MOMENT MX (MY)	MOMENT MY (MX)	VELOCITY X (Y)	VELOCITY Y (X)	DISPLACEMENT X (Y)
	.372E+02	-.131E+04	.696E+04	-.952E+04	-.921E-01	-.207E+01	-.411E+01	-.600E+01	.476E-04
	-.189E+05	-.189E+05	-.481E+05	-.176E+05	-.439E+02	-.439E+02	-.742E+02	-.102E+03	-.76E-04
			.450E+04	.264E+04	-.833E+02	-.833E+02	-.833E+02	-.344E+02	.890E-01
									.890E-01
									.166E+00
									.242E+00
									.261E+00
									.283E+00


```

1 C FLAT PLATE PROGRAM FOR FIXED GRID SIZE (13X13)
C PARABOLICAL RUN *****
5 C PROGRAM MAIN(OUTPUT,TAPE6=OUTPUT)
C ASSIGNING THE TIME-VARYING VARIABLES
C DIMENSION M(13,13),MO(13,13),W0(13,13),OX(13,13),OY(13,13),VK(13,
10 C13),VY(13,13),Q(13,13),VX0(13),VK1(13),VY0(13),VY1(13)
REAL M(13,13),MY(13,13)
REAL KO,KW,KMD
C INPUT DATA REQUIRED (NUMERICAL EXAMPLE IS ARBITRARY)
15 C
DS=6.
EI=20000.
DM=.002
KM=10000.
KMD=1.
KO=10000.
OT=.002
NEND=1250
NP=250
C BEGIN OF RUN *****MODIFICATION
20 DO 2 NN=1,2
IF(NN.EQ.2) OT=.0001
IF(NN.EQ.2) NEND=2500
IF(NN.EQ.2) NP=500
C END OF RUN *****MODIFICATION
30 C
C SET INITIAL CONDITIONS
C WRITE(6,1)
FORMAT(IH1)
DO 10 J=1,13
DO 10 I=1,13
Q(I,J)=1
W(I,J)=0
MO(I,J)=0
OX(I,J)=0
OY(I,J)=0
VX(I,J)=0
VY(I,J)=0
VX(I,J)=0
VY(I,J)=0
35 DO 100 NNN=1,NEND
C MAIN DO-LOOP OF COMPUTATION PER TIME STEP NNNN
C BEGIN OF RUN *****MODIFICATION
Q(7,7)=1+NNN
IF(NNN.GT.500) Q(7,7)=500.
GO TO 4
3  Q(7,7)=.05*NNNN

```

PROGRAM MAIN 74/74 OPT=1

```

4      IF(NNNN.GT.10000) Q(7,7)=500.
      T=OT*NNNN
      C END OF RUN ***** MODIFICATION
      C DEFINE O, M AND V VALUES IN 13*13 ARRAYS
      C
      DO 25 J=1,13,2
      C OX,OY INSIDE/BOUNDARY
      C
      DO 30 I=2,12,2
      OX(I,J)=(M(I+1,J)-M(I-1,J))/DS
      OY(I,J)=(M(I,J,I+1)-M(I,J,I-1))/DS
      OX(I,J)=OX(I+2,J)/(1.+DS*KO/(2.*EI))
      OY(I,J)=OY(I+2,J)/(1.+DS*KO/(2.*EI))
      OY(J,I)=OY(J,12)/(1.+DS*KO/(2.*EI))
      C MX,MY,VX,VY ON BOUNDARY
      C
      DO 40 II=1,13,12
      SIGN=1.
      IF(II.EQ.1) SIGN=-1.
      MX(II,J)=-KO*OX(II,J)*SIGN
      MY(J,II)=-KO*OY(J,II)*SIGN
      VX(II,J)=(KM*W(II,J)+KMD*MD(II,J))*SIGN
      VY(J,II)=(KM*W(J,II)+KMD*MD(J,II))*SIGN
      C
      C MX,MY INSIDE/BOUNDARY
      C
      DO 50 II=3,11,2
      MX(II,J)=(OX(II+1,J)-OX(II-1,J))*EI/DS
      MY(J,II)=(OY(J,II+1)-OY(J,II-1))*EI/DS
      C
      C JX,JY INSIDE/BOUNDARY
      C
      DO 60 II=2,12,2
      VX(II,J)=(MX(II+1,J)-MX(II-1,J))/DS
      VY(J,II)=(MY(J,II+1)-MY(J,II-1))/DS
      C
      C JX,JY OUTSIDE BOUNDARY
      C
      DO 70 I=1,13,2
      VX(I)=2.*VX(I,I)-VX(2,I)
      VX(1,I)=2.*VX(13,I)-VX(12,I)
      VY(I)=2.*VY(I,1)-VY(I,2)
      VY(1,I)=2.*VY(11,I)-VY(10,I)
      C
      C CALCULATE WDD AND INTEGRATE
      C
      DO 80 J=1,13,2
      DO 86 I=1,13,2
      VXP=VX(I,J)
      IF(I.NE.13) JXP=VX(I+1,J)
      VXM=VY(I,J)
      IF(I.NE.1) VXM=VX(I-1,J)
  
```

```

115 VYP=VY14(I)
    IF(J.NE.13) VYP=VY(I,J+1)
    VYM=VY0(I)
    IF(J.NE.1) VYM=VY(I,J-1)
120 MD(I,J)=0(I,I,J)-JXP+VXM-JYP+JVM/JDM
    MD(I,J)=MD(I,J)+DT*MOD(I,J)
    M(I,J)=M(I,J)+DT*MD(I,J)
    CONTINUE
    IF(MOD(NNNN,NP).NE.0) GO TO 1000
C IDENTIFICATION OF VARIABLES FOR PRINT-OUT
C
130 WRITE(6,100)
    FORMAT(* TIME SLOPE OX (OY) SHEAR JX (JY)*)
C MX (MY) MOMENT
C WRITING OUTPUT VARIABLES
C
135 WRITE(6,101) T,OX(2,1),OX(2,3),OX(2,5),OX(2,7),MX(1,1),MX(1,3),
    CHX(1,5),MX(1,7),VX(2,1),VX(2,3),VX(2,5),VX(2,7)
    FORMAT(13E10.3)
136 WRITE(6,132) OX(4,1),OX(4,3),OX(4,5),OX(4,7),MX(3,3),MX(3,5),
    CHX(3,7),VX(4,1),VX(4,3),VX(4,5),VX(4,7)
    FORMAT(10X,4E10.3,10X,3E10.3,4E10.3)
140 WRITE(6,133) OX(6,1),OX(6,3),OX(6,5),OX(6,7),MX(5,5),MX(5,7),
    CUX(6,1),VX(6,3),VX(6,5),VX(6,7)
    FORMAT(10X,4E10.3,20X,2E10.3,4E10.3)
145 WRITE(6,104) MX(7,7)
    FORMAT(80X,E10.3)
    WRITE(6,200)
    FORMAT(* ACCELERATION MDD DISPLACEMENT M*)
    JELOCI
150 WRITE(6,201) MDD(1,1),MDD(1,3),MDD(1,5),MDD(1,7),MD(1,1),MD(1,3),
    MD(1,5),MD(1,7),M(1,1),M(1,3),M(1,5),M(1,7)
    FORMAT(10X,12E10.3)
155 WRITE(6,202) MDD(3,3),MDD(3,5),MDD(3,7),MD(3,3),MD(3,5),MD(3,7),
    CM(3,3),M(3,5),M(3,7)
    FORMAT(20X,3E10.3,10X,3E10.3,10X,3E10.3)
160 WRITE(6,203) MDD(5,5),MDD(5,7),MD(5,5),MD(5,7),M(5,5),M(5,7)
    FORMAT(30X,2E10.3,20X,2E10.3,20X,2E10.3)
165 WRITE(6,204) MDD(7,7),MD(7,7),M(7,7)
    FORMAT(40X,E10.3,30X,E10.3,30X,E10.3)
C
C END OF MAIN DO-LOOP
C
1000 CONTINUE
C BEGIN OF RUN *****TWO***** MODIFICATION
2 CONTINUE
C END OF RUN *****TWO***** MODIFICATION
STOP
END

```

TIME	SLOPE OX (OY)	ACCELERATION WDD	VELOCITY WC	MOMENT MX (MY)	VELOCITY MX (VY)	DISPLACEMENT W
.500E+01	.202E-03 .152E-03 -.169E-04	.244E-02 .971E-02 .418E-02	.178E-01 .239E-01 .135E-01	.412E+02 .733E+01 -.518E+02	.115E+03 .560E+02 -.269E+02	.847E+01 -.875E+01 -.353E+01
	ACCELERATION WDD	VELOCITY WC	MOMENT MX (MY)	VELOCITY MX (VY)	DISPLACEMENT W	
	.642E+00 .169E+02 .328E+03	.228E+02 .367E+03 .364E+03	.220E-01 .337E+00 .145E+03 .251E+03 -.639E+03	.220E-02 .603E-01 .149E+03	.402E-01 -.404E+00 .136E+00 .134E+01	.843E-03 .338E-01 .168E+00 .334E+00
TIME	SLOPE OX (OY)	ACCELERATION WDD	VELOCITY WC	MOMENT MX (MY)	VELOCITY MX (VY)	DISPLACEMENT W
.100E+00	.413E-03 .303E-03 -.384E-04	.166E-01 .194E-01 .831E-02	.357E-01 .477E-01 .270E-01	.831E+02 .138E+02 -.104E+03	.220E+03 .111E+03 -.545E+02 -.555E+03	-.173E+02 -.409E+02 -.415E+02 -.415E+03
	ACCELERATION WDD	VELOCITY WC	MOMENT MX (MY)	VELOCITY MX (VY)	DISPLACEMENT W	
	-.161E+01 .237E+02	.155E+02 .481E+03 .729E+03	.193E+02 .260E+03 .271E+03 -.598E+02	-.189E-01 -.313E+00 .338E+03	-.286E-01 -.346E-01 .810E+00 .226E+01	.172E-02 .681E-01 .337E+00 .667E+00
TIME	SLOPE OX (OY)	ACCELERATION WDD	VELOCITY WC	MOMENT MX (MY)	VELOCITY MX (VY)	DISPLACEMENT W
.150E+00	.418E-03 .314E-03 -.366E-04	.168E-01 .195E-01 .826E-02	.359E-01 .476E-01 .268E-01	.830E+02 .137E+02 -.104E+03	.221E+03 .110E+03 -.548E+02 -.552E+03	-.175E+02 -.466E+02 -.412E+02 -.411E+02
	ACCELERATION WDD	VELOCITY WC	MOMENT MX (MY)	VELOCITY MX (VY)	DISPLACEMENT W	
	.209E+01 -.285E+02	.389E+02 -.204E+03 .547E+03 .132E+04	.665E+01 .932E+02 .547E+03 .132E+04	-.987E-02 -.161E+00 .518E+03	-.697E-02 .383E+00 .139E+01 .233E+01	.292E-02 .146E+00 .337E+00 .667E+00
TIME	SLOPE OX (OY)	ACCELERATION WDD	VELOCITY WC	MOMENT MX (MY)	VELOCITY MX (VY)	DISPLACEMENT W
.200E+00	.423E-03 .313E-03 -.368E-04	.169E-01 .195E-01 .825E-02	.361E-01 .477E-01 .268E-01	.843E+02 .133E+02 -.105E+03	.222E+03 .109E+03 -.552E+02 -.552E+03	-.177E+02 -.407E+02 -.408E+02 -.408E+02
	ACCELERATION WDD	VELOCITY WC	MOMENT MX (MY)	VELOCITY MX (VY)	DISPLACEMENT W	
	-.131E+01 -.262E+03	.216E+02 -.280E+03 .102E+03 .163E+04	.205E+02 .462E+02 .781E+03 .163E+04	.916E-02 .312E+00 .853E+00 .193E+01	.215E-01 .551E+00 .133E+01 .193E+01	.302E-02 .147E+00 .338E+00 .666E+00
TIME	SLOPE OX (OY)	ACCELERATION WDD	VELOCITY WC	MOMENT MX (MY)	VELOCITY MX (VY)	DISPLACEMENT W
.250E+00	.420E-03 .309E-03 -.352E-04	.168E-01 .196E-01 .832E-02	.361E-01 .480E-01 .269E-01	.842E+02 .137E+02 -.105E+03	.222E+03 .110E+03 -.599E+02 -.554E+03	-.176E+02 -.411E+02 -.469E+02 -.469E+02
	ACCELERATION WDD	VELOCITY WC	MOMENT MX (MY)	VELOCITY MX (VY)	DISPLACEMENT W	
	-.160E+01 -.118E+02 -.113E+03	.214E+02 .127E+03 -.147E+03	.557E-01 .106E+01 .131E+01 .106E+01	.340E-01 .703E+00 .131E+01	.742E-01 .122E+01 .135E+01 .106E+01	.300E-02 .148E+00 .339E+00 .668E+00

TIME	SLOPE OX (OY)	ACCELERATION MDD	VELOCITY MD	MOMENT MX (MY)	SHEAR VX (VY)	DISPLACEMENT W
.500E+01	.202E-03 .824E-02	.366E+00 .129E+02	.327E-03 .671E-03	.101E+01 .412E+02	-.316E+00 -.848E+01	-.147E+02 -.135E+02
	.152E-03 .971E-02	.297E+03	.179E-01	.732E+01	-.147E+00 -.872E+01	-.205E+02 -.207E+02
	-.164E-04 .419E-02	.449E+03	.106E+00	-.517E+02	.251E+00 -.359E+01	-.289E+02 -.628E+02
TIME	SLOPE OX (OY)	ACCELERATION MDD	VELOCITY MD	MOMENT MX (MY)	SHEAR VX (VY)	DISPLACEMENT W
.100E+00	.413E-03 .166E-01	.389E-01 .121E+01	.327E-03 .671E-03	.101E+01 .412E+02	-.316E+00 -.848E+01	-.147E+02 -.135E+02
	.304E-03 .194E-01	.343E+03	.179E-01	.732E+01	-.147E+00 -.872E+01	-.205E+02 -.207E+02
	-.404E-04 .829E-02	.766E+03	.106E+00	-.517E+02	.251E+00 -.359E+01	-.289E+02 -.628E+02
TIME	SLOPE OX (OY)	ACCELERATION MDD	VELOCITY MD	MOMENT MX (MY)	SHEAR VX (VY)	DISPLACEMENT W
.150E+00	.419E-03 .166E-01	.389E-01 .121E+01	.327E-03 .671E-03	.101E+01 .412E+02	-.316E+00 -.848E+01	-.147E+02 -.135E+02
	.312E-03 .195E-01	.343E+03	.179E-01	.732E+01	-.147E+00 -.872E+01	-.205E+02 -.207E+02
	-.369E-04 .828E-02	.766E+03	.106E+00	-.517E+02	.251E+00 -.359E+01	-.289E+02 -.628E+02
TIME	SLOPE OX (OY)	ACCELERATION MDD	VELOCITY MD	MOMENT MX (MY)	SHEAR VX (VY)	DISPLACEMENT W
.200E+00	.422E-03 .168E-01	.361E-01 .136E+02	.165E-02 .250E-01	.210E+01 .838E+02	-.658E+00 -.176E+02	-.303E+02 -.279E+02
	.312E-03 .195E-01	.343E+03	.179E-01	.732E+01	-.147E+00 -.872E+01	-.205E+02 -.207E+02
	-.363E-04 .825E-02	.766E+03	.106E+00	-.517E+02	.251E+00 -.359E+01	-.289E+02 -.628E+02
TIME	SLOPE OX (OY)	ACCELERATION MDD	VELOCITY MD	MOMENT MX (MY)	SHEAR VX (VY)	DISPLACEMENT W
.250E+00	.418E-03 .168E-01	.361E-01 .136E+02	.165E-02 .250E-01	.210E+01 .838E+02	-.658E+00 -.176E+02	-.303E+02 -.279E+02
	.311E-03 .195E-01	.343E+03	.179E-01	.732E+01	-.147E+00 -.872E+01	-.205E+02 -.207E+02
	-.368E-04 .838E-02	.766E+03	.106E+00	-.517E+02	.251E+00 -.359E+01	-.289E+02 -.628E+02

```

1  C FLAT PLATE PROGRAM FOR VARIABLE GRID SIZE (UP TO 21*21)
  C SET UP FOR CASE WT-18
  C
  C PROGRAM MAIN(OUTPUT, TAPE5=OUTPUT)
  C
  C ASSIGNING THE TIME-VARYING VARIABLES
  C
  C DIMENSION M(21,21),MD(21,21),MDD(21,21),OX(21,21),OY(21,21),VX(21,
  C21),VY(21,21),Q(21,21),MMOT(21,21),OKMOT(21,21),OYMDT(21,21),OXD(2
  C1,21),OYD(21,21),JX0(21),JY0(21),JVP1(21)
  C REAL MX(21,21),MY(21,21),MXEL(21,21),MYEL(21,21),MXVC(21,21),
  C CHVC(21,21),MX(21,21),KMD(21,21),KXD(21),KOY(21),KOD(21),KODD(21)
  C REAL KOXC,KOXDC,KOYDC,KOYDC,KJXYC,KJXYC,KJXYC,KJXYC,KVSYF,KHDC,
  C KMDN,KMUP,MFRANE,MPANE
  C
  C VARIABLES FOR DIFFERENT GRID SIZES
  C
  C DIMENSION L(8),A(8),B(8)
  C DATA L(1),L(2),L(3),L(4),L(5),L(6),L(7),L(8)/5,9,13,17,21,25,
  C29,33/
  C DATA A(1),A(2),A(3),A(4),A(5),A(6),A(7),A(8)/2.,20.,7.,168.,
  C330.,572.,913.,1160./
  C DATA B(1),B(2),B(3),B(4),B(5),B(6),B(7),B(8)/5.,17.,37.,65.,
  C11.,145.,197.,257./
  C
  C INPUT DATA REQUIRED (CASE WT-18)
  C
  X=25.
  Y=25
  N1=5
  EMOD=.329E+06
  THCK=.956
  EIXF=.129E+06
  EIJF=.129E+06
  MPANE=.0615
  MFRANE=.1613
  KMDN=.1E+06
  KMUP=.1E-10
  KHDC=.1E-10
  KOXC=10000.
  KOYDC=10000.
  KOXC=.1E-10
  KOYDC=.1E-10
  KJXY=.1E-10
  KJXY=.1E-10
  KVSYF=.5E-10
  KVSYF=.5E-10
  QTOT=25000.
  TQ=.0013
  OT=.0001
  NEND=400
  NP=4
  C
  C CALCULATION OF DEPENDENT VARIABLES
  C
  NG=L(N1)

```


PROGRAM MAIN 74/74 OPT=1

```

115      KM(1,13,2)=.1E+06
        KM(2,13,2)=.1E+06
        KM(2,13,2)=.1E+06
120      C JISTRIBUTE STABILIZING PERMANENT LOAD
        C
        DO 29 I=1,NG
          DO 20 J=1,NGP6
            G(I,J)=.1
        2C
        C SUPERPOSE PYRAMIDAL IMPACT LOAD WT-19
        C
        DO 25 J=3,NGC,2
          K=NGP1-J
          DO 25 I=J,K,2
            DO 25 II=J,K,2
              G(II,II)=(J-1)*QTOT/NQ
        25
        C MAIN DO-LOOP CF COMPUTATION PER TIME STEP.NNNN
        C
        DO 100 NNNN=1,NNNN
          T=DT*NNNN
        C IMPACT TIMING WT-18
        C
        IF(I.EQ.0008) GO TO 30
        GO TO 35
        DO 40 J=3,NGM2,2
          DO 40 I=3,NGM2,2
            G(I,J)=Q(I,J+6)
        4C
        35 IF(I.LI.TOH.OR.T.GT.TOP) GO TO 45
          DO 50 J=3,NGM2,2
            DO 50 I=3,NGM2,2
              G(I,J)=.1
            CONTINUE
        50
        45
        C
        C DEFINE O,M AND J VALUES IN NG*NS ARRAYS
        C
        DO 55 J=1,NG,2
        C OX,OY INSIDE/BOUNDARY
        C
        DO 60 I=2,NGM1,2
          OXMDT(I,J)=OX(I,J)
          OX(I,J)=(M(I+1,J)-M(I-1,J))/DX
          OKD(I,J)=(OX(I,J)-OXMDT(I,J))/DT
          OYMDT(J,I)=OY(J,I)
          OY(J,I)=(M(J,I+1)-M(J,I-1))/DY
          OYD(J,I)=(OY(J,I)-OYMDT(J,I))/DT
        60
        C ON BOUNDARY
        C
          EIXG=EIX
          IF(J.EQ.1.OR.J.EQ.NG) EIXC=EIXF
          OXMDT(1,J)=OX(1,J)
          OX(1,J)=OX(2,J)/(1.+OX*KOX(J)/(2.*EIXC))
          OXDI(J)=(OX(1,J)-OXMDT(1,J))/DT

```

```

175 OXMDT(NG,J)=OX(NG,J)
    OX(NG,J)=OX(NGM1,J)/(1.+OX*KOX(J)/(2.*EIXC))
    OXD(NG,J)=(OX(NG,J)-OXMDT(NG,J))/DT
    EIYC=EIX
    IF(J.EQ.1.OR.J.EQ.NG) EIYC=EIYF
    OYMDT(J,1)=OY(J,1)
    OY(J,1)=OY(J,2)/(1.+OY*KOY(J)/(2.*EIYC))
    OYD(J,1)=(OY(J,1)-OYMDT(J,1))/DT
180 OYMDT(J,NG)=OY(J,NG)
    OY(J,NG)=OY(J,NGM1)/(1.+OY*KOY(J)/(2.*EIYC))
    OYD(J,NG)=(OY(J,NG)-OYMDT(J,NG))/DT
    C MX,MY,JX,JY ON BOUNDARY
    C
185 DO 65 IZ=1,NG,NGM1
    SIGN=-1
    IF(IZ.EQ.1) SIGN=-1.
    MXEL(II,J)=-KOX(J)*OX(II,J)*SIGN
    MXJC(II,J)=-KOX(J)*OXD(II,J)*SIGN
    MYEL(II,J)=MYEL(II,J)+MXVC(II,J)
    MYJC(II,J)=-KOY(J)*OY(J,II)*SIGN
    MYVC(II,J)=-KOYD(J)*OYD(J,II)*SIGN
    MY(J,II)=MYEL(J,II)+MYVC(J,II)
    I=1
    IF(M(II,J).LE.0.) I=2
    VA(II,J)=(KM(II,J,I)*M(II,J)+KMD(J)*MD(II,J))*SIGN
    I=1
    IF(M(J,II).LE.0.) I=2
    VV(J,II)=(KM(J,II,I)*M(J,II)+KMD(J)*MD(J,II))*SIGN
200 C MA,MY INSIDE/BOUNDARY
    C
205 DO 70 II=3,NGM2,2
    EIXG=EIX
    IF(J.EQ.1.OR.J.EQ.NG) EIXG=EIXF
    KVSXC=KVSX
    IF(J.EQ.1.OR.J.EQ.NG) KJSXC=KJSXF
    MXEL(II,J)=(OX(II+1,J)-OX(II-1,J))*EIXC/OX
    MXVC(II,J)=(OXD(II+1,J)-OXD(II-1,J))*KVSXC/OX
    MYEL(II,J)=MYEL(II,J)+MYVC(II,J)
    EIXG=EIX
    IF(J.EQ.1.OR.J.EQ.NG) EIXG=EIXF
    KJSYC=KJSY
    IF(J.EQ.1.OR.J.EQ.NG) KVSYC=KVSYF
    MYEL(J,II)=(OY(J,II+1)-OY(J,II-1))*EIXC/OY
    MYVC(J,II)=(OYD(J,II+1)-OYD(J,II-1))*KVSYC/OY
    MY(J,II)=MYEL(J,II)+MYVC(J,II)
210 C
215 DO 75 II=2,NGM1,2
    VV(II,J)=(MX(II+1,J)-MX(II-1,J))/DX
    VV(J,II)=(MY(J,II+1)-MY(J,II-1))/DY
220 C
225 C VV,VY OUTSIDE BOUNDARY
    C

```

PROGRAM MAIN 74774 OP.=1

```

230 DO 80 I=1,NG,2
      VX(I)=2.*VX(I,I)-VX(I,2,I)
      VXP1(I)=2.*VX(NG,I)-VX(NG+1,I)
      VY(I)=2.*VY(I,I)-VY(I,2)
      VYP1(I)=2.*VY(NG,I)-VY(NG+1,I)
80   C
235 C CALCULATE MOD AND INTEGRATE
      DO 85 J=1,NG,2
      DO 85 I=1,NG,2
      DM=DMH
      IF(I.EQ.1.OR.I.EQ.NG.OR.J.EQ.1.OR.J.EQ.NG) DM=DMF
      VXP=VXP1(J)
      IF(I.NE.NG) VXP=VX(I+1,J)
      VXH=VX(I,J)
      IF(I.NE.1) VXH=VX(I-1,J)
      VYP=VYP1(I)
      IF(J.NE.NG) VYP=VY(I,J+1)
      VYH=VY(I,I)
      IF(I.NE.1) VYH=VY(I,J-1)
      MOD(I,J)=CO(I,J)-VXP1*VXH-VYP+VYH/DM
      MOD(I,J)=MOD(I,J)+DT*MOD(I,J)
      MODT(I,J)=MOD(I,J)
      M(I,J)=M(I,J)+DT*MOD(I,J)
85   CONTINUE
      IF(MOD(NM,NK,NP).NE.0) GO TO 1800
255 C IDENTIFICATION OF VARIABLES FOR PRINT-OUT
      C
      WRITE(6,100)
100  FORMAT(4 TIME M(1,1) M(5,1) M(11,1) M(1,5) M(11,7)
      C M(11,9) M(1,11) M(7,11) M(1,21) M(5,21) M(11,21)
      C)
260 C
      C PRINTING OF OUTPUT DEFLECTIONS FOR WT-16
      C
      WRITE(6,200) T,M(1,1),M(5,1),M(11,1),M(1,5),M(11,7),M(11,9),
      C M(1,11),M(7,11),M(1,21),M(5,21),M(11,21)
200  FORMAT(F6.4,12E10.3)
      C
      C END OF MAIN DO-LOOP
270 C
      1000 CONTINUE
      STOP
      END

```


0228	M(1,1)	M(5,1)	M(11,1)	M(11,7)	M(11,9)	M(1,11)	M(7,11)	M(11,11)	M(1,21)	M(5,21)	M(11,21)
	-629E-01	-947E-02	-436E+00	-932E+00	-115E+01	-532E-02	-392E-02	-112E+01	-546E+00	-275E+00	-124E-01
0229	M(1,1)	M(5,1)	M(11,1)	M(11,7)	M(11,9)	M(1,11)	M(7,11)	M(11,11)	M(1,21)	M(5,21)	M(11,21)
	-849E-01	-81E-01	-447E+00	-602E+00	-832E+00	-777E-02	-592E+00	-812E+00	-588E+00	-353E+00	-177E-01
0230	M(1,1)	M(5,1)	M(11,1)	M(11,7)	M(11,9)	M(1,11)	M(7,11)	M(11,11)	M(1,21)	M(5,21)	M(11,21)
	-129E+00	-75E-01	-414E+00	-430E+00	-362E+00	-147E-01	-351E+00	-357E+00	-792E+00	-11E+00	-356E-03
0231	M(1,1)	M(5,1)	M(11,1)	M(11,7)	M(11,9)	M(1,11)	M(7,11)	M(11,11)	M(1,21)	M(5,21)	M(11,21)
	-121E+00	-552E-02	-315E+00	-121E+00	-102E+00	-217E-01	-205E-01	-901E-01	-900E+00	-456E+00	-159E-01
0240	M(1,1)	M(5,1)	M(11,1)	M(11,7)	M(11,9)	M(1,11)	M(7,11)	M(11,11)	M(1,21)	M(5,21)	M(11,21)
	-336E-01	-105E-01	-291E+00	-149E+00	-272E+00	-963E-03	-152E+00	-532E+00	-987E+00	-505E+00	-739E-01
0241	M(1,1)	M(5,1)	M(11,1)	M(11,7)	M(11,9)	M(1,11)	M(7,11)	M(11,11)	M(1,21)	M(5,21)	M(11,21)
	-146E-02	-133E-01	-247E+00	-649E+00	-452E+00	-131E-02	-336E+00	-413E+00	-196E+01	-589E+00	-152E+00
0248	M(1,1)	M(5,1)	M(11,1)	M(11,7)	M(11,9)	M(1,11)	M(7,11)	M(11,11)	M(1,21)	M(5,21)	M(11,21)
	-751E-01	-539E-02	-662E-01	-746E+00	-711E+00	-267E-01	-952E+00	-533E+00	-114E+01	-665E+00	-347E+00
0252	M(1,1)	M(5,1)	M(11,1)	M(11,7)	M(11,9)	M(1,11)	M(7,11)	M(11,11)	M(1,21)	M(5,21)	M(11,21)
	-861E-01	-697E-02	-567E-01	-912E+00	-867E+00	-292E-02	-562E+00	-662E+00	-125E+01	-722E+00	-509E+00
0256	M(1,1)	M(5,1)	M(11,1)	M(11,7)	M(11,9)	M(1,11)	M(7,11)	M(11,11)	M(1,21)	M(5,21)	M(11,21)
	-245E-01	-226E-03	-299E-01	-823E+00	-896E+00	-152E-01	-768E+00	-951E+00	-129E+01	-793E+00	-497E+00
0260	M(1,1)	M(5,1)	M(11,1)	M(11,7)	M(11,9)	M(1,11)	M(7,11)	M(11,11)	M(1,21)	M(5,21)	M(11,21)
	-14E-01	-136E-01	-148E+00	-952E+00	-112E+01	-950E-03	-336E+00	-123E+01	-126E+01	-823E+00	-482E+00
0264	M(1,1)	M(5,1)	M(11,1)	M(11,7)	M(11,9)	M(1,11)	M(7,11)	M(11,11)	M(1,21)	M(5,21)	M(11,21)
	-144E+00	-852E-02	-205E+00	-116E+00	-152E+01	-712E-02	-101E+01	-142E+01	-118E+01	-338E+00	-491E+00
0268	M(1,1)	M(5,1)	M(11,1)	M(11,7)	M(11,9)	M(1,11)	M(7,11)	M(11,11)	M(1,21)	M(5,21)	M(11,21)
	-206E+00	-450E-02	-135E+00	-119E+01	-147E+01	-301E-02	-102E+01	-132E+01	-103E+01	-334E+00	-524E+00
0272	M(1,1)	M(5,1)	M(11,1)	M(11,7)	M(11,9)	M(1,11)	M(7,11)	M(11,11)	M(1,21)	M(5,21)	M(11,21)
	-157E+00	-140E-01	-145E+00	-102E+01	-119E+01	-682E-02	-34E+00	-113E+01	-872E+00	-891E+00	-603E+00
0276	M(1,1)	M(5,1)	M(11,1)	M(11,7)	M(11,9)	M(1,11)	M(7,11)	M(11,11)	M(1,21)	M(5,21)	M(11,21)
	-725E-02	-652E-02	-138E+00	-756E+00	-805E+00	-805E-02	-710E+00	-883E+00	-762E+00	-313E+00	-701E+00
0280	M(1,1)	M(5,1)	M(11,1)	M(11,7)	M(11,9)	M(1,11)	M(7,11)	M(11,11)	M(1,21)	M(5,21)	M(11,21)
	-382E-01	-132E-01	-256E-01	-532E+00	-643E+00	-111E-02	-477E+00	-672E+00	-525E+00	-587E+00	-795E+00
0284	M(1,1)	M(5,1)	M(11,1)	M(11,7)	M(11,9)	M(1,11)	M(7,11)	M(11,11)	M(1,21)	M(5,21)	M(11,21)
	-134E+00	-298E-02	-362E-01	-329E-01	-526E+00	-117E-01	-397E+00	-502E+00	-472E+00	-525E+00	-825E+00
0288	M(1,1)	M(5,1)	M(11,1)	M(11,7)	M(11,9)	M(1,11)	M(7,11)	M(11,11)	M(1,21)	M(5,21)	M(11,21)
	-777E-01	-112E-01	-716E-01	-281E+00	-307E+00	-108E-01	-204E+00	-371E+00	-335E+00	-391E+00	-731E+00
0292	M(1,1)	M(5,1)	M(11,1)	M(11,7)	M(11,9)	M(1,11)	M(7,11)	M(11,11)	M(1,21)	M(5,21)	M(11,21)
	-233E-01	-106E-01	-258E+00	-144E+00	-179E+00	-218E-01	-576E-01	-102E+00	-143E+00	-257E+00	-632E+00
0296	M(1,1)	M(5,1)	M(11,1)	M(11,7)	M(11,9)	M(1,11)	M(7,11)	M(11,11)	M(1,21)	M(5,21)	M(11,21)
	-481E-01	-212E-02	-372E+00	-492E-01	-302E-01	-337E-01	-112E+00	-132E+00	-467E-01	-183E+00	-518E+00
0300	M(1,1)	M(5,1)	M(11,1)	M(11,7)	M(11,9)	M(1,11)	M(7,11)	M(11,11)	M(1,21)	M(5,21)	M(11,21)
	-584E-01	-206E-01	-392E+00	-259E+00	-284E+00	-614E-02	-482E+00	-522E+00	-616E-01	-144E+00	-388E+00
0304	M(1,1)	M(5,1)	M(11,1)	M(11,7)	M(11,9)	M(1,11)	M(7,11)	M(11,11)	M(1,21)	M(5,21)	M(11,21)
	-450E-01	-152E-01	-426E+00	-608E+00	-836E+00	-359E-01	-719E+00	-911E+00	-428E-01	-586E-01	-304E+00
0308	M(1,1)	M(5,1)	M(11,1)	M(11,7)	M(11,9)	M(1,11)	M(7,11)	M(11,11)	M(1,21)	M(5,21)	M(11,21)
	-682E-01	-203E-01	-424E+00	-912E+00	-115E+01	-702E-02	-325E+00	-120E+01	-446E-01	-956E-01	-241E+00
0312	M(1,1)	M(5,1)	M(11,1)	M(11,7)	M(11,9)	M(1,11)	M(7,11)	M(11,11)	M(1,21)	M(5,21)	M(11,21)
	-593E-01	-397E-02	-382E+00	-131E+01	-128E+01	-782E-02	-112E+01	-137E+01	-899E-01	-126E+00	-351E+00
0316	M(1,1)	M(5,1)	M(11,1)	M(11,7)	M(11,9)	M(1,11)	M(7,11)	M(11,11)	M(1,21)	M(5,21)	M(11,21)
	-917E-01	-177E-01	-334E+00	-127E+01	-140E+01	-258E-02	-116E+01	-142E+01	-193E+00	-110E+00	-616E-01
0320	M(1,1)	M(5,1)	M(11,1)	M(11,7)	M(11,9)	M(1,11)	M(7,11)	M(11,11)	M(1,21)	M(5,21)	M(11,21)
	-14E+00	-693E-02	-149E+00	-152E+01	-153E+01	-239E-01	-119E+01	-143E+01	-379E+00	-133E+00	-496E-01
0324	M(1,1)	M(5,1)	M(11,1)	M(11,7)	M(11,9)	M(1,11)	M(7,11)	M(11,11)	M(1,21)	M(5,21)	M(11,21)
	-932E-01	-192E-01	-123E+00	-135E+01	-179E+01	-562E-02	-130E+01	-155E+01	-532E+00	-139E+00	-185E+00
0328	M(1,1)	M(5,1)	M(11,1)	M(11,7)	M(11,9)	M(1,11)	M(7,11)	M(11,11)	M(1,21)	M(5,21)	M(11,21)
	-170E-01	-170E-01	-256E+00	-161E+01	-178E+01	-424E-02	-129E+01	-168E+01	-675E+00	-154E+00	-242E+00
0332	M(1,1)	M(5,1)	M(11,1)	M(11,7)	M(11,9)	M(1,11)	M(7,11)	M(11,11)	M(1,21)	M(5,21)	M(11,21)
	-267E-01	-170E-02	-377E+00	-136E+01	-162E+01	-128E-01	-116E+01	-164E+01	-794E+00	-731E+00	-289E+00


```

1 C DYNAMIC CONICAL SMELL PROGRAM (17X17)
C ANY LOADING HISTORY, FIXED TANGENTIAL SUPPORT
C X-VARIABLES --M,UM,FT AND OX,FM,UT (6 FIRST ORDER DIFF.EQ.S)
C Y-DIRECTION --MY,UN AND OY,V (4 EQ.S COUPLED WITH X-VAR.S)
C PROGRAM MAIN(OUTPUT, IAPES=OUTPUT)
C ASSIGNING THE TIME-VARYING VARIABLES
C DIMENSION UN(17,17), UNO(17,17), UNDO(17,17), UT(17,17), OX(17,17),
20 2OHK(17,17), FN(17,17), FT(17,17), V(17,17), VN(17,17), QN(17,17), QT(17,17),
C DIMENSION FNO(17), FNI(17), V0(17), V10(17), R(17), ROX(17), OS(17),
15 1DTHX(17), THX(17), EIX(17)
REAL *K(17,17), MY(17,17)
REAL KOX,KOY,KUN,KUNO,KY,KYO
C INPUT DATA REQUIRED (NUMERICAL EXAMPLE IS ARBITRARY)
C
20 SIOE=100.
RMAX=25.
KMIN=20.
THETA=3.1416
THICK=1.
E=340000.
SPOEN=.0012
KUN=10000.
KY=10000.
KUNO=.1
KYO=.1
KOX=100000.
KOY=100000.
DT=.0001
NEND=4000
NF=4000
C CALCULATION OF REMAINING INPUT
C (1) FINITE DIFFERENCES OF CONE SEGMENT
C
40 OY=SIOE/8.
OR=(RMAX-RMIN)/16.
OTHEI=THETA/16.
SMOIN=2.*SIN(OTHEI)
DO 100 J=1,17
R(J)=RMIN+OR*(J-1)
DX(J)=SNOI2*R(J)
100 OS(J)=THETA*R(J)/8.
THX(1)=0.
DTHX(1)=.5*THETA
DO 105 J=2,17
105 DTHX(J)=DTHX(J-1)+OTHEI
165 DTHX(J)=.5*THETA-DTHX(J)
C (2) AVERAGE DENSITY OF ELEMENT
C
CO 110 I=1,17

```

PROGRAM MAIN 74/74 OPT=1

```

60      DO 110 J=1,17
        110 DM(I,J)=DS(J)*OY*THICK*SPDEN
        C (3) APPROX. EY(J)=EY + EFFECT OF CURVATURE
        C ASSUMPTION -- FRAME = 5 X SHELL STIFFNESS
        C
        65      CSTHTH=.125*THICK*(1.-COS(OTHEI))**2
            THCK=THICK**3/12.
            EYF=L.
        DO 115 J=1,17,2
        115 EY(J)=OS(J)*(THCK+(CSTHTH*(J)**2))**E
            EYF=EYF+EY(J)/9.
            EIX=E*OY*THCK
            EIXF=5.*EIX
        C SET INITIAL CONDITIONS
        C
        75      DO 120 J=1,17
        120 I=1,17
            UN(I,J)=0.
            UNO(I,J)=50.
            UT(I,J)=0.
            OX(I,J)=0.
            OY(I,J)=0.
            PX(I,J)=0.
            PY(I,J)=0.
            FV(I,J)=0.
            FT(I,J)=0.
            V(I,J)=0.
            OM(I,J)=.01
            QT(I,J)=.01
            OT(9,J)=0.
        DO 130 I=10,17
        130 QT(I,J)=.01
        120 CONTINUE
        C MAIN DO-LOOP OF COMPUTATION PER TIME STEP MNHN
        C DEFINE O,M, AND V (UN,UT) VALUES IN 17*17 ARAYS
        C
        100      DO 1000 MNHN=1,REND
            T=OT*MNHN
            DO 135 J=1,17,2
        C OX,OY INSIDE BY ALL UN AND UT INSIDE
        C
        DO 140 I=2,16,2
        140 OY(I,J)=((UN(I+1,J)-UN(I-1,J))/SNODH2-UT(I,J))/R(J)
            OY(J,I)=((UN(J,I+1)-UN(J,I-1))/DY)
        C OX,OY AT BOUNDARY BY INSIDE OX,OY, BOUND. COND. MX,MY AND OX,OY APPROX.
        C
            EIXC=EIX
            EYIC1=EY(I)
            EYIC17=EY(I7)
            IF(J.NE.1.OR.J.NE.17) GO TO 145
    
```

```

115 EIXC=EIXF
    EIVCI=EIVF
    EIVC17=EIVF
145 OX(1,J)=OX(2,J)/(1.+OX(J)*KOX/(2.*EIXC))
    OX(17,J)=OX(16,J)/(1.+OX(J)*KOX/(2.*EIXC))
    OY(J,1)=OY(J,2)/(1.+OY*KOY/(2.*EIVC1))
    OY(J,17)=OY(J,16)/(1.+OY*KOY/(2.*EIVC17))
C
C MX,MY AND FN,V AT BOUNDARY
C
    DO 155 II=1,17,16
    SIGN=1.
    IF(II.EQ.1) SIGN=-1.
    KX(II,J)=-KOX*OX(II,J)*SIGN
    KY(J,II)=-KOY*OY(J,II)*SIGN
    FN(II,J)=(KUN*UN(II,J)+KUN*UND(II,J))*SIGN
150 V(J,II)=(KY*UN(J,II)+KYO*UND(J,II))*SIGN
    GO 155 II=3,15,2
C
C MX,MY INSIDE/EDGE BY OX,OY INSIDE
C
    EIXC=EIX
    EIVC=EIV(III)
    IF(J.EQ.1.OR.J.EQ.17) EIXC=EIXF
    IF(J.EQ.1.OR.J.EQ.17) EIVC=EIVF
140 KX(II,J)=(OX(II+1,J)-OX(II-1,J))*EIXC/OX(J)
    KY(J,II)=(OY(J,II+1)-OY(J,II-1))*EIVC/OY
    DO 160 II=2,16,2
C
C FN,V INSIDE/EDGE BY MX,MY
C
    FN(II,J)=(KX(II+1,J)-KX(II-1,J))/DX(J)
160 V(J,II)=(KY(J,II+1)-KY(J,II-1))/DY
C
C FN,V OUTSIDE BOUNDARY
C
    FNC(J)=2.*FN(1,J)-FN(2,J)
    FNI(J)=2.*FN(17,J)-FN(16,J)
    VC(J)=2.*V(J,1)-V(J,2)
    VI(J)=2.*V(J,17)-V(J,16)
155 I=1,17,2
C
C FORWARD/BACKWARD CALCULATION OF FT
C
    FT(I,J)=FT(I-2,J)-FN(I-1,J)*SNDI+2*QT(I-1,J)
    K=18-I
160 FT(K,J)=FT(K+2,J)+FN(K+1,J)*SNDI+2*QT(K+1,J)
135 CONTINUE
    DO 170 J=1,17,2
C
C CALCULATE UNOD AND INTEGRATE
C
    DO 175 I=1,17,2
    CH=DMH(I,J)
    IF(I.EQ.1.OR.I.EQ.17.OR.J.EQ.1.OR.J.EQ.17) DM=DMH(I,J)/2.
    FNP=FN18(J)
170 IF(I.NE.17) FNP=FN(I+1,J)

```

```

175 FNM=FND(J)
    IF(I,NE,1) FNM=FN(I-1,J)
    VP=V18(I)
    IF(I,NE,17) VP=V(I,J+1)
    VM=V0(I)
    IF(I,NE,1) VM=V(I,J-1)
    UNDD(I,J)=(QN(I,J)-FNP*FNM+FT(I,J)*SNDTH2-(P+JM)/DM
    UN(I,J)=UN(I,J)+DT*UNDD(I,J)
180 UN(I,J)=UN(I,J)+DT*UNDD(I,J)
    175 CONTINUE
C FOREWARD/BACKW. CALC. OF UT
C
185 UI(2,J)=-.5*UN(1,J)*SNDTH2
    UT(16,J)=-.5*UN(17,J)*SNDTH2
    DO 186 I=4,8,2
    UI(I,J)=UT(I-2,J)-UN(I-1,J)*SNDTH2
    K=18-I
190 UT(K,J)=UT(K+2,J)+UN(K+1,J)*SNDTH2
    176 CONTINUE
C IDENTIFICATION AND WRITING OF VARIABLES FOR PRINT-OUT
C
195 IF(MNHN,EG,1) GO TO 185
    IF(MOD(MNHN,MP),NE,0) GO TO 1000
    185 WRITE(6,1)
        WRITE(6,365) ((QN(I,J),I=1,17,2),I),J=1,17,2)
        WRITE(6,370) ((QT(I,J),I=2,16,2),I),J=1,17,2)
        WRITE(6,375) ((OX(I,J),OX(I,J),I=2,16,2),OX(17,J),I),J=1,17,2)
        WRITE(6,380) ((OY(I,1),I=1,17,2),I),
            1 ((OY(1,J),I=1,17,2),I),J=2,16,2),
            2 ((OY(1,17),I=1,17,2),I)
        WRITE(6,1)
        WRITE(6,365) ((FM(I,J),I=1,17,2),I),J=1,17,2)
        WRITE(6,390) ((FM(I,J),I=1,17,2),I),J=1,17,2)
        WRITE(6,395) ((FN(I,J),I=2,16,2),FN(17,J),I),J=1,17,2)
        WRITE(6,400) ((V(I,1),I=1,17,2),I),
            1 ((V(1,J),I=1,17,2),I),J=2,16,2),
            2 ((V(1,17),I=1,17,2),I)
        WRITE(6,405) ((FT(I,J),I=1,17,2),I),J=1,17,2)
        WRITE(6,1)
        WRITE(6,410) ((UN(I,J),I=1,17,2),I),J=1,17,2)
        WRITE(6,415) ((UND(I,J),I=1,17,2),I),J=1,17,2)
        WRITE(6,420) ((UND(I,J),I=1,17,2),I),J=1,17,2)
        WRITE(6,425) ((UT(I,J),I=2,16,2),I),J=1,17,2)
        FORMAT(1H)
1 365 FORMAT(9I5X,9E10.3,15X,E10.3,5X,'QNP')
    370 FORMAT(9I10X,9E10.3,20X,E10.3,5X,'QT')
    375 FORMAT(10I5X,10X,E10.3,10X,E10.3,5X,'OX')
    380 FORMAT(10I5X,9E10.3,15X,E10.3,15X,'OX')
    385 FORMAT(9I5X,9E10.3,15X,E10.3,5X,'OY')
    390 FORMAT(9I5X,9E10.3,15X,E10.3,5X,'FM')
    395 FORMAT(9I10E10.3,10X,E10.3,5X,'V')
    400 FORMAT(10I5X,9E10.3,15X,E10.3,5X,'FT')
    405 FORMAT(9I5X,9E10.3,15X,E10.3,5X,'UN')
    410 FORMAT(9I5X,9E10.3,15X,E10.3,5X,'UND')
    415 FORMAT(9I5X,9E10.3,15X,E10.3,5X,'UT')

```

PROGRAM MAIN

74/74 OPT=1

FTN 4.4+2401

09/26/75

09.10.53.

PAGE

5

230 420 FORMAT(9(5X,9E10.3,15X,E10.3,3X,*JM00*/))
425 FORMAT(9(10X,8E10.3,20X,E10.3,5X,*UT*/))
C END OF MAIN DO-LOOP
C
235 1000 CONTINUE
STOP
END

.739E-02	.220E-01	.729E-02	UN	.400E+00
.165E-01	.167E+00	.165E-01	UN	.400E+00
.10E-01	.218E+00	.120E-01	UN	.400E+00
.515E-01	.333E+00	.515E-01	UN	.400E+00
.308E-02	.472E+00	.308E-02	UN	.400E+00
.745E-01	.679E+00	.745E-01	UN	.400E+00
.833E-01	.592E+00	.833E-01	UN	.400E+00
.572E-01	.339E+00	.572E-01	UN	.400E+00
.352E-02	.127E-01	.352E-02	UN	.400E+00
.989E+01	.035E+01	.989E+01	UND	.400E+00
.481E+01	.481E+01	.481E+01	UND	.400E+00
.830E+01	.833E+01	.833E+01	UND	.400E+00
.234E+01	.257E+02	.234E+01	UND	.400E+00
.142E+02	.142E+02	.142E+02	UND	.400E+00
.190E+02	.190E+02	.190E+02	UND	.400E+00
.195E+02	.213E+02	.195E+02	UND	.400E+00
.233E+01	.173E+02	.233E+01	UND	.400E+00
.265E+01	.221E+01	.265E+01	UND	.400E+00
.148E+04	.730E+04	.148E+04	UNDD	.400E+00
.152E+04	.215E+04	.152E+04	UNDD	.400E+00
.648E+04	.598E+03	.648E+04	UNDD	.400E+00
.205E+05	.598E+03	.205E+05	UNDD	.400E+00
.613E+04	.146E+04	.613E+04	UNDD	.400E+00
.142E+05	.438E+04	.142E+05	UNDD	.400E+00
.161E+05	.156E+04	.161E+05	UNDD	.400E+00
.102E+05	.230E+04	.102E+05	UNDD	.400E+00
.252E+03	.214E+04	.252E+03	UNDD	.400E+00
.142E-02	.999E-02	.142E-02	UT	.400E+00
.322E-02	.683E-01	.322E-02	UT	.400E+00
.235E-02	.235E-02	.235E-02	UT	.400E+00
.101E-01	.101E-01	.101E-01	UT	.400E+00
.601E-03	.601E-03	.601E-03	UT	.400E+00
.145E-01	.145E-01	.145E-01	UT	.400E+00
.163E-01	.163E-01	.163E-01	UT	.400E+00
.112E-01	.112E-01	.112E-01	UT	.400E+00
.686E-03	.686E-03	.686E-03	UT	.400E+00

```

1 C IMPACT ANALYSIS OF F-111 MODULE/WIND SHIELD (CASE FM-1)
C ANY LOADING HISTORY, FIXED TANGENTIAL SUPPORT
C X-VARIABLES --RX,UN,FT AND OX,FM,UT (6 FIRST ORDER DIFF.E.L.S)
5 C Y-DIRECTION --RY,UN AND OY,V (4 EQ.S COUPLED WITH X-VAR.S)
C
C PROGRAM MAIN(OUTPUT,TAPE6=OUTPUT,PLOT)
COMMON DATA(603),XX(102),Y(100,18),YY(102)
C ASSIGNING THE TIME-VARYING AND PERMANENT VARIABLES
C
C DIMENSION UN(17,17),UNMD(17,17),UNDO(17,17),UF(17,17),
10X(17,17),OXND(17,17),OXD(17,17),OY(17,17),OYMD(17,17),
20YD(17,17),FY(17,17),FY(17,17),V(17,17),QNC(17,17),QF(17,17),
JOH(17,17),THX(17,17),OS(17,17),OTM(17,17),SNOT(17,17),DX(17,17),
40Y(17,17),CSTHTH(17,17),EIX(17,17),EIV(17,17)
DIMENSION FNO(17),FNI(17),VU(17),VU(17),RD(17),THE(17),CIRC(17),
15G(17),ST(20)
REAL KUN(17,17),KOX(17,17),KOY(17,17),KUND(17,17),KXKD(17,17),
20YOYD(17,17),MX(17,17),MY(17,17),MXV(17,17),MYV(17,17),
..VEL(17,17),MYVC(17,17)
REAL KUNSL,KUNBK,KUNAC,KOSIL,KOBOM,KOASC,KUNOSL,KUNDB4,KUNDAC,
1KQDSIL,KOQBOM,KODARC,LHEA,LSIL,MHEA,MSIL,MBOM,MARC
C INPUT DATA REQUIRED (NUMERICAL EXAMPLE IS ARBITRARY)
C
C DATA DT,NEND,NP,FRC,CURV,ISHEAR,COR/.0001,500,5,15,15,5,2,./
C D-MENSIONS OF WINDOW
C DATA THICK,LHEA,MHEA,LSIL,MSIL/.3,51.5,3.44,5,3,5/
30 DATA RMIN,THN,MBOM,RMAX,THM,MARC/26,1,100,6,3,30,5,146,6,2,./
C MASS PROPERTIES (DENSITY AND PER INCH)
C DATA SPDEN,MHEA,MSIL,MBOM,MARC/.00122,0.0054,0.0085,.0038,./
C STIFFNESSES (MODULE AND PER INCH), VISCOUS DAMPING, BOUNDARY CONSTANTS
EPANE=315000.
VISC=.1E-10
ELARC=2860000.
EITAC=70000.
KUNAC=230.
KOARC=10000.
EIHEA=640000.
EITHD=78000.
EISIL=10000000.
EITSL=1800000.
KUNSL=10000.
KOSIL=100000.
EIBOM=100000000.
EITBM=100000.
KUNBM=10000.
KOBOM=1000000.
DATA KUNDSL,KUNDB4,KUNDAC,KQDSIL,KOQBOM,KOARC/.1,1,1,1E-10,
50 C.1E-10,.1E-10/
C OUTPUT OPTIONS (FM-1)
C PRINT=1 OR 0 -- WRITE (OR NOT) AEC STRAIN GAGE DATA
C PRINT=1 OR 0 -- WRITE (OR NOT) CHOSEN TIME HISTORY OF VARIABLES
55 CALCOMP PLOTTING -- PLOT=3 (NO), PLOT=1 (YES)

```

```

DATA PRINT1,PRINT2,PLOT/1,1,0/
C CALCULATION OF REMAINING INPUT
C (1) FINITE DIFFERENCES OF CONE SEGMENT (X-DIRECTION)
C
RD(1)=RMIN
RD(17)=RMAX
GRD=RMAX-RMIN
RD(2)=RD(1)*GRD*NBOW/(LSIL+LHEA)
RD(16)=RD(17)-GRD*WARC/(LSIL+LHEA)
TH(1)=3.14159*THHN/180.
TH(17)=3.14159*THNX/180.
DTHET=TH(17)-TH(1)
TH(2)=TH(1)+DTHET*NBOW/(LSIL+LHEA)
TH(16)=TH(17)-DTHET*WARC/(LSIL+LHEA)
DO 100 J=3,15
RD(J)=RD(1)+(J-1)*GRD/16.
TH(J)=TH(1)+(J-1)*DTHET/16.
100 CONTINUE
DO 135 J=1,17
CIRC(J)=TH(J)*RD(J)
THX(1,J)=TH(J)*.5
THX(2,J)=.5*TH(J)*(1.-MSIL/CIRC(J))
DO 110 I=3,7
THX(1,I)=TH(I)*(.5-(I-3)*.0625)
THX(8,I)=.5*WHEA*TR(I)/CIRC(I)
THX(9,I)=0.
DO 115 I=1,8
THX(18-I,I)=THX(I,I)
115 CONTINUE
DO 120 J=1,17
OS(1,J)=MSIL
OS(2,J)=CIRC(J)*.125
OS(3,J)=CIRC(J)*.1875-MSIL*.5
DO 125 I=4,6
OS(I,J)=CIRC(J)*.125
OS(7,J)=CIRC(J)*.1875-WHEA*.5
OS(8,J)=CIRC(J)*.125
OS(9,J)=WHEA
DO 130 I=4,8
OS(18-I,I)=OS(I,I)
130 CONTINUE
DO 135 I=1,17
DTH(I,J)=OS(I,J)/RD(I)
SNOTH(I,J)=2.*SIN(OTH(I,J)/2.)
135 DX(I,J)=SNOTH(I,J)*RD(J)
C (2) FINITE DIFFERENCES Y-DIRECTION
C
SO(1)=LSIL
SO(2)=LSIL+(LHEA-LSIL)*MSIL/CIRC(9)
DO 140 I=3,7
SO(I)=(9-I)*LSIL+(I-3)*LHEA*.125
SO(8)=LHEA-(LHEA-LSIL)*WHEA/CIRC(9)
SO(9)=LHEA
DO 145 I=1,8
SO(18-I)=SO(I)
145 CONTINUE

```

```

115 DO 150 I=1,17
    DY(I,1)=WSON
    DY(I,2)=SD(I)*.125
    DY(I,3)=SD(I)*.1875-WBOM/2.
    DO 155 J=4,14
120   DY(I,J)=SD(I)*.125
    DY(I,15)=SD(I)*.1875-WARG/2.
    DY(I,16)=SD(I)*.125
    DY(I,17)=WARG
125 C (3) EIX AND *PROX. EIX=EIX+EFFECT OF CURVATURE
    C
    THICK=THICK*.12.
    DO 160 I=1,17
    DO 160 J=1,17
    EIX(I,J)=DY(I,J)*THICK*EPANE
130   CSINTH(I,J)=CURV*THICK*(1.-COS(OTH(I,J)/2.))*2
    EIX(I,J)=OS(I,J)*(THICK*CSINTH(I,J)*RO(J)+2)*EPANE
    C
135 C (4) STIFFNESS DISTRIBUTIONS AT EDGES
    DO 155 J=2,16
    EIX(1,J)=EITSL*DY(1,J)
    EIX(9,J)=EITMD*DY(9,J)
    EIX(17,J)=EITSL*DY(17,J)
    EIX(1,J)=EISIL
    EIX(9,J)=EIMEA
    EIX(17,J)=EISIL
140   :65 EIX(17,J)=EISIL
    DO 170 I=2,8
    EIX(I,1)=EIBOM
    EIX(I,17)=EIBOM
    EIX(I,17)=EIBOM
    EIX(I,17)=EIBOM
145   EIX(I,17)=EIBOM*DX(I,1)
    EIX(I,17)=EIBOM*DX(I,1)
    EIX(I,17)=EIBOM*DX(I,1)
    EIX(I,17)=EIBOM*DX(I,1)
150   EIX(I,17)=EIBOM*DX(I,1)
    EIX(I,17)=EIBOM*DX(I,1)
    EIX(I,17)=EIBOM*DX(I,1)
    EIX(I,17)=EIBOM*DX(I,1)
155 C (5) CORNER STIFFNESSES (ASSUMPTION)
    DO 180 I=1,17,6
    EIX(I,1)=EIBOM*COR
    EIX(I,17)=EIBOM*COR
160   DO 185 I=1,17,16
    EIX(I,1)=EIBOM*COR
    EIX(I,17)=EIBOM*COR
165   EIX(I,1)=EIBOM*COR
    EIX(I,17)=EIBOM*COR
    C
170 C (6) BOUNDARY CONDITIONS AT CORNERS, EDGES (ADJUSTMENTS FOR FM=1)
    C
    DO 190 J=1,17
    KUN(J,1)=KUNBM
    KUN(J,1)=KUNBM
    KOY(J,1)=KOBOM
    KOY(J,1)=KOBOM
    KOYD(J,1)=KOBOM
    KOYD(J,1)=KOBOM

```

```

175 KUN(I,17)=KUNAC
    KUND(J,17)=KUNDAC
    KOY(J,17)=KOARC
    KOYD(J,17)=KODARC
    DO 195 I=1,17,16
    KUN(I,J)=KUNSL
    KUND(I,J)=KUNDSL
    KOY(I,J)=CSIL
    KOYD(I,J)=KODSIL
190 CONTINUE
    EY(9,7)=EY(9,7)*2.
    EY(9,9)=EY(9,9)*2.
    EY(9,11)=EY(9,11)*2.
    EY(9,17)=EY(9,17)/2.
    KOY(9,17)=KOY(9,17)*2.
    KUN(9,17)=KUN(9,17)/2.
    EIX(9,17)=EIX(9,17)/2.
    KOY(7,17)=OY(7,17)*2.
    EY(7,17)=EY(7,17)/2.
    KUN(5,17)=KUN(5,17)/2.
    EIX(5,17)=EIX(5,17)/2.
195 C (7) MASS DISTRIBUTIONS
    DO 200 I=1,17
    DO 200 J=1,17
    DM(I,J)=OS(I,J)*OY(I,J)*TMZCK*SPJEN
    DO 205 I=1,17,16
    DM(I,1)=DX(I,1)*HBOH+DY(I,1)*HSIL
    DM(I,17)=DX(I,17)*MARC+OY(I,17)*MSIL
    DM(9,1)=OX(9,1)*HBOH+OY(9,1)*MHEA
    DM(9,17)=OX(9,17)*MARC+OY(9,17)*MHEA
    DO 210 I=2,8
    DM(I,1)=DX(I,1)*HBOH
    DM(I,8,1)=DX(I+8,1)*HBOH
    DM(I,17)=DX(I,17)*MARC
    DM(I+8,17)=OX(I+8,17)*MARC
    DO 215 J=2,16
    DM(9,J)=OY(9,J)*MHEA
    DO 220 I=1,17,16
    DM(I,J)=OY(I,J)*HSIL
    215 CONTINUE
215 C SET INITIAL CONDITIONS
    DO 225 J=1,17
    DO 230 I=1,17
    UN(I,J)=0.
    UNMDT(I,J)=G.
    UNOD(I,J)=0.
    UNOD(I,J)=0.
    UT(I,J)=0.
    OX(I,J)=0.
    OXMDT(I,J)=0.
    OXOD(I,J)=0.
    OY(I,J)=0.
    OYMDT(I,J)=0.

```

```

230 OYD(I,J)=0.
    MX(I,J)=0.
    MXEL(I,J)=0.
    MY(I,J)=0.
    MYEL(I,J)=0.
    FN(I,J)=0.
    FT(I,J)=0.
    Y(I,J)=0.
    QN(I,J)=.01
    QT(I,J)=.01
    DO 235 I=10,17
    235 QT(I,J)=-.01
    225 CONTINUE
240 C MAIN DO-LOOP OF COMPUTATION PER TIME STEP NNNN
    C DEFINE N, M, AND J (UN,UT) VALUES IN 17*17 ARRAYS
    C
    DO 1000 NANN=1, NEND
    T=DT*NNNN
    C LOADING CASE "FM-1"
    C
    IF (NANN.EQ.1) GO TO 240
    IF (NANN.EQ.5) GO TO 245
    IF (NANN.EQ.9) GO TO 256
    IF (NANN.EQ.13) GO TO 255
    IF (NANN.EQ.17) GO TO 263
    GO TO 265
240 QT(4,9)=SIN(THX(4,9))*63600.*FRC
    QN(5,9)=COS(THX(5,9))*127200.*FRC
    QT(6,9)=SIN(THX(6,9))*63600.*FRC
    GO TO 265
245 QT(4,9)=QT(4,9)*.5
    QN(5,9)=QN(5,9)*.5
    QT(6,9)=QT(6,9)*.5
    QT(4,11)=SIN(THX(4,11))*31800.*FRC
    QN(5,11)=COS(THX(5,11))*63600.*FRC
    QT(6,11)=SIN(THX(6,11))*31800.*FRC
    GO TO 265
250 QT(4,9)=.J1
    QN(5,9)=.01
    QT(6,9)=.01
    QT(4,11)=QT(4,11)*.5
    QN(5,11)=QN(5,11)*.5
    QT(6,11)=QT(6,11)*.5
    QT(4,13)=SIN(THX(4,13))*15900.*FRC
    QN(5,13)=COS(THX(5,13))*31800.*FRC
    QT(6,13)=SIN(THX(6,13))*15900.*FRC
    GO TO 265
255 QT(4,11)=.01
    QN(5,11)=.01
    QT(6,11)=.01
    QN(5,13)=QN(5,13)*.5
    QT(4,13)=QT(4,13)*.5

```

250

PROGRAM MAIN 74/74 OPT=1

```

290 QT(6,13)=QT(6,13)*.5
    QT(4,15)=SIN(THX(4,15))*7950.*FRC
    QN(5,15)=COS(THX(5,15))*15900.*FRC
    QT(6,15)=SIN(THX(6,15))*7950.*FRC
    GO TO 265
295 QT(4,13)=.61
    QN(5,13)=.01
    QT(6,13)=.01
    QT(6,15)=QT(4,15)*.5
    QN(5,15)=QN(5,15)*.5
    QT(6,15)=QT(6,15)*.5
    QT(4,17)=SIN(THX(4,17))*3975.*FRC
    QN(5,17)=COS(THX(5,17))*7950.*FRC
    QT(6,17)=SIN(THX(6,17))*3975.*FRC

```

C END OF IMPACT AT NNNN=21 (CASE FM-1)

C 265 IF (I.LI..00209.0R.I.GT..00211) GO TO 270

```

305 DO 275 J=1,17,2
    DO 280 I=1,17,2
280 QN(I,J)=.01
295 QT(K,J)=.01
310 DO 290 K=10,16,2
275 CONTINUE
270 CONTINUE
    DO 295 J=1,17,2

```

C OX,OY INSIDE BY ALL UN AND UT INSIDE

```

315 DO 306 I=2,16,2
    OXHD(I,J)=OX(I,J)
    OX(I,J)=(UN(I+1,J)-UN(I-1,J))/SNDTH(L,J)-UT(I,J)/ZO(J)
    OY(I,J)=(OX(I,J)-OXHD(I,J))/DT
    OYHD(I,J)=OY(I,J)
    OY(J,I)=(UN(I,I+1)-UN(I,I-1))/DY(J,I)
    OY(J,I)=(OY(J,I)-OYHD(J,I))/DT
320 OX(J,I)=OX(I,J)
    OY(J,I)=OY(I,J)
    OXHD(I,J)=OX(I,J)
    OYHD(I,J)=OY(I,J)
    OX(I,J)=OX(I,J)/(2.*EIX(I,J))
    OY(I,J)=OY(I,J)/(2.*EIX(I,J))
    OX(17,J)=OX(15,J)/(1.+OX(17,J)*KX(17,J)/(2.*EIX(17,J)))
    OY(17,J)=OY(15,J)/(1.+OY(17,J)*KY(17,J)/(2.*EIX(17,J)))
    OX(J,1)=OX(J,2)/(1.+OX(J,1)*KX(J,1)/(2.*EIX(J,1)))
    OY(J,1)=OY(J,2)/(1.+OY(J,1)*KY(J,1)/(2.*EIX(J,1)))
    OY(J,17)=OY(J,17)
    OY(J,17)=OY(J,17)/(1.+OY(J,17)*KY(J,17)/(2.*EIX(J,17)))
    OY(J,17)=OY(J,17)/DT

```

C OX,OY AT BOUNDARY BY INSIDE OX,OY, BOUND. COND. MX,MY A=0 OX,OY APPROX.

C 306 I=2,16,2

```

330 OXHD(I,J)=OX(I,J)
    OX(I,J)=(UN(I+1,J)-UN(I-1,J))/SNDTH(L,J)-UT(I,J)/ZO(J)
    OY(I,J)=(OX(I,J)-OXHD(I,J))/DT
    OYHD(I,J)=OY(I,J)
    OY(J,I)=(UN(I,I+1)-UN(I,I-1))/DY(J,I)
    OY(J,I)=(OY(J,I)-OYHD(J,I))/DT
335 OX(J,I)=OX(I,J)
    OY(J,I)=OY(I,J)
    OXHD(I,J)=OX(I,J)
    OYHD(I,J)=OY(I,J)
    OX(I,J)=OX(I,J)/(2.*EIX(I,J))
    OY(I,J)=OY(I,J)/(2.*EIX(I,J))
    OX(17,J)=OX(15,J)/(1.+OX(17,J)*KX(17,J)/(2.*EIX(17,J)))
    OY(17,J)=OY(15,J)/(1.+OY(17,J)*KY(17,J)/(2.*EIX(17,J)))
    OX(J,1)=OX(J,2)/(1.+OX(J,1)*KX(J,1)/(2.*EIX(J,1)))
    OY(J,1)=OY(J,2)/(1.+OY(J,1)*KY(J,1)/(2.*EIX(J,1)))
    OY(J,17)=OY(J,17)
    OY(J,17)=OY(J,17)/(1.+OY(J,17)*KY(J,17)/(2.*EIX(J,17)))
    OY(J,17)=OY(J,17)/DT

```

C MX,MY AND FN,V AT BOUNDARY

C 60 305 II=1,17,16

```

345 IF(I1.EQ.1) SIGN=-1.
    MXEL(II,J)=-KXD(II,J)*OX(II,J)*SIGN
    MXVC(II,J)=-KXD(II,J)*OXD(II,J)*SIGN
    MX(II,J)=MXEL(II,J)+MXVC(II,J)
    MYEL(J,II)=-KOY(J,II)*OY(J,II)*SIGN
    MYVC(J,II)=-KOYD(J,II)*OYD(J,II)*SIGN
    MY(J,II)=MYEL(J,II)+MYVC(J,II)
    FN(II,J)=(KUN(II,J)*UN(II,J)+KUND(II,J)*UND(II,J))*SIGN
    DO 310 II=3,15,2
355 C MX,MY INSIDE/EDGE BY OX,OY INSIDE, INCLUDING DAMPING
    C
    MXEL(II,J)=(OX(II+1,J)-OX(II-1,J))*EIX(II,J)/DX(II,J)
    MXVC(II,J)=(OXD(II+1,J)-OXD(II-1,J))*VISC/DX(II,J)
    MX(II,J)=MXEL(II,J)+MXVC(II,J)
    MYEL(J,II)=(OY(J,II+1)-OY(J,II-1))*EY(J,II)/OY(J,II)
    MYVC(J,II)=(OYD(J,II+1)-OYD(J,II-1))*VISC/OY(J,II)
    MY(J,II)=MYEL(J,II)+MYVC(J,II)
    DO 315 II=2,16,2
365 C FN,J INSIDE/EDGE BY MX,MY
    C
    FN(II,J)=(MX(II+1,J)-MX(II-1,J))/DX(II,J)
    V(J,II)=(MY(J,II+1)-MY(J,II-1))/OY(J,II)
370 C FN,V OUTSIDE BOUNDARY
    C
    FN(J)=2.*FN(1,J)-FN(2,J)
    V(J)=2.*V(J,1)-V(J,2)
    V18(J)=2.*V(J,17)-V(J,16)
375 C FOREWARD/BACKWARD CALCULATION OF FT
    C
    ISHFMO=ISHEAR+2
    ISHMD=20-ISHEAR
    DO 320 I=ISHFMO,17,2
    FT(I,J)=FT(I-2,J)-FN(I-1,J)*SNOT+(I-1,J)+QT(I-1,J)
    DO 325 I=ISHMD,17,2
    K=18-I
    FT(K,J)=FT(K+2,J)+FN(K+1,J)*SNOT+(K+1,J)-QT(K+1,J)
295 CONTINUE
    DO 330 J=1,17,2
390 C CALCULATE UNDO AND INTEGRATE
    C
    DO 335 I=1,17,2
    FNP=FN18(J)
    IF(I.NE.17) FNP=FN(I+1,J)
    FNM=FM0(J)
    IF(I.NE.1) FNM=FN(I-1,J)
    VP=V18(I)
    IF(J.NE.17) VP=V(I,J+1)
    VM=V0(I)
    IF(J.NE.1) VM=V(I,J-1)

```

```

400 UNDD(I,J) = (QN(I,J) - FNP + FMH + FT(I,J) * SNOTH(I,J) - VP + VM) / UM(I,J)
    UNO(I,J) = UNO(I,J) + DT * UNDD(I,J)
    UN(I,J) = UN(I,J) + DT * UNO(I,J)
335 CONTINUE
C FORWARD/BACKW. CALC. OF UT
C
    UT(2,J) = -.5 * UN(1,J) * SNOTH(1,J)
    UT(16,J) = .5 * UN(17,J) * SNOTH(17,J)
    ISHFWD = ISHEAR - 1
    ISHBWD = 17 - ISHEAR
    DO 340 I = 4, ISHFWD + 2
340  UT(I,J) = UT(I-2,J) - UM(I-1,J) * SNOT4(I-1,J)
    DO 345 I = 4, ISHBWD + 2
    K = 18 - I
345  UT(K,J) = UT(K+2,J) + UM(K+1,J) * SNOT4(K+1,J)
330 CONTINUE
C IDENTIFICATION AND WRITING OF VARIABLES FOR PRINT-OUT
C
    IF (PRINT1.EQ.0) GO TO 350
    IF (MOD(NNN,NP).NE.0) GO TO 1000
    ST(1) = NY( 9, 9) * .98 / EIX( 9, 9)
    ST(2) = NY( 9,17) * .98 / EIX( 9,17)
    ST(3) = NY( 7,17) * .50 / EIX( 7,17)
    ST(4) = MX( 9,13) * .50 / EIX( 9,13)
    ST(5) = MX(13,17) * .90 / EIX(13,17)
    ST(6) = MX( 9,17) * .90 / EIX( 9,17)
    ST(7) = MX( 5,17) * .90 / EIX( 5,17)
    ST(8) = MX( 5, 9) * .5 * THICK / EIX( 5, 9)
    ST(9) = NY( 5, 9) * .5 * THICK / EIX( 5, 9)
    ST(10) = UN( 5, 9)
    ST(11) = UN( 5,13)
    ST(12) = UN( 5,17)
    ST(13) = UN( 9, 9)
    ST(14) = UN( 9,13)
    ST(15) = UN( 9,17)
    ST(16) = UN(13, 9)
    ST(17) = UN(13,13)
    ST(18) = UN(13,17)
    NN = NNN / NP
    XX(NN) = I
    NEND = NN
    DO 355 I = 1, 18
355  Y(NN,I) = ST(I)
350 CONTINUE
    IF (PRINT2.EQ.0) GO TO 1000
    WRITE(6,360)
360  FORMAT(1H1)
    WRITE(6,365) ((QN(I,J), I=1,17,2), J=1,17,2)
    WRITE(6,370) ((QT(I,J), I=2,16,2), J=1,17,2)
    WRITE(6,375) ((OX(I,J), OX(I,J), I=2,16,2), OX(17,J), J=1,17,2)
    WRITE(6,380) ((OY(I,1), I=1,17,2), I,
    1 ((OY(I,J), I=1,17,2), J=2,16,2),
    2 ((OY(I,17), I=1,17,2), I)
    WRITE(6,360)

```

```

460 WRITE(6,385) ((MX(I,J),I=1,17,2),J=1,17,2)
    WRITE(6,390) ((MY(I,J),I=1,17,2),J=1,17,2)
    WRITE(6,395) ((FN(I,J),I=1,17,2),J=1,17,2)
    WRITE(6,400) ((V(I,J),I=1,17,2),J=1,17,2)
1
2
    WRITE(6,405) ((FT(I,J),I=1,17,2),J=1,17,2)
    WRITE(6,360)
    WRITE(6,410) ((UN(I,J),I=1,17,2),J=1,17,2)
    WRITE(6,415) ((UND(I,J),I=1,17,2),J=1,17,2)
    WRITE(6,420) ((UND(I,J),I=1,17,2),J=1,17,2)
    WRITE(6,425) ((UT(I,J),I=2,16,2),J=1,17,2)
365 FORMAT(9(5X,9E10.3,15X,E10.3,5X,*QN*//))
370 FORMAT(9(10X,0E10.3,20X,E10.3,5X,*QT*//))
375 FORMAT(9(10E10.3,10X,E10.3,5X,*OX*//))
385 FORMAT(9(5X,9E10.3,15X,E10.3,5X,*MX*//))
390 FORMAT(9(5X,9E10.3,15X,E10.3,5X,*MY*//))
395 FORMAT(9(10E10.3,10X,E10.3,5X,*FN*//))
400 FORMAT(10(5X,9E10.3,15X,E10.3,5X,*V*//))
405 FORMAT(9(5X,9E10.3,15X,E10.3,5X,*FT*//))
410 FORMAT(9(5X,9E10.3,15X,E10.3,5X,*UN*//))
415 FORMAT(9(5X,9E10.3,15X,E10.3,4X,*UND*//))
420 FORMAT(9(5X,9E10.3,15X,E10.3,3X,*UND0*//))
425 FORMAT(9(10X,0E10.3,20X,E10.3,5X,*UT*//))
C END OF MAIN DO-LOOP
C
1000 CONTINUE
C PLOTS OF TIME HISTORIES (FM=1)
C
    IF (PRINT.EQ.0) GO TO 430
    WRITE(6,435)
    FORMAT(1H1,* TIME SY(9,9) SY(9,17) SY(7,17) SX(9,13) SX(13,17)
C) SX(9,17) SX(5,17) SX(5,9) SY(5,9)*
    WRITE(6,440) ((XX(NN),Y(NN,I),I=1,9)),NN=1,NNEND)
440 FORMAT(6,4,9E10.3)
    WRITE(6,445)
    FORMAT(1H1,* TIME UN(5,9) UN(5,13) UN(5,17) UN(3,9) UN(9,13)
C) UN(9,17) UN(13,9) UN(13,13) UN(13,17)*
    WRITE(6,446) ((XX(NN),Y(NN,I),I=10,18)),NN=1,NNEND)
    IF (PLOT.EQ.0) GO TO 430
    CALL GRAPH
    CALL PLOTE
130 CONTINUE
    STOP
    END

```

SUBROUTINE GRAPH 74/74 OPT=1

```

1      SUBROUTINE GRAPH
C      C PLOTTING OF TIME HISTORIES OF STRAINS
C
5      COMMON DATA(603),XX(102),Y(100,10),YY(102)
DIMENSION BXAX1(2),BYAX1(3)
DATA BXAX1(1)/12H TIME (SEC) /,BYAX1(1)/10H STRAINS (IN/IN) /
DATA YSCAL1,YSCAL2/-.61,.0025/
XX(101)=.0
XX(102)=.005
DO 100 NNN=1,2
KKB=1
KKE=3
IF (NNN.EQ.2) KKB=4
IF (NNN.EQ.2) KKE=7
CALL PLOT(.0,.0,-3)
CALL AXIS (.0,1.5,BXAX1,-12,10,.0,.0,.005)
YY(101)=YSCAL1
YY(102)=YSCAL2
CALL AXIS (.0,1.5,BYAX1,10,0,90,YY(101),YY(102))
CALL PLOT (.0,3.5,3)
CALL PLOT (10.3,5,2)
CALL PLOT (10.5,5,3)
CALL PLOT (.0,5.5,2)
CALL PLOT (.0,7.5,3)
CALL PLOT (10.7,5,2)
CALL PLOT (10.9,5,3)
CALL PLOT (.0,9.5,2)
CALL PLOT (2.9,5,3)
CALL PLOT (2.1,5,2)
CALL PLOT (4.1,5,3)
CALL PLOT (4.9,5,2)
CALL PLOT (6.9,5,3)
CALL PLOT (6.1,5,2)
CALL PLOT (8.1,5,3)
CALL PLOT (8.9,5,2)
CALL PLOT (10.9,5,3)
CALL PLOT (10.1,5,2)
CALL PLOT (.0,1.5,-3)
DO 101 KK=KKB,KKE
DO 102 NN=1,100
102 YY(NN)=Y(NN,KK)
101 CALL LINE (XX,YY,100,1,1,KK)
CALL PLOT (12.-1.5,-3)
100 CONTINUE
END
END
    
```


.500E+02	-.123E+04	-.514E+04	-.903E+04	-.276E+04	.638E+04	.484E+04	.312E+03	-.165E+02	MX
.385E+03	-.110E+04	.136E+04	-.984E+03	.748E+03	.230E+02	.257E+02	.257E+02	.250E-01	MX
.101E+04	-.267E+04	.294E+04	-.121E+04	.482E+03	-.143E+03	.256E+02	.375E+02	.250E-01	MX
.637E+03	-.251E+04	.370E+04	-.890E+03	-.222E+04	-.159E+03	-.200E+03	-.272E+03	.250E-01	MX
.379E+03	-.110E+04	.926E+03	.276E+03	.155E+04	.406E+02	-.777E+03	.513E+03	.250E-01	MX
.215E+03	-.482E+03	-.805E+02	.638E+03	.356E+03	-.438E+03	-.223E+03	.639E+03	.250E-01	MX
-.923E+02	.638E+03	.234E+04	.128E+04	.953E+03	-.549E+03	-.108E+03	-.499E+03	.250E-01	MX
-.207E+03	.159E+04	-.390E+04	.187E+04	.104E+04	.351E+03	-.481E+03	.731E+03	.250E-01	MX
.984E+00	.414E+04	-.598E+04	.256E+04	.726E+03	-.239E+03	-.357E+04	.655E+04	.250E-01	MX
-.821E+03	.265E+04	-.292E+03	.346E+04	.273E+04	.169E+04	.594E+03	.738E+03	.250E-01	MY
-.319E+03	.104E+04	-.558E+03	-.598E+03	-.133E+04	.195E+01	.207E+02	.575E+02	.250E-01	MY
.136E+04	-.452E+04	-.172E+04	-.305E+04	-.299E+04	-.187E+03	.882E+03	.855E+03	.250E-01	MY
.149E+05	.763E+03	.478E+04	.177E+04	.201E+04	.121E+03	.505E+03	.568E+03	.250E-01	MY
.217E+05	.104E+04	-.110E+04	.120E+04	.312E+04	.901E+03	-.184E+04	-.131E+04	.250E-01	MY
.164E+05	-.916E+03	.274E+04	.127E+04	.203E+04	-.659E+03	.800E+02	-.118E+04	.250E-01	MY
.520E+04	.190E+04	-.222E+04	.980E+02	.463E+03	.392E+02	-.502E+03	.118E+04	.250E-01	MY
-.244E+04	.290E+04	-.439E+04	.254E+04	.435E+04	.300E+04	.641E+03	.122E+04	.250E-01	MY
-.208E+03	-.532E+03	.941E+04	-.133E+04	-.137E+03	.288E+03	-.999E+02	.154E+03	.250E-01	MY
-.178E+02	-.207E+03	-.633E+03	-.629E+03	.101E+04	.148E+04	-.250E+03	-.733E+03	.250E-01	FN
.337E+02	-.225E+03	.377E+03	.380E+03	.112E+03	.490E+02	-.846E+01	.356E+02	.250E-01	FN
.917E+02	-.424E+03	.831E+03	-.594E+03	.285E+03	-.132E+03	.564E+02	-.419E+02	.250E-01	FN
.154E+03	-.189E+03	.258E+03	-.619E+03	-.179E+03	.277E+03	-.554E+01	-.973E+01	.250E-01	FN
.972E+02	-.839E+02	.483E+02	.865E+02	-.238E+03	.208E+03	-.104E+03	.342E+02	.250E-01	FN
-.131E+02	.106E+03	-.362E+03	.413E+03	-.373E+02	-.171E+03	.503E+02	-.411E+02	.250E-01	FN
-.134E+03	.195E+03	-.594E+03	.624E+03	-.590E+02	.212E+03	.155E+03	.174E+03	.250E-01	FN
-.243E+03	.425E+03	-.104E+04	.878E+03	-.188E+03	-.381E+03	-.601E+02	-.513E+03	.250E-01	FN
-.178E+02	-.418E+03	-.638E+03	-.713E+03	.366E+03	.134E+03	.261E+03	.198E+03	.250E-01	V
-.425E+03	-.279E+03	-.443E+02	-.669E+03	-.631E+03	-.272E+03	-.940E+02	.232E+03	.250E-01	V
.806E+03	.962E+03	-.194E+03	-.379E+03	.252E+03	.304E+02	.143E+02	.436E+02	.250E-01	V
.244E+04	.915E+03	.108E+04	.775E+03	.777E+03	.496E+02	-.627E+02	.513E+02	.250E-01	V
.122E+04	.474E+02	-.940E+03	-.915E+02	.119E+03	.119E+03	-.391E+03	-.427E+03	.250E-01	V
-.936E+03	-.338E+03	.641E+03	-.112E+02	-.175E+03	.244E+03	.320E+03	.122E+03	.250E-01	V
-.202E+04	.446E+03	-.827E+03	-.188E+03	.244E+03	.122E+03	-.981E+02	.435E+03	.250E-01	V
-.137E+04	-.174E+03	-.362E+03	.933E+03	-.928E+02	.498E+03	.192E+03	-.413E+03	.250E-01	V
.461E+03	-.594E+03	.889E+03	-.622E+03	-.469E+02	.328E+03	-.124E+03	.239E+03	.250E-01	V
.243E+03	.236E+02	-.167E+02	.243E+02	.255E+02	.155E+03	.131E+03	.655E+02	.250E-01	V
-.159E+03	-.150E+03	.0	.149E+03	-.913E+02	-.442E+03	-.363E+03	-.239E+03	.250E-01	FT
.375E+02	.930E+02	.0	.889E+02	.611E+02	.493E+02	.511E+02	.423E+02	.250E-01	FT
.711E+02	.206E+03	.0	.153E+03	.795E+02	.113E+03	.988E+02	.110E+03	.250E-01	FT
.111E+03	.224E+03	.0	.166E+03	.215E+03	.159E+03	.141E+03	.142E+03	.250E-01	FT
.193E+02	.717E+02	.0	.230E+02	.890E+02	.313E+02	.602E+02	.507E+02	.250E-01	FT
-.103E+02	.139E+02	.0	-.249E+02	.151E+02	.124E+02	.483E+01	.139E+02	.250E-01	FT
-.764E+02	-.108E+03	.0	-.123E+03	-.112E+03	-.509E+02	-.759E+02	-.636E+02	.250E-01	FT
-.123E+03	-.183E+03	.0	-.193E+03	-.165E+03	-.983E+02	-.145E+03	-.134E+03	.250E-01	FT
-.196E+03	-.332E+03	.0	-.280E+03	-.220E+03	-.983E+02	-.791E+02	-.645E+02	.250E-01	FT

.181E-01	.422E-01	.625E-01	.695E-01	.300E-01	-.120E-01	-.260E-01	-.204E-01	-.121E-01	.250E-01	UN
-.339E-01	.214E+00	.740E-01	.314E+00	.222E+00	.114E+00	.178E-01	-.685E-01	-.563E-01	.250E-01	UN
-.978E-01	.661E+00	-.143E+00	.411E+00	.309E+00	.234E+00	.639E-01	.166E-01	-.051E-01	.250E-01	UN
-.154E+00	.343E+00	-.778E+00	-.357E-01	.205E+00	.337E+00	.324E+00	.256E+00	-.103E+00	.250E-01	UN
-.160E+00	.135E+00	-.345E+00	-.197E+00	.163E+00	.448E+00	.700E+00	.504E+00	-.133E+00	.250E-01	UN
-.969E-01	.534E-01	-.120E+00	-.219E+00	.222E+00	.874E+00	.707E+00	.542E+00	-.183E+00	.250E-01	UN
.129E-01	-.921E-01	.643E+00	-.918E-01	.342E+00	.814E+00	.734E+00	.481E+00	-.237E+00	.250E-01	UN
.134E+00	-.751E-01	.908E+00	.430E-01	.491E+00	.374E+00	.662E+00	.516E+00	-.268E+00	.250E-01	UN
.242E+00	.225E+00	.332E+00	.425E+00	.617E+00	.796E+00	.694E+00	.432E+00	-.266E+00	.250E-01	UN
.705E+02	.425E+01	.145E+02	-.205E+02	-.716E+01	.636E+01	.410E+00	-.175E+02	-.353E+02	.250E-01	UN
.113E+02	-.114E+03	.318E+03	-.145E+03	-.522E+02	.202E+02	.225E+01	.286E+02	-.167E+02	.250E-01	UN
-.468E+02	.246E+03	.188E+03	-.473E+02	-.603E+02	-.445E+02	-.398E+02	.149E+03	-.239E+01	.250E-01	UN
-.667E+02	-.986E+01	.136E+02	-.159E+03	.375E+02	.447E+02	-.639E+02	.174E+03	.591E+01	.250E-01	UN
-.434E+02	-.190E+03	-.705E+02	-.911E+02	-.488E+02	.231E+02	-.515E+02	.128E+03	.434E+01	.250E-01	UN
-.507E+01	-.564E+03	.138E+02	-.174E+03	-.723E+02	.326E+02	.401E+02	.385E+02	.141E+02	.250E-01	UN
-.547E+01	-.216E+03	.315E+03	-.214E+03	-.143E+03	-.644E+02	.173E+03	.404E+02	.640E+02	.250E-01	UN
-.549E+02	-.159E+03	.189E+03	-.286E+03	-.215E+03	-.382E+02	.190E+03	.243E+02	.729E+02	.250E-01	UN
-.130E+03	-.266E+03	-.558E+03	-.769E+03	-.403E+03	-.360E+02	-.996E+02	-.212E+03	.856E+02	.250E-01	UN
.267E+05	.267E+04	-.371E+05	-.418E+05	.102E+05	.597E+05	.343E+05	-.211E+05	-.350E+05	.250E-01	UN
-.122E+05	.173E+05	.163E+06	-.102E+06	-.682E+05	-.234E+05	-.495E+05	.427E+05	.152E+05	.250E-01	UN
-.808E+04	-.563E+06	.253E+05	-.322E+06	-.172E+06	-.374E+05	.713E+05	.127E+05	.318E+05	.250E-01	UN
.507E+05	-.532E+05	.717E+06	.733E+05	.482E+05	.596E+05	.754E+05	.541E+05	-.490E+04	.250E-01	UN
.603E+05	-.562E+04	-.246E+06	.862E+04	-.251E+05	.373E+05	-.160E+06	-.134E+06	-.219E+05	.250E-01	UN
.306E+05	-.139E+06	.260E+06	.412E+05	.575E+05	-.543E+05	.903E+05	-.732E+05	-.200E+02	.250E-01	UN
-.189E+05	.103E+06	-.214E+06	-.225E+05	-.813E+04	.568E+05	-.381E+05	.837E+05	.472E+05	.250E-01	UN
-.352E+05	.142E+06	-.303E+06	.145E+06	.132E+05	-.126E+06	.689E+05	-.975E+05	.414E+05	.250E-01	UN
-.569E+05	.186E+05	-.290E+05	-.699E+05	.122E+05	.770E+05	-.220E+05	-.223E+06	-.612E+04	.250E-01	UN
-.121E-02	-.134E-01	.745E-02	-.132E-01	.167E-01	-.128E-01	-.669E-02	-.812E-03	.250E-01	UT	
.222E-02	-.630E-01	.139E+00	.407E-01	.157E-01	-.202E-01	-.246E-01	-.370E-02	.250E-01	UT	
.629E-02	-.206E+00	.264E+00	.128E+00	.937E-01	.163E-01	-.124E-03	-.547E-02	.250E-01	UT	
.970E-02	-.106E+00	.283E+00	.296E+00	.273E+00	.156E+00	.697E-01	-.652E-02	.250E-01	UT	
.987E-02	-.382E-01	.473E+00	.542E+00	.528E+00	.365E+00	.171E+00	-.820E-02	.250E-01	UT	
.587E-02	-.139E-01	.592E+00	.675E+00	.652E+00	.397E+00	.193E+00	-.111E-01	.250E-01	UT	
.786E-03	.342E-01	.712E+00	.748E+00	.713E+00	.391E+00	.172E+00	.714E-01	.250E-01	UT	
-.782E-02	.225E-01	.865E+00	.847E+00	.798E+00	.397E+00	.193E+00	-.157E-01	.250E-01	UT	
-.139E-01	-.104E+00	.958E+00	.776E+00	.715E+00	.375E+00	.153E+00	-.153E-01	.250E-01	UT	

..145E+03	.765E+04	.578E+04	.416E+04	.543E+04	.605E+04	.675E+04	.237E+04	..953E+02	MX	.500E-01
..463E+03	.103E+04	..864E+03	.632E+03	.254E+03	..164E+03	..370E+02	..430E+03	.144E+03	MX	.500E-01
..896E+02	.507E+03	..139E+04	.752E+03	.262E+03	.702E+03	..135E+04	.675E+03	..273E+03	MX	.500E-01
..239E+03	.350E+02	..176E+04	.900E+03	.349E+03	.611E+03	..157E+04	.111E+04	..533E+03	MX	.500E-01
..233E+03	.233E+02	..162E+04	.982E+03	.172E+04	.864E+03	..179E+04	.117E+04	..660E+03	MX	.500E-01
..119E+03	.569E+03	..203E+04	.143E+04	..241E+04	.625E+03	..944E+03	.556E+03	..155E+03	MX	.500E-01
..409E+03	.145E+04	..308E+04	.139E+04	.101E+04	.259E+03	.170E+03	.355E+03	..145E+03	MX	.500E-01
..371E+03	.162E+04	..295E+04	.926E+03	.173E+04	.151E+03	.616E+03	..474E+03	..923E+02	MX	.500E-01
..227E+02	.268E+04	..341E+04	.302E+03	.110E+04	..353E+03	.474E+04	.431E+04	..287E+03	MX	.500E-01
..196E+04	..478E+04	..218E+04	..454E+04	..277E+04	..711E+03	.113E+03	.432E+03	..222E+03	MY	.500E-01
..508E+04	.224E+04	.135E+04	.125E+04	.549E+03	..151E+04	..567E+03	..225E+04	..102E+05	MY	.500E-01
..250E+05	.676E+05	..243E+02	..515E+02	.635E+03	.135E+04	..123E+03	.633E+03	.278E+04	MY	.500E-01
..279E+05	..172E+04	..128E+04	..107E+04	..116E+04	..871E+03	.783E+02	.934E+03	.183E+05	MY	.500E-01
..145E+05	..179E+04	..201E+02	..862E+03	.295E+04	.134E+04	..421E+03	.221E+04	.259E+05	MY	.500E-01
..430E+04	.884E+02	.237E+04	.468E+04	.723E+04	.264E+04	.994E+03	.334E+04	.198E+05	MY	.500E-01
..139E+05	.272E+04	..248E+04	.290E+04	.501E+04	.210E+04	.115E+04	.308E+04	.611E+04	MY	.500E-01
..852E+04	.311E+04	..193E+04	..120E+04	.891E+03	.721E+03	..230E+04	..334E+03	..500E-01	MY	.500E-01
..307E+02	..668E+03	.665E+03	..113E+04	..133E+04	..599E+03	..432E+03	.219E+03	..118E+03	MY	.500E-01
..183E+03	.126E+04	..303E+03	..262E+03	..205E+03	.101E+03	.113E+03	..709E+03	..398E+03	FN	.500E-01
..279E+02	.227E+03	..288E+03	.258E+03	..878E+02	.634E+02	.192E+02	..597E+02	.871E+02	FN	.500E-01
..247E+02	.852E+02	..271E+03	.306E+03	..700E+02	.629E+02	..293E+03	.289E+03	..136E+03	FN	.500E-01
..516E+02	..343E+02	..241E+03	.358E+03	.349E+03	..388E+03	..293E+03	.360E+03	..221E+03	FN	.500E-01
..981E+01	..267E+02	..209E+03	.331E+03	.942E+02	..109E+03	..337E+03	.375E+03	..409E+03	FN	.500E-01
..121E+03	.827E+02	..312E+03	.416E+03	..462E+03	.365E+03	..169E+03	.182E+03	..435E+03	FN	.500E-01
..220E+03	.212E+03	.516E+03	.509E+03	..435E+02	..856E+02	..102E+02	..609E+02	.251E+02	FN	.500E-01
..273E+03	.215E+03	..488E+03	.413E+03	.874E+02	..171E+03	.503E+02	..118E+03	.413E+02	FN	.500E-01
..291E+03	.273E+03	..626E+03	.382E+03	.821E+02	..149E+03	.524E+03	.706E+01	..524E+03	FN	.500E-01
..183E+03	..816E+03	..192E+03	.520E+03	.935E+02	.809E+02	..231E+03	..739E+03	..140E+04	/	.500E-01
..127E+04	.122E+04	.587E+03	.931E+03	.345E+03	..145E+03	..113E+03	..439E+03	..142E+04	V	.500E-01
..364E+04	..271E+03	..228E+03	..209E+03	..184E+03	.477E+03	.740E+02	.428E+03	..233E+04	V	.500E-01
..166E+04	..414E+03	..202E+03	..164E+03	..273E+03	..358E+03	.335E+02	.625E+02	.273E+04	/	.500E-01
..240E+04	..126E+02	.210E+03	.340E+03	.649E+02	.356E+03	..833E+02	.210E+03	.136E+04	V	.500E-01
..338E+04	.325E+03	.398E+03	.890E+03	.662E+03	.209E+03	.236E+03	.195E+03	..109E+04	V	.500E-01
..173E+04	.454E+03	..889E+03	..285E+03	..334E+03	..873E+02	.271E+02	..111E+04	..210E+04	/	.500E-01
..967E+03	.675E+02	.910E+02	..660E+03	..743E+03	.194E+03	..726E+02	.135E+03	..152E+04	V	.500E-01
..153E+04	..653E+03	.432E+03	.121E+02	..242E+03	..256E+03	..192E+03	.436E+03	.388E+02	V	.500E-01
..291E+03	.453E+02	.288E+02	.332E+02	..695E+01	..657E+02	..112E+03	..115E+03	..231E+03	/	.500E-01
..272E+03	..717E+02	..151E+02	.621E+02	.135E+02	..104E+02	..371E+02	.131E+03	.225E+03	FT	.500E-01
..151E+02	..712E+02	..698E+02	..636E+02	..413E+02	..263E+02	..311E+02	.153E+02	..378E+02	FT	.500E-01
..737E+02	..645E+02	..645E+02	..788E+02	..608E+02	..770E+02	..167E+01	.738E+02	..413E+02	FT	.500E-01
..657E+02	..582E+02	..582E+02	..921E+02	..109E+03	..833E+02	..676E+01	.113E+03	..441E+02	FT	.500E-01
..662E+02	..900E+02	..900E+02	..120E+03	.132E+02	..320E+02	..375E+02	.839E+02	..510E+02	FT	.500E-01
..907E+02	..154E+03	..154E+03	..152E+03	.139E+03	..110E+03	..922E+02	.922E+02	..937E+02	FT	.500E-01
..843E+02	..151E+03	..151E+03	..126E+03	.155E+03	..102E+03	..117E+03	.839E+02	..936E+02	FT	.500E-01
..113E+03	..200E+03	..200E+03	..122E+03	..143E+03	..103E+03	..267E+03	..273E+03	..102E+03	FT	.500E-01

.162E+00	.672E+01	.282E+01	.261E+02	.823E+02	.338E+02	.247E+01	.827E+01	.145E+00	UN
.699E+01	.239E+00	.113E+00	.307E+00	.194E+00	.193E+01	.392E+01	.952E+01	.191E+01	UN
.243E+01	.103E+00	.130E+00	.369E+00	.445E+00	.510E+00	.157E+00	.355E+00	.146E+00	UN
.510E+01	.193E+00	.331E+00	.390E+00	.645E+00	.723E+00	.342E+00	.713E+00	.304E+00	UN
.101E+01	.221E+00	.331E+00	.594E+00	.887E+00	.108E+01	.542E+00	.958E+00	.409E+00	UN
.121E+00	.236E+01	.378E+00	.917E+00	.104E+01	.125E+01	.798E+03	.916E+00	.433E+00	UN
.220E+00	.161E+00	.797E+00	.695E+00	.945E+00	.111E+01	.907E+00	.526E+00	.387E+00	UN
.275E+00	.849E+01	.810E+00	.204E+00	.529E+00	.764E+00	.774E+00	.426E+00	.309E+00	UN
.592E+00	.286E+00	.380E+00	.156E+00	.918E+01	.328E+00	.534E+00	.533E+00	.231E+00	UN
.855E+02	.623E+02	.412E+02	.293E+02	.121E+02	.325E+01	.177E+02	.422E+02	.574E+02	UN
.680E+02	.213E+03	.308E+03	.359E+03	.142E+03	.351E+02	.785E+02	.143E+03	.537E+02	UN
.343E+02	.107E+03	.227E+02	.660E+02	.692E+02	.355E+02	.119E+03	.555E+02	.521E+02	UN
.478E+01	.266E+03	.109E+03	.267E+03	.727E+02	.254E+02	.933E+02	.317E+02	.275E+02	UN
.261E+02	.194E+03	.366E+03	.251E+03	.857E+02	.104E+03	.271E+02	.227E+03	.257E+02	UN
.508E+01	.646E+02	.152E+02	.175E+03	.457E+02	.126E+03	.161E+03	.205E+03	.711E+02	UN
.374E+02	.287E+02	.173E+02	.216E+03	.518E+02	.809E+02	.435E+02	.136E+03	.385E+02	UN
.887E+02	.459E+02	.137E+03	.905E+02	.349E+02	.413E+01	.173E+03	.277E+03	.720E+02	UN
.724E+02	.163E+03	.109E+03	.302E+02	.119E+02	.283E+02	.564E+02	.658E+02	.201E+03	UN
.132E+06	.645E+05	.437E+05	.547E+05	.231E+05	.108E+05	.180E+05	.234E+05	.808E+05	UN
.407E+05	.308E+06	.496E+05	.263E+06	.292E+05	.985E+05	.214E+05	.174E+06	.822E+05	UN
.391E+05	.855E+05	.129E+06	.495E+05	.923E+05	.189E+06	.117E+06	.150E+06	.946E+04	UN
.767E+05	.361E+05	.207E+06	.337E+05	.581E+05	.127E+06	.110E+06	.657E+05	.336E+05	UN
.211E+05	.273E+05	.140E+06	.925E+05	.485E+05	.485E+05	.198E+06	.918E+05	.592E+05	UN
.437E+05	.335E+05	.889E+05	.267E+06	.485E+05	.108E+05	.314E+05	.233E+06	.340E+05	UN
.755E+05	.145E+06	.332E+06	.108E+06	.127E+06	.173E+04	.203E+05	.138E+06	.802E+04	UN
.248E+05	.135E+06	.152E+06	.351E+05	.557E+05	.178E+05	.309E+05	.430E+05	.139E+05	UN
.723E+05	.119E+06	.543E+05	.414E+05	.117E+06	.221E+06	.735E+05	.312E+06	.328E+04	UN
.122E+01	.373E+01	.352E+01	.368E+01	.368E+01	.369E+01	.394E+01	.335E+01	.974E+02	UT
.459E+02	.654E+01	.965E+01	.233E+03	.216E+03	.216E+01	.403E+01	.366E+01	.125E+02	UT
.156E+02	.345E+01	.503E+00	.381E+00	.332E+00	.164E+00	.123E+00	.123E+00	.936E+02	UT
.321E+02	.649E+01	.808E+00	.672E+00	.502E+00	.352E+00	.268E+00	.268E+00	.192E+01	UT
.621E+03	.790E+01	.122E+01	.108E+01	.905E+00	.515E+00	.365E+00	.365E+00	.253E+01	UT
.731E+02	.161E+01	.152E+01	.118E+01	.187E+01	.596E+00	.366E+00	.366E+00	.282E+01	UT
.131E+01	.493E+01	.131E+01	.105E+01	.937E+00	.497E+00	.227E+00	.227E+00	.230E+01	UT
.160E+01	.174E+01	.881E+00	.797E+00	.744E+00	.429E+00	.190E+00	.190E+00	.181E+01	UT
.168E+01	.137E+00	.490E+00	.557E+00	.548E+00	.407E+00	.237E+00	.237E+00	.132E+01	UT

TIME	SY(9,9)	SY(9,17)	SY(7,17)	SX(9,13)	SX(13,17)	SX(9,17)	SX(5,17)	SX(5,9)	SY(5,9)
0005	-459E-03	-260E-07	-264E-08	589E-05	125E-06	-101E-06	-320E-07	-458E-02	-757E-02
0010	-560E-03	-247E-05	-389E-06	182E-04	253E-06	-303E-05	-283E-05	-155E-01	-222E-01
0015	-810E-03	-680E-05	-836E-06	-136E-03	-120E-05	363E-04	251E-04	-237E-01	-277E-01
0020	-139E-02	193E-04	116E-04	-246E-03	217E-04	137E-03	344E-04	-269E-01	-231E-01
0025	-120E-02	193E-04	314E-04	773E-03	142E-04	146E-03	-155E-03	-259E-01	-144E-01
0030	-173E-02	153E-03	791E-04	515E-03	-101E-03	633E-04	755E-03	-228E-01	-152E-02
0035	-208E-02	270E-03	212E-03	711E-03	107E-04	352E-03	205E-02	-192E-01	448E-02
0040	-184E-02	487E-03	487E-03	101E-02	138E-03	565E-03	272E-02	160E-01	411E-02
0045	-259E-02	817E-03	902E-03	125E-02	153E-03	674E-03	245E-02	-130E-01	-356E-03
0050	-273E-02	118E-02	139E-02	137E-02	293E-04	595E-03	173E-02	320E-01	-472E-02
0055	-267E-02	149E-02	184E-02	116E-02	-263E-03	510E-03	104E-02	430E-02	-533E-02
0060	-311E-02	168E-02	219E-02	721E-03	-440E-03	-244E-03	240E-02	-135E-02	-232E-02
0065	-275E-02	173E-02	236E-02	400E-03	655E-03	131E-03	-107E-02	355E-02	232E-02
0070	-305E-02	164E-02	232E-02	201E-04	950E-03	749E-03	-284E-02	103E-01	553E-02
0075	-340E-02	140E-02	203E-02	328E-03	-110E-02	136E-02	-442E-02	118E-01	177E-02
0080	-306E-02	103E-02	159E-02	550E-03	800E-03	153E-02	-516E-02	-112E-01	866E-03
0085	-370E-02	829E-03	102E-02	-102E-02	-438E-04	134E-02	-496E-02	915E-02	-432E-02
0090	-377E-02	299E-03	602E-03	187E-03	817E-03	686E-03	-427E-02	334E-02	-757E-02
0095	-332E-02	122E-03	448E-03	166E-02	148E-02	-101E-03	-351E-02	-115E-02	-691E-02
0100	-366E-02	304E-04	586E-03	-211E-02	192E-02	846E-03	-279E-02	-27E-03	341E-02
0105	-242E-02	155E-03	926E-03	212E-02	221E-02	157E-02	-205E-02	-254E-02	138E-03
0110	-176E-02	263E-03	129E-02	171E-02	231E-02	203E-02	-147E-02	-316E-02	810E-03
0115	-134E-02	367E-03	151E-02	111E-02	218E-02	-213E-02	-147E-02	-137E-01	-252E-02
0120	-216E-03	440E-03	149E-02	393E-03	176E-02	190E-02	-222E-02	-174E-01	-833E-02
0125	-125E-03	459E-03	124E-02	152E-03	176E-02	160E-02	-329E-02	-189E-01	-133E-01
0130	-222E-05	356E-03	873E-03	466E-03	178E-02	142E-02	-452E-02	178E-01	-140E-01
0135	-832E-03	453E-03	567E-03	356E-04	132E-02	149E-02	-417E-02	-139E-01	-593E-02
0140	-154E-02	597E-03	548E-03	602E-04	165E-02	149E-02	-437E-02	-172E-02	804E-02
0145	-271E-02	800E-03	757E-03	106E-03	141E-02	134E-02	-495E-02	359E-02	128E-01
0150	-415E-02	100E-02	932E-03	419E-04	115E-02	103E-02	-526E-02	390E-02	113E-01
0155	-425E-02	115E-02	100E-02	284E-04	882E-03	975E-03	-477E-02	304E-02	623E-02
0160	-458E-02	126E-02	101E-02	153E-04	684E-03	108E-02	-355E-02	755E-02	-444E-03
0165	-264E-02	355E-02	125E-02	565E-04	338E-03	141E-02	-173E-02	399E-02	-404E-02
0180	-158E-02	134E-02	147E-02	203E-03	-427E-04	119E-02	-200E-02	369E-02	139E-04
0185	-182E-03	128E-02	162E-02	372E-04	524E-03	982E-03	-259E-02	205E-02	448E-02
0190	618E-03	116E-02	157E-02	403E-03	790E-03	101E-02	-243E-02	334E-03	593E-02
0195	397E-03	356E-03	130E-02	650E-03	593E-03	147E-02	-236E-02	340E-02	276E-02
0200	808E-03	677E-03	919E-03	380E-03	-280E-04	225E-02	-135E-02	-366E-02	-378E-02
0205	384E-03	541E-03	561E-03	542E-03	644E-03	308E-02	-203E-03	838E-02	-103E-01
0210	-246E-03	-111E-04	-246E-03	152E-02	120E-02	373E-02	656E-03	763E-02	133E-01
0215	101E-04	470E-03	761E-04	215E-02	159E-02	400E-02	899E-02	-108E-02	-110E-01
0220	201E-03	909E-03	245E-03	246E-02	157E-02	364E-02	323E-03	-399E-03	458E-02
0225	445E-03	-127E-02	-771E-03	192E-02	109E-02	-277E-02	-108E-02	343E-02	257E-02
0230	143E-02	149E-02	147E-02	713E-03	252E-03	169E-02	-294E-02	314E-02	692E-02
0235	167E-02	153E-02	204E-02	280E-03	499E-03	580E-03	-455E-02	-386E-02	-674E-02
0240	266E-02	-339E-02	-232E-02	859E-03	787E-04	787E-04	-524E-02	500E-02	300E-02
0245	294E-02	-108E-02	231E-02	997E-03	943E-03	281E-03	-481E-02	-129E-02	-129E-02
0250	241E-02	-568E-03	142E-02	943E-03	-109E-02	221E-03	-164E-02	363E-02	-281E-02

.0255	.224E-02	.263E-03	.627E-03	.103E-02	.145E-02	.657E-04	.235E-02	.352E-02	.330E-04
.0260	.109E-03	.567E-04	.111E-04	.119E-02	.192E-02	.109E-03	.126E-02	.367E-02	.629E-02
.0265	.209E-02	.193E-03	.205E-03	.156E-02	.238E-02	.212E-03	.298E-03	.361E-02	.130E-01
.0270	.340E-03	.179E-03	.604E-04	.189E-02	.269E-02	.398E-03	.558E-03	.249E-02	.167E-01
.0275	.150E-02	.665E-04	.558E-03	.178E-02	.275E-02	.595E-03	.101E-02	.448E-03	.154E-01
.0280	.152E-02	.279E-04	.972E-03	.134E-02	.251E-02	.101E-02	.740E-03	.462E-02	.916E-02
.0285	.159E-02	.162E-04	.110E-02	.556E-03	.273E-02	.138E-02	.619E-04	.309E-02	.465E-03
.0290	.210E-02	.584E-04	.935E-03	.229E-03	.164E-02	.163E-02	.639E-03	.127E-01	.767E-02
.0295	.167E-02	.135E-03	.610E-03	.479E-03	.145E-02	.151E-02	.311E-03	.144E-01	.128E-01
.0300	.184E-02	.235E-03	.316E-03	.508E-03	.123E-02	.106E-02	.940E-03	.836E-01	.141E-01
.0305	.188E-02	.365E-03	.103E-03	.407E-03	.908E-03	.373E-03	.256E-02	.104E-01	.123E-01
.0310	.140E-02	.518E-03	.457E-04	.242E-03	.487E-03	.435E-03	.402E-02	.522E-02	.975E-02
.0315	.166E-02	.719E-03	.194E-03	.505E-03	.375E-04	.144E-02	.527E-02	.376E-03	.663E-02
.0320	.107E-02	.713E-03	.600E-03	.141E-02	.631E-03	.163E-02	.735E-02	.127E-01	.187E-02
.0325	.481E-03	.664E-03	.762E-03	.117E-02	.555E-03	.154E-02	.764E-02	.167E-01	.133E-02
.0330	.673E-03	.589E-03	.783E-03	.502E-03	.860E-04	.121E-02	.698E-02	.191E-01	.541E-02
.0335	.176E-03	.503E-03	.617E-03	.231E-02	.572E-03	.544E-03	.558E-02	.195E-01	.942E-02
.0340	.312E-03	.429E-03	.307E-03	.337E-03	.110E-02	.116E-03	.400E-02	.180E-01	.117E-01
.0345	.554E-03	.393E-03	.329E-04	.491E-03	.131E-02	.499E-03	.279E-02	.145E-01	.109E-01
.0350	.324E-03	.387E-03	.275E-03	.815E-03	.126E-02	.750E-03	.214E-02	.343E-02	.685E-02
.0355	.108E-02	.363E-03	.374E-03	.987E-03	.117E-02	.933E-03	.195E-02	.344E-02	.965E-03
.0360	.102E-02	.265E-03	.360E-03	.899E-03	.118E-02	.123E-02	.204E-02	.243E-02	.419E-02
.0365	.376E-03	.713E-04	.368E-03	.583E-03	.125E-02	.165E-02	.219E-02	.714E-02	.621E-02
.0370	.314E-03	.187E-03	.497E-03	.211E-03	.126E-02	.201E-02	.211E-02	.997E-02	.419E-02
.0375	.602E-03	.457E-03	.823E-03	.101E-02	.112E-02	.226E-02	.157E-02	.109E-01	.705E-03
.0380	.114E-02	.697E-03	.128E-02	.136E-02	.751E-03	.241E-02	.706E-03	.105E-01	.572E-02
.0385	.137E-02	.893E-03	.172E-02	.124E-02	.253E-03	.227E-02	.392E-04	.946E-02	.798E-02
.0390	.203E-02	.104E-02	.196E-02	.698E-03	.429E-03	.187E-02	.150E-03	.840E-02	.604E-02
.0395	.148E-02	.112E-02	.182E-02	.775E-04	.104E-02	.128E-02	.112E-02	.718E-02	.730E-03
.0400	.111E-02	.112E-02	.150E-02	.461E-03	.130E-02	.708E-03	.238E-02	.523E-02	.523E-02
.0405	.116E-02	.112E-02	.150E-02	.461E-03	.130E-02	.473E-03	.308E-02	.194E-02	.876E-02
.0410	.567E-03	.102E-02	.935E-03	.713E-03	.112E-02	.478E-03	.277E-02	.332E-02	.283E-02
.0415	.998E-03	.859E-03	.416E-03	.330E-03	.158E-03	.743E-03	.175E-02	.332E-02	.283E-02
.0420	.138E-02	.675E-03	.136E-03	.135E-03	.158E-03	.106E-02	.618E-03	.134E-01	.402E-02
.0425	.143E-02	.496E-03	.150E-03	.435E-03	.168E-03	.104E-02	.620E-03	.169E-01	.963E-02
.0430	.224E-02	.306E-03	.333E-03	.847E-03	.308E-03	.799E-03	.127E-02	.181E-01	.117E-01
.0435	.210E-02	.870E-04	.457E-03	.995E-03	.243E-03	.432E-03	.239E-02	.188E-01	.983E-02
.0440	.193E-02	.370E-03	.341E-03	.741E-03	.617E-04	.432E-03	.341E-02	.137E-02	.552E-02
.0445	.225E-02	.316E-03	.252E-04	.305E-03	.631E-05	.166E-03	.390E-02	.961E-02	.903E-03
.0450	.165E-02	.388E-03	.462E-03	.111E-03	.644E-03	.496E-03	.365E-02	.518E-02	.203E-02
.0455	.175E-02	.599E-03	.709E-03	.111E-03	.644E-03	.913E-03	.271E-02	.749E-03	.274E-02
.0460	.209E-02	.386E-04	.576E-03	.327E-03	.139E-02	.134E-02	.137E-02	.354E-02	.197E-02
.0465	.222E-02	.353E-03	.594E-04	.704E-03	.139E-02	.162E-02	.260E-04	.755E-02	.118E-02
.0470	.326E-02	.799E-03	.650E-03	.116E-02	.912E-03	.162E-02	.122E-02	.110E-01	.147E-02
.0475	.342E-02	.122E-02	.131E-02	.113E-02	.568E-03	.182E-02	.122E-02	.110E-01	.147E-02
.0480	.332E-02	.158E-02	.169E-02	.719E-03	.892E-04	.189E-02	.210E-02	.133E-01	.294E-02
.0485	.372E-02	.183E-02	.175E-02	.279E-03	.470E-03	.170E-02	.264E-02	.141E-01	.459E-02
.0490	.294E-02	.190E-02	.159E-02	.298E-05	.979E-03	.138E-02	.276E-02	.130E-01	.593E-02
.0495	.245E-02	.204E-02	.138E-02	.382E-03	.130E-02	.856E-03	.255E-02	.103E-01	.346E-02
.0500	.227E-02	.203E-02	.124E-02	.101E-02	.144E-02	.334E-03	.207E-02	.537E-02	.514E-04

TIME	UN(5,9)	UN(5,13)	UN(5,17)	UN(9,9)	UN(9,13)	JN(9,17)	UN(13,9)	JN(13,13)	UN(13,17)
.0005	.439E+06	-.160E-02	.589E-05	.145E-01	-.440E-03	.658E-05	.293E-01	-.107E-03	.747E-06
.0010	.118E+01	.837E-02	.203E-03	.325E-01	.473E-03	.788E-04	.806E-01	.824E-03	.148E-04
.0015	.170E+01	.156E+00	-.245E-02	.581E-01	.176E-01	-.120E-02	.120E+00	.126E-01	-.182E-03
.0020	.191E+01	.395E+00	.665E-02	.919E-01	.404E-01	-.397E-02	.143E+00	.315E-01	.754E-03
.0025	.189E+01	.692E+00	.359E-02	.129E+00	.615E-01	.745E-02	.151E+00	.553E-01	.268E-03
.0030	.175E+01	.105E+01	-.512E-01	.187E+00	.932E-01	.117E-01	.154E+00	.851E-01	-.811E-02
.0035	.162E+01	.142E+01	-.134E+00	.246E+00	.149E+00	-.324E-01	.155E+00	.119E+00	-.249E-01
.0040	.154E+01	.173E+01	-.219E+00	.310E+00	.207E+00	-.683E-01	.158E+00	.153E+00	-.413E-01
.0045	.148E+01	.190E+01	-.286E+00	.392E+00	.270E+00	-.120E+00	.160E+00	.179E+00	-.448E-01
.0050	.137E+01	.187E+01	-.351E+00	.468E+00	.336E+00	-.173E+00	.154E+00	.190E+00	-.296E-01
.0055	.119E+01	.165E+01	-.399E+00	.648E+00	.408E+00	-.208E+00	.134E+00	.143E+00	.178E-02
.0060	.936E+00	.131E+01	-.387E+00	.548E+00	.480E+00	-.211E+00	.997E-01	.158E+00	.464E-01
.0065	.694E+00	.969E+00	-.274E+00	.702E+00	.544E+00	-.172E+00	.555E-01	.124E+00	.102E+00
.0070	.540E+00	.723E+00	-.549E-01	.777E+00	.606E+00	-.991E-01	.945E-02	.884E-01	.157E+00
.0075	.519E+00	.231E+00	.837E+00	.837E+00	.658E+00	.367E-01	-.318E-01	.589E-01	.133E+00
.0080	.620E+00	.614E+00	.518E+00	.881E+00	.699E+00	.200E+00	-.664E-01	.372E-01	.178E+00
.0085	.788E+00	.652E+00	.755E+00	.926E+00	.734E+00	.375E+00	-.979E-01	.204E-01	.130E+00
.0090	.958E+00	.651E+00	.912E+00	.944E+00	.779E+00	.539E+00	-.131E+00	.322E-02	.700E-01
.0095	.115E+01	.575E+00	.974E+00	.952E+00	.810E+00	.766E+00	-.201E+00	-.471E-01	.234E-01
.0100	.121E+01	.451E+00	.920E+00	.929E+00	.843E+00	.831E+00	-.219E+00	-.793E-01	.130E-01
.0105	.134E+01	.350E+00	.867E+00	.907E+00	.882E+00	.872E+00	-.210E+00	-.111E+00	.528E-01
.0110	.152E+01	.353E+00	.856E+00	.882E+00	.920E+00	.897E+00	-.170E+00	-.139E+00	.114E+00
.0115	.173E+01	.506E+00	.856E+00	.854E+00	.972E+00	.916E+00	-.106E+00	-.161E+00	.176E+00
.0120	.191E+01	.794E+00	.942E+00	.846E+00	.101E+01	.933E+00	-.360E-01	-.178E+00	.222E+00
.0125	.198E+01	.115E+01	.944E+00	.846E+00	.105E+01	.948E+00	.212E-01	-.186E+00	.244E+00
.0130	.188E+01	.149E+01	.968E+00	.842E+00	.108E+01	.953E+00	.539E-01	-.182E+00	.250E+00
.0135	.160E+00	.173E+01	.904E+00	.883E+00	.111E+01	.939E+00	.623E-01	-.158E+00	.252E+00
.0140	.120E+00	.187E+01	.861E+00	.913E+00	.112E+01	.857E+00	.573E-01	-.108E+00	.259E+00
.0145	.804E+00	.193E+01	.827E+00	.951E+00	.115E+01	.857E+00	.522E-01	-.328E-01	.273E+00
.0150	.503E+00	.195E+01	.790E+00	.978E+00	.118E+01	.811E+00	.546E-01	.582E-01	.292E+00
.0155	.350E+00	.196E+01	.739E+00	.977E+00	.121E+01	.781E+00	.623E-01	.150E+00	.314E+00
.0160	.326E+00	.196E+01	.739E+00	.977E+00	.123E+01	.772E+00	.656E-01	.226E+00	.377E+00
.0165	.362E+00	.190E+01	.677E+00	.967E+00	.126E+01	.720E+00	.551E-01	.276E+00	.364E+00
.0170	.386E+00	.175E+01	.635E+00	.929E+00	.126E+01	.780E+00	.304E-01	.308E+00	.403E+00
.0175	.360E+00	.148E+01	.633E+00	.868E+00	.128E+01	.798E+00	.269E-02	.328E+00	.435E+00
.0180	.304E+00	.110E+01	.669E+00	.804E+00	.130E+01	.822E+00	.914E-02	.352E+00	.504E+00
.0185	.273E+00	.671E+00	.716E+00	.733E+00	.130E+01	.859E+00	.120E-01	.389E+00	.530E+00
.0190	.316E+00	.274E+00	.744E+00	.676E+00	.128E+01	.914E+00	.722E-01	.437E+00	.518E+00
.0195	.439E+00	-.305E-01	.748E+00	.626E+00	.123E+01	.988E+00	.163E+00	.483E+00	.477E+00
.0200	.592E+00	-.217E+00	.714E+00	.571E+00	.116E+01	.108E+01	.163E+00	.483E+00	.477E+00
.0205	.693E+00	-.300E+00	.689E+00	.532E+00	.107E+01	.117E+01	.264E+00	.511E+00	.428E+00
.0210	.659E+00	-.315E+00	.688E+00	.496E+00	.967E+00	.125E+01	.356E+00	.486E+00	.402E+00
.0215	.500E+00	-.298E+00	.724E+00	.866E+00	.866E+00	.132E+01	.428E+00	.499E+00	.453E+00
.0220	.233E+00	-.262E+00	.797E+00	.418E+00	.779E+00	.135E+01	.482E+00	.449E+00	.425E+00
.0225	-.463E-01	-.200E+00	.885E+00	.367E+00	.695E+00	.134E+01	.528E+00	.425E+00	.655E+00
.0230	-.253E+00	-.944E-01	.948E+00	.315E+00	.816E+00	.127E+01	.578E+00	.432E+00	.655E+00
.0235	-.349E+00	.633E-01	.819E+00	.270E+00	.547E+00	.116E+01	.633E+00	.477E+00	.734E+00
.0240	-.355E+00	.260E+00	.819E+00	.219E+00	.479E+00	.100E+01	.682E+00	.553E+00	.761E+00
.0245	-.333E+00	.466E+00	.604E+00	.186E+00	.412E+00	.818E+00	.709E+00	.544E+00	.740E+00
.0250	-.345E+00	.643E+00	.332E+00	.163E+00	.342E+00	.617E+00	.700E+00	.734E+00	.694E+00

0255	.415E+00	.763E+00	.646E-01	.142E+00	.273E+00	.423E+00	.653E+00	.315E+00	.645E+00
0260	.513E+00	.814E+00	.154E+00	.31E+00	.212E+00	.256E+00	.584E+00	.387E+00	.601E+00
0265	.573E+00	.796E+00	.300E+00	.115E+00	.157E+00	.131E+00	.520E+00	.960E+00	.564E+00
0270	.531E+00	.710E+00	.363E+00	.100E+00	.110E+00	.44E-01	.488E+00	.104E+01	.526E+00
0275	.363E+00	.551E+00	.347E+00	.915E-01	.714E-01	.163E-01	.500E+00	.112E+01	.478E+00
0280	.971E-01	.308E+00	.273E+00	.686E-01	.338E-01	.667E-01	.553E+00	.118E+01	.416E+00
0285	.191E+00	.240E-01	.194E+00	.519E-01	.330E-02	.119E+00	.631E+00	.121E+01	.347E+00
0290	.414E+00	.432E+00	.171E+00	.379E-01	.254E-01	.17E+00	.714E+00	.119E+01	.281E+00
0295	.503E+00	.871E+00	.242E+00	.183E-01	.559E-01	.223E+00	.788E+00	.112E+01	.227E+00
0300	.430E+00	.127E+01	.396E+00	.141E-01	.785E-01	.269E+00	.847E+00	.100E+01	.182E+00
0305	.231E+00	.156E+01	.590E+00	.115E-01	.100E+00	.309E+00	.892E+00	.872E+00	.146E+00
0310	.633E-01	.169E+01	.783E+00	.119E-01	.124E+00	.346E+00	.923E+00	.742E+00	.120E+00
0315	.398E+00	.167E+01	.953E+00	.195E-01	.13E+00	.381E+00	.934E+00	.624E+00	.105E+00
0320	.737E+00	.154E+01	.109E+01	.119E-01	.155E+00	.413E+00	.911E+00	.315E+00	.104E+00
0325	.105E+01	.138E+01	.120E+01	.636E-02	.193E+00	.444E+00	.841E+00	.055E+00	.119E+00
0330	.135E+01	.127E+01	.126E+01	.326E-01	.233E+00	.478E+00	.718E+00	.282E+00	.151E+00
0335	.155E+01	.123E+01	.127E+01	.129E-01	.275E+00	.517E+00	.550E+00	.146E+00	.190E+00
0340	.166E+01	.126E+01	.124E+01	.279E-01	.306E+00	.564E+00	.361E+00	.769E-02	.213E+00
0345	.165E+01	.131E+01	.120E+01	.556E-01	.341E+00	.613E+00	.179E+00	.113E+00	.213E+00
0350	.140E+01	.130E+01	.115E+01	.337E-01	.322E+00	.663E+00	.303E-01	.197E+00	.172E+00
0355	.120E+01	.121E+01	.109E+01	.132E+00	.456E+00	.709E+00	.741E-01	.234E+00	.106E+00
0360	.860E+00	.104E+01	.100E+01	.195E+00	.532E+00	.745E+00	.138E+00	.229E+00	.364E-01
0365	.552E+00	.888E+00	.892E+00	.609E+00	.609E+00	.764E+00	.173E+00	.195E+00	.208E-01
0370	.342E+00	.661E+00	.749E+00	.343E+00	.678E+00	.731E+00	.193E+00	.149E+00	.632E-01
0375	.257E+00	.560E+00	.581E+00	.423E+00	.742E+00	.761E+00	.197E+00	.104E+00	.975E-01
0380	.272E+00	.549E+00	.406E+00	.491E+00	.795E+00	.688E+00	.176E+00	.627E-01	.133E+00
0385	.330E+00	.605E+00	.258E+00	.553E+00	.843E+00	.641E+00	.114E+00	.239E-01	.179E+00
0390	.37E+00	.688E+00	.177E+00	.610E+00	.844E+00	.593E+00	.458E-02	.150E-01	.237E+00
0400	.365E+00	.817E+00	.276E+00	.678E+00	.927E+00	.568E+00	.142E+00	.509E-01	.300E+00
0405	.382E+00	.860E+00	.393E+00	.704E+00	.978E+00	.557E+00	.294E+00	.747E-01	.380E+00
0410	.500E+00	.909E+00	.485E+00	.717E+00	.966E+00	.581E+00	.439E+00	.439E-01	.379E+00
0415	.719E+00	.973E+00	.523E+00	.735E+00	.934E+00	.616E+00	.374E+00	.150E-01	.368E+00
0420	.101E+01	.104E+01	.517E+00	.751E+00	.821E+00	.703E+00	.274E-01	.164E+00	.403E+00
0425	.130E+01	.108E+01	.502E+00	.751E+00	.821E+00	.703E+00	.274E-01	.164E+00	.403E+00
0430	.149E+01	.106E+01	.505E+00	.767E+00	.784E+00	.745E+00	.171E+00	.230E+00	.488E+00
0435	.154E+01	.955E+00	.530E+00	.773E+00	.753E+00	.788E+00	.339E+00	.290E+00	.556E+00
0440	.143E+01	.792E+00	.559E+00	.788E+00	.735E+00	.822E+00	.459E+00	.358E+00	.542E+00
0445	.120E+01	.606E+00	.565E+00	.807E+00	.747E+00	.841E+00	.575E+00	.452E+00	.694E+00
0450	.909E+00	.441E+00	.529E+00	.819E+00	.741E+00	.835E+00	.682E+00	.578E+00	.693E+00
0455	.609E+00	.321E+00	.441E+00	.844E+00	.740E+00	.792E+00	.799E+00	.726E+00	.543E+00
0460	.333E+00	.255E+00	.307E+00	.871E+00	.773E+00	.714E+00	.917E+00	.370E+00	.560E+00
0465	.852E-01	.200E+00	.144E+00	.904E+00	.773E+00	.611E+00	.101E+01	.977E+00	.486E+00
0470	.140E+00	.118E+00	.261E-01	.945E+00	.816E+00	.497E+00	.103E-01	.102E+01	.422E+00
0475	.342E+00	.197E-01	.185E+00	.966E+00	.863E+00	.387E+00	.983E+00	.101E+01	.386E+00
0480	.506E+00	.213E+00	.316E+00	.979E+00	.907E+00	.291E+00	.971E+00	.362E+00	.333E+00
0485	.604E+00	.431E+00	.404E+00	.980E+00	.939E+00	.211E+00	.734E+00	.309E+00	.410E+00
0490	.608E+00	.626E+00	.441E+00	.954E+00	.953E+00	.151E+00	.516E+00	.381E+00	.454E+00
0495	.516E+00	.755E+00	.427E+00	.924E+00	.959E+00	.109E+00	.550E+00	.885E+00	.499E+00
0500	.351E+00	.797E+00	.380E+00	.887E+00	.945E+00	.918E-01	.542E+00	.307E+00	.534E+00

REFERENCES

1. R.E. Whittman, Bird Resistant Aircraft Windshields, AF Materials Laboratory Briefs, Wright-Patterson AFB, May 1972.
2. USAF Bird Strike Summary 1 January 1971 thru 31 December 1971, Directorate of Aerospace Safety, AF Inspection and Safety Center, Norton AFB, California.
3. R. Kerker, Effect of Air Deflectors or Fuselage Shock Waves on Bird Trajectory, Douglas Aircraft Company Interim Report, Contract F33615-74-C-3038, May 1974.
4. J.W. Noonan, J.B.R. Heath, NAE Flight Impact Simulator, Quarterly Bulletin of the Div. of Mech. Engineering and the National Aeronautical Establishment, 1969, AD-707780.
5. G.E. Meyer, M.J. Boulter, Bird Control at the Airport, AIAA Journal, Dec. 73.
6. Unclassified DDC Literature Search, Shock-Absorbing Structure, Feb. 72.
7. R.D. Bennett, NASTRAN Differential Stiffness Analysis of an Aircraft Canopy, in NASA TM X-2378, September, 1971.
8. Sierracin Field Report, Bird Impact Test Windshield, Ref. Douglas Aircraft Co. Report DAC 33494, 1966.
9. P.A. Miller, Anti-Icing Aspects of Helicopter Windshield Design, International Helicopter Icing Conference, Ottawa, Canada, May 72.
10. A.J. Holland, The Development of Glass Transparencies for Modern Aircraft, Aircraft Engineering, Dec. 64.
11. R.J. Hayduk, Hail Damage to Typical Aircraft Surfaces, Journal of Aircraft, Vol. 10, Jan. 73.
12. M.J. Mott, Experimental Investigation into the Bird Impact Resistance of Flat Windscreen Panels with Clamped Edges, 2nd Symposium on Optical Transparencies, London U.K., June 71, A 72-27013.

AFFDL-TR-74-155

13. E.G. Barber, Reliability and Performance of Aircraft Transparencies in Civil Airline Service, Aircraft Engineering, Dec. 1964.
14. J.B. Olson, Design Considerations Affecting Performance of Glass/Plastic Windshields in Airline Service, Sierracin Corp., Las Vegas Conf. on Bird Strike, AFML-TR-73-126, June 73.
15. Windshield Flight Environment Simulator Capabilities (WFES), Sierracin/Sylmar Ca. Marketing Dept., 1974.
16. R.S. Hassard, Plastics for Aerospace Vehicles, Part II Transparent Glazing Materials, Proposed MIL-HDBK-12A, Part II, AFML-Contract F-33615-71-C-1465, Goodyear Aerospace Co., Jan. 73.
17. AFSC Design Hdbk. Chap. 3 Detail Design, Sect. 3A Substructures, April 73.
18. I.I. McNaughtan, The Resistance of Transparencies to Bird Impact at High Speeds, Aircraft Engineering, Vol. 36, Dec. 64.
19. G. Poullain, Clamagirand, Windscreens to Resist Bird Strikes, 2nd Symposium on Optical Transparencies, London U.K., June 71, A 72-27014.
20. The Boeing Co., Cockpit Window Damage Limits, Boeing Airliner, March 1961.
21. Douglas Aircraft Co., Windshield Bird Strike Structure Criteria - Phase I, F33615-73-C-3030, AFFDL-TR-73-103, Oct. 73.
22. Stress Analysis Manual, AFFDL-TR-69-42, February 1970.
23. A.W. Leissa, Vibration of Plates, NASA SP-160, 1969.
24. General Dynamics, F-111B Production Configuration Improvement Program, Vol. V, Crew Module Study, Fort Worth Div., FZM-12-4590-5, Feb. 67.

AFFDL-TR-74-155

25. L.M. Polentz, Tailor Your Shock Absorbers to Fit Your Needs, Hydraulics and Pneumatics, Vol. 26, No. 5, May 73.
26. H.W. Kriebel, A Study of the Practicality of Active Shock Isolation, University Microfilms, Ann Arbor, Mich., 1966.
27. C.E. Crede, Vibration and Shock Isolation, John Wiley & Sons.
28. R.L. Ketter, S.P. Prawl, Modern Methods of Engineering Computation, McGraw-Hill Book Co., 1969.
29. Dubbel, Hdbk f.d. Maschinenbau, Springer, 1956.
30. J.N. Macduff, J.R. Curreri, Vibration Control, McGraw-Hill, 1958.
31. E.A. Bakirzis, Stiffness Characteristics of Rubber Impact Absorbers, Journal of Strain Analysis, Vol. 7, No. 1, January 1972.
32. G.W. Underwood, Transparencies for Supersonic and Hypersonic Flight, Aircraft Engineering, Dec. 64.
33. Hawker Siddeley Aviation Ltd., Bird Impact Resistance Experimental Program. T.R.M. 430-432, 442, 452, 1970-71.
34. MIL-Hdbk-17, Part II, Transparent Glazing Materials, DoD, Washington, D.C., Jan. 57.
35. E. J. Sanders, Bird Impact Test Program, Data Package, Strain Gage Data for Shots FM-1, FM-2, FM-6, FM-7, ARO Inc., Aeroballistics Branch, Von Karman Gas Dynamics Facility, Jan. 73.
36. L.F. Richardson, The Approximate Arithmetical Solutions by Finite Differences of Physical Problems Involving Differential Equations with an Application to the Stresses in a Masonry Dam, Philosophical Transactions, Royal Society, London, Vol. 210, 307-357, May 24, 1910.
37. R.H. MacNeal, Electrical Circuit Analogies for Elastic Structures, John Wiley & Sons Inc., 1962.

AFFDL-TR-74-155

38. NACA TN 3280, Electrical Analogies for Stiffened Shells with Flexible Rings, Dec. 54.
39. W. Fluegge, Stresses in Shells, Springer-Verlag, New York, NY, 1972.
40. Roark, Formulas for Stress and Strain, McGraw Hill, NY.
41. J. Mitchell, More Thoughts on Forces Associated with a Bird Strike, Associate Committee on Bird Hazards to Aircraft of the National Research Council of Canada, Field Note 37, March 1966.
42. G.A. MacAulay, Some Thoughts on the Forces Associated with a Birdstrike, Field Note 24, Dept. of Transportation, National Res. Council of Canada, Jan. 65.
43. Analog/Hybrid Computation Branch, Computer Center, Shock Mount for Bird Strike, ASD Internal Memo 73-2, Feb. 73.
44. J.E. Mahaffey, B-1 Windshield Materials Study, NAR Rep. TFD 70-835-1, Jan. 71.
45. F-111 Crew Module Aerodynamic Review, GD/FW Rpts, FZM-12-057 and FZS-12, Fig. 2-1, 1967.
46. G.L. Wiser, New Materials in Aircraft Windshields, Interavia, Sep 73.
47. Monthly Progress Reports of PPG Industries, F-111 Bird Resistant Windshield, AFFDL Contract F33615-73-C-3099, 1973.
48. S.J. Hashmi et al., Dynamic Plastic Deformation of Rings Under Impulsive Load and Large Deflexion Elastic-Plastic Response of Certain Structures to Impulsive Load; Numerical Solutions and Experimental Results, Int. J. Mech. Sci. Pergamon Press, Vol. 14, December 72.
49. F.D. Sanson, H.E. Petersen, MIMIC Programming Manual, SEG-TR-67-31, July 67.
50. Control Data 6000 Computer Systems MIMIC Digital Simulation Language Reference Manual, Rev. E., 1 January 1972.

AFFDL-TR-74-155

51. Special Report on Windshield Programs, Sierracin Field Report, Summer 74.
52. G.E. Wintermute, Design Criteria on the Response of Transparent Aircraft Windshield Materials to Bird Impact, Contract F33615-72-C-1896, in AFML-TR-73-126, June 73.
53. P.W. Taylor, Test Methods to Establish Strength and Reliability, Aircraft Engineering, Dec. 64.
54. M.J. Mott, Experimental Investigation Into the Bird Impact Resistance of Flat Windscreen Panels with Clamped Edges, in Conference of Transparent Aircraft Enclosures, AFFDL-TR-73-126, June 73.
55. AFSC News Review, A-10 Tests, Results Show Survivability of Support Aircraft, June 74.
56. I.I. McNaughtan, The Temperature of a Vinyl Layer in an Electrically Heated Windscreen During Warm-Up, R.A.E. Rpt. No. TR-65215, AD-476093, Sep 65.
57. W.G. Roberts, Ten-Twenty High Strength Glass, Triplex Safety Glass Co. Ltd, in AFML-TR-73-126, June 73.
58. Triplex Windscreens for 747, Flight International, April 73.
59. D.L. Voss, Protective Coatings, Sierracin Corp., Las Vegas Conf. on Bird Strike, AFML-TR-73-126, June 73.
60. G.E. Husman, R.J. Kuhbander, Environmental Data and Machining Techniques of Polycarbonates, USAF Conference on Transparent Aircraft Enclosures, Las Vegas, NV, Feb 73.
61. H.R. Hazell, Study of Polycarbonate as a Glazing Material for Aircraft Windows and Canopies, Directorate of Materials Research and Development (Aviation), London, Rpt No. D MAT-181, AD-903844, January 1972.
62. Goodyear Aerospace Corp., Design Criteria on the Response of Transparent Aircraft Windshield Materials to Bird Impact, AFML-F33615-72-C-1896, 1972.

AFFDL-TR-74-155

63. Rockwell International Tech. Briefing TSP71-17639, 1971.
64. W. Miller, Polycarbonate Aircraft Transparencies, 6th National SAMPE Tech. Conf. in Dayton, Ohio, Session 3C-Special Materials Application, Oct. 74.
65. B-1 Windshields, Aviation Week and Space Technology, Feb. 72.
66. B-1 to Fly with Metal-Coated Windows, Goodyear Publ., May 72.
67. LOF Glass Aircraft and Defense Manual, Libbey-Owens-Ford Company, June 69.
68. W.E. Pryor, Reliability and Performance of Aircraft Transparencies in Military Service, Aircraft Engineering, Dec. 64.
69. MIL Hdbk-17A, Plastics for Aerospace Vehicles, Part I, Reinforced Plastics, Jan. 1971.
70. F.A. Cleveland, Size Effects in Conventional Aircraft Design, AIAA J. Aircraft, Vol. 7, Nov.-Dec. 1970.
71. MCAIR Status Report No. 3, Development of Bird Resistant Windshield Support Structure, Contract No. F33615-73-C-3142, Sep. 73.
72. I.I. McNaughtan, The Design of Leading-Edge and Intake Wall Structure to Resist Bird Impact, Royal Aircraft Establishment T.R. 72056, AD-903942, Apr. 1972.
73. Swedlow Inc., Swedlow Acrylic Plastic Windshield Bird Impact Tests, Company Paper.
74. R.L. Lyon, J.L. Zable, Impact-Force Source and Impact-Force Calibrator, Experimental Mechanics, Vol. 13, June 73.
75. F.P. Wang, The Conceptual, Analytical and Computational Aspects of Bird/Aircraft Windshield Impact, Douglas A/C Co. Interim Rpt., Contract F33615-74-C-3038, May 74.

AFFDL-TR-74-155

76. G.E. Freeman, J.B. Perkins, Helicopter and Other VTOL Transparencies - An Updating, in Conference Transparent Aircraft Enclosures, AFML-TR-73-126, June 73.

77. D.J. Peake, Some Additional Low Speed Bird Impact Tests on a Modified Windshield of the CL-41 Tutor A/C, National Research Council of Canada, NAE LR-488, Aug. 67.

78. Dayton University Research Institute, Responsive Materials to Impulsive Loading, AFML Contract F33615-73-C-5027, 1973.

79. G.M. Korb et al., Development and Experimental Verification of a Computer Program for Predicting Temperature Distribution and Heat Transfer Through Coated and Uncoated, Single or Multi-Glaze Window Systems, AFFDL-TR-69-28, April 1969.

80. General Dynamics, Temperature-Time History of Original Glass-Windshield of F-111, GD Rpt, M303-2033, Dec. 65.

81. C.D. Bailey, D.P. Beres, Non-Stationary Dynamic Response of a Free-Free Beam with a Step Load Applied at its Center, Technical Note, The Ohio State University, Feb. 73.

82. N.S. Phillips, R.W. Carr, A Statistical Investigation Into the Development of Energy Absorber Design Criteria, Beta Industries Inc., Dayton, OH, AD-749333.

83. J.W. Leech, Finite-Difference Calculation Method for Large Elastic-Plastic Dynamically Induced Deformations of General Thin Shells, AFFDL-TR-66-171, Wright-Patt. AFB Ohio, December 1966.